Pipeline Research Council International
LEADING PIPELINE RESEARCH

Catalog No. L5XXXX

Second Generation Models for Strain-Based Design

Contract PR-ABD-1 – Project 2

Contract DTPH56-06-T000014
"Consolidated Research & Development Program on Validation & Documentation of Tensile Strain Limit Design Models for Pipelines"

Final Approved Report

Prepared by the

Pipeline Research Council International, Inc.
Design, Materials, and Construction Technical Committee

For

US Department of Transportation
Pipeline and Hazardous Materials Safety Administration (PHMSA)

July 31, 2011

Sponsors' Preface

The Pipeline Research Council International, Inc. (PRCI) has completed a research project entitled "Consolidated Research & Development Program on Validation & Documentation of Tensile Strain Limit Design Models for Pipelines." This project was completed in collaboration with the research project funded by United States Department of Transportation, Pipeline and Hazardous Materials Safety Administration (DOT PHMSA) under contract DOT Project DTPH56-06-T000014. The research was completed by the Center for Reliable Energy Systems (CRES), C-FER Technologies (C-FER) and Microalloying International. The final technical report developed by the researchers is attached to this Sponsors' Preface. The combination of this Sponsors' Preface and the researchers' final technical report represent the final PRCI report that has been endorsed by the PRCI funding project team.

A contractual obligation exists for the project report to be released to the Public Domain because this program was funded, in part, by DOT PHMSA. Both PRCI and DOT PHMSA are concerned that a potential exists to apply the results of this report inappropriately, and this concern has resulted in the inclusion of the Sponsor's Preface. PRCI and DOT PHMSA have identified limitations in the application of the report as follows:

The technology is not yet sufficiently validated, and because strain-based design procedures have direct implications to pipeline integrity, users are strongly advised to use the results of this report with caution. Significant further work is required to fully validate and vet the technology documented herein. All users of the prediction model described in the report would need to ensure the model is appropriate for their unique material, design, construction, operational and environmental conditions.

As shown in the report, a tensile strain capacity prediction model was developed. The experimental data were then used to evaluate the model by comparing the measured failure strains with those predicted. The experimental program showed a wide range of failure strains for very similar test conditions. Differences of up to 75% exist between experimentally measured failure strains and the predictions. The report suggests that flat stress strain curves may be the cause of the wide scatter in the experimental results, and that Y/T alone is insufficient to describe flatness. However, additional work is necessary to establish whether this is a primary cause of the lack of agreement between model and experimental results or one of several contributing factors. The user is advised to exercise caution in using the results of the model, as a basis to account for potential failure strains less than predicted has not been established.

Additionally, the limited testing program did not fully investigate all of the key materials and geometric variables included in the model. With the exception of internal pressure, key variables were not experimentally evaluated across the full range of geometry and material property values that can be realistically expected within the pipeline industry. The table below delineates the variables included as model inputs and describes the extent to which these variables were explored experimentally in the full-scale test matrix. As such, the data in this table provide limits of model evaluation. Caution is advised when applying the results of this program outside of the tested range.

The major model variables that were not explored in the test program are high-low misalignment, wall thickness, and pipe diameter. Among those three parameters, the high-low misalignment and wall thickness are known from previous research to have a strong effect on the tensile strain capacity. Available test data and models indicate that the pipe diameter in itself is not a significant variable.

Model Input Parameters	**Experimentally Explored Range**
Geometric Parameters	
Pipe wall thickness	single wall thickness: 12.7 mm
Flaw depth	2 and 3 mm (primarily 3mm)
Flaw length	35, 50 and 70 mm (primarily 50mm)
Flaw location	Base pipe, weld metal centerline and HAZ (all were surface breaking)
Girth weld high-low misalignment	essentially zero nominal misalignment
Weld Geometry	Narrow groove GMAW (see note 1)
Material Parameters	
Pipe Yield Strength	Two levels separated by about 14 ksi in yield strength. Both pipes defined as X65 from the manufacturers (see note 2)
Pipe longitudinal Y/T ratio	Mean Y/T ratios of 0.88 and 0.92. The measured range of Y/T ratio is greater. (see note 3)
Weld/Pipe UTS mismatch	Mean levels of UTS mismatch: 1.04, 1.14, and 1.19. Mean levels of Yield Strength mismatch: 0.96, 1.08, and 1.09.
Weld metal toughness	Three procedures with two weld consumables: Lincoln LH56 and Thyssen K-Nova(Ni)
Loading Parameter	
Internal pressure	Low pressure (zero) and high pressure (hoop stress = 70-75% of actual yield strength)

Notes:

1. The model offers two equations; one for narrow groove GMAW and one for FCAW and SMAW welds with a wider bevel.
2. NPS12 ERW pipes were sourced from two manufacturers. On the basis of actual strength, the pipes were denoted as X56 and X70 and were treated as two grades in the program.
3. The difference in the strength and Y/T ratio was recognized in the test program and post-test analysis. The pipes were treated as being two grades.

Pipeline Research Council International
LEADING PIPELINE RESEARCH

Catalog No. L5XXXX

Second Generation Models for Strain-Based Design

Contract PR-ABD-1 – Project 2
Final Approved Report

Prepared for the
Design, Materials, and Construction Technical Committee
of
Pipeline Research Council International, Inc

Prepared by

Center for Reliable Energy Systems
Yong-Yi Wang, Ming Liu, and Yaxin Song

With Assistance from

C-FER Technologies (1999) Inc.
Mark Stephens and Randy Petersen

Microalloying International
Robin Gordon

August 30, 2011

Version	Date of Last Revision	Date of Uploading	Comments
1.1	February 22, 2011	February 22, 2011	
1.2	May 31, 2011	May 31, 2011	
1.3	July 1, 2011	July 1, 2011	
1.4	July 25, 2011	July 25, 2011	
1.5	August 30, 2011	August 30, 2011	Final

Notice

This report is furnished to Pipeline Research Council International, Inc. (PRCI) under the terms of PRCI contract PR-ABD-1-Project 2, between PRCI and ABD-1 contractor Center for Reliable Energy Systems ("CRES").

The contents of this report are published as received from the ABD-1 contractor. The opinions, findings, and conclusions expressed in the report are those of the authors and not necessarily those of PRCI, its member companies, or their representatives. Publication and dissemination of this report by PRCI should not be considered an endorsement by PRCI of the ABD-1 contractor, or the accuracy or validity of any opinions, findings, or conclusions expressed herein.

In publishing this report, PRCI and the ABD-1 contractor make no warranty or representation, expressed or implied, with respect to the accuracy, completeness, usefulness, or fitness for purpose of the information contained herein, or that the use of any information, method, process, or apparatus disclosed in this report may not infringe on privately owned rights. PRCI and the ABD-1 contractor assume no liability with respect to the use of, or for damages resulting from the use of, any information, method, process, or apparatus disclosed in this report. By accepting the report and utilizing it, you agree to waive any and all claims you may have, resulting from your voluntary use of the report, against PRCI and the ABD-1 contractor.

Pipeline Research Council International Catalog No. L5XXXX

PRCI Reports are Published by Technical Toolboxes, Inc.
3801 Kirby Drive, Suite 520
Houston, Texas 77098
Tel: 713-630-0505
Fax: 713-630-0560
Email: info@ttoolboxes.com

Funding Partners

The following organizations provided financial support to this project:

Alliance
BP
Chevron
ConocoPhillips Company
El Paso
Enbridge
Evraz Inc NA
ExxonMobil
Gassco
Gaz de France
JFE
Lincoln Electric
National Grid
Nippon Steel
NiSource
PG&E
PHMSA
PRCI
Saudi Aramco
Southern California Gas Company
Spectra Energy
Sumitomo Metal Industries
TAMSA
TransCanada
TransGas

Responsibilities and Acknowledgement

The report was prepared for PRCI as a deliverable under a consolidated program with the US Department of Transportation Pipeline and Hazardous Materials Safety Administration (PHMSA). This report specifically covers the work of the second project aimed at the development of second generation tensile strain design models. The work of the first project is covered in a separate report[1]. The first project was carried out jointly by the Center for Reliable Energy Systems (CRES), C-FER Technologies, and Microalloying International. CRES has the principal responsibility for the second project. This report is principally prepared by CRES with assistance from C-FER and Microalloying.

Many individuals provided valuable contributions throughout this multi-year effort. The project team is particularly grateful for the guidance and encouragement of Mr. David Horsley of BP for the entire duration of this project. Mr. David Horsley, Dr. Joe Zhou of TransCanada, and Dr. Laurie Collins of Evraz NA served as the project technical managers during various phases of this project. Mr. Chris McLaren of PHMSA served as the technical manager from the US Department of Transportation. He has provided many insightful inputs to the project. Mr. Ken Lorang of PRCI, who was the project manager from PRCI, was a constant and persistent driving force behind all project activities.

Representatives of project funding partners have provided constructive suggestions throughout the course of this project. Of particular note, in recognition of their active participation, are Dr. Paulo Gioielli of ExxonMobil, Dr. Pedro Vargas of Chevron, and Dr. V. B. Rajan of Lincoln. The project team is grateful to Dr. Tom Zimmerman of Enbridge for his central role in the preliminary development of the large-scale experimental test program.

The project team wishes to dedicate this work to the late Ms. Marina Smith whose enthusiasm and support for this project were evident whenever and wherever she was present.

Finally, we wish to thank the linepipe manufacturers for their donation of the pipe materials.

[1] Wang, Y.-Y., Liu, M., Long, X., Stephens, M., Petersen, R., and Gordon, R., "Validation & Documentation of Tensile Strain Limit Design Models for Pipelines," PRCI Project ABD-1, Project 1, DOT Agreement DTPH56-06-T000014, Final report, August 2, 2011.

Second Generation Models for Strain-Based Design

Executive Summary

This project covers the development of tensile strain design models which form a key part of the strain-based design of pipelines. The strain-based design includes at least two limit states, tensile rupture, and compressive buckling. The tensile strain limit state is considered as an ultimate limit state in pipeline design. The breach of the limit state can lead to loss of life and property, damage to the environment, and disruption of pipeline operations. The development of tensile strain design models has a direct impact on the safety and integrity of pipeline systems. The tensile strain design models are also an enabling technology for pipelines in the northern climate and deep-water offshore area.

This multi-year research program was undertaken to develop tensile strain design models using a multidisciplinary approach, involving fundamental fracture mechanics, small-scale material characterization tests, and large-scale tests of full-size pipes. The central output of this project is the tensile strain design procedures for pipelines when the applied longitudinal strain exceeds the yield strain (typically defined as 0.5% total strain). The tensile strain design procedures are strain-based and complementary to the typical stress-based design procedures which focus on the control of hoop stress.

The tensile strain design procedures consist of three essential elements: (1) linepipe specifications, (2) welding procedure qualifications, and (3) tensile strain design models. The main focus of this project is the third element, i.e., tensile strain design models. A set of overall tensile strain design procedures is recommended. However, those recommendations are not meant to be all-inclusive. Appropriate national and international standards shall be followed in conjunction with those recommendations. All phases of a pipeline life, including installation, commissioning, and operation, should be considered to ensure safe operation over its entire life.

The tensile strain design models are structured with the following overarching principles. First, a flexible framework is established for the adoption of the current technology and the incorporation of future development. Secondly, the most appropriate approach for the tensile strain design of a particular project depends on the scale of the project and many design and maintenance considerations. No single approach may be appropriate for all projects. Thirdly, a framework of a multi-level approach is proposed which allows the use of a wide variety of material toughness test options.

A four-level approach is proposed for the tensile strain design models. The Level 1 procedure provides estimated tensile strain capacity (TSC) in a tabular format for quick initial assessment. The apparent toughness is estimated from upper shelf Charpy impact energy. The Level 2 procedure contains a set of parametric equations based on an initiation-control limit state. The tensile strain capacity can be computed from these equations with the input of a pipe's dimensional parameters and material property parameters, including the apparent toughness. The apparent toughness is estimated from either upper shelf Charpy energy or upper shelf toughness of standard CTOD test specimens. The Level 3 procedure uses the same set of

equations as in Level 2 and the toughness values are obtained from low-constraint tests. In the Level 3 procedure, two limit states based on either initiation control or ductile instability may be used. The Level 4 procedure allows the use of direct FEA calculation to develop crack driving force relations. The same limit states as those in Level 3 may be used. The Level 4 procedures should only be used by seasoned experts in special circumstances where lower level procedures are judged inappropriate.

The tensile strain design models may be used for the following purposes:

(1) The determination of tensile strain capacity for given material properties and flaw size.

(2) The determination of acceptable flaw sizes for given material properties and target tensile strain capacity.

(3) The selection of material properties to achieve a target strain capacity for a given flaw size.

(4) The optimization of the tensile strain capacity by balancing the requirements of material parameters, such as weld strength (thus weld strength mismatch level) versus toughness.

The essential features of the tensile strain design models are as follows

(1) Two limit states are recognized: (a) initiation control and (b) ductile instability.

(2) Two weld bevel geometries are recognized: (a) narrow-groove, typical of mechanized GMAW welds and (b) standard groove, typical of FCAW and SMAW welds.

(3) The pipes are assumed to have uniform and isotropic tensile properties.

(4) The pipes on either side of the girth welds are assumed to have the same properties.

(5) There are no inherent limits on pipe grade. The linepipe tensile properties are represented by its longitudinal Y/T ratio, which serves as a representation of linepipe's strain hardening capacity.

(6) The predictive equations have no embedded safety factor.

(7) The welds should not have gross strength undermatching.

(8) The target optimum strain range of the models is from 1.0% to one half of the pipe's uniform elongation.

(9) The models are applicable to one single flaw in a girth weld. If multiple flaws were to exist in a single girth weld, the flaws need to be sufficiently far apart so the existence of other flaws does not affect the behavior of the flaw being evaluated.

(10) No flaw interaction rules are established and applied in the models.

(11) The models should not be used for flaw acceptance after repair welding without further evaluation.

(12) The potential impact of material anisotropy on the tensile strain capacity is not considered in the models.

The tensile strain models were not based on the particular pipe grades tested in the experiment program. The fundamental basis of the models is fracture mechanics. The parametric representation of the tensile property of the linepipes and welds were developed using

a material database which covered grades from X65 to X100. The tensile strain models are, in principle, applicable to all GMAW and FCAW/SMAW processes, provided that appropriate material property data are within the applicable range of the models.

The tensile strain models recognized a strong relationship between strain capacities and some key pipeline material and geometry parameters, including wall thickness, weld strength mismatch, girth weld high-low misalignment, internal pressure, and flaw size. The experimental program within this project evaluated the effects of internal pressure, weld strength mismatch, Y/T ratio, flaw location, flaw size, and toughness. The specific relationships between the other key parameters and strain capacities were not experimentally evaluated. For example, the weld high-low misalignment and pipe wall thickness were not assessed within the large-scale experimental test program. Further work is required to evaluate the relationship which is established in the model, but not covered in the current experimental test matrix.

The large-scale experimental program included two 12" OD 0.5" WT linepipes which were manufactured by two manufacturers. The separation of the actual yield strength between those two linepipes was approximately 14 ksi. Three welding procedures were applied to those two pipes, creating three weld strength levels. Pipes of different diameter and wall thickness should be tested to further evaluate the model.

A total of 24 full-scale tests were conducted with and without internal pressure. The tensile strain capacities (TSC) measured from those tests were evaluated and compared with the predicted TSCs of the models. Fifteen of the 24 tests had measured TSCs in the range of 0.7% to 3.5%. There was a good conformity within this strain range between the test data and the prediction. Seven of the 24 tests had measured TSCs greater than 3.5%, and in some cases much greater. The predicted TSCs for those 7 tests were lower than the test data. The most significant contributor to the difference between the measured and predicted TSCs is likely the strength variation along the length of the pipe and the flat stress-strain curves of the tested pipes. A small variation in the strength can lead to a large variation of the measured remote strain even when the flaw behaves consistently. The evaluation of the pipe property variation indicates that the strain values greater than approximately 3.5% are not likely repeatable or consistent. Two out of the 24 tests had measured TSCs lower than 0.7% for which the predicted TSCs are higher. For one of two cases, there was a duplicate test which produced a much higher TSC value which was predicted well by the models. Extensive analyses, both experimental and numerical, were conducted to examine those two low TSC tests. The variation of pipe property along pipe length could be partially responsible for the difference. The other possible contributor is the high oxygen content of those welds and associated high driving force. However, the exact causes of the low values have not been identified at the time of this writing.

Finally, it should be noted that the strain-based design, including tensile strain design, is an evolving field of engineering disciplines. The stated objective of this work is to provide a solid technical basis for the development of industry guidelines and possible recognition by codes and standards. The tensile strain design procedures, including the tensile strain prediction models, provide a sound starting point towards these stated objectives. However variations in material

properties and service conditions can be greater than those analyzed in this project. These conditions must be accounted for when the procedures are applied in actual pipeline projects.

Table of Contents

1 Introduction

1.1 Background and Incentive

Strain-based design (SBD) refers to pipeline design methodologies which have a specific goal of maintaining pipeline service and integrity under large longitudinal plastic strains (>0.5%). Such large strains may come from frost heave and thaw settlements in arctic regions, seismic activities, mine subsidence, and other events. For offshore pipelines, large longitudinal strains may be induced by thermal expansion or displacement of pipelines due to underwater landslides. In North America, the need for SBD is primarily driven by northern pipeline projects where these pipelines may traverse regions of discontinuous permafrost. In other parts of the world, SBD is playing an increasingly important role for pipelines going through areas of seismic activities and mine subsidence.

Traditional pipeline design primarily focuses on pressure containment through limiting the hoop stress to a certain percentage of the specified minimum yield stress (SMYS). For instance, the concept of class location is based on the ranking of the maximum applied hoop stress as a percentage of SMYS.

Events leading to large longitudinal plastic strains are often displacement-controlled, although combined displacement- and load-controlled events are possible. Designing for large ground movement events is a complex undertaking. Although the owners and contractors are legally required to construct and operate pipelines safely under all anticipated conditions, design methods specifically for large ground movements are often lacking sufficiently actionable details. A project sponsored by US DOT PHMSA focused on the identification and evaluation of geo-hazards in the areas of landslide and subsidence [1]. The project did not address the tolerance level of pipelines against such geo-hazards.

To assess the structural integrity and safety of a pipeline against large ground movement hazards, it is necessary to know the magnitude of strain demand (applied strain) and strain capacity (strain limit). The assessment is performed by evaluating two limit states: *tensile rupture* and *compressive buckling*. The *tensile rupture* is an ultimate limit state which is related to the breach of the pressure boundary. The *compressive buckling* could be either a service limit state or an ultimate limit state. This project focuses on one of the key components of the assessment, the tensile strain capacity, or TSC.

The tensile strain capacity of a pipeline is controlled by the tensile strain capacity of its girth welds. The girth welds here refer to the entire weld region, including the weld metal, fusion boundary, and the heat-affected zone (HAZ). Girth welds tend to be the weakest link due to the possible existence of weld defects and often deteriorative metallurgical and/or mechanical property changes from welding thermal cycles. Consequently, TSC is intrinsically related to the girth welding procedure qualification and flaw acceptance criteria. The welding procedure qualification involves the control of essential variables to ensure the equivalence of procedure qualification welds and field production welds, and the definition and execution of mechanical tests of welds. The flaw acceptance criteria are implemented in field production welds to ensure a certain level of performance, in this case TSC, is achieved.

Presently, the most recognized procedures for tensile strain design are DNV OS F101 and RP F108 for offshore, and CSA Z662 Annex C for onshore applications. Both methods are useful under certain circumstances, but with many limitations.

1.2 Objectives of this Project

The primary objective of this project is to provide a set of tensile strain design models for the strain-based design of pipelines. The implementation of the tensile strain design models involves (1) linepipe specifications, (2) welding procedure qualification, (3) field girth weld flaw acceptance criteria, and (4) field construction practice. In the case of welding procedure qualification, the testing and requirements of tensile and toughness properties are some of the key elements. These relevant areas are covered as a part of the overall development of tensile strain design models. In a longer term, this project should provide substantial technical basis for the standardization of the treatment of TSC.

1.3 Scope and Structure of the Report

This report covers the development of tensile strain design models. In Section 2 of the report, a brief state-of-the-art review of the tensile strain design procedure is provided. In Section 3, the experimental tests in support of the development of the tensile strain design models are briefly reviewed. The test data and post-test analysis are covered in the Project 1 report [2]. In Section 4, the general concept of tensile strain design and material response under tensile straining is covered. In Section 5, the framework of the tensile strain design models is established. The key components of these models are listed along with the limit state assumptions. In Section 6, the development of crack-driving force relations is described in detail. In Section 7, the development of TSC equations from FEA results is fully described. Sample trends of TSC and flaw acceptance criteria are given. In Section 8, the fundamental concepts of apparent toughness are first explained. The significance of apparent toughness from various experimental test forms is described. In Section 9 the central output of this project, the tensile strain design procedures, is given. The three essential elements of tensile strain design: linepipe specifications, welding procedure qualification, and tensile strain design models, are covered in this section. The tensile strain design models presented in Section 9 are evaluated against the full-scale test data from Project 1 in Section 10. The applicable range of the models is illustrated. A few key issues are discussed in Section 11. The concluding remarks are given in Section 12. The unresolved issues and possible future work are also highlighted in this section.

The appendices of the report provide support information to the main body of the report. These appendices are mostly self-contained for easy reading.

2 Tensile Strain Capacity (TSC)

2.1 Overview

A brief review of the current status of tensile strain design procedures is provided in this section. More extensive coverage is given in the Project 1 report [2].

2.2 State-of-Art in Tensile Strain Design

2.2.1 Wide Plate Testing

Wide plate testing has been one of the most recognized tools for determining girth weld tensile strain capacity [3,4]. Many organizations now have CWP testing capabilities, including the University of Gent, C-FER, Stress Engineering Services, National Institute of Standards and Technology (NIST), Evraz, JFE, Nippon Steel Corporation, POSCO, etc.

A few notable shortcomings of the past CWP tests are the lack of consistent and standardized test procedures [5] and its inability to evaluate the effects of internal pressure and girth weld high-low misalignment on TSC. The importance of having standardized testing is being recognized [5]. Denys, et al., has published a recommended testing procedure of CWP specimens [6]. The research team of a joint US DOT PHMSA and PRCI project is also working on a "standard" CWP testing procedure [7].

2.2.2 Extension of Stress-Based Design Procedures

Section G100 of DNV OS-F101 [8] provides guidance on the determination of girth weld defect acceptance criteria for strain-based design conditions. A number of key input parameters are covered in the guidelines, including (1) the selection of appropriate stress-strain curves for flaws located in the weld metal and HAZ, (2) the treatment of strain concentration, and (3) the treatment of residual stress. Extensive guidance is provided on the fracture toughness testing. DNV OS RP F108 [9] provides further guidance on the engineering critical assessment (ECA) of girth welds for installation by reeling. The recommended toughness testing procedure is a multiple-specimen SENT (single-edge-notched tension) procedure with further qualification and validation by the so-called "sector" specimens. The sector specimen is similar to a miniature curved wide plate specimen.

DNV F101 and F108 collectively provide insightful comments related to many complex factors affecting TSC. The implementation procedures of those comments are, in many instances, not prescribed. Therefore, the application of F101 and F108 requires the involvement of well-seasoned experts. The platform of ECA, i.e., Level 3 of BS 7910, is not the most suitable format for strain-based design, although it serves as a useful intermediate step before more suitable formats are developed and validated. The full implementation of F101 and F108 can be prohibitively expensive for large onshore projects.

2.2.3 PRCI Approach to TSC

In the PRCI approach, the TSC is established by equating the crack driving force with the apparent toughness of the structure. The crack driving force, i.e., $CTOD_F$, is related to the remote longitudinal strain. The relationship depends on the flaw size, flaw location, linepipe

tensile properties, weld metal tensile properties (weld strength mismatch), weld geometry, and other parameters [10,11,12,13,14].

The apparent toughness represents the resistance of the material to the applied strain in the presence weld flaws. The term "apparent" is adopted in the recognition that the traditional single-parameter based fracture mechanics is no longer strictly valid in the presence of large crack-tip plasticity, which is almost always the case for strain-based design. Consequently, the toughness as a "material parameter", as often viewed, does not exist anymore. The so-called "toughness", in the presence of large crack-tip plasticity, represents the intrinsic material toughness modified by the material response specific to the structure of interest. In other words, the "toughness" of the material becomes dependent on the flaw size relative to the rest of the structure and the strain redistribution in the vicinity of the flaw and the rest of the structure.

One of the original conceptual developments in TSC is the grouping of the girth weld response to the longitudinal straining into three distinctive regions [10], see Figure 2-1. In Region 1, the crack-driving force, as represented by the crack-tip-opening displacement (CTOD), increases rapidly with a small amount of applied strain. This condition is associated with large flaw size and/or weld strength undermatching. In Region 3, the crack-driving force remains small, even with a large applied strain. This condition is associated with small flaw size and or highly overmatching weld metal. Continued straining under this condition would lead to failure in the pipe body, not in the girth weld. In Region 2, there is a gradual rise in the crack-driving force as a function of the applied strain. The strain capacity is dependent on a material's toughness.

The boundaries of the three regions are not clear cut. The characterization of these regions helps to visualize the different possible responses.

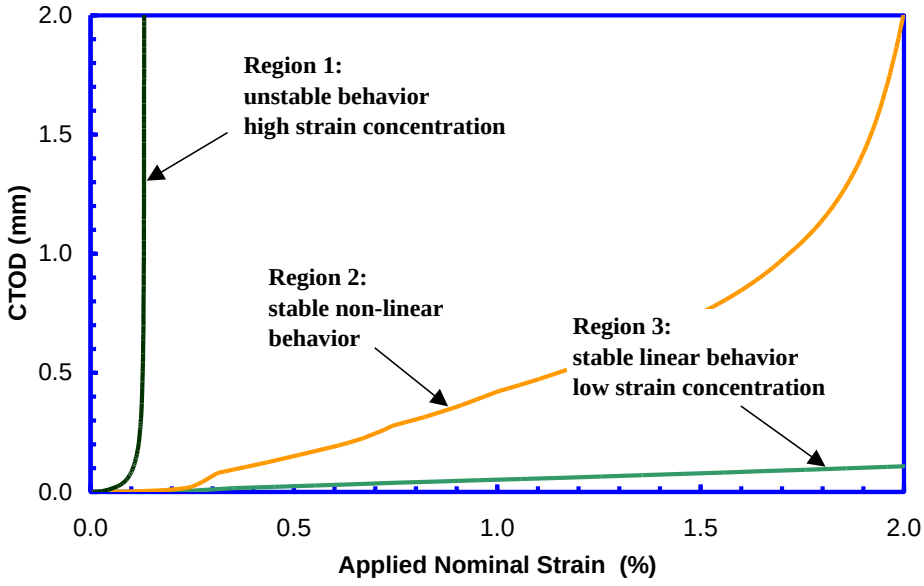

Figure 2-1 Characteristic response of CTODF as a function of applied nominal strain [10]

2.2.4 Adoption of PRCI Approach in CSA

The PRCI approach described above was formally recognized in Annex C of CSA Z662 2007 Edition [15]. The overall approach is structured into two tiers. The Tier 1 approach is non-prescriptive. It allows for essentially all validated approaches for the tensile strain design. The Tier 2 approach is a direct adoption of the PRCI approach. A set of parametric equations is provided which allows the calculation of TSC from known material properties and flaw size. Alternatively, the critical flaw size may be computed for a given set of material properties and anticipated strain demand.

No exclusive test methods were defined in Annex C for the determination of apparent toughness. A procedure to convert the traditional high-constraint CTOD toughness to apparent toughness was suggested. This conversion process contains three critical elements: (1) the material response is assumed to be on the upper shelf in the toughness brittle-to-ductile transition response, (2) the CTOD toughness from the traditional high-constraint CTOD tests has to satisfy the validity criteria for single-parameter dominance of the crack-tip fields, and (3) when the above conditions are satisfied, the apparent toughness is set as the smaller of (1) three-times of the minimum value and (2) two-times of the averaged values. The first condition was supposed to be achieved by specifying the minimum and averaged Charpy energy values, although the actual numerical values are too low for modern mechanized GMAW welds. It should be noted that the assumption about upper-shelf behavior precludes the use of pop-in controlled CTOD toughness as a basis for determining the apparent toughness. Such use would imply that the entire material of interest behaves in a brittle manner, which clearly can't be the case for a strain-based design.

Some factors which were later found to affect TSC, such as internal pressure, were little known at the time of Annex C adoption. The effects of internal pressure were not explicitly included in the TSC parametric equations. The effect was considered by setting a hard limit on the maximum value of the apparent toughness 0.3 mm to prevent non-conservative TSC predictions.

2.2.5 Resistance-Curve Approach (i.e., the Tangency Approach)

The resistance-curve approach is a failure criterion where fracture instability is predicted to occur when the driving force for fracture exceeds the materials resistance to fracture. The failure mode is assumed to be ductile fracture. The crack driving force, in terms of CTOD or *J*-integral, is derived from finite element analysis for various structural geometries (including flaw size) and material properties. The resistance curve (*R*-curve) is directly measured from test specimens. The failure point or the unstable ductile tearing point is determined by the traditional tangency criteria (discussed in 5.3.3). There are several organizations pursuing tensile strain capacity prediction using the tangency approach, two of which are SINTEF [16,17,18] and ExxonMobil [19,20,21,22].

The tensile strain models developed within this project recognize two limit states: (1) initiation control using apparent toughness as the toughness parameter and (2) ductile instability (or tangency method) using resistance curve as the toughness parameter. The initial control limit state is similar to the apparent toughness approach proposed in prior PRCI projects. It should be

noted that although the tangency approaches adopted by different organizations were based on the same fracture mechanics principles, variations can exist in the details of implementations. The instability analysis developed within this program is an independent piece of work.

2.2.6 Osaka University and JFE Approach

The Osaka/JFE approach relies on the failure loci relating the stress triaxiality and equivalent plastic strain at a crack tip. The so-called two-parameter approach has been applied to a wide variety of fracture mechanics applications [23,24]. Igi and Suzuki applied this methodology for the prediction of tensile strain limit of X80 pipes [25]. The SENT and CWP specimens were tested to establish the failure loci. Igi and Suzuki demonstrated the effects of internal pressure and Y/T on tensile strain limits using this method. The reduction of tensile strain limits were shown to be a factor of 1.8 for low Y/T material (Y/T=0.76) and over 5.0 for high Y/T material (Y/T=0.95).

2.3 Incentives for this Work - Effects of Internal Pressure

Research performed in the early to mid-2000's indicated that a softened HAZ and the presence of internal pressure can potentially reduce the TSC of pipeline girth welds [26,27,28]. The possible reduction in tensile strain capacity due to internal pressure is a major concern because previous project-specific experimental studies have all been conducted under uniaxial loading. For instance, the PRCI TSC approach was validated against CWP test results obtained under uniaxial tension [29].

There were no validated models which accounted for the effects of internal pressure. The development of such models was hampered by the lack of experimental test data. The consolidated program, of which this project is a part, was initiated to provide such experimental data. It was also envisioned that such data in conjunction with analytical and numerical analysis could lead to the development of second generation models. It may be noted that full-scale test data generated since the start of this project have demonstrated the detrimental effects of internal pressure on TSC [30,31,32].

2.4 Other Significant Factor - Girth Weld Strength Mismatch and High-Low Misalignment

In addition to internal pressure, girth weld high-low misalignment was found to potentially have significant impact on the girth weld tensile strain capacity. Sample crack driving force relations are given in Figure 2-2 for a nominal X80 girth weld with ½-inch (12.7-mm) pipe wall thickness [33,34]. At a high level of misalignment (> 3.2 mm), the strain capacity is shown to be greatly reduced even with a relatively small flaw (3-mm deep and 50-mm long). The detrimental effects of misalignment on tensile strain capacity have also been reported recently by Kibey, et al. [35].

With adequate toughness, overmatched welds can greatly improve the tensile strain capacity. The effect of weld strength mismatch on tensile strain capacities, however, was not explicitly considered in existing codes and standards. For example, in CSA Z662, it is generally required that weld strength must overmatch pipe strength.

2.5 Objectives

The overall objective of this project is the development of second generation TSC models which incorporate additional factors, such as internal pressure, weld strength mismatch, and weld high-low misalignment, which were not included in the first-generation models. Practical and comprehensive guidelines on the use of these models are to be provided. The ultimate objective of this work is to provide the industry with a set of tensile strain design procedures which are suitable for incorporation into pipeline design standards.

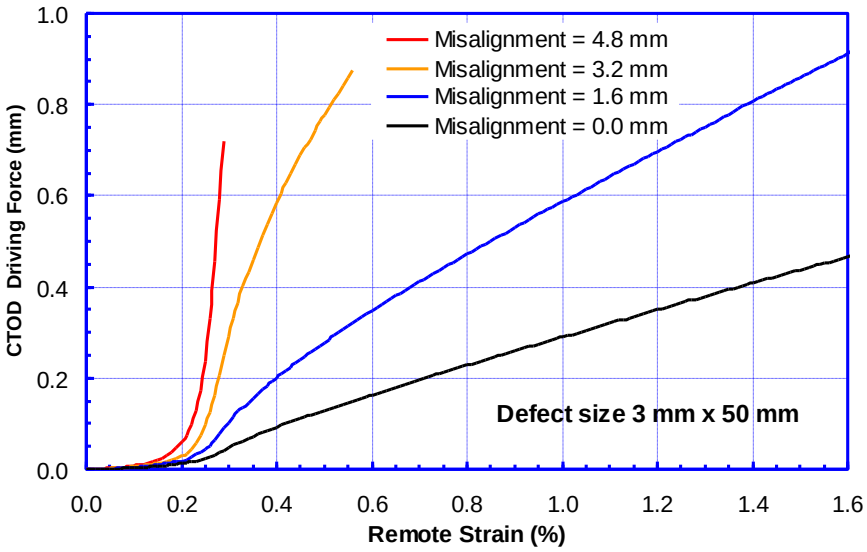

Figure 2-2 Crack driving force as a function of remote stress at various levels of misalignment [34]

3 Experimental Tests

3.1 Pipes and Welds Tested for this Program

Three types of pipes, supplied by three different manufacturers, including two groups of X65 electric-resistance welded (ERW) pipes and one group of X80 UOE pipes, were tested in this program. The pipe types and geometries are shown in Table 3-1.

Table 3-1 Pipe groups tested in the program

Pipe Group #	Pipe Designation	Pipe Grade	Pipe Type	Diamater		Wall Thickness		Weld
				(inch)	(mm)	(inch)	(mm)	
1	X65 High Y/T	X65	ERW	12.75	324	0.5	12.7	First Production
								Second Production
2	X65 Low Y/T	X65	ERW	12.75	324	0.5	12.7	One Procedure
3	X80	X80	UOE	24	610	0.5	12.7	One Procedure

The two X65 groups of pipes were designated as high *Y*/*T* and low *Y*/*T* pipes, respectively, where the *Y* and *T* refer to the yield and ultimate tensile strength, respectively.

Girth welds in all three groups of pipes were made with mechanized GMAW processes. The root pass was deposited from the OD side in a 5G position. The hot, fill, and cap passes were deposited in a 1G position, by rolling the pipe while holding the welding head steady, with the intent to produce as uniform as possible weld properties around the circumference.

Two different girth welding procedures were applied to the X65 high *Y*/*T* pipes, resulting in two girth weld strength levels. The two welds are referred to as the first and second production welds, respectively (see Table 3-1). One girth welding procedure was applied to the X65 low *Y*/*T* pipes and another welding procedure was applied to the X80 pipes.

In summary, there are four types of girth welds from three different groups of pipes. Two groups of the pipes are nominally 12-inch X65 pipes and one group of the pipes is nominally 24-inch X80 pipes.

3.2 Small-Scale Tests

The following material characterization tests were conducted:

(1) Weld macro,

(2) Microhardness map (for selected welds),

(3) Pipe tensile properties at room temperature and at -20ºC (for selected pipes),

a. Longitudinal properties,

b. Hoop properties,

(4) All weld metal tensile properties at room temperature and -20C,

(5) Charpy transition curves,

(6) CTOD transition curves with standard deeply-notched SENB specimens, and

(7) J-resistance curves with low-constraint SENT (i.e., SE(T) in ASTM notation) specimens.

The details of the test results are covered in Project 1 report [2].

3.3 Large-Scale Tests

The large-scale experimental program was carried out by C-FER. The entire test program consisted of 34 axial tension tests on specimens fabricated from nominally 12-inch (324-mm) Grade X65 (448 MPa) ERW pipes and 8 axial tension tests on specimens fabricated from nominally 24-inch (610-mm) diameter Grade X80 (551 MPa) UOE DSAW pipes.

In the large scale tests, the specimen fabrications and test conditions were chosen to exercise a number of parameters which are known to have significant impacts on the tensile strain capacity. The parameters included the internal pressure, the strain hardening characteristics of the pipe body and weld materials, the degree of weld strength overmatch, and the size and location of the weld flaws. The majority of the pipe and curved wide plate tests were performed at room temperature to ensure effectively ductile material behavior. Selected tests were performed at a reduced temperature to assess the effects of cold temperature on the strain capacity.

For the 12.75-inch OD X65 pipes, 24 tests were performed on full pipe specimens and 10 tests were performed on curved wide plate panels cut from pipes. All specimens contained circumferentially oriented, surface breaking flaws intended to simulate girth weld flaws in field production welds. The majority of the pipe specimens were tested with high internal pressure; others were tested with very low internal pressure (effectively no pressure) to clearly establish the effects of pressure on strain capacity. The test parameters for the CWP panels were chosen to align with the test parameters for the effectively unpressurized pipe specimens to assess the degree to which the strain capacity of the CWPs agree with the strain capacity obtained from full scale pipe tests.

Testing of the 24-inch OD X80 pipe material was limited to eight tests on CWP panels cut from girth welded pipes. All specimens contained circumferentially oriented, surface breaking flaws intended to simulate weld flaws in a field girth welding environment.

4 General Concept of Tensile Strain Failure

4.1 Physical Process of Tensile Strain Failure

Girth welds may contain planar flaws, which are considered more detrimental to the integrity of welds than volumetric flaws. Tensile ruptures are postulated to start from those planar weld flaws. The tensile failure process of a girth weld under longitudinal straining may be viewed by examining test specimens designed to emulate the failure process. Figure 4-1 shows the residual opening of a flaw taken from a full-scale pipe test [36]. The flaw was artificially introduced to simulate a planar flaw. The same flaw is viewed in Figure 4-2 by cutting the specimen perpendicular to the flaw plane, revealing the weld profile and the flaw opening, and growth in the middle of the weld. An overall profile of flaw surface is shown in Figure 4-3, showing the flaw growth before the termination of the test.

For a ductile girth weld under longitudinal straining, the flaw first starts to open while the crack tip blunts to form a notch with finite radius. After some blunting, a single or multiple sharp flaws would initiate at the tip of the notch, forming a sharp growing flaw. At some point, the flaw may grow through the wall thickness as in the case of a pressurized full-scale test, and the test would be terminated.

Figure 4-1 Residual flaw opening view from the pipe OD surface after a test

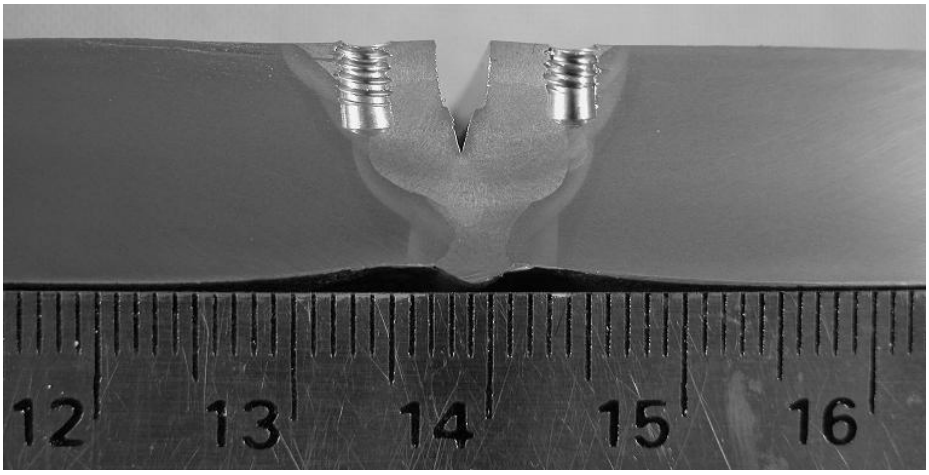

Figure 4-2 Residual flaw opening viewed along a cross-section along the pipe axis

Figure 4-3 A flaw profile showing the initial machined flaw and the stable growth prior to the termination of the test

4.2 Failure Modes under Tensile Strain Loading

By observing large-scale test results of this program and the CWP tests conducted at NIST on the girth welds of 36-inch OD and 0.75-inch WT X100 pipes, the tensile failure modes are generalized and shown in Figure 4-4 and Figure 4-5. The failure modes are currently categorized as a function of normalized flaw size, for illustration purposes. There are many factors which can affect the tensile strain capacity. In the context of Figure 4-4, the other parameters, except flaw size, are held constant. The categorization of the failure modes is intended to facilitate the rationalization of a material's tensile strain response. The boundaries among those modes can overlap and are not absolute.

4.2.1 Category I Failure: Failure in the Pipe Body

When there is a small flaw in an overmatching weld, the crack driving force imparted on the flaw increases upon the initial application of remote straining. The driving force can become saturated as the flaw is effectively protected by the overmatching weld metal. Almost all of the subsequently applied longitudinal displacement acts only to deform the pipe body, leading to the failure in the pipe body. The driving force is never large enough to cause a failure in the flawed plane.

4.2.2 Category II Failure: Flaw Failure with Limited Flaw Growth

When the flaws are shallow and long or moderately deep and short, there is a dynamic equilibrium between the crack-driving force needed to grow the flaw and the straining of the pipe body. There is limited flaw growth when the applied load approaches the maximum load. Substantial straining can occur in the pipe body before the attainment of the maximum load. This dynamic equilibrium between the straining of flawed plane and the pipe body means that

the eventual failure location is highly dependent on the strain hardening behavior of the materials around the flawed plane and the pipe body. Although the final failure is in the flawed plane, high strain capacity approaching pipe uniform strain can be achieved.

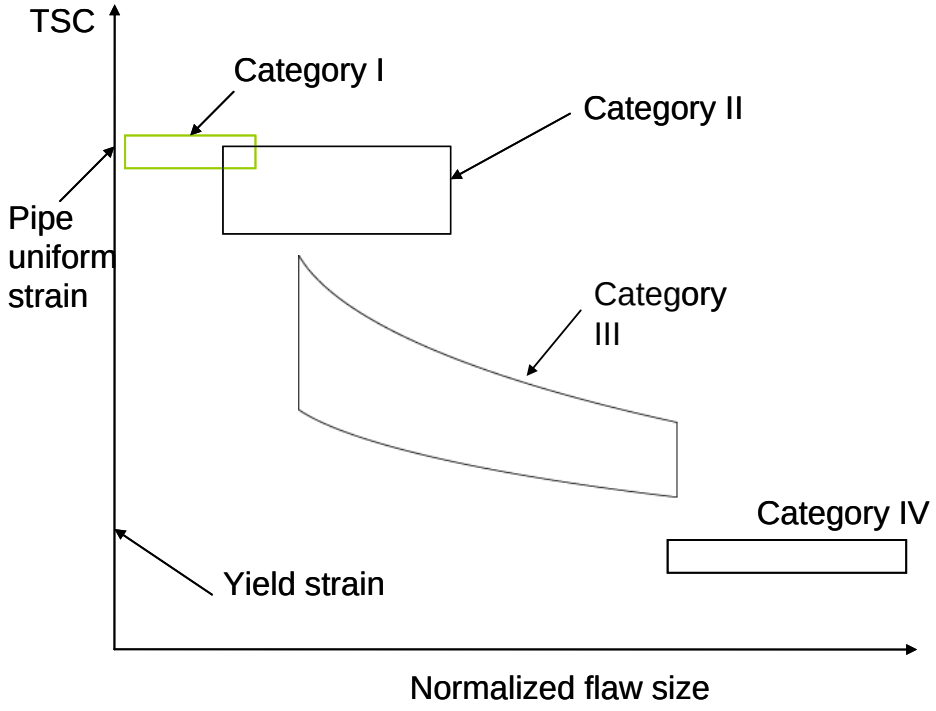

Figure 4-4 Categories of responses to remote longitudinal straining

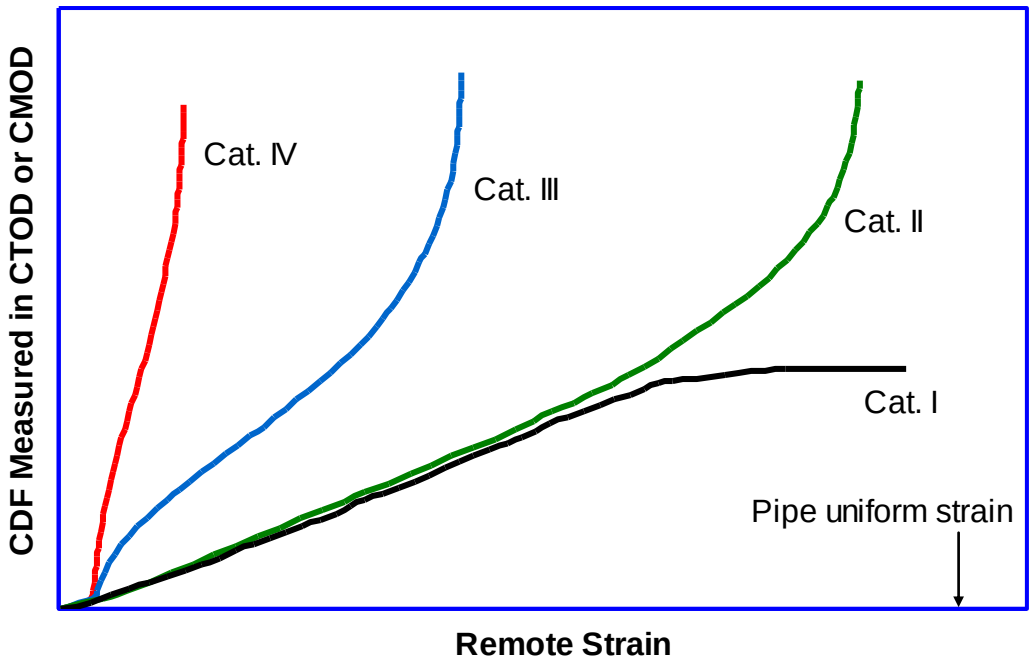

Figure 4-5 Categories of responses expressed in crack driving force (CDF) vs. remote strain relations

4.2.3 Category III Flaw Failure with Finite Flaw Growth

If the increase of the crack-driving force is gradual after gross section yielding of the pipe body, flaw growth occurs gradually with the remote straining. The flaw may fail by (1) local instability, i.e., flaw popping-through the wall, but the overall load capacity of the specimen may still increase, or (2) global instability if the loading of the specimen is load-controlled, i.e., the rapid propagation of the flaw in the circumferential direction. Many large-scale tests are performed in displacement-controlled mode and the tests are stopped when the overall maximum load is reached. In displacement-controlled mode, the attainment of maximum load does not necessarily lead to instantaneous overall instability.

4.2.4 Category IV Flaw Failure in Elastic Strain Range

If the flaw is large, or there is a gross weld strength undermatching, or there is a large magnitude of high-low misalignment, or the combination of those conditions, the growth of the crack-driving force may be unbounded. The remotely applied displacement is almost entirely taken up by the flawed plane. The failure strain under this scenario is near or less than the yield strain.

4.3 Examples of Tensile Strain Behavior

An example of Category II behavior is shown in Figure 4-6. This full-scale specimen had four nominally identical initial flaws, 3 mm × 35 mm located in the heat-affected zone (HAZ). The two curves in Figure 4-6 represent upper and lower bound CMOD responses as a function of the averaged remote strain measured at the pipe body. The final failure strain, as evident from the upper bound CMOD response, is approximately 9%, which is very close to the pipe uniform strain. This indicates that high failure strains are possible even when the final failure is in the flawed plane.

An example of Category III behavior is shown in Figure 4-7. The specimen setup is the same as that of Figure 4-6, i.e., four nominally identical initial flaws of 3 mm × 50 mm located in the heat-affected zone (HAZ). There is considerable difference between the upper and lower bound behavior after approximately 1% strain. For instance, at CMOD = 2 mm, the remote strain corresponding to the upper-bound flaw is at 1.2%, while the remote strain corresponding to the lower-bound flaw is at 2.0%. At a remote strain of 2.6% (CMOD = 4 mm), the growth of CMOD of the upper-bound flaw starts to accelerate, indicating accelerated flaw growth through the pipe wall. At the same strain level, the CMOD of the lower-bound flaw is much less, at approximately 2.3 mm. For the overall specimen, the failure strain around 2.7% indicates a Category III behavior.

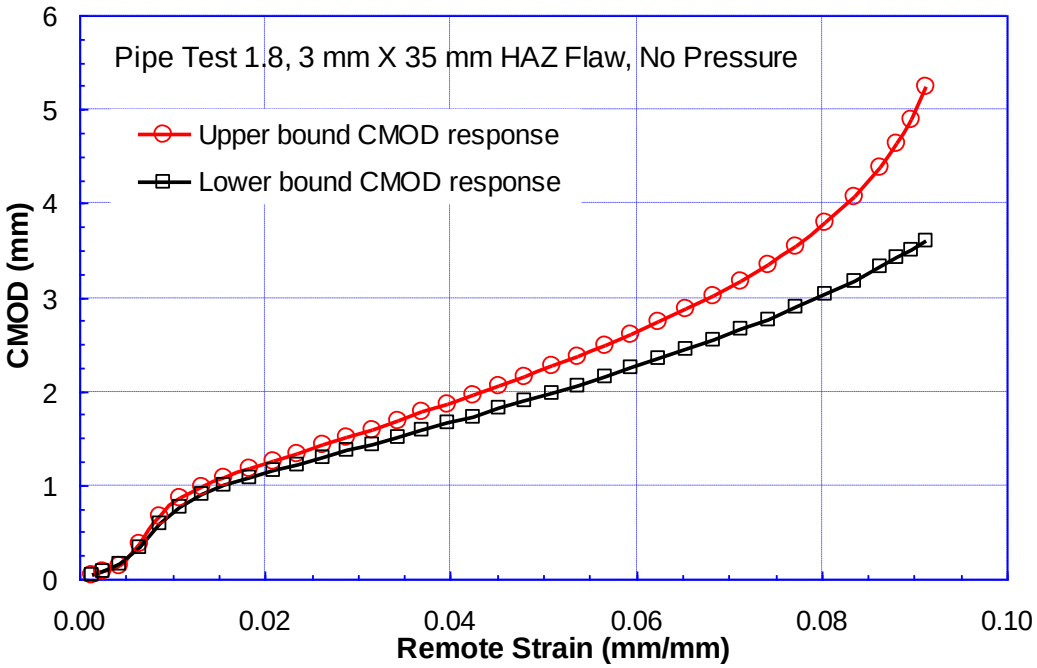

Figure 4-6 Example of Category II behavior from a full-scale pipe test

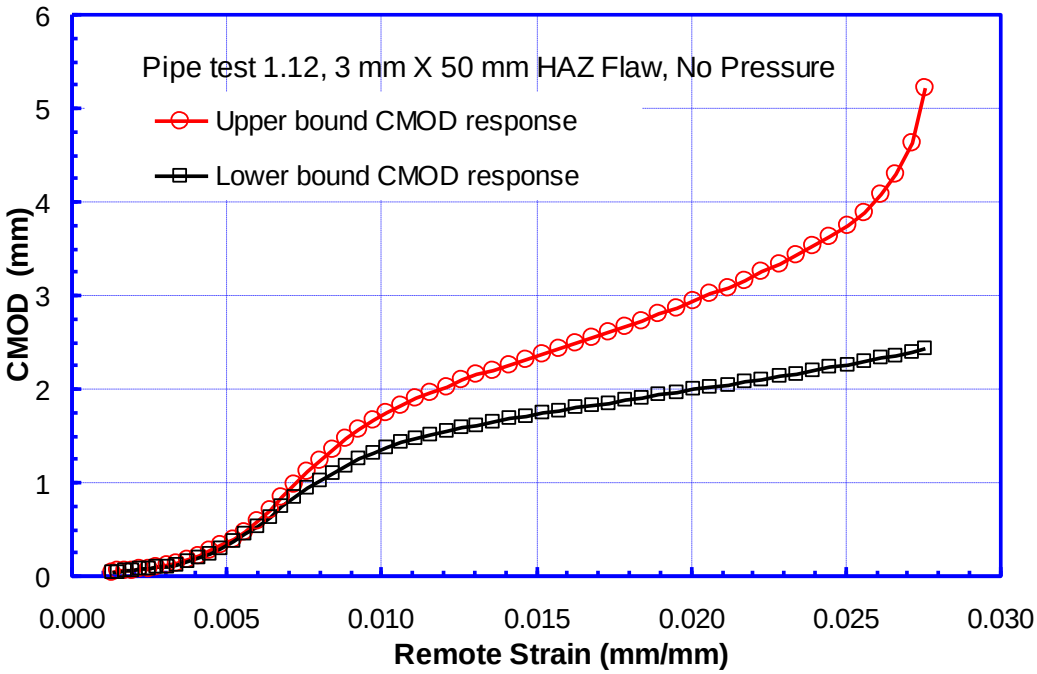

Figure 4-7 Example of Category III behavior from a full-scale pipe test

5 Development of Tensile Strain Models

5.1 Factors Affecting Tensile Strain Capacity

The following factors are known to affect tensile strain capacity:

- Linepipe material
  - Longitudinal tensile property (strength level, strain hardening, and the shape of the stress-strain curve)
  - Transverse (hoop) tensile property (strength level, strain hardening, and the shape of the stress-strain curve)
  - Steel chemical composition
- Girth weld
  - Weld metal tensile property (strength level or mismatch level w.r.t. the base pipe, strain hardening, and the shape of the stress-strain curve)
  - Weld metal toughness
  - Weld bevel geometry
  - High-low misalignment
- Interface between the linepipe and weld
  - HAZ toughness
  - HAZ softening
- Weld flaws
  - Flaw location (weld vs. HAZ)
  - Flaw orientation
  - Flaw size (length and height)
  - Flaw position in thickness direction (for buried flaws)
  - Flaw interaction
- Pipe Geometry
  - Pipe wall thickness
  - Pipe diameter
- Loading
  - Internal pressure
  - Accumulation of plastic strain (low cycle fatigue)
  - Loading rate

The parameters for the current model development were selected using the following criteria:

(1) The parameters are known to have strong impact on TSC,

(2) The parameters are quantifiable with the current technology or technology expected to be available in the foreseeable future.

Some of the parameters, such as flaw size and tensile properties, were treated as continuous variables within certain ranges. Other parameters, such as bevel geometry, were given a few distinctive values.

5.2 Limit States

5.2.1 Tensile Failure and Flaw Growth Process

The physical process of flaw growth and tensile strain failure was briefly described in Section 4.1. For ductile fracture, the flaw growth usually consists of two components: blunting and ductile tearing. As applied stress or strain increases, the flaw first blunts from its initial sharp tip and then the blunted flaw initiates stable ductile tearing. Upon further loading, the ductile tearing will grow in size, forming a growing flaw with a sharp tip. The initial blunted profile remains behind the newly formed sharp flaw. Further stable ductile flaw tearing eventually triggers the onset of unstable flaw growth, i.e., the failure or instability. The evolution of the flaw profile is schematically shown in Figure 5-1.

The limit state corresponding to the onset of stable flaw extension is referred to as initiation-control based limit state. The limit state corresponding to the onset of unstable flaw growth is referred to as ductile-instability based limit state. The initiation-control based limit state is, in general, more conservative than the ductile-instability based limit state, as the initiation control is established at the transition from blunting to ductile tearing. The degree of the conservatism, as measured by the failure strains, is discussed in the next section.

The initiation-control based limit state permits the usage of conventional initiation-based fracture toughness measures, such as upper shelf Charpy impact energy and standard deeply-notched SENB specimens, to obtain single-value toughness.

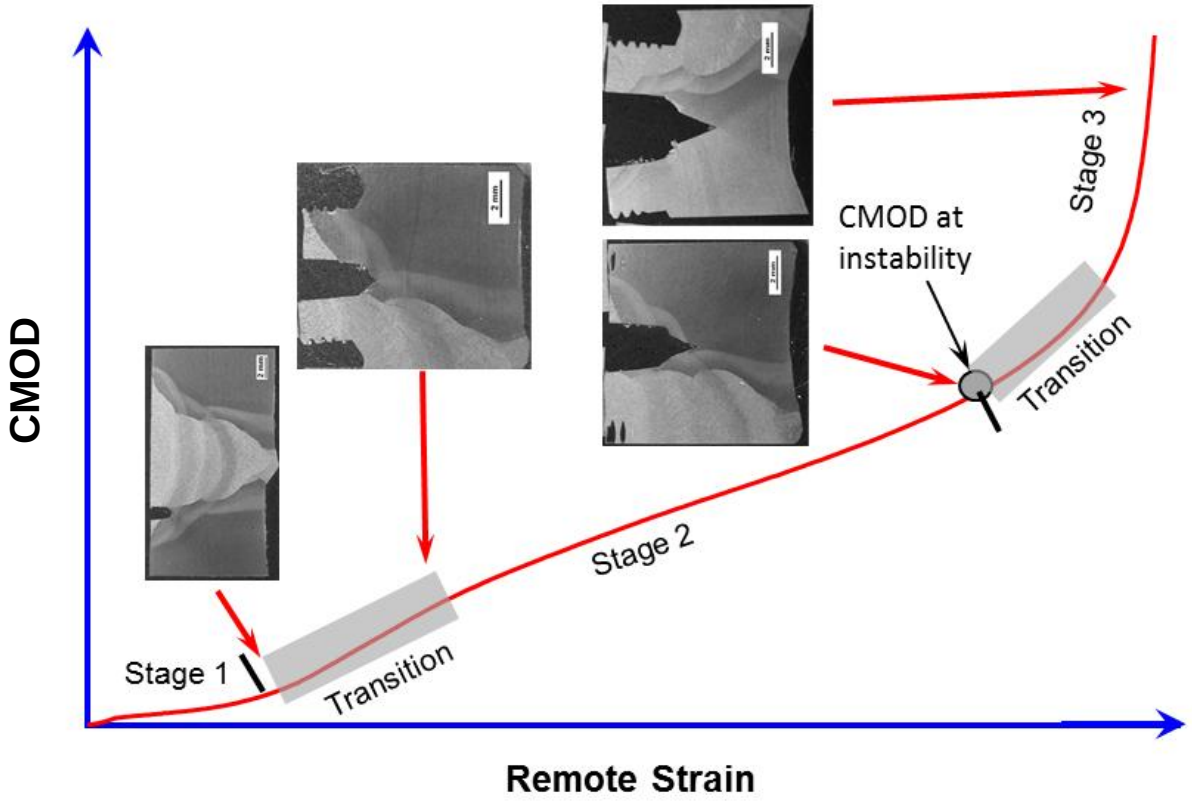

Figure 5-1 Schematic drawing of flaw growth profiles

5.2.2 Role of Stable Flaw Growth on Tensile Strain Failure

The other critical consideration is the timing/sequence of the stable flaw growth relative to the tensile strain value at the failure events. As mentioned in the previous section, the stable flaw growth includes both flaw blunting and stable ductile tearing. The strain vs. flaw growth history of full-scale tests by JFE is shown in Figure 5-2. It is evident that the strain at 0.5 mm flaw growth is very close to the strain of leakage. The flaw growth at the point of leakage is much greater than 0.5 mm. However, most of growth occurs near the final leakage point accompanied by a small increase of remote strain.

The CTOD vs. strain history from Østby is shown in Figure 5-3. The amount of flaw growth is about 0.65 mm at the point when the CTOD and strain relation turns nearly vertical, indicating a small increment of strain with the increase of CTOD. In addition, the inserted crack profile indicates that most of the flaw growth was actually from blunting at that moment and the stable tearing was just initiated.

The flaw growth history vs. strain by Minnaar, et al, is shown in Figure 5-4. Similar to the above observations, it is seen that at a flaw growth of 0.5-0.6 mm, the strains are very close to the final failure strains.

5.3 Framework of Tensile Strain Models

The framework of the tensile strain models was built upon two major components: crack driving force relations and limit states (i.e., definition of failure). The two limit states, initiation-control based and ductile-instability based limit states, were both incorporated in the tensile strain models.

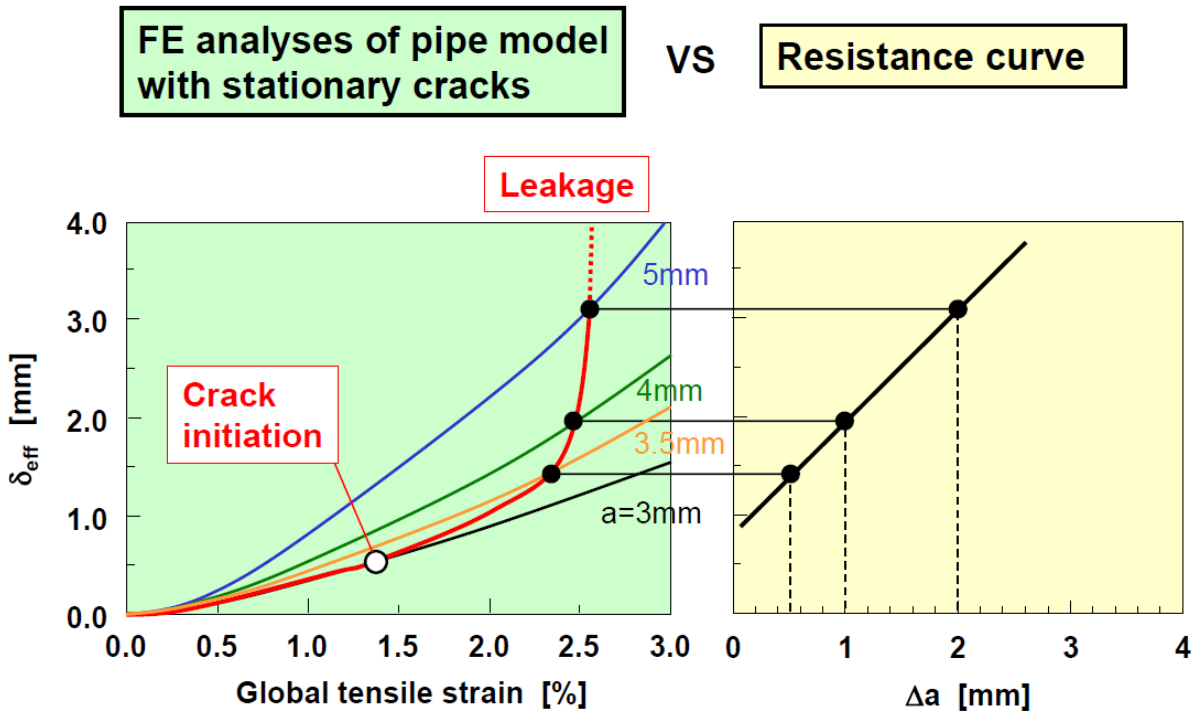

Figure 5-2 Flaw growth vs. strain history from full-scale pipe tests [37]

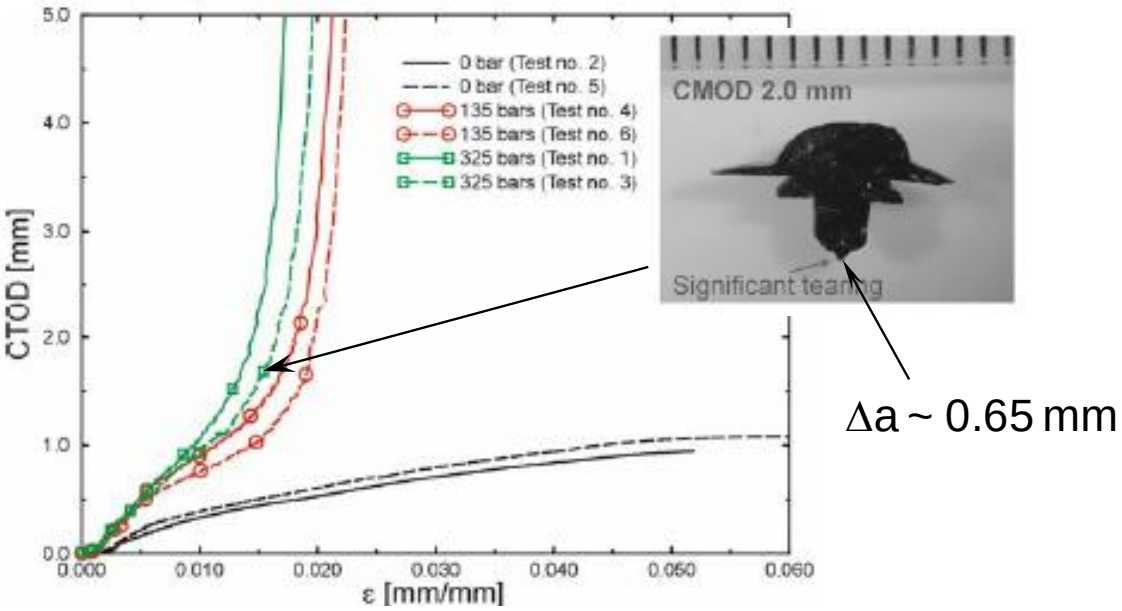

Figure 5-3 Crack opening profile vs. CTOD-strain history from full-scale pipe tests [30]

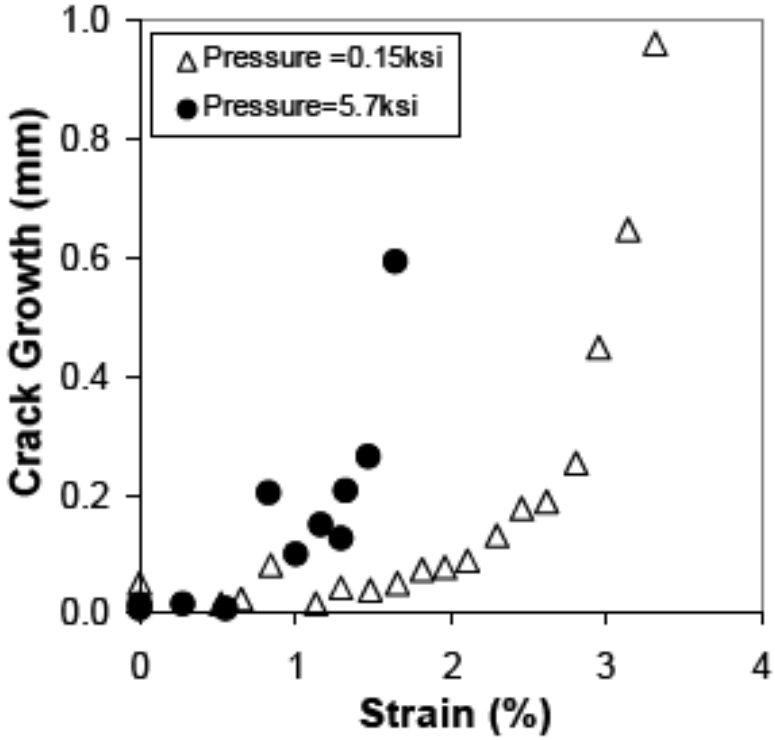

Figure 5-4 Crack growth vs. strain history from full-scale pipe tests [19]

5.3.1 Crack Driving Force Relations

The crack-driving force relations were developed independent of the limit states. The crack driving force, $CTOD_F$, is expressed as a function of remotely applied strain for any given geometry (including flaw size) and material parameters, as shown in Figure 5-5. The details on the development of $CTOD_F$ can be found in Section 6.

5.3.2 Limit State Based on Initiation Control

The initiation-based tensile limit state is defined as $CTOD_F = CTOD_A$, where $CTOD_F$ is the crack-driving force and $CTOD_A$ (or δ_A) is the apparent toughness. The apparent toughness is the toughness corresponding to the onset of stable tearing. The significance and the determination of the apparent toughness are explained in detail in Section 8.

Both $CTOD_F$ and $CTOD_A$ are represented by the crack tip opening displacement, i.e., CTOD. The initiation-based limit state is schematically illustrated in Figure 5-5.

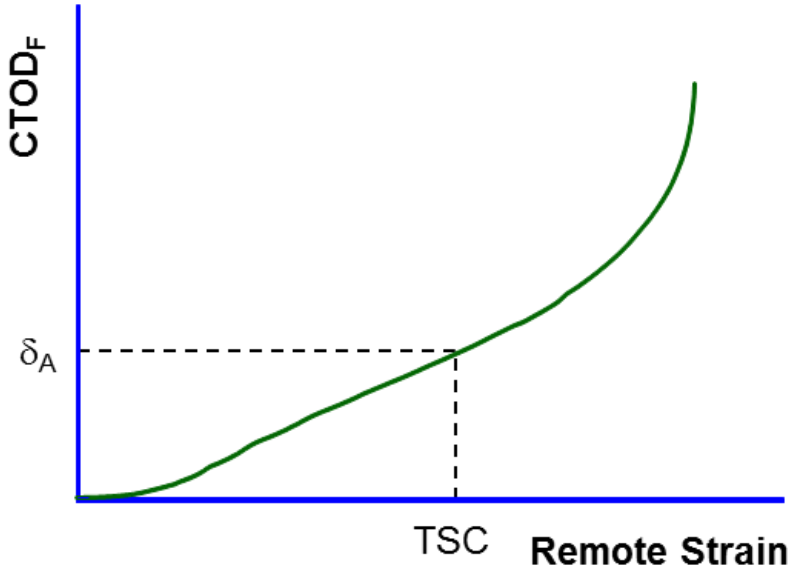

Figure 5-5 Typical $CTOD_F$ and definition of initiation-control based limit state

5.3.3 Limit Stated Based on Ductile Instability

The ductile-instability based limit state is illustrated in Figure 5-6. The fracture toughness is expressed as a function of flaw growth, as shown in Figure 5-6, which is usually termed as tearing resistance curve (i.e., $CTOD_R$). The limit state is defined as the tangent point of the crack driving force curve and the fracture toughness curve as shown in Figure 5-6.

The crack driving force relations discussed in Section 5.3.1 were re-organized to implement the limit state. For any given flaw size, the crack driving forces ($CTOD_F$) were presented as a group of curves (i.e., iso-strain $CTOD_F$ curves) of different strain levels. Each iso-strain $CTOD_F$ curve is expressed as a function of flaw growth (see Figure 5-6). The difference between the iso-strain $CTOD_F$ curves and the $CTOD_F$ curves in Section 5.3.1 is the format of presentation. The two types of crack driving force curves share the same dependence on the input parameters and were developed in the same way. They have one-to-one correlations (see Figure 5-7).

5.4 Process of Model Development

The development of the crack driving force includes the following steps:

1. Determine the representation of pipe and weld tensile properties,
2. Determine the key input parameters,
3. Construct finite element models,

4. Develop finite element analysis matrix,
5. Post-process FEA results and construct TSC database,
6. Develop TSC parametric equations from the database, and
7. Compare the results of TSC equations with TSC database.

The development of the crack-driving force relations is given in Section 6.

The resistance curve and apparent toughness may be determined from a number of experimental test methods. The full process is detailed in Section 8.

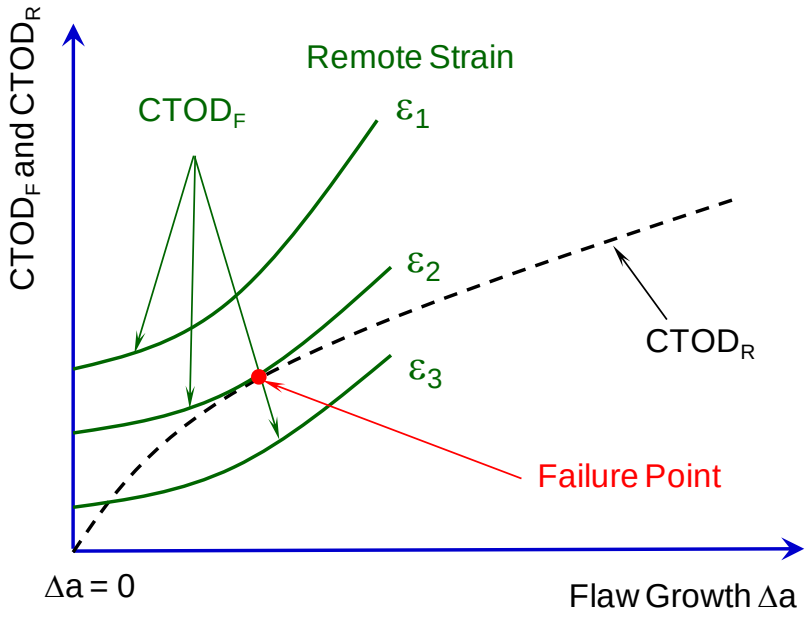

Figure 5-6 Definition of ductile-instability based limit state

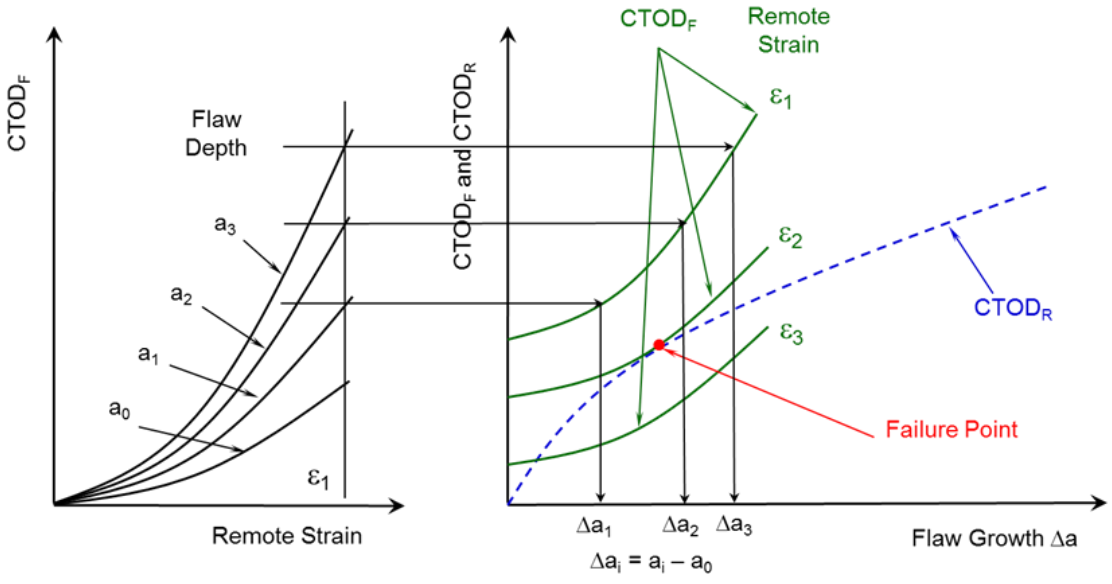

Figure 5-7 Schematic drawing of iso-strain CTOD$_F$ curve creation

6 Development of Driving Force Relations

6.1 Mathematical Representation of Pipe and Weld Tensile Properties

6.1.1 Background

The complete representation of a material's tensile property is its full stress-strain curve. In engineering code implementations, however, it can be difficult to use a full stress-strain curve as an input parameter. The stress-strain curve is often simplified and represented by three key material parameters: yield strength (YS), ultimate tensile strength (UTS), and uniform strain (uEL). For example, in some stress-based ECA codes, the YS and flow stress (average of YS and UTS) are often used as the input parameters for characterizing material properties.

The crack driving forces used in the strain-based TSC models are known to be more dependent on the materials' strain hardening properties than on the strength properties. In most of the current TSC models, the material properties are often represented by Y/T ratio and sometimes uEL as well. Although full stress-strain curves were indeed used in those TSC model developments, the exact shape of those stress-strain curves was usually not the focus and has not been thoroughly investigated. It should be noted that the three parameters, YS, UTS (or Y/T), and uEL, cannot completely determine a stress-strain curve. For example, three stress-strain curves are shown in Figure 6-1, they all have the same YS, UTS, and uEL, but the actual shapes of the curves are different. It has been found that the crack driving force can be affected by the shape of the stress-strain curves. In general, the higher the pipe stress-strain curves are, the higher the crack driving forces are, if all the other conditions, such as weld stress-strain curves, flaw sizes and locations, and pipe wall thickness etc., are kept the same.

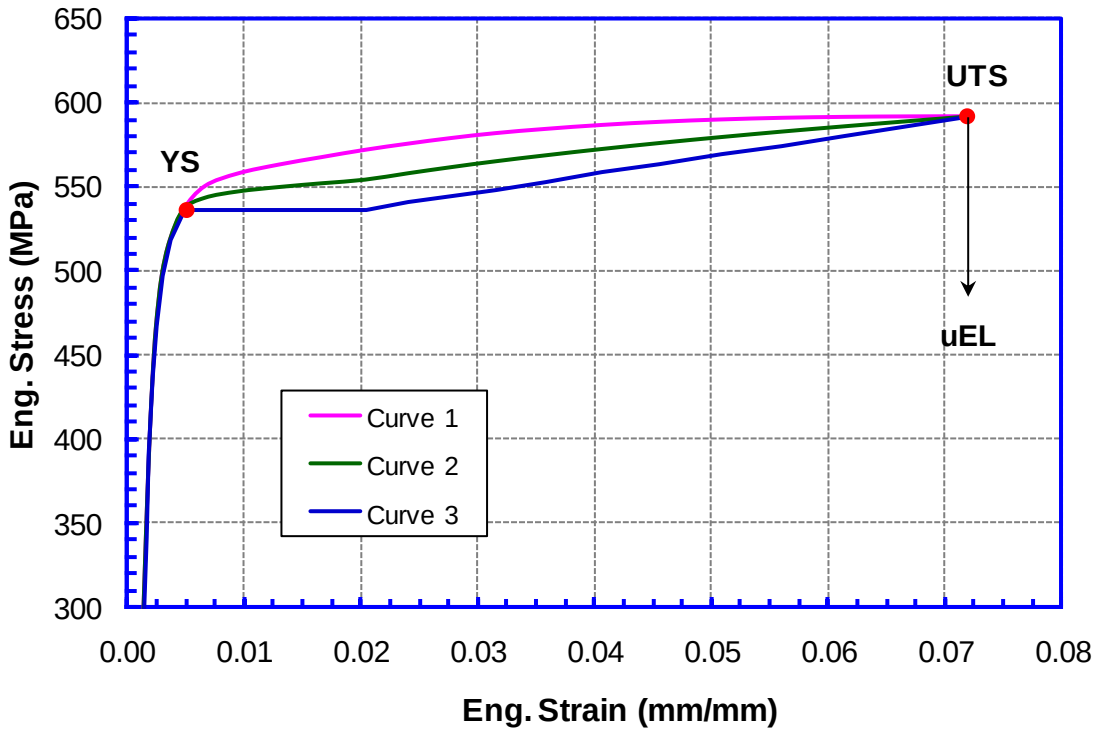

Figure 6-1 Stress-strain curves of same YS, UTS, and uEL

For strain-based TSC models, the shape of the stress-strain curves is important to the crack driving force prediction. Therefore, the mathematical equations used to represent the stress-strain curves need to be designed to capture the actual shape of the curves in real materials. The mathematical equations should be able to (1) uniquely determine a full stress-strain curve using the three material parameters, i.e., YS, UTS (or Y/T), and uEL; and (2) statistically give a reasonable representation of the stress-strain curves of actual pipe and weld materials.

6.1.2 Ramberg-Osgood vs. CSA Stress-Strain Curve Equations

Two widely used stress-strain curve equations, i.e., the Ramberg-Osgood (RO) equation and the CSA Z662 equation are examined in this section. Both equations create smooth stress-strain curves (i.e., the round-house shape). The discontinuities in the stress-strain curve, such as the Lüder's strain, are not created. The Lüder's strain of the pipe material is highly detrimental to the compressive strain capacity of the pipeline and therefore is usually prohibited in strain-based design. The Lüder's strain, on the other hand, may increase the tensile strain capacity due to the lower crack driving forces it generated, as discussed in the previous section. Therefore, the omission of the Lüder's strain in pipe stress-strain curve is deemed to be acceptable to the TSC model development.

The RO equation shows the relationship between the true stress (σ_T) and true strain (ε_T) as in the following,

$$\varepsilon_T = \frac{\sigma_T}{E} + 0.002\left(\frac{\sigma_T}{\sigma_0}\right)^m , \tag{6.1}$$

where E and σ_0 are the Yong's modulus and reference stress, respectively. The m is the strain hardening exponent of the RO equation. By definition, the reference stress σ_0 is the true stress corresponding to a plastic strain of 0.2% and therefore is usually very close to the YS at 0.5% strain. The engineering stress-strain curve calculated from the RO equation usually consists of a natural peak, i.e., UTS and uEL. By calibrating σ_0 and n, the RO equation can generate a stress-strain curve for given YS and UTS. The uEL, however, is an outcome of the equation and cannot be independently varied.

In Figure 6-2, the relationship between the uEL and Y/T ratio is shown for some real pipe materials with YS in the 56-ksi and 70-ksi range. The experimental data show that the uEL can be affected by both YS and Y/T. In general, the uEL decreases as the Y/T and YS increase. For comparison, the uEL from the stress-strain curves generated by the RO equations are also included where the RO equations cover a large range of YS and Y/T ratio. It is shown that the uEL created by the RO equation is almost independent of the YS and only depends on the Y/T. Most importantly, the uEL calculated from a RO equation can be significantly lower than the actual uEL from an experimentally measured stress-strain curve of the same YS and UTS (or Y/T). It is especially true for low YS pipe materials.

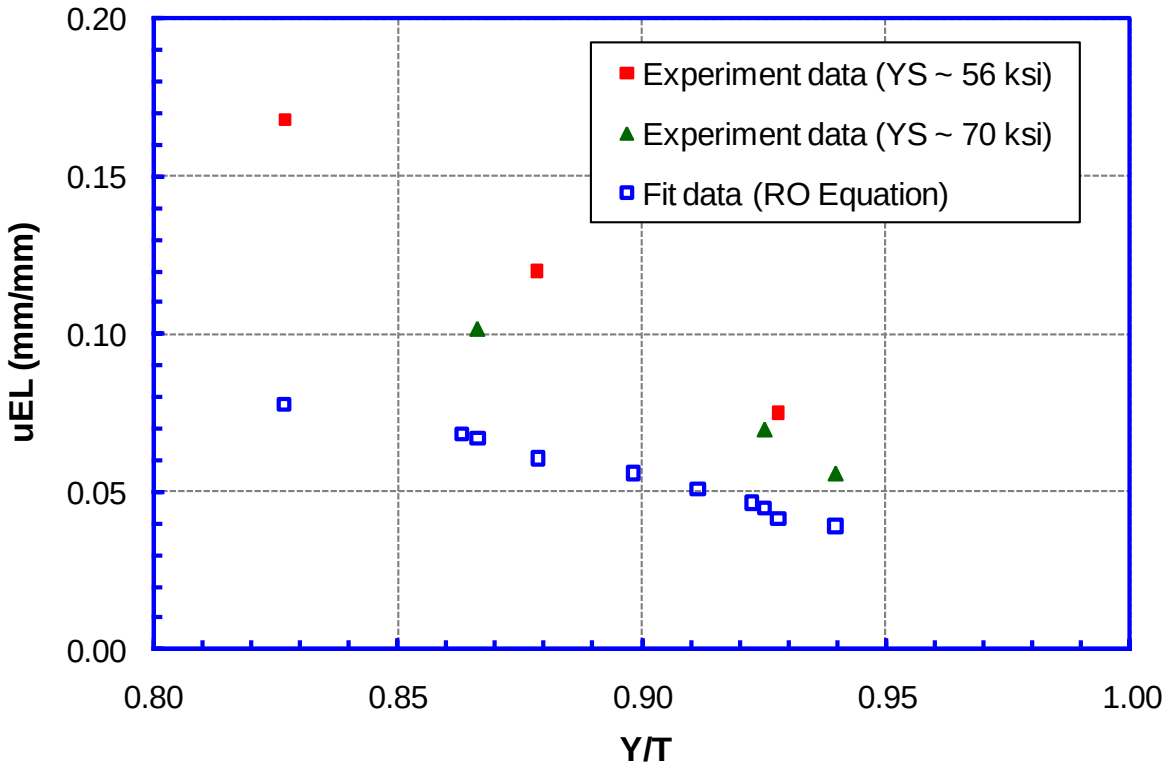

Figure 6-2 Correlation between uEL and Y/T (experiment vs. RO equation)

In contrast to the RO equation, the equation given in CSA Z662 defines the relationship between the engineering stress (σ) and engineering strain (ε) as in the following:

$$\varepsilon = \frac{\sigma}{E} + \left(0.005 - \frac{\sigma_y}{E}\right)\left(\frac{\sigma}{\sigma_y}\right)^n , \tag{6.2}$$

where σ_y is the YS at 0.5% strain and n is the strain hardening exponent of the CSA equation. For any given set of YS, UTS, and uEL, a unique n can be determined by Eq. (6.3). Therefore, the CSA equation can uniquely determine a full stress-strain curve which satisfies the YS, UTS (or Y/T), and uEL exactly.

$$n = \ln\left(\frac{\text{uEL} - \text{UTS}/E}{0.005 - \text{YS}/E}\right) / \ln\left(\frac{1}{\text{Y/T}}\right) \tag{6.3}$$

Based on the above observations, the CSA Z662 equation is selected to represent and generate the full stress-strain curves for the crack driving force development in this project.

6.1.3 Representation of Pipe Stress-Strain Curves

A representative pipe stress-strain curve is shown in Figure 6-3. The curve is of round-house shape but becomes very flat near the UTS. The flat part near the UTS is typical for modern linepipe steels which can raise some challenges in stress-strain curve representations, especially for determining the uEL. For example, the uEL of the same curve can be measured quite differently due to slightly different interpretations (or processing) of the experiment data. In

addition, a trivial difference in the slope of the flat part of the curve, may not affect the crack driving force calculation, but can result in a significant difference in the uEL.

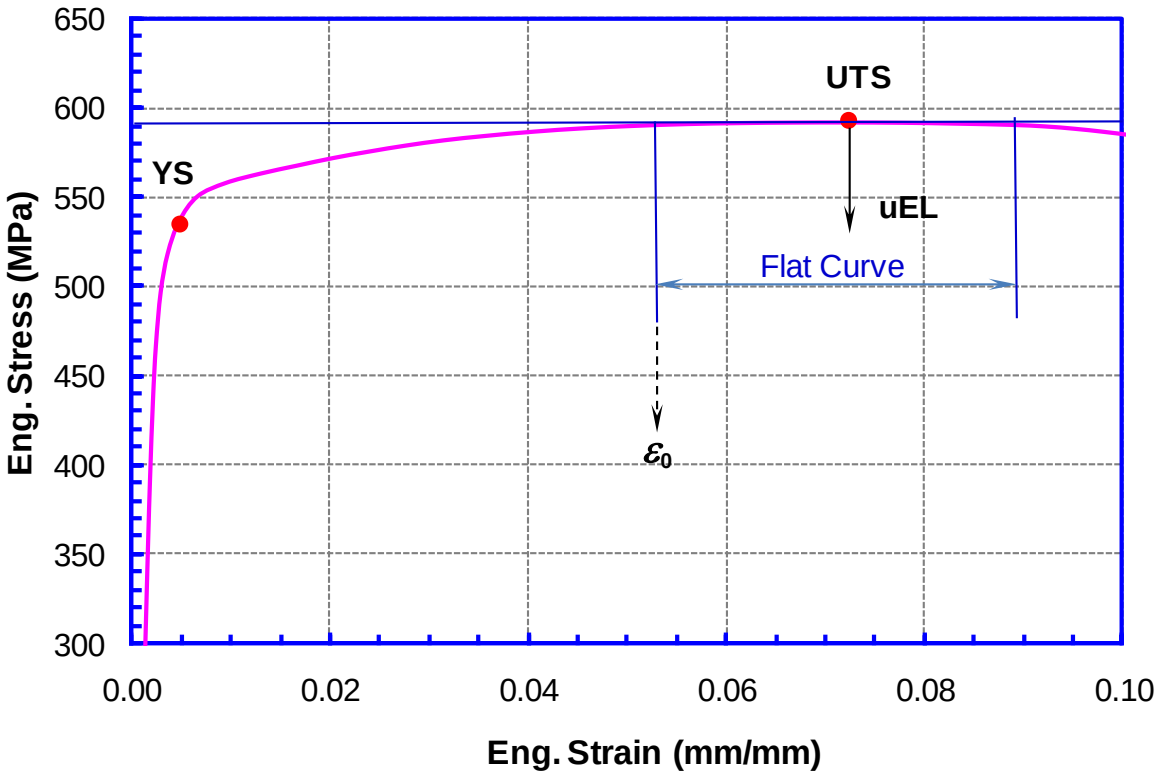

Figure 6-3 Sample pipe stress-strain curves

To better understand the linepipe properties (especially the uEL), the material parameters were analyzed using a collected material database. The database contains 76 pipe longitudinal stress-strain curves. The range of the material properties in the database is summarized in Table 6-1. The YS (in longitudinal direction) ranges from 56 ksi to 114 ksi, and therefore roughly covers pipe grades from X65 to X100. The uEL varies from 5% to 17%. The key material parameters, such as the YS, UTS, and uEL, were directly measured from the stress-strain curves and used to calculate the Y/T and the strain hardening exponent *n* of the CSA equation. The relationship between the strain hardening exponent *n* and the Y/T ratio was shown in Figure 6-4, where a clear correlation can be observed. A fitting equation for the correlation was developed and given in the following:

$$n = \frac{3.14}{1 - \mathrm{Y/T}}. \tag{6.4}$$

The correlation observed in Figure 6-4 indicates that the linepipe properties, i.e., YS, UTS (or Y/T), and uEL are interrelated to a certain degree. The uEL of the material can be dismissed as an independent material parameter. Instead, in an average sense, the uEL can be estimated from the YS and UTS with satisfactory accuracy.

Table 6-1 Summary of the material database (pipe)

	YS-0.5%	UTS	uEL	YT	*n* (CSA)
	ksi	ksi	mm/mm		
Minimum	56	68	0.05	0.74	11.9
Maximum	114	125	0.17	0.95	75.3
Median	84	100	0.07	0.88	29.8

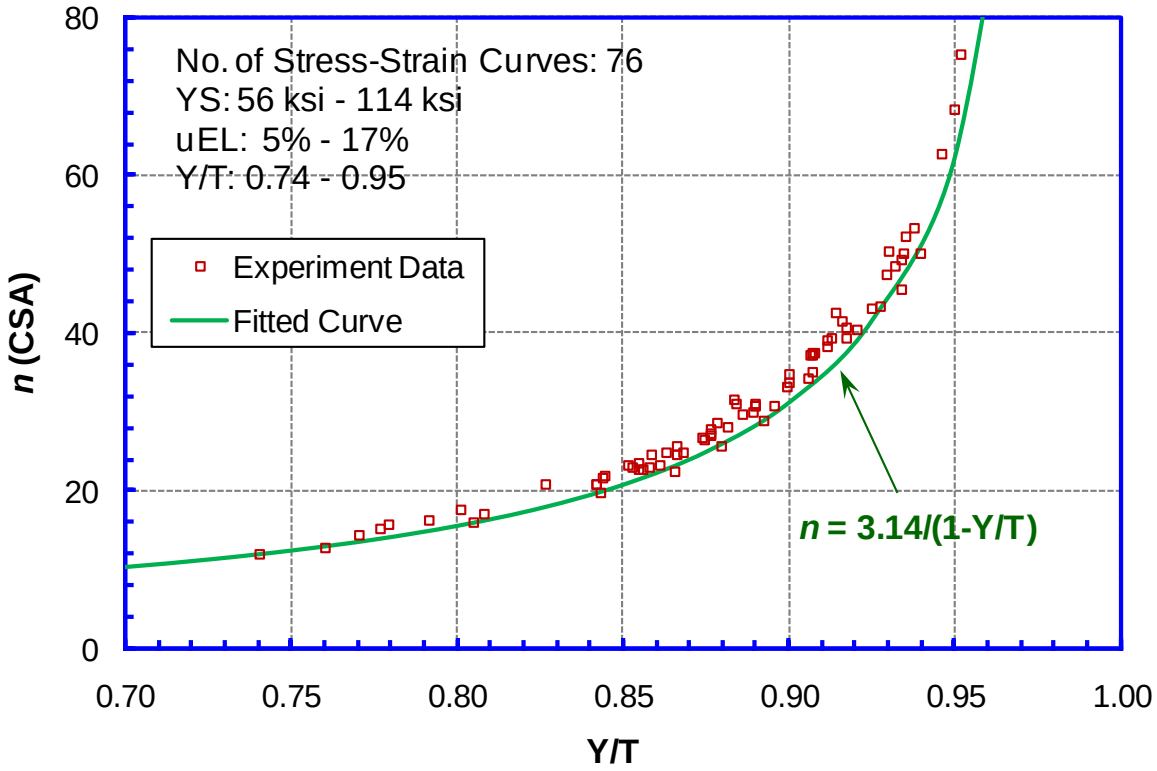

Figure 6-4 Correlation between strain hardening exponent and Y/T (pipe)

The flat part of the stress-strain curve also makes the representation of the curve with a single mathematical equation difficult. To obtain a better representation of the stress-strain curves, the curve is divided into two parts and represented by two different equations, respectively. As shown in Figure 6-3, the first part of the curve ($\varepsilon \le \varepsilon_0$) can be represented by the CSA equation, i.e., Eq. (6.2), and the second part of the curve ($\varepsilon_0 \le \varepsilon \le$ uEL) can be simply represented as a horizontal line (i.e., constant stress of UTS). The ε_0 is the strain calculated from Eqs. (6.2) and (6.4) when $\sigma =$ UTS, i.e.,

$$\varepsilon_0 = \frac{\text{UTS}}{E} + \left(0.005 - \frac{\text{YS}}{E}\right)\left(\frac{1}{\text{Y/T}}\right)^n \quad \text{and} \quad n = \frac{3.14}{1 - \text{Y/T}}. \tag{6.5}$$

The uEL is the strain at the end of the curve, which is calculated from the following equation:

$$\text{uEL} = 1.25\varepsilon_0 \tag{6.6}$$

The uEL was calculated using Eqs. (6.5) and (6.6) for all the stress-strain curves given in the material database and is compared with the original values. As shown in Figure 6-5, on average, the calculated uEL matches the original values fairly well.

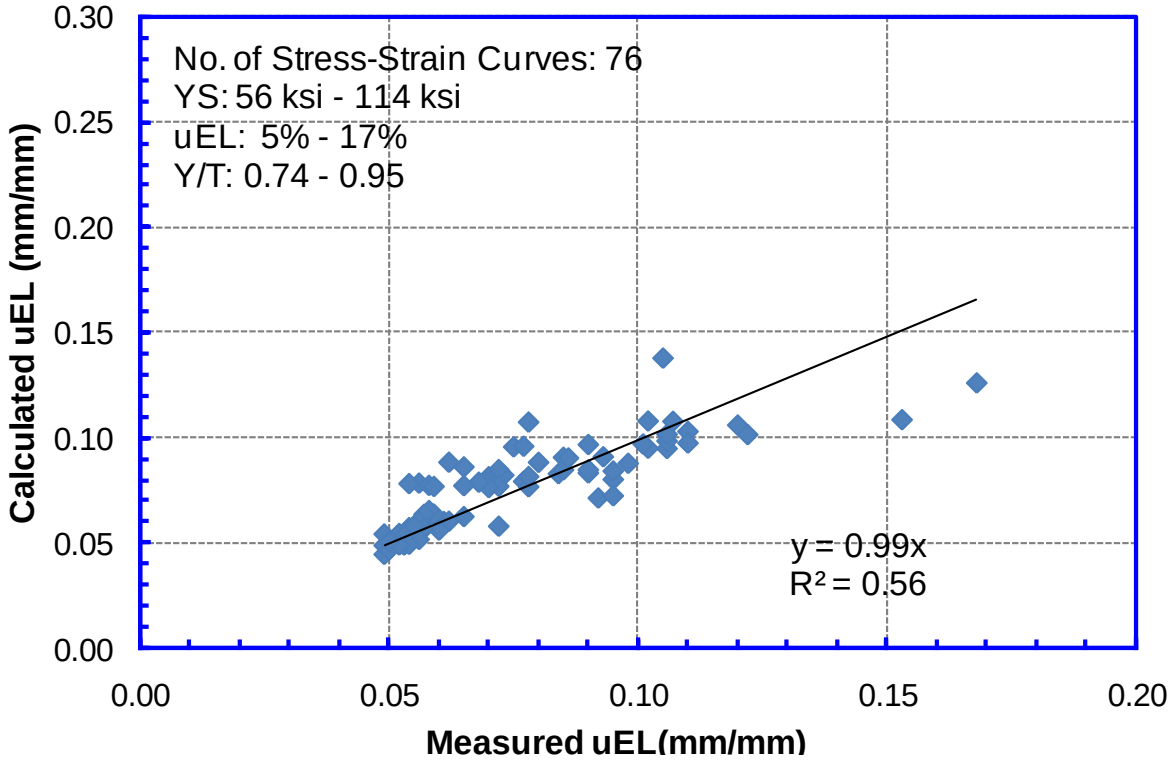

Figure 6-5 Calculated uEL v.s. measured uEL

In summary, the following steps are recommended to create a full pipe stress-strain curve for given YS and UTS:

(1) Determine YS and UTS,

(2) Calculate Y/T using YS and UTS,

(3) Calculate n using Eq. (6.4),

(4) Calculate ε_0 using Eqs. (6.5),

(5) Calculate uEL using Eq. (6.6),

(6) Construct the 1st part of the stress-strain curve using Eq. (6.2) for strains up to ε_0,

(7) Construct the 2nd part of the stress-strain curve by extending a horizontal line of constant stress from ε_0 to uEL.

6.1.4 Representation of the Weld Metal Stress-Strain Curves

Two sample weld stress-strain curves are shown in Figure 6-6, one for X65 pipe and the other for X100 pipe. Different from the round-house type of pipe stress-strain curves, the weld metal curves usually show a discontinuous yielding point, and before reaching the yielding point, the curves are almost a straight line.

In addition, it has been frequently observed that the weld stress-strain curves sometimes contain a Lüder's strain as high as 2%, but sometimes do not. The most recent data suggest that

the existence of the Lüder's strain is closely related to specimen locations. The Lüder's strain usually exists in specimens extracted near pipe ID, while OD specimens usually do not show the Lüder's strain. This difference is believed to be caused by the different thermal histories experienced by the ID and OD weld materials. When the full thickness specimens are tested, the weld stress-strain curves usually do not show an obvious Lüder's strain. Therefore, it was decided to include a 1% Lüder's strain in the weld stress-strain curve equations.

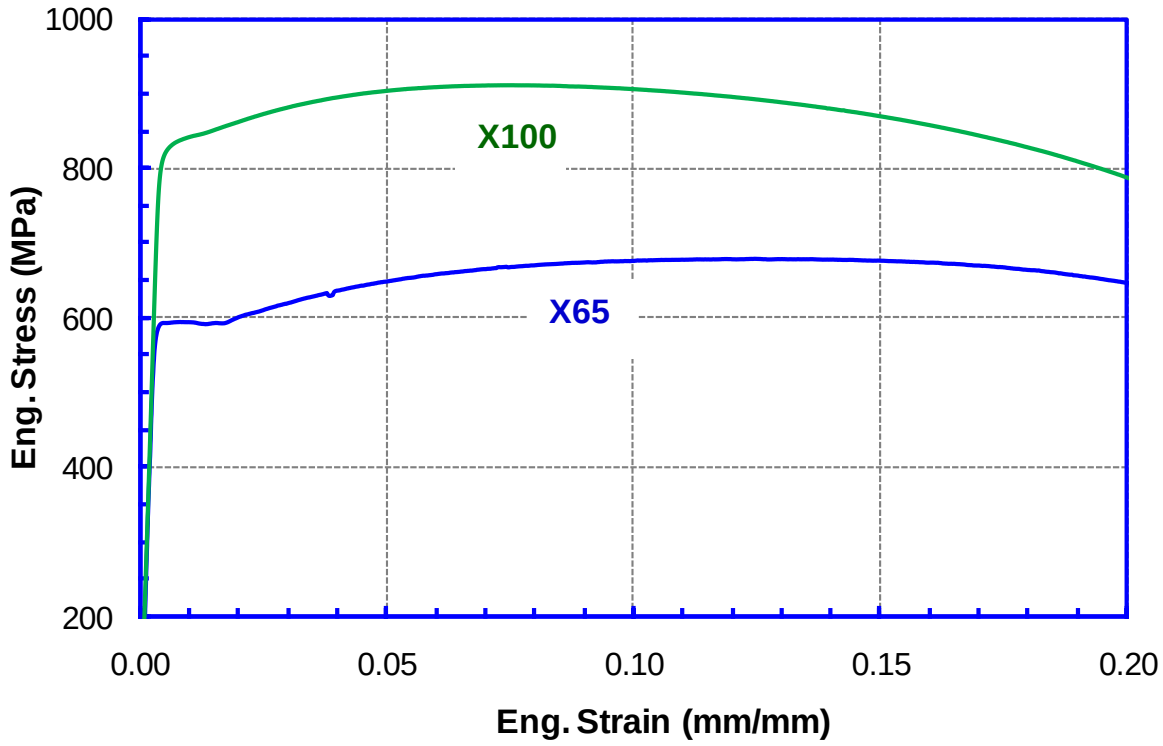

Figure 6-6 Sample weld metal stress-strain curves

Based on the above observations, it was decided to divide the weld stress-strain curve into three sections. The first section is represented as a straight line of slope E (the Young's modulus). The second section represents the Lüder's extension, which is of constant stress on σ_y (the YS). The third section characterizes the strain hardening of the curve and is in the form of a modified CSA equation. The equations are shown in the following:

$$\begin{aligned} \varepsilon &= \frac{\sigma}{E} && \text{if } \varepsilon \le \sigma_y / E \\ \sigma &= \sigma_y && \text{if } \sigma_y / E < \varepsilon \le 1\% \\ \varepsilon &= \frac{\sigma}{E} + \left(0.005 - \frac{\sigma_y}{E}\right)\left(\frac{\sigma}{\sigma_y}\right)^n + 0.005 && \text{if } 1\% < \varepsilon \le \text{uEL} \end{aligned} \tag{6.7}$$

A material database of weld stress-strain curves was also collected. The database contains approximately 64 weld stress-strain curves with YS ranging from 66 ksi to 132 ksi. The range of the material properties is summarized in Table 6-2. Specimens, of different types and extracted

at different locations, are not distinguished in the database. By examining the database, a similar correlation equation for the strain hardening exponent *n* and Y/T ratio was found for weld metal stress-strain curves. As shown in Figure 6-7, the correlation equation is given as:

$$n = \frac{2.58}{(1 - \mathrm{Y/T})^{1.17}} . \tag{6.8}$$

With the correlation equation (in Figure 6.8), the uEL of the weld materials can be determined from the YS and the UTS, and is not an independent parameter.

To further reduce the number of independent parameters for generating a weld stress-strain curve, a correlation equation for the YS and UTS of the weld was established based on the weld material database. As shown in Figure 6-8, the correlation equation is given as:

$$\mathrm{YS} = \mathrm{UTS} - 13.2, \tag{6.9}$$

where the unit of YS and UTS is ksi. Using Eqs. (6.7), (6.8), and (6.9), a unique weld metal stress-strain curve can be generated for a given UTS.

Table 6-2 Summary of the material database (weld)

	YS	UTS	uEL	YT	*n* (CSA)
	ksi	ksi	mm/mm		
Minimum	66	82	0.04	0.81	15.9
Maximum	132	138	0.13	0.96	96.9
Median	112	127	0.08	0.89	34.2

In summary, the following steps are recommended to create a full weld stress-strain curve for given UTS:

(1) Determine UTS,

(2) Calculate YS using Eq. (6.9),

(3) Calculate Y/T using YS and UTS,

(4) Calculate *n* using Eq. (6.8),

(5) Construct the stress-strain curve using Eq. (6.7).

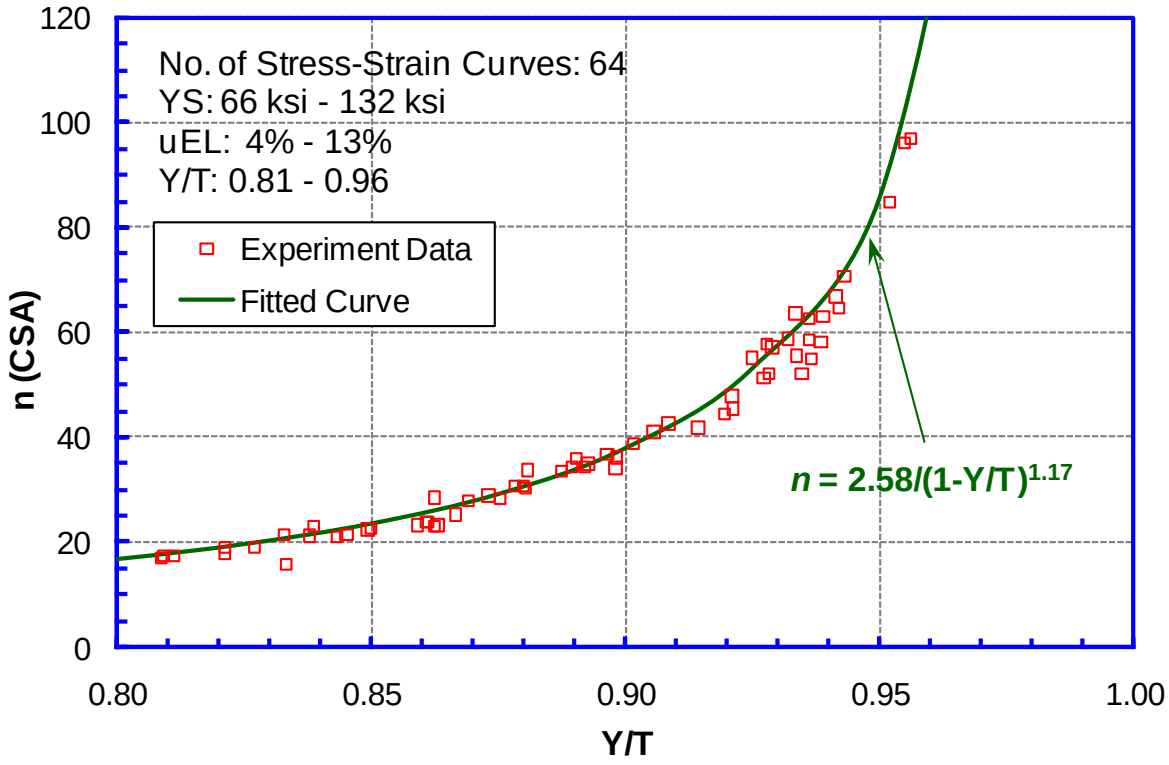

Figure 6-7 Correlation between strain hardening exponent and Y/T (weld)

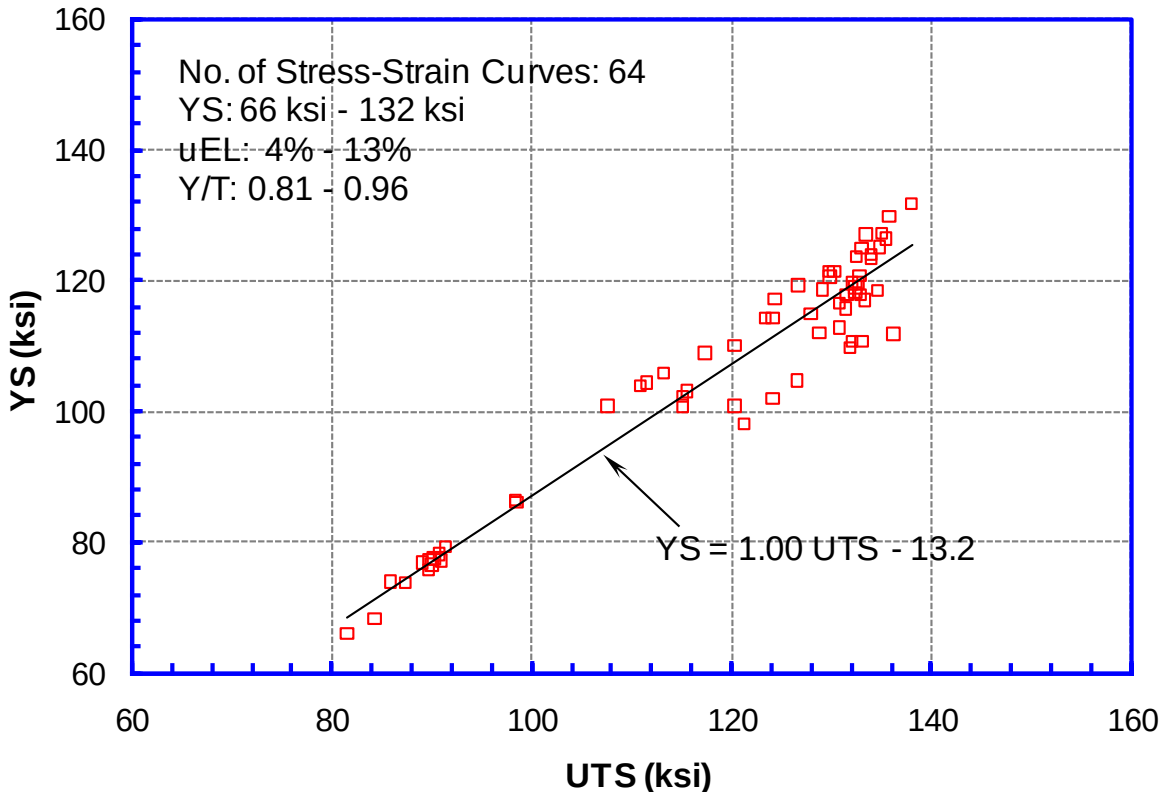

Figure 6-8 Correlation between YS and UTS (weld)

6.2 Finite Element Models and Analysis Procedures

6.2.1 FE Models

The commercial finite element software ABAQUS® was used to conduct the crack driving force calculations. A typical finite element model is shown in Figure 6-9, where due to symmetry boundary conditions in the circumference direction, only half of the pipe was modeled. The overall length of the model is kept as 6 times that of the pipe OD to eliminate the end effect on crack opening and to obtain a finite uniform strain zone. Eight node brick (three-dimensional solid linear) elements with hybrid interpolation functions were used where the non-linear geometric (large-deformation) effect was enabled. The selected element type is proved to be effective on large plasticity analysis, especially associated with cracks.

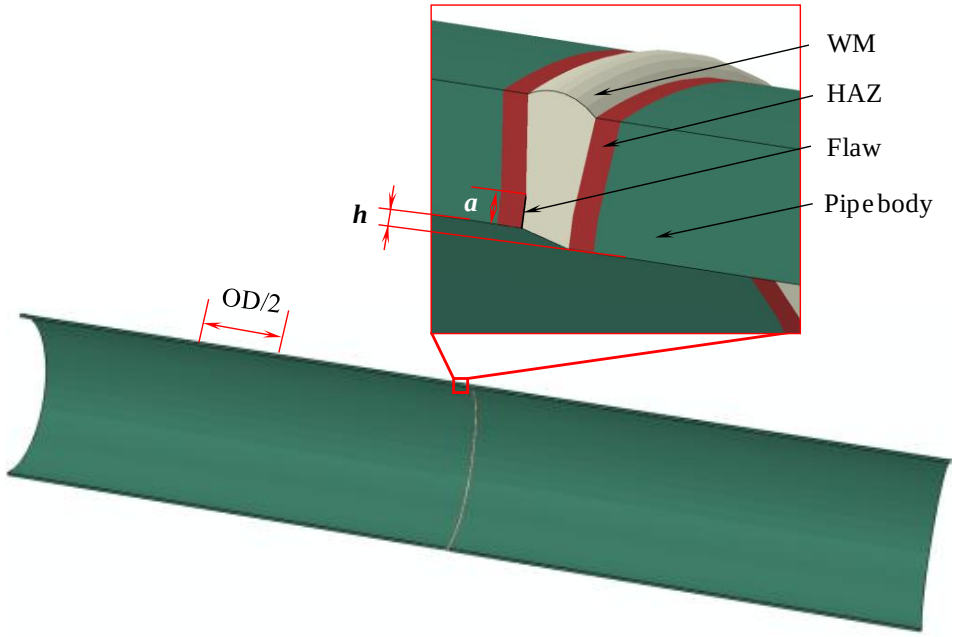

Figure 6-9 Finite element model

The flaw was modeled in a semi-elliptical shape. The flaw was located on the ID surface of the pipe and along the fusion line (i.e., HAZ flaws). Due to weld metal overmatching, which is generally required in strain-based design, the HAZ flaws usually see larger crack driving force than the weld metal flaws. To improve convergence, a small key hole of about 0.05-mm radius was created at the flaw tip. The element size near the flaw tip was about 0.05 mm, as well. The girth weld high-low misalignment was modeled as a relative shift of the two pipes on either side of the welds. The flaw depth was defined as the distance of the tip to the pipe ID surface, which is adjacent to the flaw, as shown in Figure 6-9. The flaw size was kept constant during simulation and no flaw growth was modeled.

6.2.2 FEA Procedures and Post Analyses

The FEA was conducted in two steps. In the first step, an internal pressure was applied to the ID surface where the two pipe ends were free of constraint and load. In the second step, a uni-axial tension was applied to the pipe while holding the internal pressure.

The objective of the FEA is to develop the crack driving force curves, i.e., the relationship between the crack tip opening displacement ($CTOD_F$) and the remote strain. The $CTOD_F$ was calculated from the deformed crack surface profile following the traditional 45°-line method as shown in Figure 6-10. The remote strain was calculated in the uniform strain zone using a gage length of half OD, as shown in Figure 6-9.

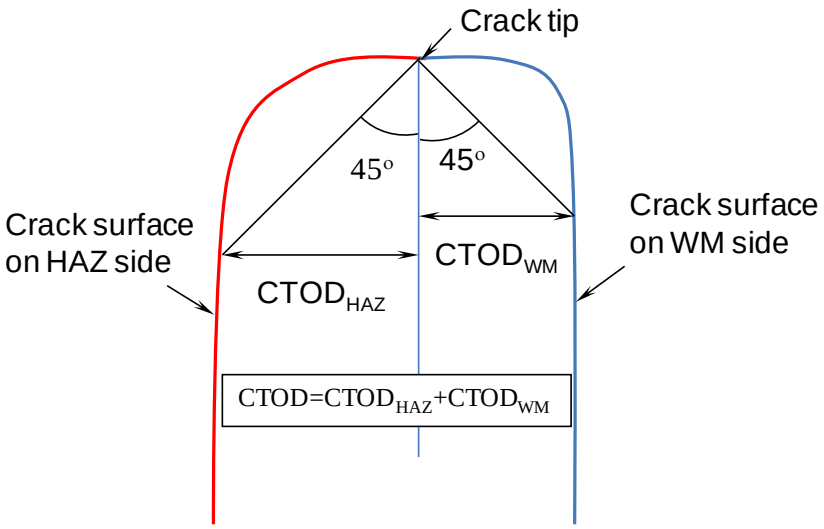

Figure 6-10 Schematic drawing of $CTOD_F$ calculation

6.3 Analysis Matrix

6.3.1 Introduction to Input Parameters

The analysis matrix is determined by input parameters (variables) which, in general, can be divided into three categories: geometry parameters, material parameters, and loading parameters.

The major geometry parameters include the following:

(1) Pipe OD and wall thickness,

(2) Flaw depth and length,

(3) Weld and HAZ geometry profile and high-low misalignment.

The material parameters are pipe and weld stress-strain curves. As discussed in Section 6.1, the material parameters are reduced to the following:

(1) Pipe yield strength and Y/T ratio,

(2) Weld overmatch level by UTS (OM),

(3) Weld Lüder's strain,

(4) HAZ softening.

The loading parameter includes:

(1) Magnitude of internal pressure.

6.3.2 Sensitivity Analysis on Selected Parameters

Different parameters can affect the crack driving forces by different degrees. Sensitivity analyses are performed to investigate the significance of each parameter on the crack driving

force. Those parameters that have small effect on the crack driving force can be fixed in the analysis. By eliminating those variables from the analysis matrix, the size of the matrix can be greatly reduced without sacrificing the accuracy.

Some parameters such as wall thickness, flaw size, weld high-low misalignment, pipe Y/T, weld OM, and internal pressure are known to have great impact on the crack driving force. Therefore, the sensitivity analysis was focused on the other parameters, i.e., pipe OD, pipe YS, weld geometry profile, HAZ softening, and weld Lüder's strain.

6.3.2.1 Pipe OD

The effect of pipe OD on the $CTOD_F$ is shown in Figure 6-11 where three OD values, i.e., 24 in, 36 in, and 48 in were analyzed. All the other input parameters are also given in the figure. The $CTOD_F$ is found independent of the pipe OD without weld high-low misalignment. The results are expected, since the relative flaw length with respect to the pipe circumference, is minimal for all three OD sizes. However, when weld high-low misalignment exists, the pipe OD does affect the $CTOD_F$ by a small amount. In general, the higher the OD is, the greater the $CTOD_F$ is. The difference is about 10% between the 24-in-OD pipe and the 48-in-OD pipe and is manageable. Therefore, since the pipe OD doesn't need to be a variable in the analysis matrix, it was decided to keep OD constant at 42 in, which can produce a slightly conservative result for most pipe ODs in use.

6.3.2.2 Weld Metal Lüder's Strain

As discussed in Section 6.1, the Lüder's strain in weld stress-strain curves can vary from zero to as much as 2%. Although it was decided to keep a constant Lüder's strain of 1% in the weld stress-strain curve equation, the effect of Lüder's strain on the $CTOD_F$ is not certain.

The effect of weld Lüder's strain on the $CTOD_F$ is shown in Figure 6-12 where two Lüder's strain values (i.e., zero and 2%) were examined. The other input parameters are listed in the figure. It is found that the Lüder's strain can slightly increase the $CTOD_F$. However, the $CTOD_F$ increase due to a 2% Lüder's strain is of no practical significance. Therefore, assuming a 1% constant Lüder's strain in the weld stress-strain curve equation is reasonable.

6.3.2.3 Pipe Yield Strength

In strain-based TSC design, it is commonly accepted that the pipe Y/T is the dominant pipe properties in affecting the $CTOD_F$. The effect of pipe YS is believed to be small, and is usually ignored. In this section, the effect of pipe YS on $CTOD_F$ is investigated.

The results are shown in Figure 6-14 and Figure 6-15 where, in general, the YS was ranged from 56 ksi to 100 ksi. In Figure 6-14, three groups of curves are shown in which each group has different combinations of weld high-low misalignment and weld strength OM. Each group consists of multiple curves of varied YS. In Figure 6-15, three groups of curves of different Y/T (i.e., 0.80, 0.85, and 0.90) are shown, and in each group the YS was varied. All results demonstrate that the effect of pipe YS has a small effect on the $CTOD_F$. Therefore, the pipe YS was kept at 80 ksi for all cases in the analysis matrix.

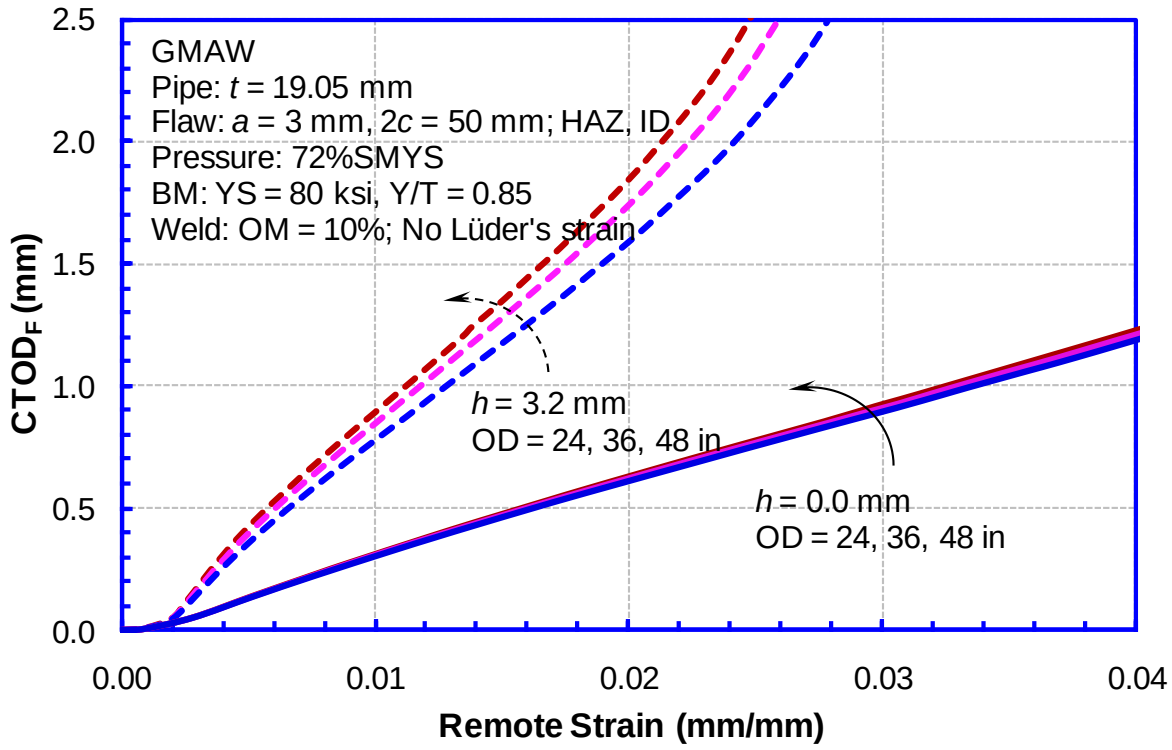

Figure 6-11 Effect of pipe OD on $CTOD_F$

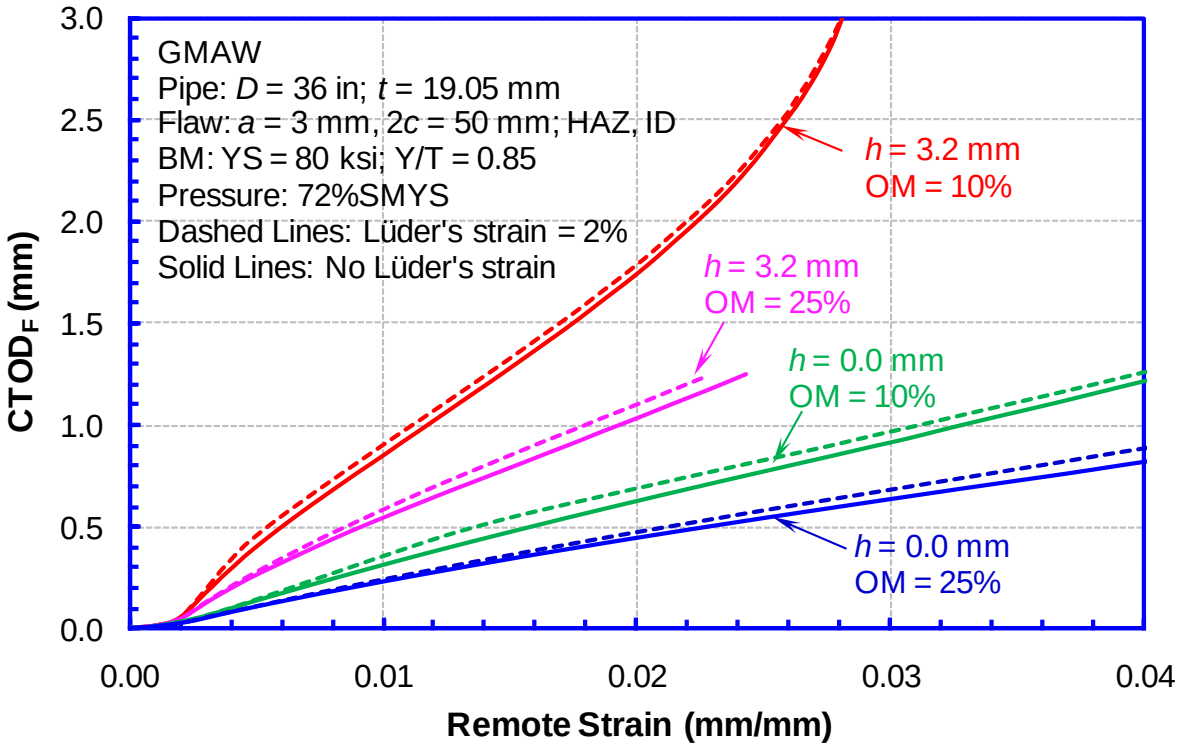

Figure 6-12 Effect of weld Lüder's strain on $CTOD_F$

6.3.2.4 Weld and HAZ Profile

A typical weld macro is shown in Figure 6-13. It shows that the actual weld geometry can be very complex. To characterize the size and shape of a weld, the simplified parameters such as bevel angle, weld root width, cap height, and HAZ width are often used.

In general, the total volume of the weld, determined by the root width and bevel angle, is the dominant parameter for the $CTOD_F$. However, the HAZ width (with softened HAZ), the shape and height of the cap (with large bevel angles), and the alignment of the bevel angle/HAZ with plastic strain shear band (with softened HAZ) can also have important effects on the $CTOD_F$.

The weld geometries are mainly determined by the welding procedures. Although the exact weld shape can be affected by many other conditions, the major parameters such as the bevel angle, root width, and HAZ width are highly repeatable for a given welding procedure. The cap shape and height, on the other hand, could vary a lot, even for the same weld. GMAW and FCAW (or SMAW) are normally considered to be two of the major welding procedures for pipeline welding. The GMAW weld normally has a lower bound bevel angle and volume, while the FCAW (or SMAW) weld has an upper bound bevel angle and volume. Due to its high heat input, the FCAW (or SMAW) weld usually contains a larger HAZ than the GMAW weld.

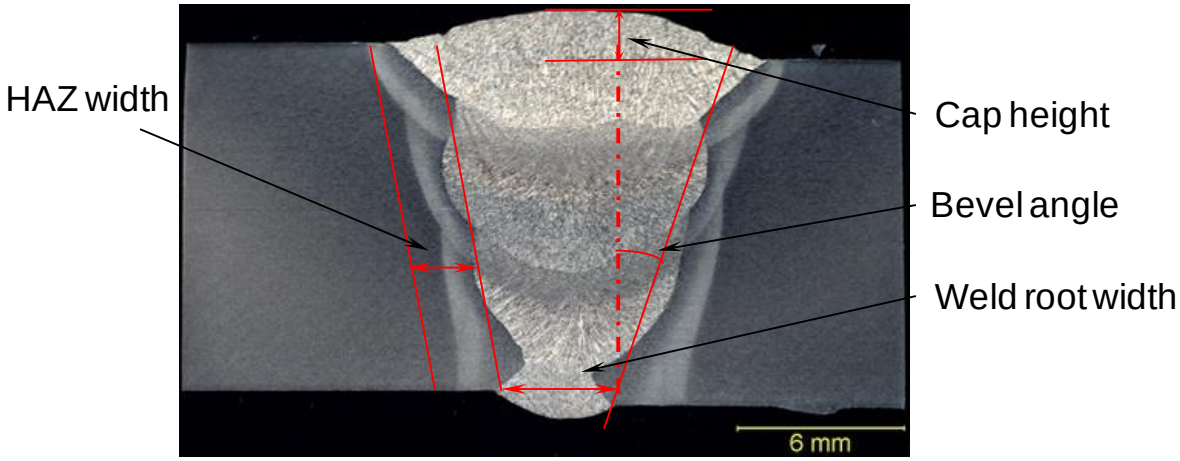

Figure 6-13 Sample weld macro

The weld profiles of those two welding procedures (i.e., GMAW and FCAW (or SMAW)) were selected in the analysis matrix. The weld geometry parameters were determined from representative welds for each welding procedure, and conservative values were used for those highly variable parameters, such as the cap height.

6.3.2.5 HAZ Softening

HAZ softening has been frequently found in modern linepipe welds, even for the pipe grades as low as X65. The hardness map in the weld area usually indicates that the strength of HAZ materials varies with location. The most softened spot is usually located at the center line of the HAZ. It should be noted that the actual softened zone can be twice as wide as the visible HAZ. By controlling the welding procedure, the level of HAZ softening can be controlled. For welds of reasonable quality, the maximum softening should be expected to be below 15% and likely

around 10%. Previous research has demonstrated that a 10%-15% softened HAZ of 2-mm wide can increase the crack driving force by 20%.

To obtain reasonably conservative solutions, a 10% softening was used in all analyses. The strength of the HAZ materials was assumed to vary with the location in the HAZ and follow a 2nd order function of a bathtub shape. The maximum softening was reached at the center of the HAZ and the strength of the HAZ material gradually changed to the strength of the pipe and weld materials, respectively at the corresponding interface.

6.3.3 Summary of Key Input Parameters

Based on the sensitivity analysis results, the key input parameters (variables in the analysis matrix) are determined as:

(1) Geometry parameters: wall thickness, flaw depth and length, and high-low misalignment,

(2) Material parameters: pipe Y/T and weld overmatch (OM),

(3) Loading parameter: internal pressure.

The other parameters listed in Section 6.3.1 are fixed at constant values:

(1) Pipe OD = 42 in,

(2) Weld Lüder's strain = 1%,

(3) Pipe yield strength = 80 ksi,

(4) HAZ softening = 10%,

(5) Weld geometries: GMAW and FCAW (the parameters are given in Figure 6-16).

6.3.4 Analysis Matrix

Two types of analysis matrix were developed for different key parameters, summarized in Section 6.3.3, according to the degree of coupling (interaction) between the parameters, namely full and partial permutation analysis matrix.

6.3.4.1 Full Permutation Matrix

The key parameters such as flaw depth, flaw length, high-low misalignment, pipe YS, and weld OM are highly interacting. Those parameters are named full permutation parameters in the following matrix. To understand and model their coupling effect, full permutation of all those parameters needs to be implemented. The corresponding FEA matrix is called the full permutation analysis matrix (see Table 6-3). The full permutation parameters are highlighted in bold. A total of 1152 cases are included in this matrix for two different welds (GMAW and FCAW). The Y/T ranges from 0.75 to 0.94; and the weld overmatch (OM) varies from 0% to 30%. The flaw depth changes from 2 mm to 8 mm; and the flaw length changes from 25 mm to 100 mm. The weld high-low misalignment varies from 0.0 mm to 3.2 mm.

6.3.4.2 Partial Permutation Matrix

The effect of wall thickness and internal pressure on $CTOD_F$ was analyzed with a partial permutation matrix as shown in Table 6-4, where complete permutation was implemented only on selected parameters.

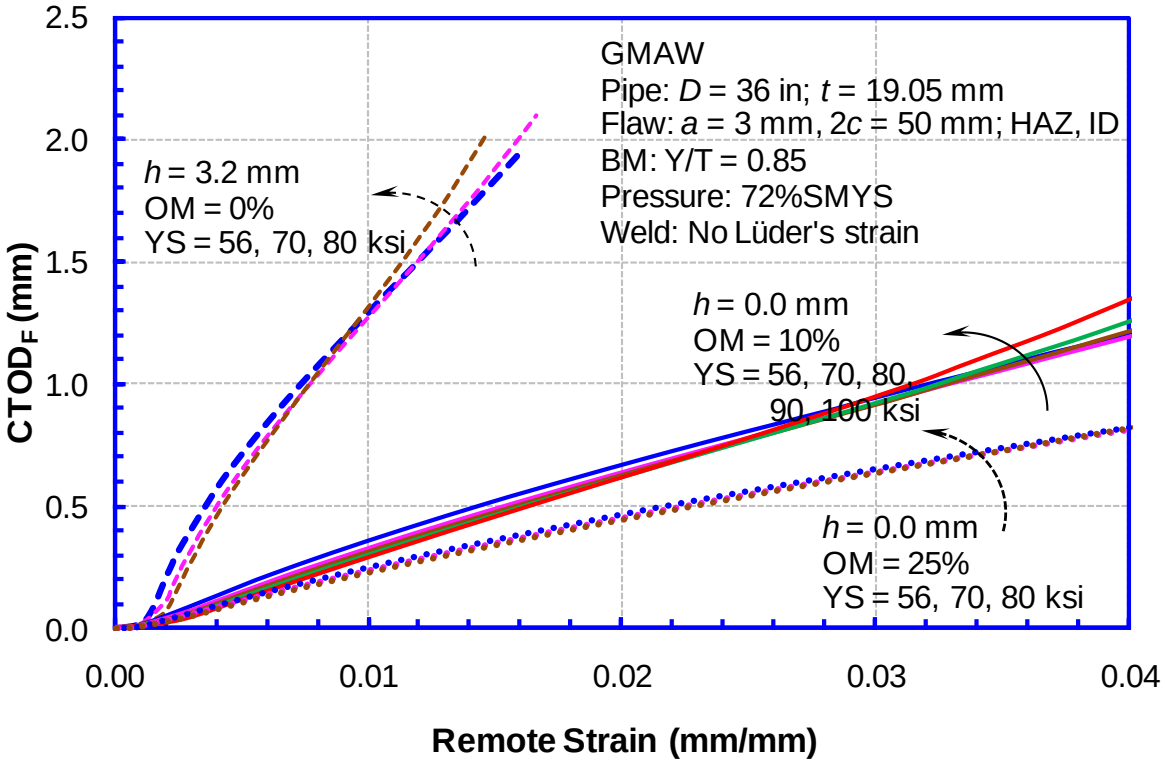

Figure 6-14 Effect of pipe YS on $CTOD_F$ (interaction with high-low and OM)

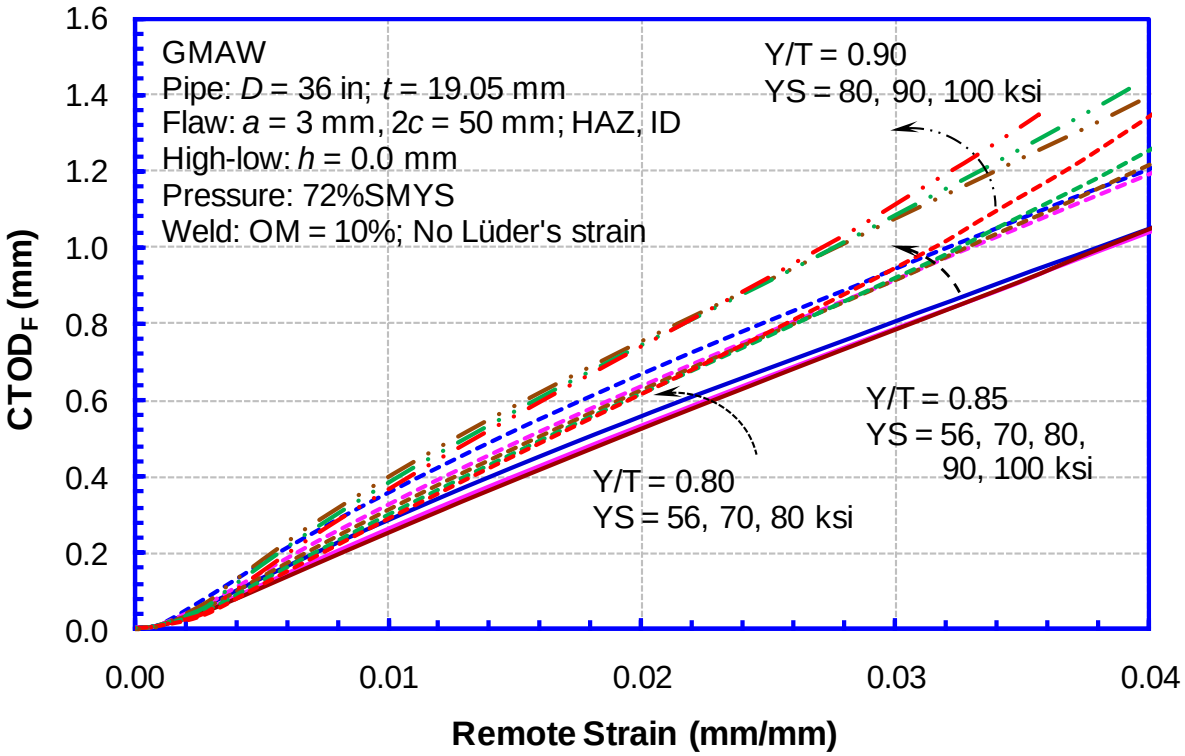

Figure 6-15 Effect of pipe YS on $CTOD_F$ (interaction with Y/T)

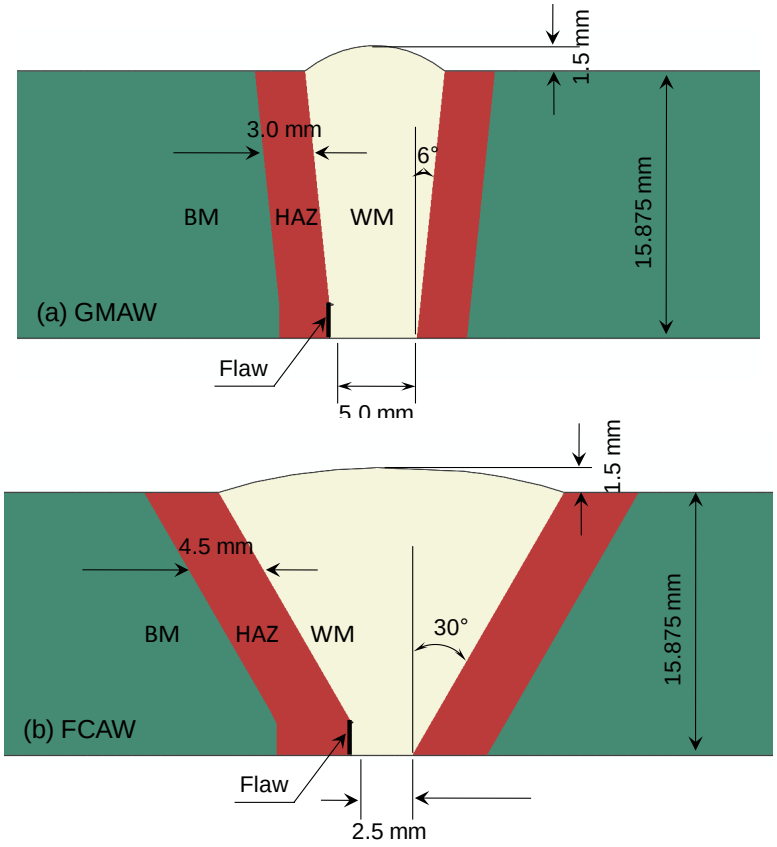

Figure 6-16 Weld geometry profiles and parameters

Table 6-3 Full permutation analysis matrix

Parameters			Values	No. of Cases
Material	Pipe	YS (ksi)	80	1
		Y/T	**0.75, 0.81, 0.87, 0.94**	**4**
	Weld	Lüder's Strain	1%	1
		OM	**0%, 15%, 30%**	**3**
	HAZ	Softening	10%	1
Geometry	Pipe	OD (inch)	42	1
		WT (in)	5/8	1
	Flaw	**Depth (mm)**	**2, 4, 6, 8**	**4**
		Length (mm)	**25, 50, 75, 100**	**4**
	Weld	**High-low (mm)**	**0.0, 1.6, 3.2**	**3**
		Type	GMAW, FCAW	2
Load	Pressure	Design Factor	0.72	1
Total Cases				1152

Table 6-4 Partial permutation analysis matrix

Parameters			Values	
			Thickness Effect	Pressure Effect
Material	Pipe	YS (ksi)	80	80
		Y/T	0.81 - 0.94	0.75, 0.87, 0.94
	Weld	Lüder's Strain	none	1%
		OM	0% - 15%	0%, 15%, 30%
	HAZ	Softening	10%	10%
Geometry	Pipe	OD (inch)	36, 42	42
		WT (in)	1/4 - 1	5/8
	Flaw	Depth (a/t)	0.10 - 0.31	0.13, 0.38, 0.50
		Length ($2c/a$)	4.2 - 25.0	4.2, 12.5, 16.7
	Weld	High-low (h/a)	0.0 - 1.6	0.0, 0.27, 0.53
		Type	GMAW	GMAW
Load	Pressure	Design Factor	0.72	0.2 ~ 0.8
Total Cases (no full permutation)			212	64

6.4 Development of Driving Force Database

The $CTOD_F$ of all the analyzed cases (i.e., with different input parameters) were extracted from the FEA results. For each case, the $CTOD_F$ was calculated at a number of remote strain values. The $CTOD_F$ was collected and put in a database as shown in Table 6-5.

Table 6-5 Sample driving force database

t (mm)	*a* (mm)	2*c* (mm)	*h* (mm)	Y/T	OM	*f*	CTOD (mm)	Strain (mm/mm)
15.9	4.0	25.0	0.00	0.75	1.00	0.72	0.00	1.12E-05
							0.16	6.87E-03
:	:	:	:	:	:	:	:	:
							2.89	5.73E-02
							3.05	5.75E-02
15.9	4.0	25.0	0.00	0.81	1.00	0.72	0.00	2.57E-05
							0.16	5.28E-03
:	:	:	:	:	:	:	:	:
							2.84	4.78E-02
							3.00	4.79E-02
:	:	:	:	:	:	:	:	:
15.9	6.0	100.0	3.20	0.94	1.30	0.72	0.00	2.34E-05
							0.25	2.04E-03
:	:	:	:	:	:	:	:	:
							4.43	6.45E-03
							4.67	6.45E-03

7 TSC Prediction Equations

7.1 TSC Equation Development Process

The development of the TSC equations follows the following process:

(1) The FEA driving force databases of the full analysis matrix in Table 6-3 were fitted with two sets of parametric equations, one for GMAW and one for FCAW/SMAW. The equations are applicable to pressurized pipes with a pressure factor of 0.72 and a pipe wall thickness of 15.9 mm (5/8").

(2) A wall thickness correlation relation was developed using a curve fitting procedure based on the FEA database of pressurized pipes shown in Table 7-3 (a subgroup of the analysis matrix in Table 6-4) with wall thicknesses of 0.5, 0.75, and 1.0".

(3) The effects of internal pressure on TSC were analyzed by comparing the TSC of pressurized pipes with the TSC of non-pressurized pipes (Table 6-4). A scaling factor for the TSC of non-pressurized pipes, as opposed to pressured pipes at a pressure factor of 0.72, was developed.

(4) An interpolation function was developed between zero pressure and high pressure based on the cases in Table 6-4.

The outcome of the above process is a set of TSC equations for a full range of internal pressure, a range of wall thickness, and two weld profiles.

7.2 Input Parameters

The TSC prediction models consider the effects of the following parameters on girth weld strain capacity.

(1) Geometric parameters:

t	pipe wall thickness, mm,
a	flaw height, mm,
$2c$	flaw length, mm, and
h	girth weld high-low misalignment, mm.

(2) Material parameters:

σ_y	pipe yield strength, MPa,
σ_U	pipe ultimate tensile strength, MPa,
σ_U^W	weld metal tensile strength, MPa, and
δ_A	girth weld apparent CTOD toughness, mm.

(3) Loading parameter:

f_p	pressure factor, ratio of applied hoop stress to pipe yield strength.

The TSC equations are given as functions of the following normalized geometric and material parameters, apparent CTOD toughness and pressure factor:

$\eta = a/t$	normalized flaw depth,

$\beta = 2c/t$ normalized flaw length,

$\psi = h/t$ normalized girth weld high-low misalignment,

$\xi = \sigma_y / \sigma_U$ base metal Y/T ratio,

$\phi = \sigma_U^W / \sigma_U$ weld metal strength mismatch ratio measured at ultimate tensile strength,

δ_A girth weld apparent CTOD toughness, mm, and

f_p pressure factor, ratio of applied hoop stress to pipe yield strength.

7.3 TSC Equations

7.3.1 TSC Equations for Default Wall Thickness and Pressure Factor

Parametric equations - TSC_p, i.e., the TSC of pipes with the wall thickness of 15.9 mm and pressure factor of 0.72, were developed for GMAW and FCAW/SMAW, respectively, through nonlinear curve fitting procedures based on the driving force database described in Table 6-3. For curve fitting purpose, each of these driving force curves were sampled by 10-14 data points to represent the relationship between the crack driving force $CTOD_F$ and the remote strain. These points were fitted to obtain the TSC equations. Figure 7-1 shows the examples of sampling points with respect to the continuous curves from FEA.

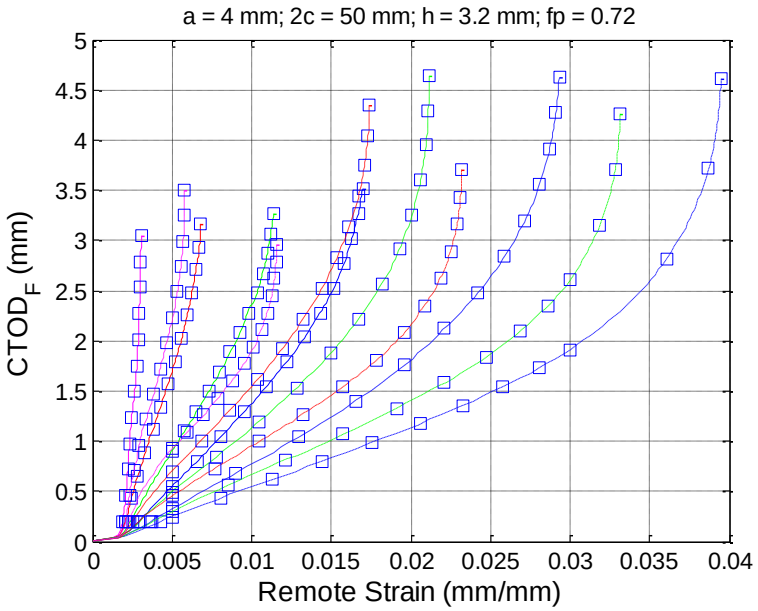

Figure 7-1 Examples of sampled driving force curves for curve fitting

The TSC_p for both GMAW and FCAW/SMAW, adopts the following form:

$$TSC_p = A\frac{f(\delta_A)}{1+f(\delta_A)}, \tag{7.1}$$

where

$$f(\delta_A) = \left(C\delta_A\right)^{B\delta_A{}^D}. \tag{7.2}$$

In Eqs. (7.1) and (7.2), the symbols *A*, *B*, *C*, and *D* represent fitted functions of normalized geometry and material parameters. Since the TSC cannot be greater than the uniform strain of the pipe material, the predicted TSC_p is set to the uniform strain if Eq. (7.1) gives a value greater than the uniform strain.

7.3.1.1 TSC_p for GMAW

The fitted functions of *A*, *B*, *C,* and *D* for GMAW TSC_p are in the following forms:

$$\begin{cases} A = a_1 e^{a_2/\beta} e^{a_3\eta\beta e^{a_4/\beta}} \left[1 + a_5\psi^{a_6} + a_7\psi(\eta\beta)^{a_8}\right]\left(1 + a_9\xi^{a_{10}}\phi^{a_{11}} + a_{12}\psi^{a_{13}}\xi^{a_{14}}\right) \\ B = \beta^{b_1}\eta^{b_2\beta^{b_3}/\eta}\left[b_4\phi^{b_5}\left(b_6\phi^{b_7}\right)^{\xi} + b_8\psi^{b_9}\right] \\ C = e^{c_1/\beta} e^{\frac{c_2\beta}{(1+c_3\beta)\eta}}\left(1 + c_4\psi^{c_5} + c_6\psi e^{-\eta} + c_7\psi e^{-\beta}\right)\left(c_8 + c_9\phi^{c_{10}} + c_{11}\xi^{c_{12}}\phi\right) \\ D = d_1\beta^{d_2}\eta^{\frac{d_3\beta}{(1+d_4\beta)}}\left(1 + d_5\psi^{d_6}\right)\left(1 + d_7\xi^{d_8} + d_9\phi^{d_{10}}\right) \end{cases} . \quad (7.3)$$

The coefficients in Eq. (7.3) are given in Table 7-1.

Table 7-1 Fitted coefficients of TSC_p equation for GMAW

a1	2.084E+00	b1	-5.005E-02	c1	1.409E+00	d1	2.209E-02
a2	2.812E-01	b2	-5.139E-03	c2	2.345E-01	d2	1.156E+00
a3	-4.950E-01	b3	4.485E-01	c3	1.125E+00	d3	1.601E+00
a4	7.373E-01	b4	1.417E+00	c4	4.181E+00	d4	8.964E-01
a5	-5.005E+00	b5	2.217E+00	c5	1.201E+00	d5	1.383E+00
a6	1.186E+00	b6	1.029E+00	c6	-5.384E+00	d6	1.333E+00
a7	1.644E+00	b7	-2.598E+00	c7	2.406E+00	d7	9.313E-02
a8	7.374E-01	b8	-2.679E+00	c8	-2.154E-01	d8	-2.240E+00
a9	-9.829E-01	b9	1.694E+00	c9	-5.237E-03	d9	8.559E+00
a10	8.655E-02			c10	9.889E+00	d10	-3.719E+00
a11	-1.029E-01			c11	3.547E-01		
a12	-1.500E-01			c12	-7.513E-01		
a13	1.025E+00						
a14	5.557E+00						

7.3.1.2 TSC_p for FCAW/SMAW

The fitted functions of *A*, *B*, *C,* and *D* for FCAW/SMAW TSC_p are in the following forms:

$$\begin{cases} A = a_1 e^{a_2/\beta} e^{a_3\eta\beta e^{a_4/\beta}} \left[1 + a_5\psi^{a_6} + a_7\psi^{a_8}(\eta\beta)^{a_9}\right]\left(1 + a_{10}\xi^{a_{11}}\phi^{a_{12}}\right) \\ B = \beta^{b_1}\eta^{b_2\beta^{b_3}/\eta}\left[b_4\phi^{b_5}\left(b_6\phi^{b_7}\right)^{\xi} + b_8\psi^{b_9}\right] \\ C = e^{c_1/\beta} e^{\frac{c_2\beta}{(1+c_3\beta)\eta}}\left(1 + c_4\psi^{c_5} + c_6\psi e^{-\eta} + c_7\psi e^{-\beta}\right)\left(c_8 + c_9\phi^{c_{10}} + c_{11}\xi^{c_{12}}\phi\right) \\ D = d_1\beta^{d_2}\eta^{d_3}\left(1 + d_4\psi^{d_5} + d_6\eta\beta\psi\right)\left(1 + d_7\xi^{d_8} + d_9\phi^{d_{10}}\right) \end{cases} . \quad (7.4)$$

The coefficients in Eq. (7.4) are given in Table 7-2.

Table 7-2 Fitted coefficients of TSC_p equation for FCAW

a1	9.281E-01	b1	-5.578E-02	c1	1.609E+00	d1	6.822E-03
a2	9.573E-02	b2	1.112E-02	c2	1.138E-01	d2	1.014E+00
a3	-5.053E-01	b3	-1.735E-01	c3	6.729E-01	d3	1.746E+00
a4	3.718E-01	b4	1.675E+00	c4	2.357E+00	d4	2.378E+00
a5	-2.023E+00	b5	2.603E-01	c5	1.057E+00	d5	9.434E-01
a6	7.585E-01	b6	1.106E+00	c6	-4.444E+00	d6	-1.243E+00
a7	6.299E-01	b7	-1.073E+00	c7	1.727E-02	d7	3.579E+01
a8	5.168E-01	b8	-1.519E+00	c8	-1.354E-02	d8	7.500E+00
a9	7.168E-01	b9	1.965E+00	c9	-1.224E-02	d9	6.294E+01
a10	-9.815E-01			c10	8.128E+00	d10	-6.930E+00
a11	2.909E-01			c11	2.007E-01		
a12	-3.141E-01			c12	-1.594E+00		

7.3.2 Thickness Correlation

The TSC_p equations described in Section 7.3.1 were derived for pipes with a wall thickness of 15.9 mm. Further FEA was conducted for three other wall thicknesses: 0.5, 0.75, and 1.0". Table 7-3 summarizes the analysis matrix. A total of 192 driving force curves were obtained for GMAW with a variety of combinations of flaw depth, flaw length, hi-low misalignment, pipe material Y/T ratio, and weld strength mismatch.

Table 7-3 FEA matrix of wall thickness effect study

Pipe		Flaw				Material				Weld	Pressure	Total
OD (in)	WT (mm)	a (mm)	2c (mm)	H (mm)	Location	Y/T	OM	Grade	HAZ	Type	fp	
42	12.7	2, 4	25, 50	0, 1.6, 3.2	HAZ, ID	0.81, 0.87	1.0, 1.15	X80	10% Softening	GMAW	0.72	48
	19.05	2, 4	25, 50	0, 1.6, 3.2		0.81, 0.87	1.0, 1.15					48
	25.4	3, 6	25, 50	0, 1.6, 3.2, 4.8		0.81, 0.87, 0.94	1.0, 1.15					96
Total												192

Using the driving force database, developed from cases shown in Table 7-3, a thickness correlation function for GMAW was developed through a curve fitting procedure. The thickness correlation is given as a function of wall thickness ratio and normalized hi-low misalignment in the following form:

$$\mathrm{sf}(t) = \left(\frac{t_0}{t}\right)^{0.8096(1+1.503\psi^{1.229})}, \tag{7.5}$$

where $t_0 = 15.9$ mm and $0.5" \le t \le 1.0"$. The TSC_p for a range of wall thickness can be calculated as:

$$TSC_p(t) = \mathrm{sf}(t) TSC_p. \tag{7.6}$$

The predicted $TSC_p(t)$ is set to the uniform strain when Eq. (7.6) gives a value of $TSC_p(t)$ greater than the uniform strain of the pipe material.

The TSC trends of FCAW/SMAW as functions of input parameters were compared with those of GMAW. The trends were found to be very similar between GMAW and FCAW/SMAW. It is therefore concluded that the thickness correlation relations in Eqs. (7.5) and (7.6) are also applicable to FCAW/SMAW.

7.3.3 Pressure Effects on TSC

The pressure effects on TSC can be quantified by a pressure effect factor C_p, defined as:

$$C_p = \frac{TSC_0}{\min\limits_{0 \le f_p \le 0.8} \{TSC\}}, \tag{7.7}$$

where TSC_0 is the TSC of non-pressurized pipes. Figure 7-2 shows schematically the definition of C_p.

A comprehensive FEA was conducted to investigate the pressure effects on girth-welded pipes. In the FE models, HAZ flaws on the ID surface of a 42" pipe were modeled. A total of 55 cases were simulated with varying pressure factor from 0.0 to 0.8. The ranges of the other parameters are as follows:

(1) Flaw depth, 2.0 mm to 8.0 mm;

(2) Flaw length, 25 mm to 100 mm;

(3) Hi-low misalignment, 0.0 mm to 3.2 mm;

(4) Pipe material Y/T ratio, 0.75 to 0.94; and

(5) Weld strength mismatch, 1.0 to 1.3.

Figure 7-3 summarizes the pressure effect factors derived from FEA results. The pressure effect factors are in the range of 1.5 to 2.5. This range is consistent with experimental observations [2].

Liu and Wang [38] investigated the pressure effects by FEA and found that crack driving force increases as pressure factor f_p increases from 0.0 to 0.6 and becomes saturated as f_p continues to increase. The TSC equations in Section 7.3.1 were developed from FEA databases with a pressure factor of 0.72. The following TSC relation as a function of internal pressure is given based on the above observations:

$$TSC = \begin{cases} TSC_p & \text{if} \quad 0.6 \le f_p \le 0.8 \\ TSC_0 + \dfrac{5 f_p}{3}(TSC_p - TSC_0) & \text{if} \quad f_p < 0.6 \end{cases}. \tag{7.8}$$

The TSC of non-pressurized pipes, TSC_0, can be conservatively estimated from TSC_p as,

$$TSC_0 = 1.5 TSC_p. \tag{7.9}$$

The predicted TSC_0 is set to the uniform strain if Eq. (7.9) gives a value of TSC_0 greater than the uniform strain of the pipe material.

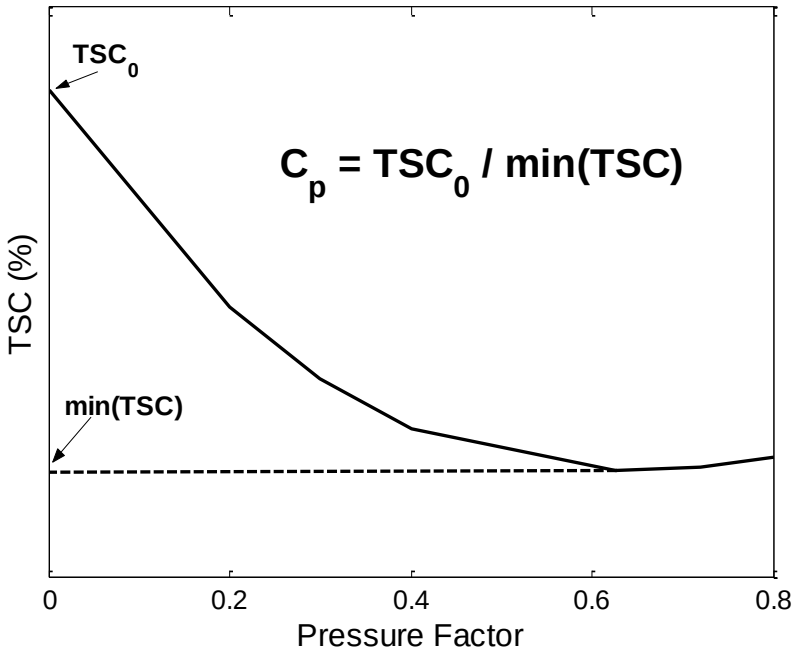

Figure 7-2 Definition of pressure effect factor C_p

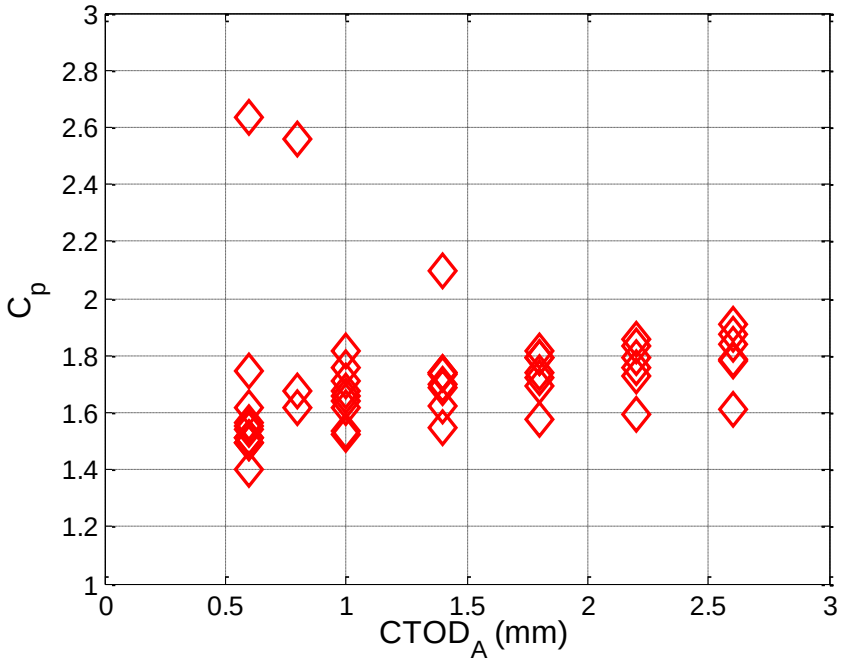

Figure 7-3 Pressure effect factors as a function of $CTOD_A$

7.4 Applicable Range

The applicable ranges of the input parameters of TSC equations are:

$\eta = a/t$ 0.05 – 0.5,

$\beta = 2c/t$ 1.0 – 20.0,

$\psi = h/t$	0.0 – 0.2,
$\xi = \sigma_y / \sigma_U$	0.75 – 0.94,
$\phi = \sigma_U{}^W / \sigma_U$	1.0 – 1.3,
δ_A	0.2 – 2.5 mm, and
f_p	0.0 – 0.8.

The applicable range of pipe wall thickness is 12.7 mm - 25.4 mm (0.5 inch - 1.0 inch). The applicable range of pipe OD is 304 mm – 1,219 mm (12 inch – 48 inch). The applicable range of pipe yield strength is 386 MPa - 690 MPa (56 ksi - 100 ksi).

7.5 Sample TSC Relations

The geometric and material parameters (η, β, ψ, ξ, and ϕ) have significant effects on the TSC of pipes. The developed TSC_p equations for GMAW and FCAW are expected to capture the effects of these parameters. Trend analysis was conducted to investigate the relationship between the geometric and material parameters and the TSC. In the analysis, TSC values are computed from the TSC_p equations by varying one parameter within its applicable range while the other parameters are held to their nominal values. The nominal values are: normalize flaw depth, $\eta = 3.0/t$; normalized flaw length, $\beta = 50/t$; normalized hi-low misalignment $\psi = 1.6/t$; pipe material Y/T ratio, $\xi = 0.88$; and weld strength mismatch, $\phi = 1.2$ (i.e., $a = 3.0$ mm, $2c = 50$ mm, and $h = 1.6$ mm). Three apparent CTOD toughness values, 0.8, 1.0, and 1.2 mm, are selected. These values represent a typical toughness range of modern mechanized GMAW/FCAW/SMAW welds.

The TSC values using the TSC_p equations for GMAW and FCAW/SMAW are plotted with regard to η, β, ψ, ξ, and ϕ in Figure 7-4 to Figure 7-8. It shows that the TSC increases as the weld strength mismatch (ϕ) increases and the TSC decrease as the flaw depth (η), flaw length (β), high-low misalignment (ψ), or pipe material Y/T ratio (ξ) increase.

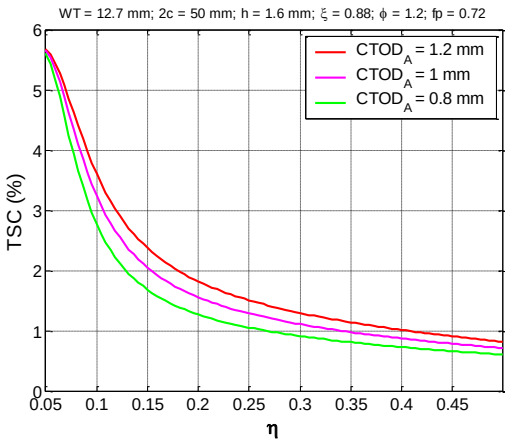

WT = 12.7 mm, GMAW

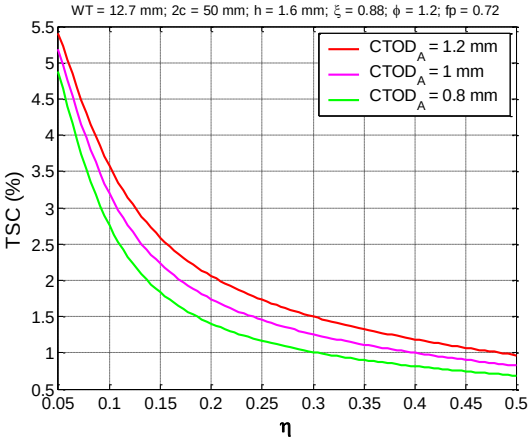

WT = 12.7 mm, FCAW

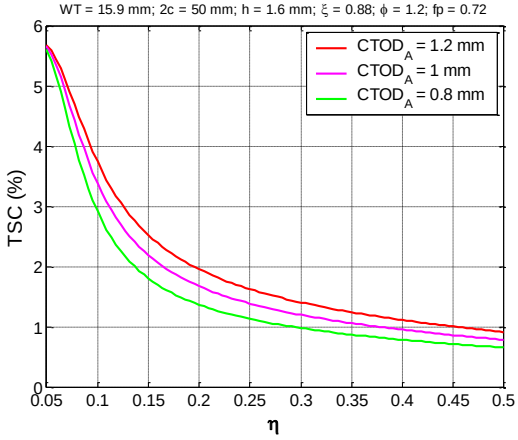

WT = 15.9 mm, GMAW

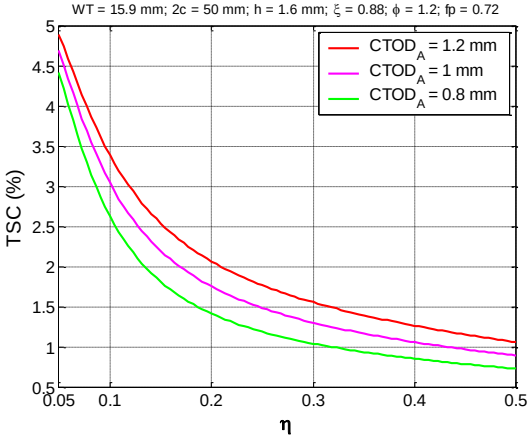

WT = 15.9 mm, FCAW

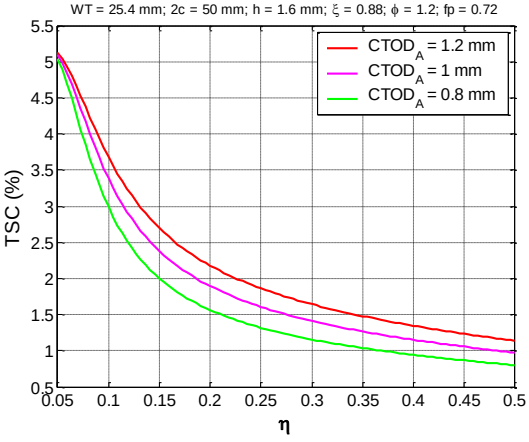

WT = 25.4 mm, GMAW

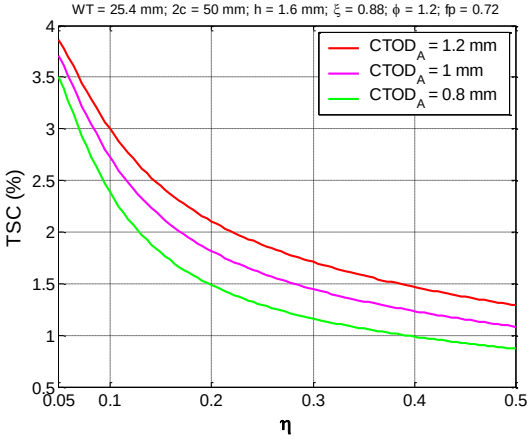

WT = 25.4 mm, FCAW

Figure 7-4 TSC as a function of normalized flaw depth

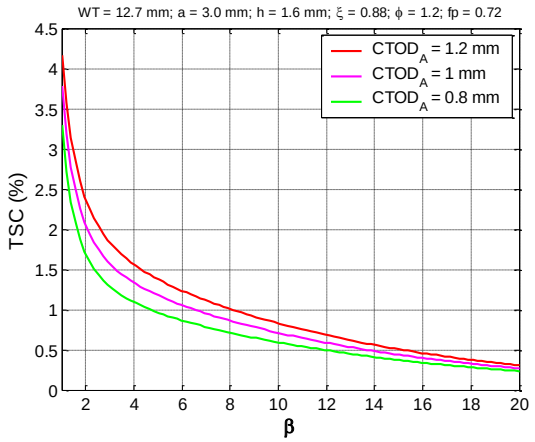

WT = 12.7 mm, GMAW

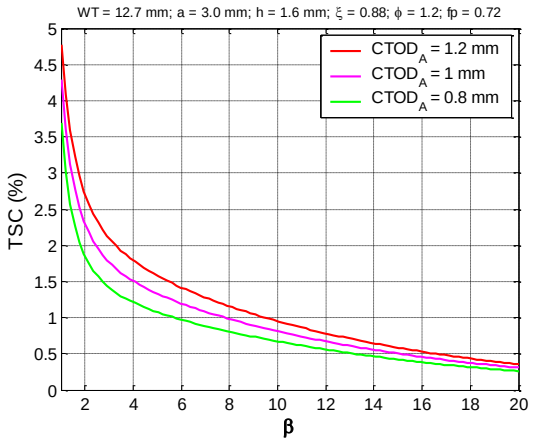

WT = 12.7 mm, FCAW

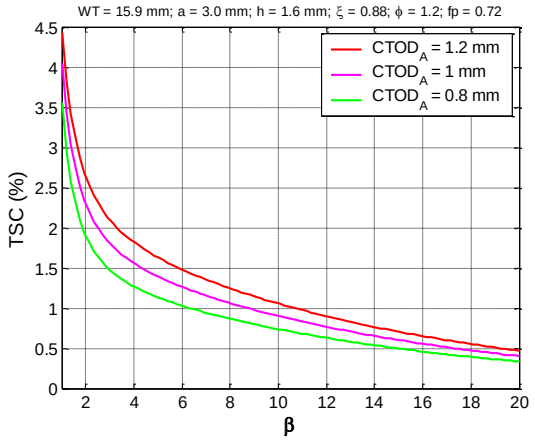

WT = 15.9 mm, GMAW

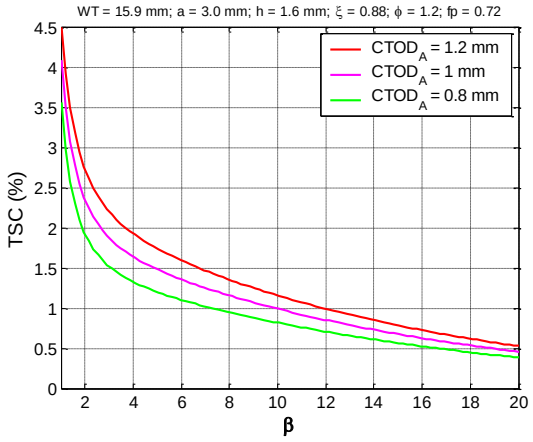

WT = 15.9 mm, FCAW

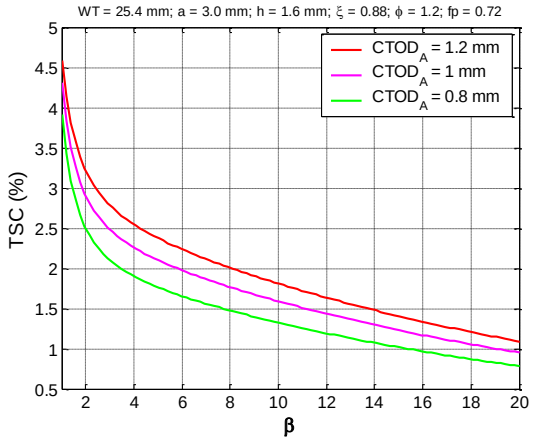

WT = 25.4 mm, GMAW

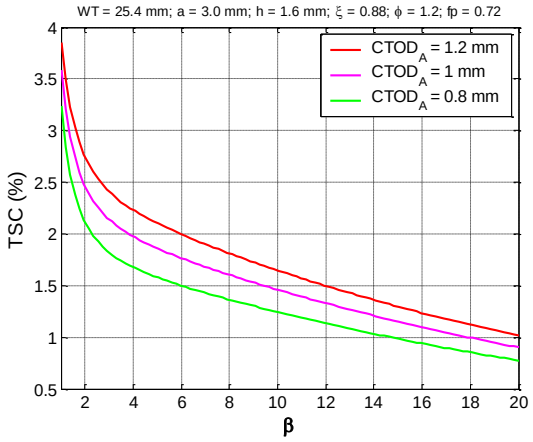

WT = 25.4 mm, FCAW

Figure 7-5 TSC as a function of normalized flaw length

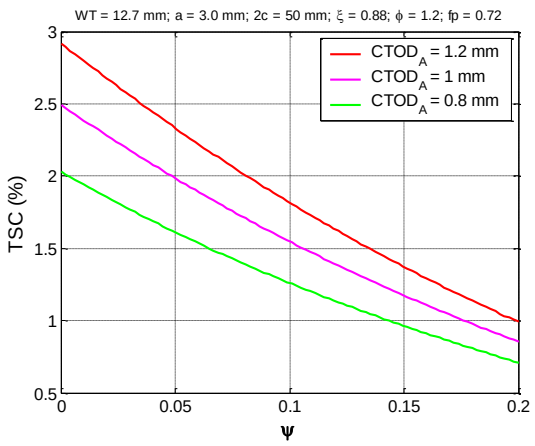

WT = 12.7 mm, GMAW

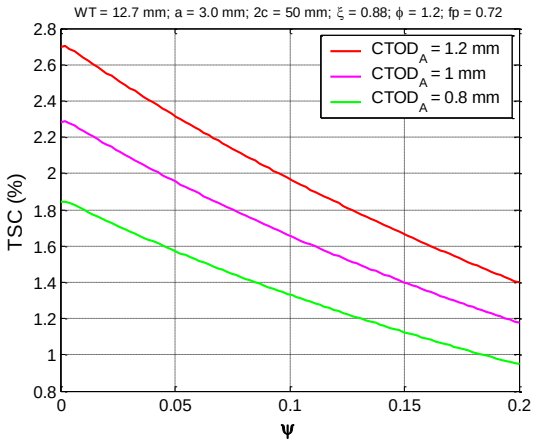

WT = 12.7 mm, FCAW

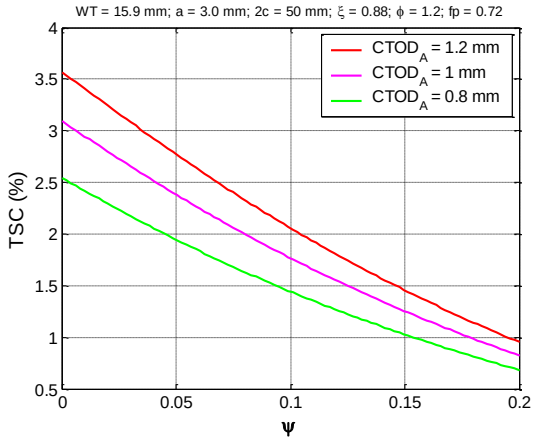

WT = 15.9 mm, GMAW

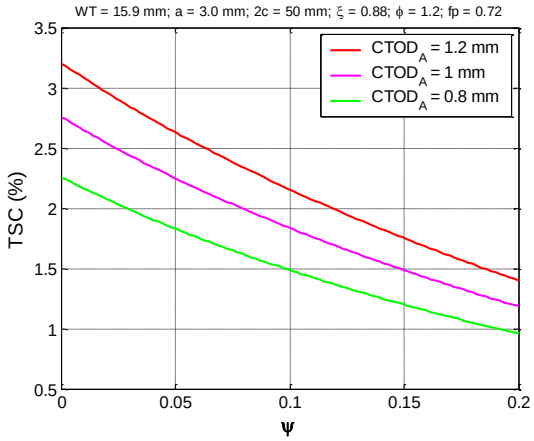

WT = 15.9 mm, FCAW

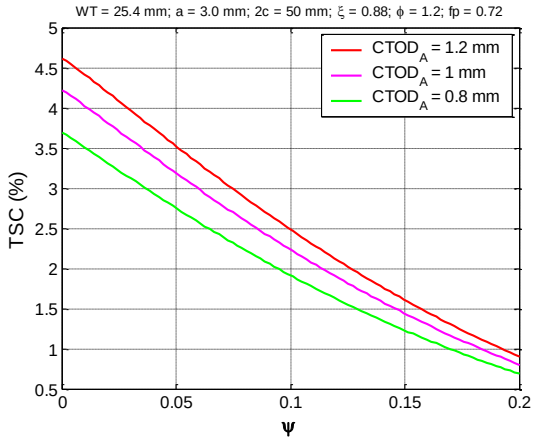

WT = 25.4 mm, GMAW

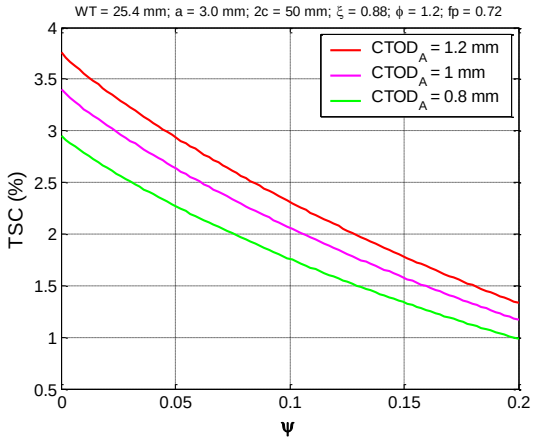

WT = 25.4 mm, FCAW

Figure 7-6 TSC as a function of normalized hi-low misalignment

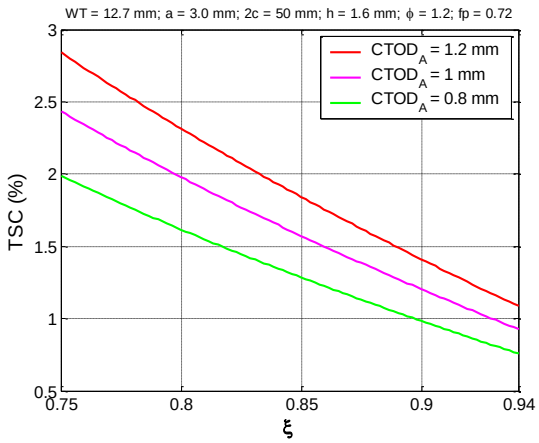

WT = 12.7 mm, GMAW

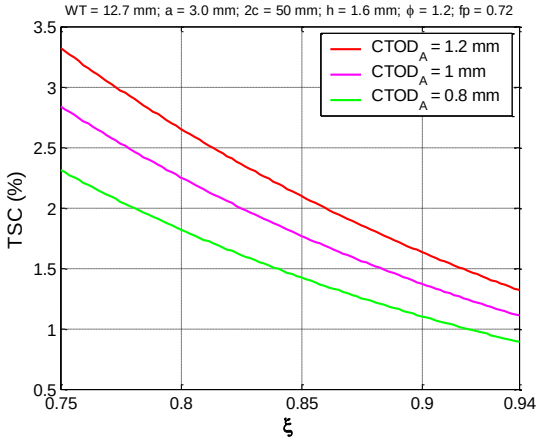

WT = 12.7 mm, FCAW

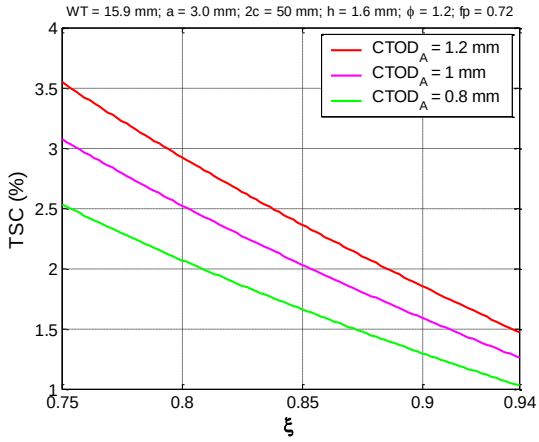

WT = 15.9 mm, GMAW

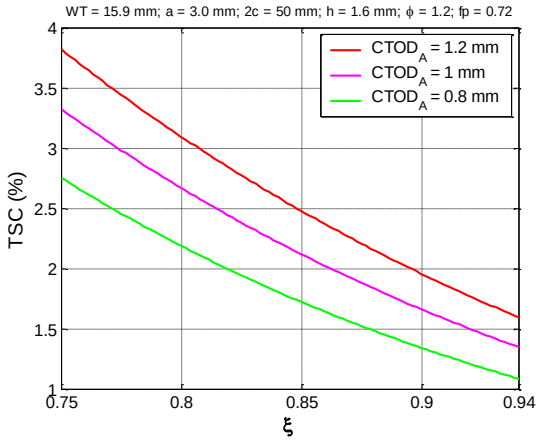

WT = 15.9 mm, FCAW

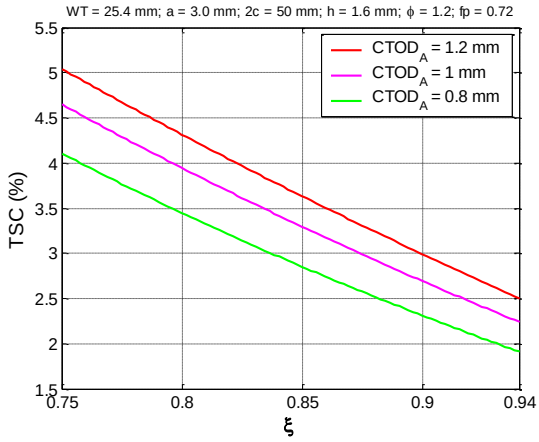

WT = 25.4 mm, GMAW

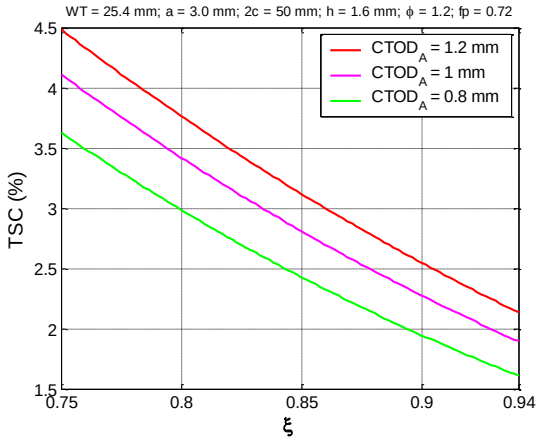

WT = 25.4 mm, FCAW

Figure 7-7 TSC as a function of pipe material Y/T ratio

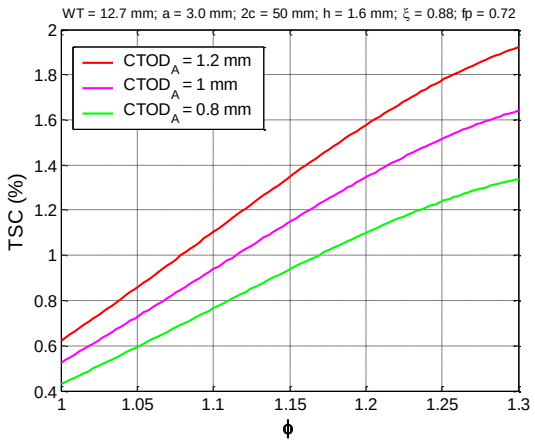

WT = 12.7 mm, GMAW

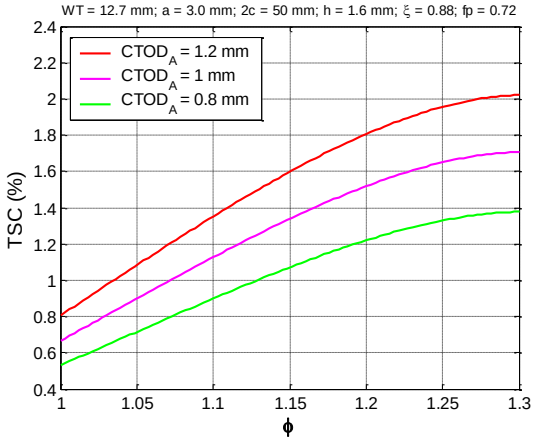

WT = 12.7 mm, FCAW

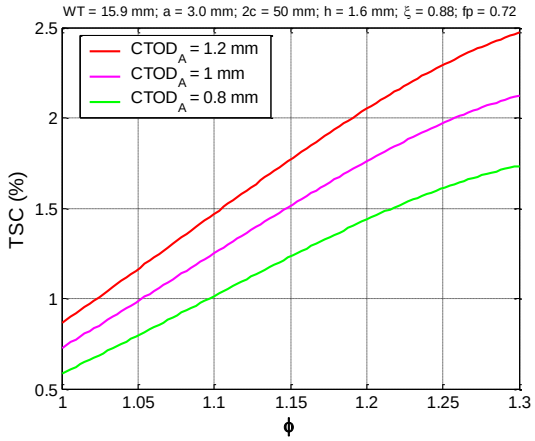

WT = 15.9 mm, GMAW

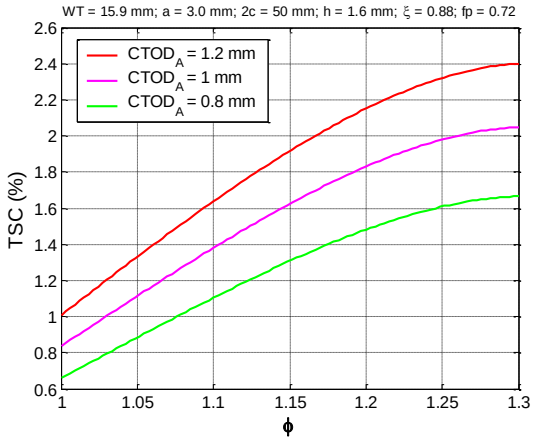

WT = 15.9 mm, FCAW

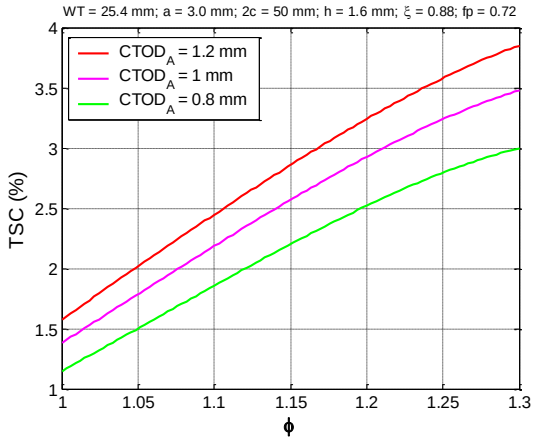

WT = 25.4 mm, GMAW

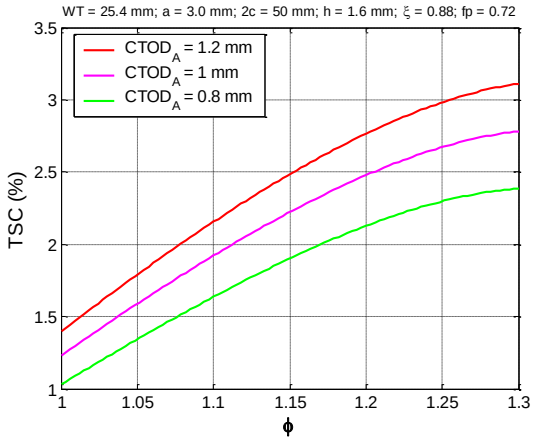

WT = 25.4 mm, FCAW

Figure 7-8 TSC as a function of weld strength mismatch

7.6 Sample Flaw Acceptance Criteria

Sample flaw acceptance criteria are generated using the $TSC_p(t)$ equations from the TSC target, apparent CTOD toughness δ_A, hi-low misalignment ψ, pipe material Y/T ratio ξ and weld strength mismatch ϕ. Figure 7-9 and Figure 7-10 show examples of such flaw acceptance graphs for GMAW, with 1.5% and 2.5% target TSCs, respectively. Similar examples of FCAW/SMAW are shown in Figure 7-11 and Figure 7-12.

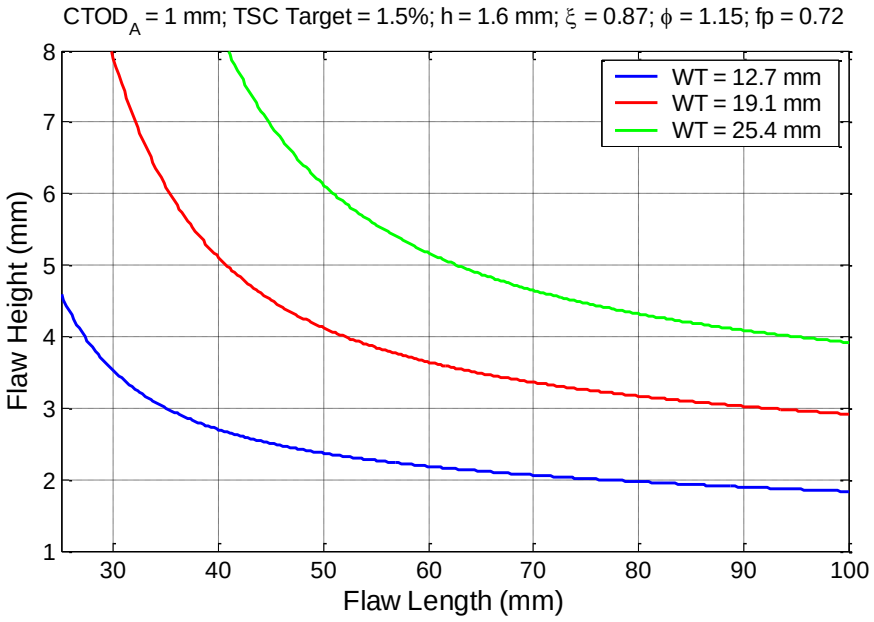

Figure 7-9 Flaw acceptance criteria, GMAW, 1.5% TSC target

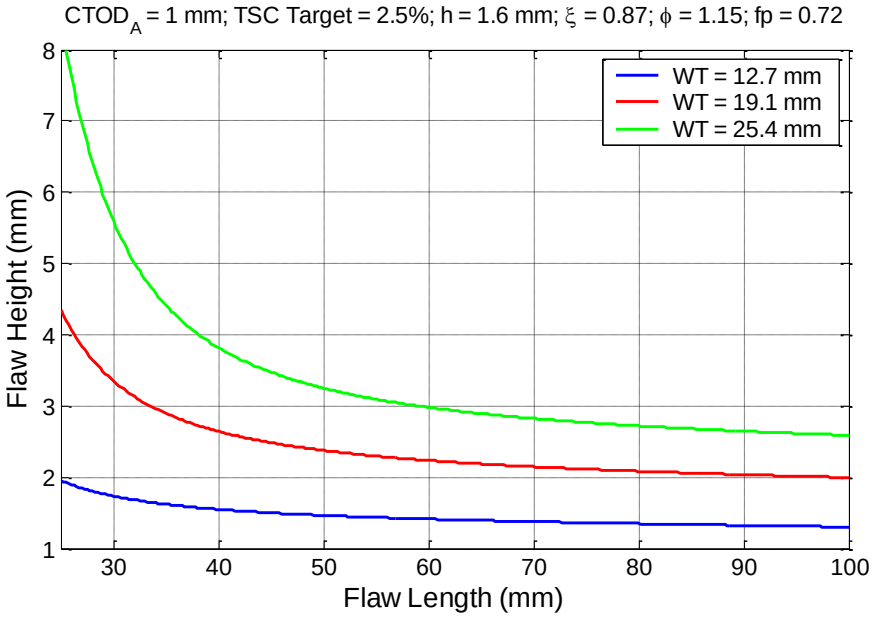

Figure 7-10 Flaw acceptance criteria, GMAW, 2.5% TSC target

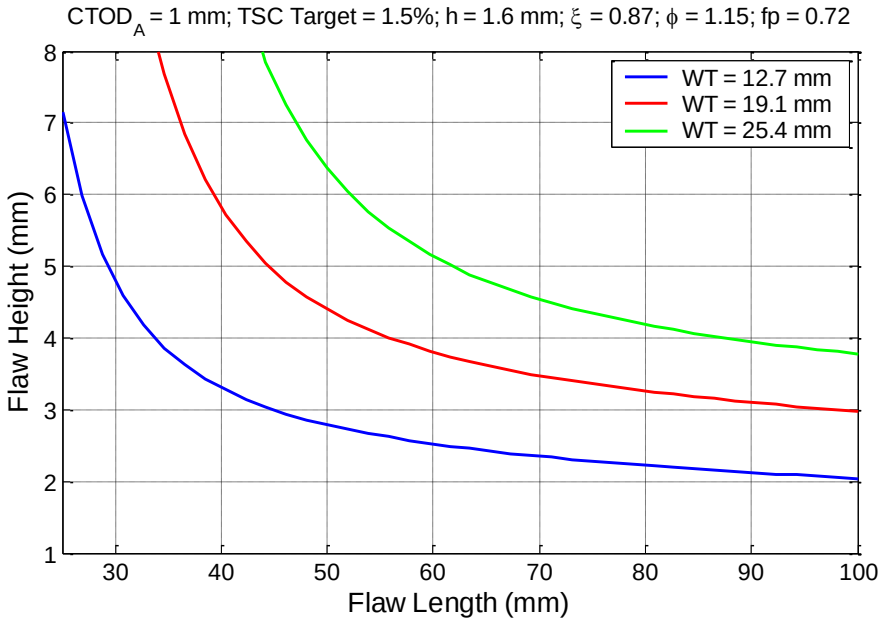

Figure 7-11 Flaw acceptance criteria, FCAW/SMAW, 1.5% TSC target

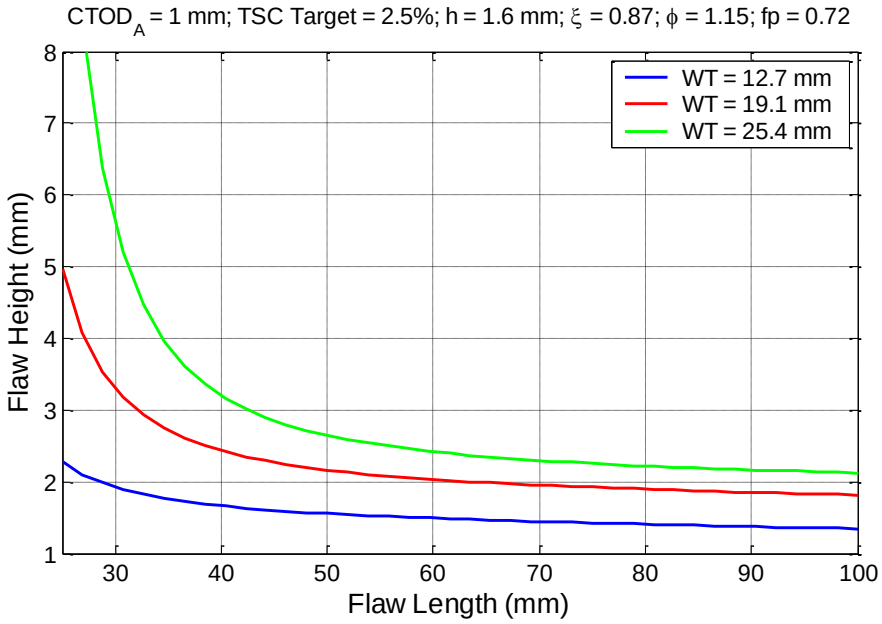

Figure 7-12 Flaw acceptance criteria, FCAW/SMAW, 2.5% TSC target

8 Concept of Apparent Toughness

8.1 Fundamentals of Apparent Toughness

8.1.1 Similitude of Crack-Tip Fields

The fundamental basis of fracture mechanics is the existence of the unique relationships between the crack-tip fields and the fracture parameters, such as the stress intensity factor *K*, *J*-Integral, and Crack Tip Opening Displacement (CTOD). When such unique relationships exist, the crack-tip fields of test specimens can be "transferred" to the structures being assessed through the fracture parameters, since those parameters uniquely represent the crack-tip fields.

8.1.2 Validity Limit on Fracture Toughness

The unique relationship between the crack-tip fields and the fracture parameters exist when the crack-tip plasticity is well-contained within the boundary of the specimens and/or structures. For fracture mechanics test specimens, such a unique relationship is enforced by specifying specimen "validity limit" as expressed in the following format:

$$J / \sigma_0 \le \frac{L}{\mu_{cr}}, \tag{8-1}$$

where L is the specimen ligament size, and μ_{cr} is 25 for bend specimen [39] and 200 for tension specimen with through wall crack [40,41]. The fracture mechanics parameter J may be converted to CTOD through the following relation [42]:

$$\delta = (0.5 - 0.7)\frac{J}{\sigma_0}. \tag{8-2}$$

If the ligament size L of a standard CTOD specimen is 25 mm (equivalent to tests done on a 25-mm wall thickness pipe), the maximum "valid" CTOD is 0.5-0.7 mm for bend specimens and less than 0.1 mm for tension specimens.

8.1.3 Toughness at the Point of Tensile Failure

When the final failure points of the large-scale test specimens are observed, it is generally found that the CTOD values associated with the final failures are well above 0.5 mm, sometimes much larger at 1.0-1.5 mm. These values are much greater than the single-parameter "valid" CTOD value (0.1 mm or less) as described in Section 8.1.2. This shows that the single-parameter approach to the welds typical of strain-based design is not valid from the rigorous viewpoint of fracture mechanics. The concept of apparent toughness is therefore necessary to apply the fracture mechanics principles. The term "apparent" implies that the traditional single-parameter based fracture mechanics was no longer strictly valid in the presence of large crack-tip plasticity. The apparent toughness represents the combined effects of the intrinsic material toughness and the structural behavior. Therefore it should not be a surprise that the value of the apparent toughness may be dependent on the flaw size, other structural dimensions, and perhaps material tensile properties. It is also necessary to recognize the applicable range of the apparent toughness derived from test specimens.

8.2 Apparent Toughness from High-Constraint Specimens

Figure 8-1 shows schematically the transition curves of a high constraint specimen and a low constraint structure. The parameter T_27J is the temperature corresponding to a Charpy value of 27 J. This parameter is taken from the Master Curve approach (ASTM standard) in order to put the temperature shift on a relative scale. The low constraint structure (e.g., girth weld under longitudinal loading) has lower transition temperatures and higher upper shelf toughness than the high constraint specimen (e.g., standard CTOD specimen). The toughness corresponding to the low constraint structure is the "apparent toughness." At a temperature greater than the lower shelf temperature, the apparent toughness is higher than that measured under the high constraint condition.

To obtain the apparent toughness from the high-constraint test data, it is necessary to determine the transition temperature shift and the increase in upper shelf toughness. A procedure was proposed by Wallin [43] to determine the transition temperature shift. For strain-based design, the material behavior has to be on the upper shelf. Therefore, it is more relevant to examine the increase of the upper shelf toughness or determine the "conversion factor" between the high-constraint test specimens and low-constraint test specimen or structures.

Wang, et al., examined the toughness conversion from standard toughness test specimens to low-constraint test specimens using constraint-sensitive fracture mechanics and experimental test data [44]. Some preliminary toughness conversion factors were proposed.

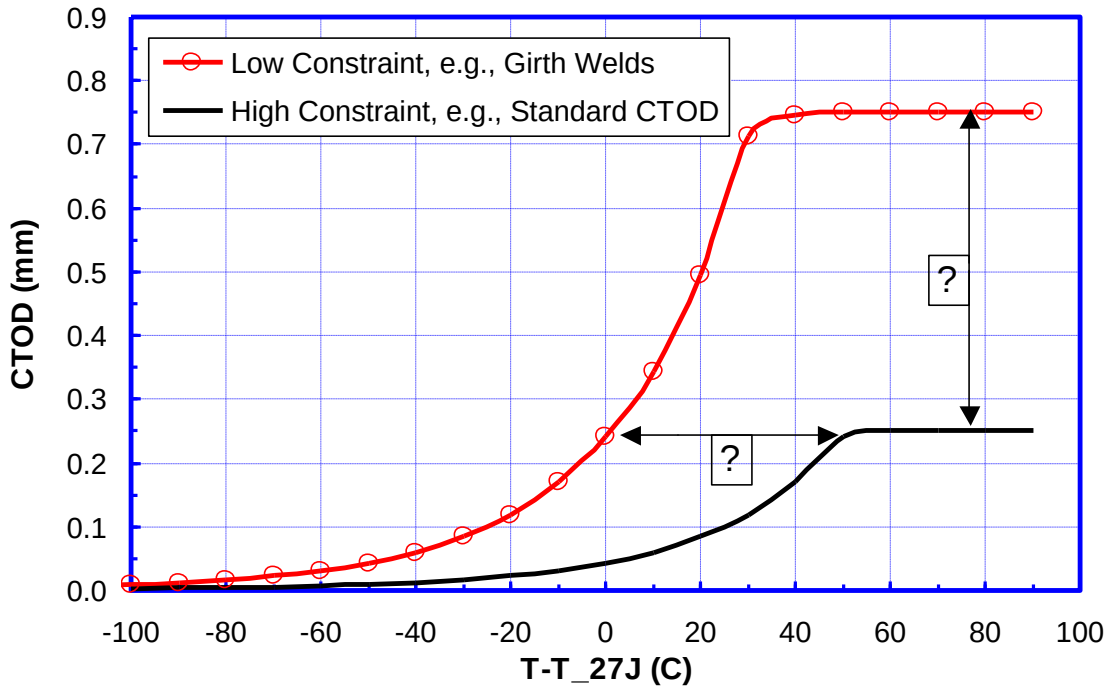

Figure 8-1 Schematic illustration of the constraint effect on fracture toughness. The test temperature (T) is subtracted by T_27J to show the relative temperature shift. The values are illustrative and not meant to depict any particular materials

8.3 Apparent Toughness from Resistance Curves

8.3.1 Physical Process of Resistance Measurement

The response of a flaw to tensile straining is schematically shown in Figure 8-2. Upon the initial straining, blunting occurs at the crack tip. A small sharp crack would initiate upon further straining. Continued straining would results in the growth of the sharp crack.

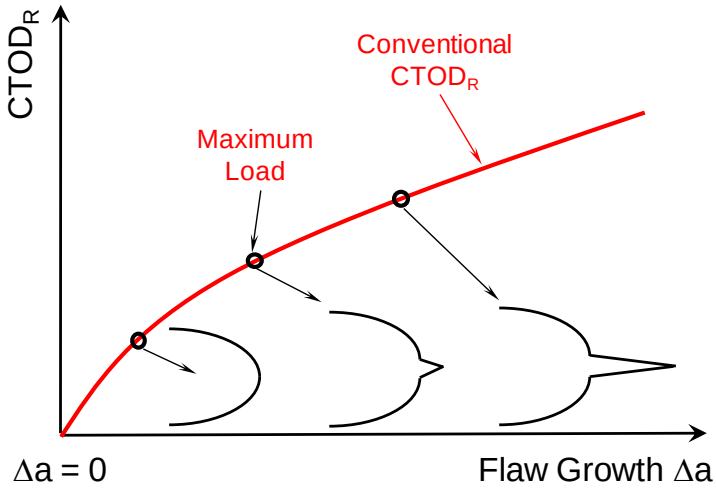

Figure 8-2 Schematic illustration of crack-tip profile vs. a conventional resistance curve

8.3.2 Contributing Factors to Apparent CTOD$_R$ and CTOD$_A$

An actual crack-tip profile from one of the full-scale test specimens is shown in Figure 8-3. This profile shows that the rise of a conventional CTOD$_R$ as the flaw grows comes from two parts: (1) blunting of the initial crack tip and (2) growth of the sharp crack. The first part is the blunting of the flaw which resulted from crack tip plastic deformation. The second part is the continued increase of crack mouth opening displacement associated with the advancing crack front. The contribution of the second part increases as the crack front advances (see Figure 8-2).

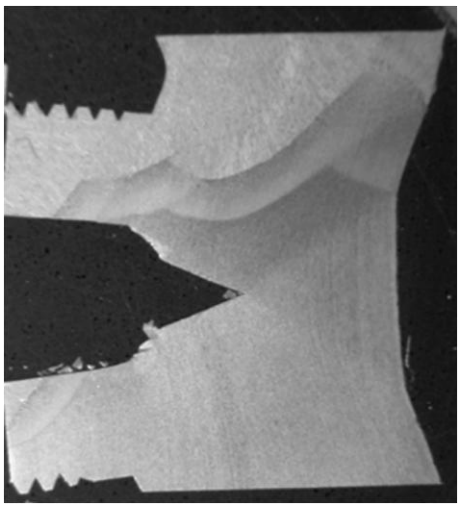

Figure 8-3 Crack-tip profile from a full-scale test specimen

The second part of the conventional $CTOD_R$ can be estimated through the use of CTOA, or crack tip opening angle (see Figure 8-4). From crack-tip profiles like those of Figure 8-3 and Figure 8-5, the contribution of advancing sharp crack is computed as CTOA multiplied by the amount of sharp crack advance, Δa_s (see Figure 8-4). The residual CTOD from the crack-tip blunting and the total residual CTOD from multiple full-scale X65 test specimens are shown in Figure 8-6.

It is evident from Figure 8-6 that the total residual CTOD follows the general trend of the conventional $CTOD_R$. The blunting part of $CTOD_R$ remains largely constant, even after a significant amount of flaw growth. The increase of conventional $CTOD_R$ after a small initial growth is largely attributable to the further opening from advancing crack front. The blunting part of $CTOD_R$ from weld center line flaws is smaller than that from HAZ flaws. This trend is consistent with the other measures of toughness, such as Charpy, traditional high-constraint CTOD, and low-constraint SENT resistance curve.

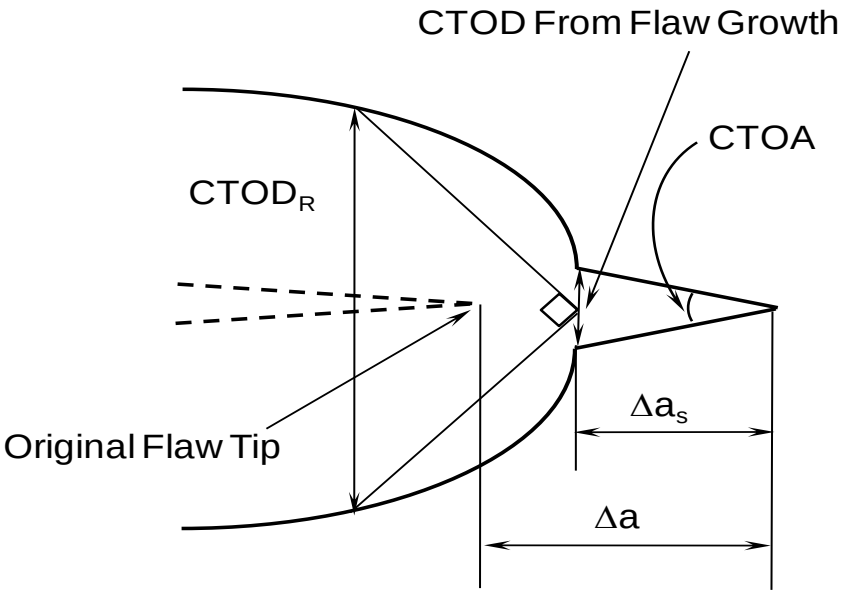

Figure 8-4 Crack opening with stable growth

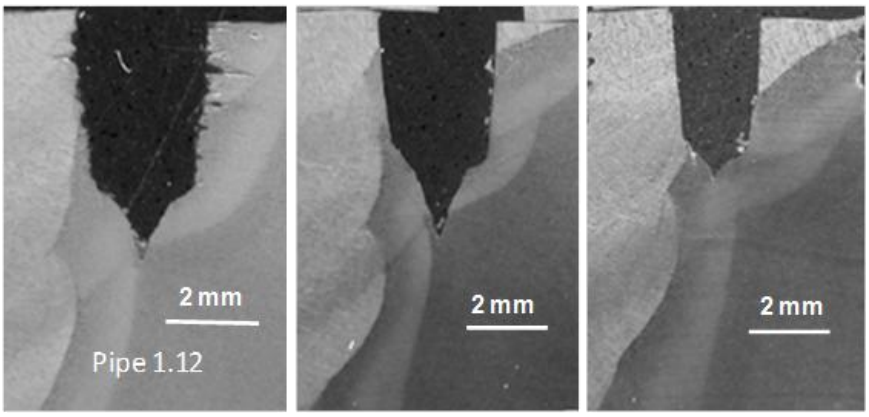

Figure 8-5 Crack-tip profile from multiple cuts along the flaw length

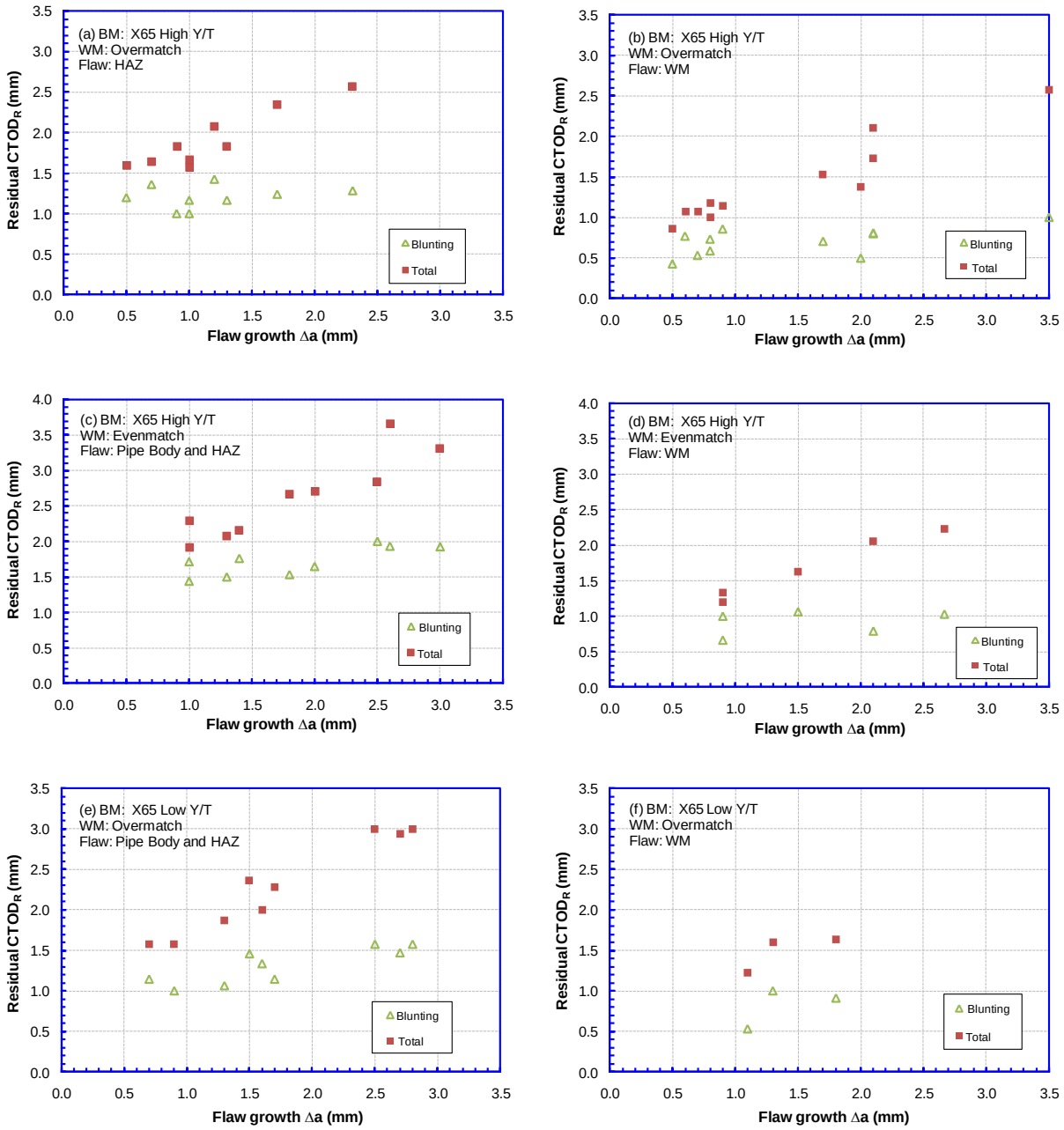

Figure 8-6 Residual CTOD as a function of flaw growth from full-scale specimens

8.3.3 Concept of Characteristic Flaw Growth

Liu, et al., analyzed the significance of the resistance curves [45]. A concept of apparent $CTOD_R$ was developed. The apparent $CTOD_R$ is the resistance calibrated to the original crack size, without crack growth. As shown in Figure 8-7, the apparent $CTOD_R$ saturates after a small amount of tearing (e.g. Δa = ~0.5 mm for this case), while the conventional $CTOD_R$ increases with flaw growth. The relatively constant value of the apparent $CTOD_R$ between 0.5 mm < Δa < 2.0 mm indicate that the apparent $CTOD_R$ obtained at a relatively small amount of flaw growth, can serve as a very close approximation to the $CTOD_A$ at the critical events. Furthermore, the relatively constant apparent $CTOD_R$ value also indicated that the material's resistance is largely

determined at the initial stage of the resistance curve. The increase of traditional $CTOD_R$ after a small initial growth is largely attributable to the advancing crack front.

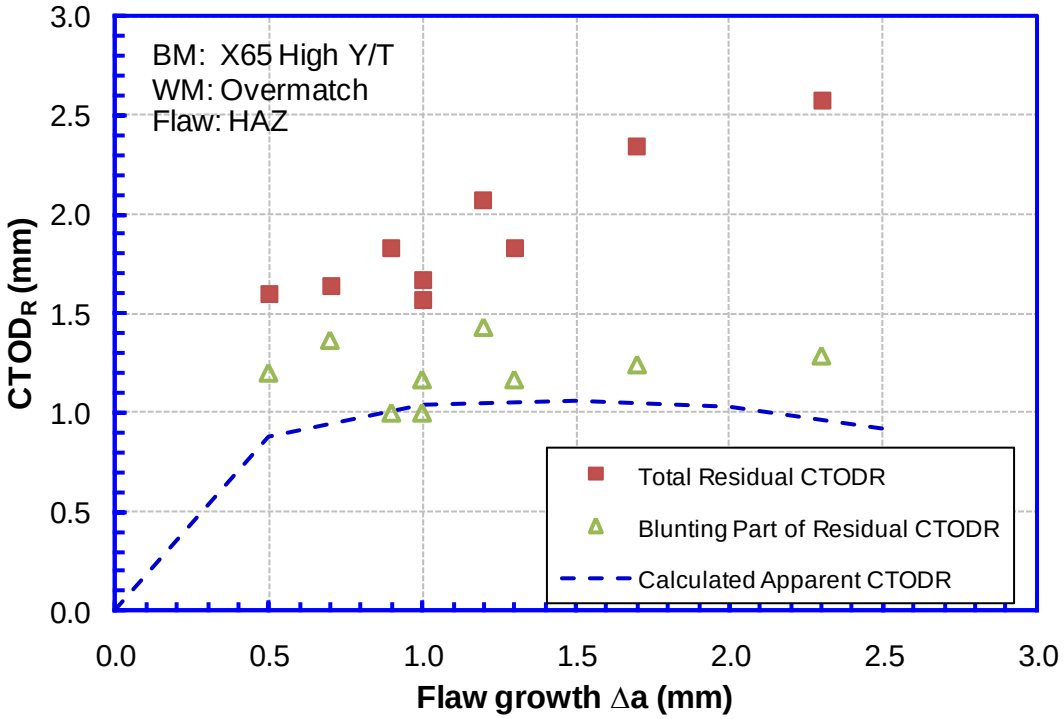

Figure 8-7 Resistance curves and their correspondence with the residual CTOD

8.4 Determination of Apparent Toughness

8.4.1 Apparent Toughness from Crack-Tip Profile

As a reference to the well-accepted CTOD definition, the crack tip profile from a standard three-point specimen is shown in Figure 8-8 [46]. The CTOD toughness associated with this crack profile (crack tip blunting) can be directly measured as shown in Figure 8-8.

As stated in Section 5, the apparent toughness ($CTOD_A$) is the initiation toughness which corresponds to the transition from flaw blunting to ductile tearing with a macroscopic sharp flaw. Similar to the conventional CTOD toughness (as shown in Figure 8-8), the apparent toughness ($CTOD_A$) can be measured directly from a crack-tip profile which contains finite ductile tearing as shown in Figure 8-9.

There are three important points to consider in the use of this approach. First, a small amount of sharp flaw growth is necessary to ensure that the full blunting has been exhausted. Secondly, the flaw profile should be obtained from structure-relevant test specimens, such as CWP and full-scale specimens. Small-scale specimens, such as SENT, may be used when the transferability of the specimens to the full-scale structure is accounted for (see Section 11). Thirdly, when the crack-tip profiles are taken from the crack-tip cross-section after the termination of a test, the crack tip opening is reduced from the elastic unloading. The effects of the unloading should be accounted for, as demonstrated later in Section 11.

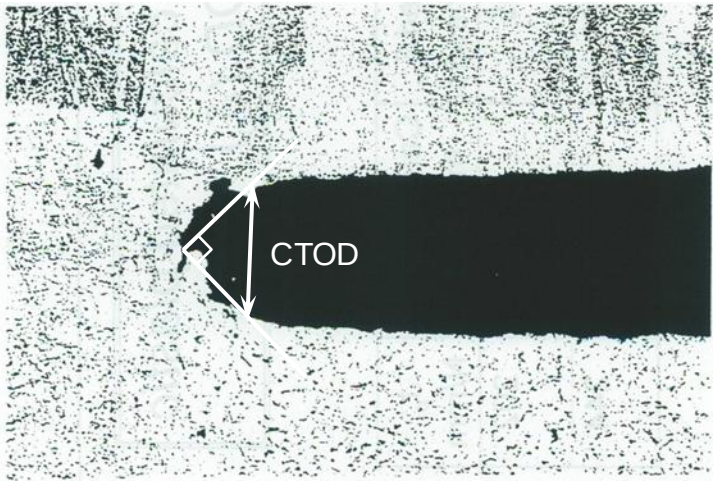

Figure 8-8 Determination of conventional CTOD toughness from crack-tip

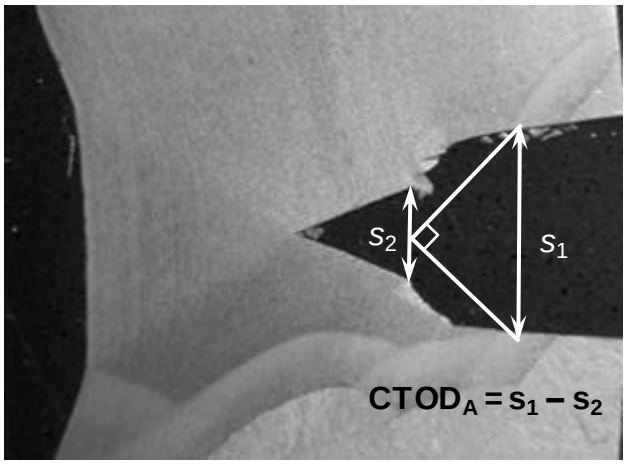

Figure 8-9 Determination of $CTOD_A$ from crack-tip with finite tearing

8.4.2 Direct Measurement from Small-Scale Specimen

Although the conventional CTOD toughness can be directly measured from the crack-tip profile in well-calibrated interrupted tests, this technique is not easy to use as a routine test procedure. Consequently, conventional CTOD tests are done by measuring load and CMOD displacement. The CTOD toughness is obtained from a set of correlation equations which relate the load vs. CMOD record with the CTOD.

The determination of $CTOD_A$ from a crack-tip profile is easier than that of conventional CTOD, as the tests do not have to be interrupted precisely. Some sharp flaw growth can be tolerated. The contribution of this sharp flaw growth can be subtracted to obtain a $CTOD_A$.

Techniques capable of measuring the transition from blunting to sharp flaw growth can be used to determine $CTOD_A$. One possibility is using the potential drop (PD) method to determine the transition between blunting and ductile tearing in low-constraint test specimens, such as SENT, shallow-notched SENB, or CWP specimens. In the PD test method a constant current power supply is connected to the test specimen and the voltage across the notch is monitored during the test. The PD response initially shows a linear increase in PD due to plasticity and crack tip blunting. As ductile tearing initiates and the remaining ligament starts to reduce in size

the PD trace exhibits an upward swing. The transition between blunting and ductile tearing corresponds to the start of the upswing in the PD trace.

The PD method is attractive, but not exercised in this project. Future work may address the following issues: (1) consistent generation of the PD trace among different labs and (2) transferability of toughness between low-constraint small-scale specimen, such as SENT and shallow-notched SENB, and large-scale structures, such as CWP and full-scale pipe. The second issue is further discussed in Section 11.

8.4.3 Apparent Toughness Converted from Standard Test Specimens

The analysis of Wang, et al., gives the conversion factor of 1.7 to 2.5 between the high-constraint standard CTOD test specimens to low-constraint test specimens [44]. Analysis of more recent data puts the conversion factor in the range of 1.5 -2.5.

8.4.4 Apparent Toughness from Resistance Curves

For SENT specimens, the maximum load in a test is usually achieved at a relatively small amount of flaw growth (see Figure 8-11) [47]. Subsequent (displacement-controlled) loading leads to continued growth of the sharp crack with some load drop.

The work of Liu, et al. [45] and Figure 8-7 show that there is characteristic flaw growth on a conventional resistance curve which can be used to determine the apparent toughness as shown in Figure 8-10. The use of the characteristic flaw growth is a practical method to determining the $CTOD_A$ when conventional CTOD resistance curve is available. The characteristic flaw growth is small, relative to the observed total flaw growth after the termination of tests. The use of this characteristic flaw growth does not contradict the observed large flaw growth in the tests.

The exact value of the characteristic flaw growth is dependent on the flaw size and the specimen dimensions. However, the range of this characteristic flaw growth is quite narrow. Presently, the characteristic flaw growth is estimated in the range of 0.5 to 1.0 mm. The characteristic flaw growth may be determined by comparing the resistance curves and the crack-tip flaw profiles as shown in Figure 8-9.

8.4.5 Apparent Toughness from Shallow-Notch SENB

Resistance curve testing was conducted at CANMET [48] on X100 base metal at room temperature and -20ºC. Both SENT and shallow-notched SENB specimens were tested. The primary difference between those two types of specimens is that the SENT specimens were loaded in tension and the SENB specimens were loaded in traditional three-point bending. The *J*-values at $\Delta a = 0.5$ mm were extracted for comparison (see Figure 8-12). The following observations can be made:

(1) The shallow-cracked SENT and SENB produced very similar results.

(2) The toughness difference between the deeply-cracked SENB and shallow-cracked SENT or SENB is about a factor of 1.7-1.8. This factor is similar to the toughness conversion factor of Section 8.4.3.

The similarity between the shallow-cracked SENB and SENT specimens introduces the possibility that the shallow-cracked SENB specimens may be used as a standardized specimen for directly obtaining the apparent toughness. The SENB specimens are easier to test in terms of

set up and test machine load requirements. There are standards readily available for testing SENB specimens.

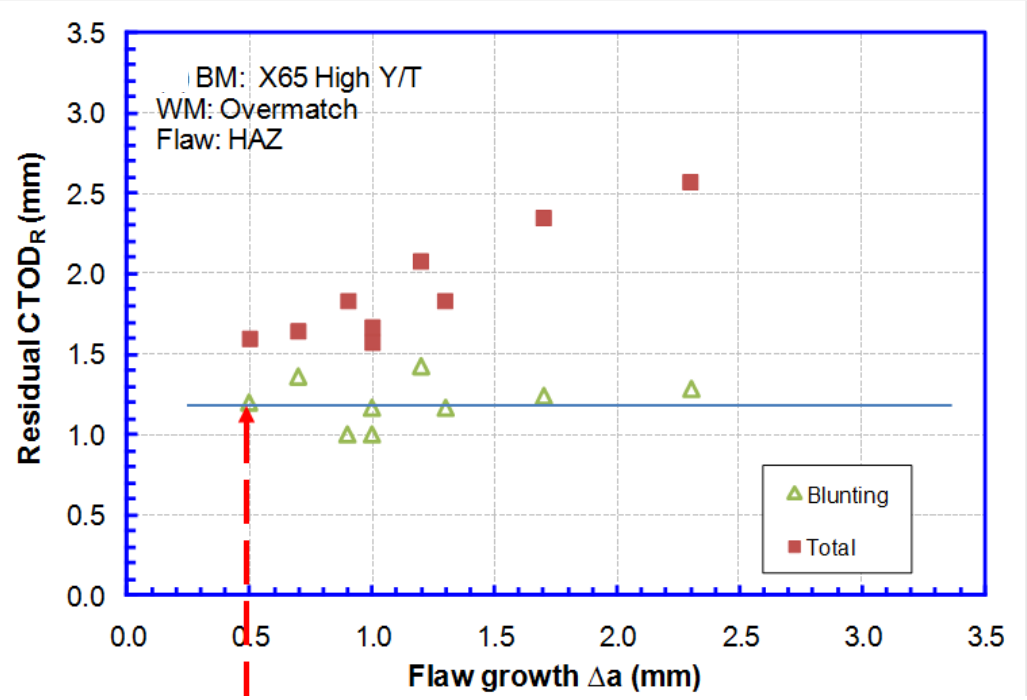

Figure 8-10 Determination of $CTOD_A$ from conventional $CTOD_R$

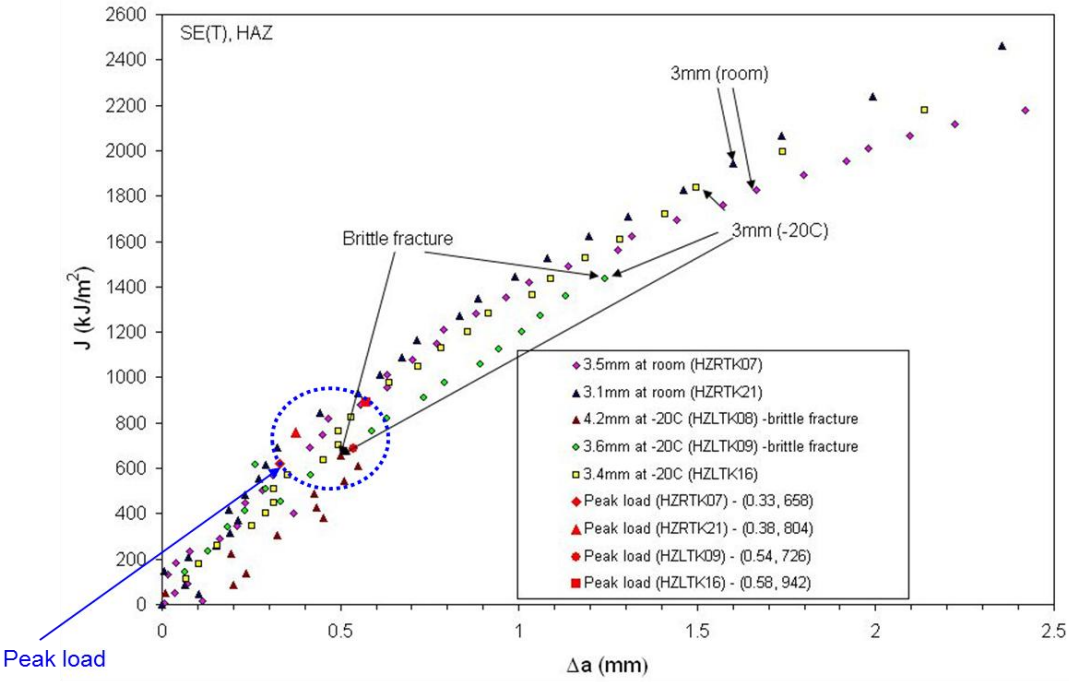

Figure 8-11 Resistance curves measured from SENT specimens of X100 girth welds with ¾" wall thickness [47]

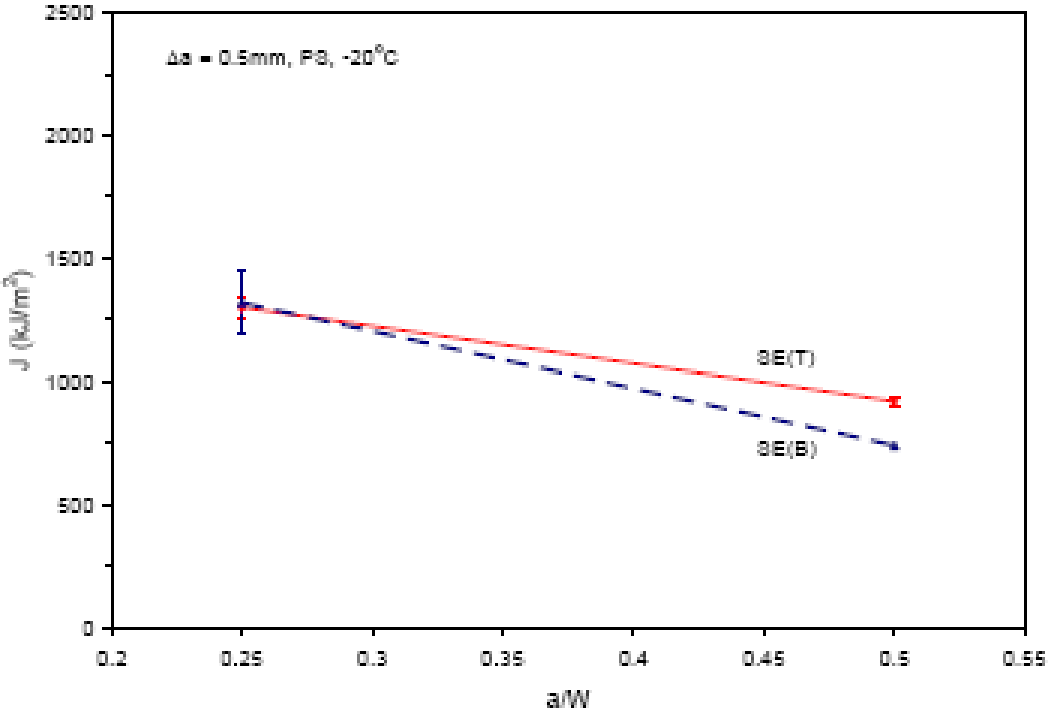

(a)

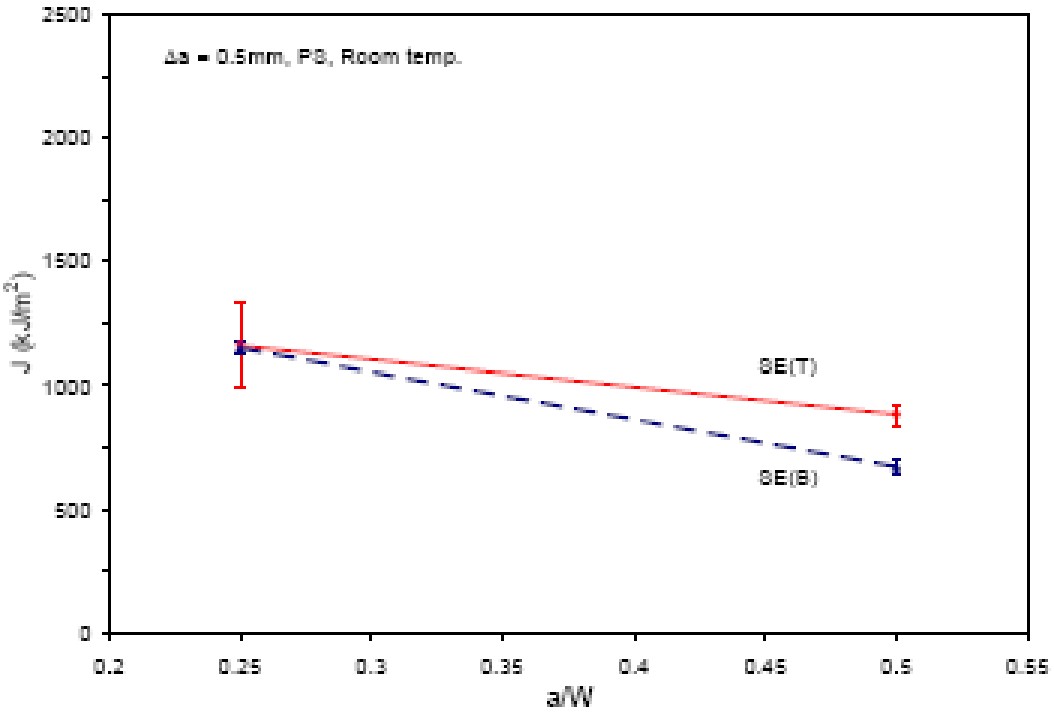

(b)

Figure 8-12 Comparison of toughness from SE(T) and SE(B) specimens [48]

9 Tensile Strain Design Procedures

9.1 Introduction

This section covers the central output of this program, the tensile strain design procedures. The tensile strain design procedures are principally used for the strain-based design of pipelines when the applied longitudinal strain on the pipelines exceeds the yield strain (typically defined as 0.5% total strain). The strain-based design is complementary to a typical stress-based design, which focuses on the control of hoop stress of the pipelines.

The tensile strain design procedures involve three essential elements: (1) linepipe specification, (2) welding procedure qualification, and (3) tensile strain design models. The main focus of this project is the third element, i.e., tensile strain design models. Some key issues in the other two elements are also covered in this section. These issues are selected on the basis of two criteria: (1) they are not sufficiently addressed in the current codes and standards and/or (2) they are not sufficiently recognized in the current industry practice.

The tensile strain design procedures consist of recommendations in the three essential elements. In most cases, background information and rationale are provided along with the recommendations. The recommendations are not meant to be all-inclusive. Appropriate national and international standards should be followed in conjunction with the recommendations presented here.

The field of strain-based design is very much a still evolving engineering discipline. Although significant progress has been made in the past decades, there is much more to be discovered and confirmed.

One critical difference between strain-based design and traditional stress-based design is that much more material information is needed for strain-based design. Furthermore, the information often needs to be defined in greater detail and higher precision in the strain-based design than in the stress-based design. Expert advice may be needed in some cases to bridge the gap between the current industry practice and the additional requirements needed for the strain-based design.

All phases of a pipeline life, including installation, commissioning, and operation should be considered to ensure safe operation throughout its' entire design life.

The tensile strain design procedures in this section are principally intended for new pipeline construction. The procedures can, in principle, be applied to the maintenance and integrity management of existing pipelines. The data required to apply the procedures to existing pipelines may not be readily available. It is possible, however, to use conservatively estimated input parameters to obtain generally conservative assessment of existing pipelines. However, it is not advisable to pile one layer of conservatism on top of other layers of conservatism. Doing so would produce unnecessarily conservative and impractical assessment results.

9.2 Overall Steps for Tensile Strain Design

The overall tensile strain design process may involve the following steps. The steps are intended to highlight some of the key considerations. They are, by no means, to be all-inclusive. Not all steps are applicable in all situations.

1. *Determine the nature of the strain demand*. The strain demand could be a one-time event, such as the strain at a fault crossing in a seismic event. The strain demand can vary and/or accumulate over time, such as in the case of frost heave and thaw settlement. Strain demand in the area of mine subsidence could be a one-time event or a time-dependent accumulative event.
2. *Determine and classify postulated failure events*. In some cases, the most critical event might be in the construction/installation phase, such as an offshore installation by reeling. For most onshore pipelines, the operation phase is the most critical as the tensile strain capacity is reduced by the internal pressure.
3. *Determine a set of target tensile strain capacity levels by introducing appropriate safety factors to the estimated strain demand.*
4. *Collect basic design and material information which affect the tensile strain capacity*. Some of the key parameters are (but are not limited to): (1) pipe wall thickness, (2) pipe tensile properties, (3) weld tensile properties, (4) weld toughness, (5) pipe dimensional tolerance, (6) field control of high-low misalignment, (7) target acceptable flaw size, and (8) inspection method.
5. *Determine if there are time-dependent degradation mechanisms of the material properties, such as strain aging or hydrogen embrittlement*. If present, these mechanisms should be considered. The effects of the material property degradation may be incorporated into the material qualification phases or monitored as a part of the pipeline integrity management program.
6. *Conduct a preliminary assessment of the tensile strain limit state for all postulated failure events*. A target category of tensile strain behavior may be selected (see Section 4). For a small project, in which the material property variations can be well defined, conditions for Category I behavior, i.e., ensuring the postulated failure locations in the pipe body, may be explored.
7. *Select an appropriate level of the tensile strain procedures if Category III behavior is targeted*. This may be done by balancing the needs for accuracy and the requirements for material property data, flaw size, and construction quality control. The higher the required accuracy, the greater the need for detailed material qualification.
8. *Develop linepipe specifications and welding procedure requirements based on the input requirements of the tensile strain design models*.
9. *Conduct material characterization tests per the requirements of No. 8*.
10. *Evaluate tensile strain capacity against the target values, taking into consideration the material property variations from No. 9*.
11. *Conduct confirmation tests of the tensile strain capacity when needed*.
12. *Develop and implement material property surveillance protocol if time-dependent degradation mechanisms exist and their effects are not fully covered in the material qualification phase*.

13. *Develop and implement strain demand monitoring systems. When needed, verify the reliability and accuracy of such systems.*
14. *Develop and implement continuous evaluation and mitigation plans if the strain demand and material properties evolve over time*.

Some of the above steps may be iterated in the design phase or in the maintenance and integrity management phase.

9.3 Generic Issues Related to Material Property Characterization

A few generic issues related to material qualification and testing are described here. The brief description presented here is intended to highlight the issues. The full coverage of those issues may be found in relevant publications and literature.

9.3.1 Material Test Temperature

Material test temperature affects the measured tensile and toughness properties. For instance, tests done within this program have shown that that both linepipe and weld metal can have high strain hardening capacity and greater uniform elongation at -20ºC than the corresponding properties at room temperature. There is some evidence that the fracture resistance curve may also increase at a cold temperature from that at the room temperature, possibly related to the rise of material's strain hardening at the cold temperature. In general, the material test temperature should be selected to correlate with the postulated failure events.

9.3.2 Hydrogen Embrittlement

Some steels may be susceptible to hydrogen embrittlement. Hydrogen may be present in the welding phase, or in the operation phase, from cathodic protection or sour service environment. In the case of possible hydrogen embrittlement from welding, the elapsed time between the completion of the welding and the qualification testing shall be appropriately selected to represent the possible elapsed time in field construction conditions. The hydrogen level of the test coupons should be at least as high as the expected hydrogen level of the field welds when those welds are subjected to the postulated high-strain events, such as reeling strains. Similar principles should be applied to the testing of materials for hydrogen environment in the operation phase. For instance, it may be necessary to pre-charge hydrogen into test specimens in the material qualification phase.

9.3.3 Cyclic Plastic Strain

Cyclic plastic strains may affect materials' tensile and toughness properties. If a postulated failure event is to occur after cyclic plastic straining, such as the postulated failure during a seismic event, the material properties may be different from those obtained at the material qualification phase. The evolution of the material property as a function of cyclic strain should be considered. For instance, some building design codes consider the effects of cyclic plastic strain when designing against earthquakes.

9.3.4 Tensile Test Data and Test Form

Tensile test data are affected by specimen dimensions, instrumentation setup, and even post-test data processing. For instance, the total elongation from round bar specimens is lower than that from rectangular cross-section specimens of the same material. A material specification

should include both required property values and the test protocols to be used to generate the data.

9.3.5 Low-Constraint Toughness Test

Low-constraint toughness tests, particularly SENT tests, are gaining popularity. Under certain conditions, such tests provide toughness data which are more representative of the pipeline girth welds than traditional deeply-notched SENB specimens. It should be recognized that there are multiple test procedures in public domain. None of them are yet recognized by the traditional test standard organizations, such as ASTM, BSI, and ISO. These procedures could produce different results even if the material behavior is the same. For instance, DNV-RP-F108 specifies 2B×B specimen dimensions and the tests are done in multiple specimen form. The toughness is represented by *J*-integral which is computed from load vs. CMOD trace. CANMET SENT test procedure calls for B×B specimen dimensions and the tests are done in single specimen form. Both *J* and CTOD can be obtained from its procedure, using the load vs. CMOD trace similar to that of DNV procedure. An ExxonMobil procedure recognizes only CTOD and its CTOD is computed near the original crack tip location (i.e., at initial flaw depth) using a triangulation method from double-clip gage measurement.

The effect of test procedures on test results should be considered in material specifications. The specifications should include both required property values and the test protocols to be used to generate the data.

9.3.6 Property Variations of Nominally the Same Material

Both tensile and toughness properties can have variations at the same grade or strength level. The tensile property variations of linepipe and weld lead to a range of weld strength mismatch levels. Toughness properties are affected by notch location and notch depth. These variations should be considered in the design and material selections.

9.4 Welding Procedure Qualification for Girth Weld

9.4.1 Scope of the Welding Procedure Qualification

A welding procedure qualification usually involves (1) making welds which cover all expected field welding conditions per welding essential variable requirements and (2) subjecting the completed welds to a set of mechanical tests to confirm their properties. The welding essential variables and scope of the mechanical tests are usually defined in relevant codes and standards. In North America, the governing standards are API 1104 and CSA Z662.

The focus of this section is the mechanical property testing.

9.4.2 Key Issues Related to Girth Welding Procedure Qualification

9.4.2.1 Cross Weld Tensile Test

Background and Rationale

Procedures for cross-weld tensile tests are well established. In the current API 1104 Appendix A requirements, the test specimens are permitted to fail in the weld, provided that the tensile strength meets the minimum UTS requirement of the pipe. This leaves the possibility of weld strength undermatching the strength of pipe. In strain based design, strain concentration in

the weld should not be allowed. This, in general terms, implies that the weld strength should be greater than the pipe strength.

In narrow-groove mechanized welds, where the weld width is less than the pipe wall thickness, failure outside the weld is possible even when the all-weld metal strength is lower than the pipe strength by a small margin, as the weld deformation is constrained by the stronger surrounding materials. This is particularly true if the weld reinforcement is not removed in the cross-weld tensile tests.

The current version API 1104 only makes distinction between two possible failure locations, weld or base metal. It is not clear if a failure in the HAZ adjacent to the fusion boundary should be classified as weld or base metal failure. For the purpose of this document, a failure in the HAZ is grouped as a weld failure.

As stated early, there should not be gross weld strength undermatching in strain-based design. A test procedure is needed to qualify such a condition.

Recommendations

The cross-weld tensile specimen form can be taken from that of API 1104 Appendix A. The concept of 2*t*-strain (see Figure 9-1), where *t* is the pipe wall thickness, strain may be used to measure and quantify the strain in the weld region [49]. The gage of the 2*t*-strain measurement is centered at the weld and covers both the deposited weld metal and the HAZ.

The strain in the 2*t* gage section should be no more than the remote strain in the base pipe at any point after the base pipe strain reaches more than 1.0%. The measured strains at low stress level may contain variations which make the comparison of the 2*t*-strain and the pipe strain difficult. Therefore, the comparison of the strains is performed after the base material passes the yield point.

A data check, similar to that for the pipe tensile test, should be performed to ensure data consistency and accuracy.

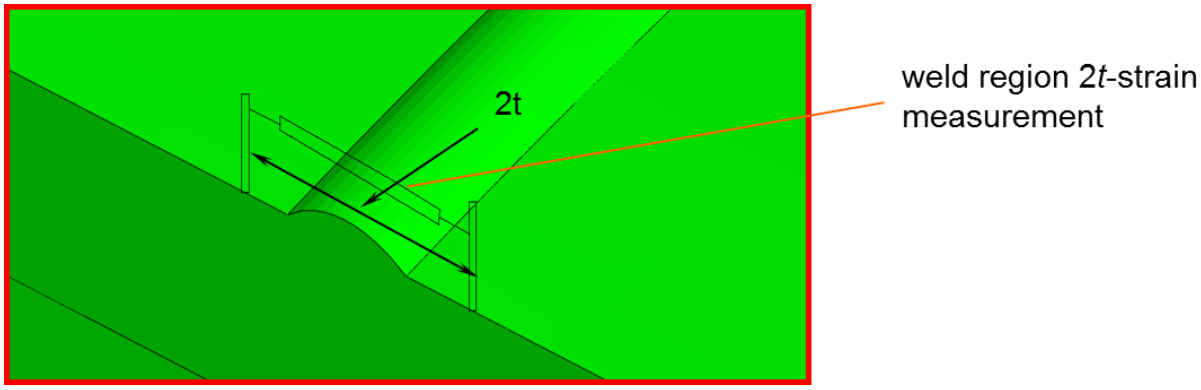

Figure 9-1 Schematic of the concept of 2*t*-strain measurement

9.4.2.2 All-Weld-Metal Tensile Test

Background and Rationale

Work performed at CANMET has shown that the all weld metal tensile test results depend on test specimen form (round bar vs. rectangular strip) and location of the specimen extraction (ID vs. OD biased).

Recommendations

Near-full thickness strip specimens should be tested per CANMET procedure [50].

A data check, similar to that used for the pipe tensile test, should be performed to ensure consistency and accuracy.

9.4.2.3 Charpy Transition Curve

Background and Rationale

The Charpy transition curve tests serve two purposes: (1) establishing the ductile-to-brittle transition temperature and (2) determining the upper shelf impact energy for the estimation of apparent CTOD toughness for the initial screening.

Recommendations

The specimen form and location should follow those in API 1104 Appendix A.

Two sets of tests should be performed. The first set consists of testing specimens of three o'clock positions at the minimum design temperature or lower, as specified in API 1104 Appendix A. The second set consists of testing specimens at one selected o'clock position at multiple temperatures to establish the transition curves.

The transition curves may be established by testing at a minimum of 5 to 6 temperatures. A set of three specimens should be tested at each temperature for each notch location (weld centerline vs. HAZ).

A suitable fit of the transition curves may be performed to develop an average transition curve for HAZ and weld centerline notched specimens, respectively.

9.4.2.4 CTOD Testing of Deeply-Notched SENB, Single Value

Background and Rationale

The testing of standard deeply-notched SENB specimens is well established. For strain-based design, the most relevant CTOD toughness is the toughness corresponding to the maximum load, or δ_m.

Recommendations

The specimen form and dimension should follow those found in API 1104 Appendix A.

The load vs. CMOD trace of the test specimen can be very flat near the point of maximum load. A curve fit near the maximum load point should be performed to smooth out local oscillations in load level and determine the maximum load point from the fitted curve.

9.4.2.5 CTOD Testing of Shallow-Notched SENB, Single Value

Background and Rationale

In comparison to deeply-notched SENB, shallow-notched SENB specimens can have the same low-constraint crack-tip conditions as a girth weld flaw, when the pipe is under tension or global bending.

Recommendations

The testing of shallow-notched SENB should follow the ASTM E1820 standard and its equivalent ISO standard.

The B×B specimen should be surface-notched with a target final flaw depth ratio of 0.25-0.35. The minimum flaw depth should be 3 mm.

The flaws should be fatigue sharpened prior to testing.

9.4.2.6 Resistance Curve Testing

Background and Rationale

The resistance curves may be obtained from (1) deeply-notched SENB, (2) shallow-notched SENB, (3) SENT, and (4) CWP. The deeply-notched SENB has the highest crack-tip constraint conditions. The resistance from this specimen can be overly conservative in predicting the girth weld behavior. The testing of CWP specimens will be covered in a separate project [51].

Recommendations – Specimen Form

The deeply-notched SENB specimens should be tested in B×2B configurations with through-wall notched flaws in accordance with ASTM E1820 and/or BS 7448.

The shallow-notched SENB specimens should be tested in B×B configurations with surface-notches of a target flaw depth ratio of 0.25-0.35. The minimum flaw depth should be 3 mm.

The SENT specimens should be tested in B×B configurations with surface-notches of a target flaw depth ratio of 0.25-0.35. The minimum flaw depth should be 3 mm.

All small-scale test specimens, including the deeply-notched SENB, shallow-notched SENB, and SENT, shall be fatigue sharpened.

Recommendations – Test Temperature

The test temperature should be determined by considering the postulated failure events. When upper shelf behavior is expected, testing at a low temperature may produce higher resistance curves than those at room temperature.

Recommendations – Data Requirements

No brittle fracture should occur prior to the maximum load.

A sufficient flaw extension, commensurate to the flaw extension at the predicted instability point of the pipe, should be obtained.

When the resistance curves are used to determine the apparent CTOD toughness, a sufficient flaw extension should be obtained beyond the flaw extension point at which the apparent toughness is determined.

9.4.3 Confirmation Tests

9.4.3.1 Curved Wide Plate Test

The procedure for the curved wide plate tests will be provided in another project report [51].

9.4.3.2 Full-Scale Test

Recommendations

The specimen dimensions, flaw spacing, and instrument plan should follow the general procedures developed within this project. The procedures are fully covered in the Project 1 report [2].

When multiple girth welds exist in a single test specimen, each section of the base pipe (pup) should be individually monitored to gage the variation of strains.

The test temperature should closely emulate the conditions of the postulated events.

There are no standardized data acquisition and post-test data analysis procedures. Since the reported test data can be significantly affected by the details of the data acquisition and post-test data analysis procedure, it is imperative that the details of tests be available for review, if the test results are to be accepted as valid confirmation tests.

9.5 Tensile Strain Design Models

9.5.1 Scope and Limitations

The tensile strain design models were developed within the framework established in Section 5. A few essential features of the models are as follows:

(1) Two limit states are recognized: (a) initiation control and (b) ductile instability.

(2) Two weld bevel geometries are recognized: (a) narrow-groove, typical of mechanized GMAW welds and (b) standard groove, typical of FCAW and SMAW welds.

(3) The pipes are assumed to have uniform and isotropic tensile properties.

(4) The pipes on either side of the girth welds are assumed to have the same properties.

(5) There are no inherent limits on pipe grade. The linepipe tensile properties are represented by its longitudinal *Y*/*T* ratio, which serves as a representation of linepipe's strain hardening capacity.

(6) The predictive equations have no embedded safety factor.

(7) The welds should not have gross strength undermatching.

(8) The target optimum strain range of the models is from 1.0% to one half of the pipe's uniform elongation.

(9) The models are applicable to one single flaw in a girth weld. If multiple flaws were to exist in a single girth weld, the flaws need to be sufficiently far apart so the existence of other flaws does not affect the behavior of the flaw being evaluated.

(10) No flaw interaction rules are established and applied in the models.

(11) The models should not be used for flaw acceptance after repair welding without further evaluation.

(12) The potential impact of material anisotropy on the tensile strain capacity is not considered in the models.

It should be noted that the tensile strain models were not based on any particular pipe grades. The fundamental basis of the models is fracture mechanics. The parametric representation of the tensile property of the linepipes and welds were developed using a material database which covered grades from X65 to X100. The tensile strain models are, in principle, applicable to all

GMAW and FCAW/SMAW processes, provided that appropriate mechanical property data are within the applicable range of the models.

9.5.2 Overarching Considerations for the Tensile Strain Design Models

The tensile strain design models are designed with the following principles.

(1) *A flexible framework is established for the adoption of current technology and the incorporation of future development*. Tensile strain design is still an evolving engineering discipline. A number of potentially valid approaches are being developed. The flexible framework allows for the incorporation of those approaches as they become mature. One example of the flexibility is the use of both CTOD and *J*-integral as fracture mechanics parameters. At the present time, CTOD is established as the fracture mechanics parameter. The models can be easily converted to use *J* as the fracture mechanics parameter. The offshore industry has been moving towards *J*-based assessment methodology in recent years.

(2) *The most appropriate approach for the tensile strain design of a particular project depends on the scale of the project and many design and maintenance considerations*. No single approach may be appropriate for all projects. There could be tradeoffs between extensive material property testing and qualification versus simply "overdesign" of the system. For instance, lower grades and thicker walls may be used to achieve high strain capacity with a simplified welding procedure qualification.

(3) *The four levels of tensile strain design models may be used with a wide variety of material toughness test options*. The material toughness options have been applied by the pipeline industry for many years. Having those options available affords flexibility, particularly when a new form of test cannot be performed.

(4) *There are no embedded hard-set parameters*. In some cases, hard-setting input parameters, such as Y/T ratio and high-low misalignment to tensile strain design models, can produce overly conservative predictions of tensile strain capacity, while limiting the use of the models in other cases.

(5) *Almost all levels of the tensile strain models are driven by the same sets of equations*. The selection of the levels is predominantly dependent on the type of toughness data available, or data which will be generated. Higher level and more sophisticated toughness tests may generate more accurate data. In certain cases, such high accuracy may not be needed when the strain capacity is higher than the strain demand by a sufficient margin, using conservative assessments.

9.5.3 Structure of the Tensile Strain Design Models

Much of the tensile strain design models are driven by a library of parametric equations which give the tensile strain capacity as a function of a number of input parameters.

The input parameters are as follows:

(1) Weld type, either narrow groove GMAW or standard groove FCAW/SMAW,

(2) Pipe wall thickness,

(3) Pipe longitudinal Y/T ratio,

(4) Weld strength mismatch,

(5) Girth weld high-low misalignment,

(6) Flaw depth,

(7) Flaw length,

(8) Apparent toughness or resistance curve, and

(9) Internal pressure.

The details of the parametric equations are given in Section 7.

9.5.4 Application of the Tensile Strain Design Models

The tensile strain design models may be used for the following purposes:

(1) The determination of tensile strain capacity for given material properties and flaw size.

(2) The determination of flaw acceptance criteria for given material properties and target tensile strain level.

(3) The selection of material properties to achieve a target strain capacity for a given flaw size.

(4) The optimization of the tensile strain capacity by balancing the requirements of material parameters, such as weld strength (thus weld strength mismatch level) versus toughness.

9.5.5 Multi-Level Tensile Strain Design Models

9.5.5.1 Level 1 Models – Initial Screening and Feasibility Studies

The Level 1 model is intended for a quick estimation of the likely tensile strain capacity. The TSC is tabulated for selected pipe dimensions, material properties, and flaw size. The apparent toughness is estimated from upper shelf Charpy impact energy. The full TSC table is given in Appendix A.

9.5.5.2 Level 2 Models – Nominal Assessment with Standard Toughness Data

The Level 2 models are given in a library of parametric equations, as shown in Section 7. The apparent toughness is estimated from either upper shelf Charpy impact energy or the upper shelf standard CTOD toughness.

9.5.5.3 Level 3 Models – Advanced Assessment with Low-Constraint Toughness

The Level 3 models have two options. Level 3a uses an initiation control limit state. Level 3b uses a ductile instability limit state.

In Level 3a, the TSC is given by the same library of parametric equations as in Level 2. The apparent toughness may be obtained by a number of low constraint test options. They include shallow-notched SENB, SENT, and CWP.

In Level 3b, the crack driving force, $CTOD_F$, is expressed by a group of iso-strain curves constructed from the same library of parametric equations as are provided in Section 7. In this application, various levels of strains are given as a function of flaw depth from the equations. The resistance curve, often expressed in an equation form with two fitted parameters, is plotted on the same $CTOD_F$ vs. flaw depth chart, as shown in Figure 5-6.

The resistance curves may be obtained from small-scale low-constraint test specimens, shallow-notched SENB and SENT. There is some evidence, however, that such resistance curves may not represent the resistance behavior of large-scale specimens, such as CWP and full-scale specimens. However, the use of the small-scale resistance is conservative, provided that the driving force and the resistance are defined and computed in the same manner.

Similarly, resistance curves from CWP specimens may be used. Obtaining resistance curves from large-scale specimens requires great care in the initial raw data generation from the tests and the post-test data processing. Additional information on the CWP testing and data processing will be available in another project report [51].

9.5.5.4 Level 4 Models – Advanced Analysis with Direct FEA Calculation

The Level4 models are structured in two options, similar to that of Level 3. In contrast to Level 3 models, where the driving force relations are expressed in parametric equations, the driving force relations are directly obtained from FEA in this level. The use of the driving force relations is the same as it is in the Level 3 models.

This option allows for special cases when the specific weld geometry and material property conditions do not allow the use of the first three options.

The Level 4 models should only be exercised by seasoned experts. A demonstrated history of consistently generating the crack driving force is necessary. There are many parameters which affect the computed crack driving forces, including but not limited to, FE mesh density and distribution throughout the model, input format of material tensile properties, and data extraction and post-processing of FEA results. Consequently, the FE modeling procedure should be fully documented. The modeling procedure should be verified by applying it in order to generate crack-driving force relations of known cases.

9.5.6 Determination of Apparent Toughness

9.5.6.1 Apparent Toughness from Upper Shelf Charpy Energy[2]

The apparent toughness may be obtained from upper shelf Charpy energy by the following relations:

$$CTOD_A = \left(0.0080 \cdot \frac{Y}{T} - 0.0014\right) \cdot CVN_{us} \text{ for X52 to X65, and}$$

$$CTOD_A = \left(0.0086 \cdot \frac{Y}{T} - 0.0021\right) \cdot CVN_{us} \text{ for X70 and X80,}$$

where the units of the Charpy energy and $CTOD_A$ are ft-lbf and mm, respectively. The graphical representation of the X80 relation is shown in Figure 9-2. The relation should only be used for $CTOD_A$ up to 1.2 mm.

The upper shelf Charpy energy to $CTOD_A$ conversion is obtained through two steps:

[2] Although Charpy to fracture toughness conversions are widely used in many industries, the conversion procedures are highly empirical. These procedures are typically only applicable to the range of materials from which the conversion procedures are developed. The conversion procedures shown here are not universal and should not be viewed as such. The users are strongly advised to confirm the relations using directly measured upper shelf Charpy energy and $CTOD_A$ for their materials of interest.

(1) Converting upper shelf Charpy energy to conventional high-constraint CTOD using a published relation [52], and

(2) Converting the high-constraint CTOD to low-constraint $CTOD_A$ using a conversion factor of 1.75.

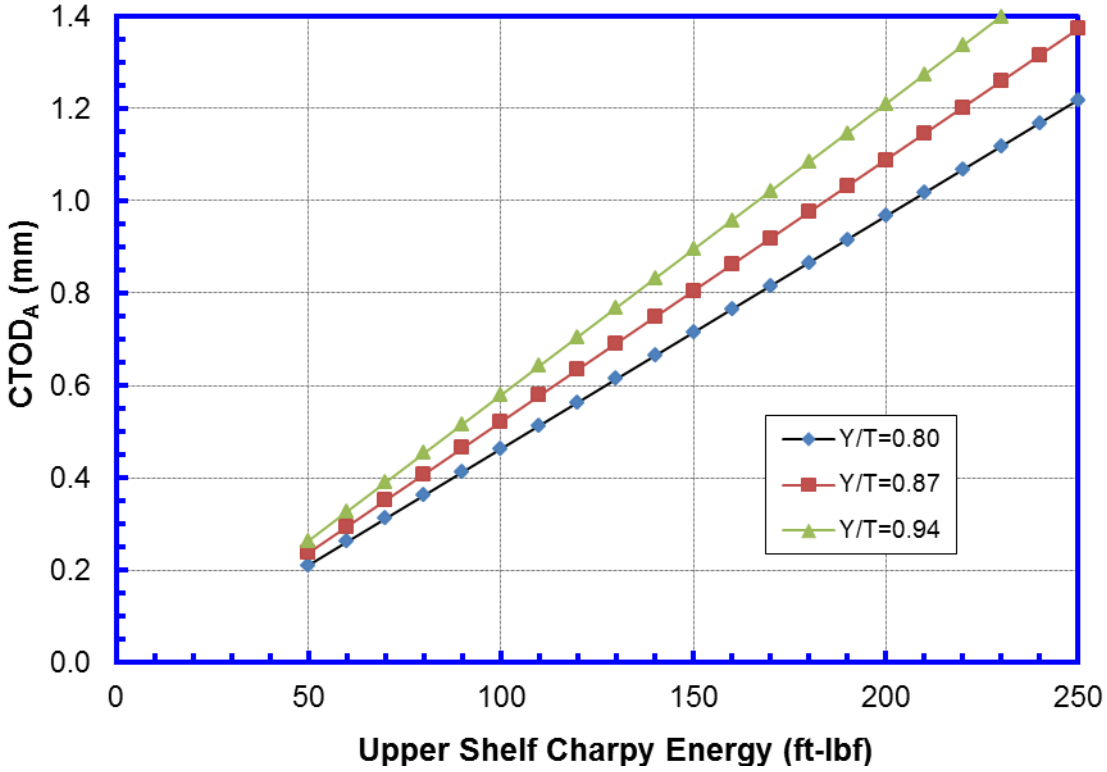

Figure 9-2 Conversion relation between upper shelf Charpy energy and $CTOD_A$

9.5.6.2 Apparent Toughness from Standard Deeply-Notched SENB

A multiplication factor of 1.5-2.0 may be applied to the upper-shelf CTOD toughness (δ_m) to obtain the apparent toughness.

This conversion factor is applicable to standard CTOD specimens without side grooves.

A default conversion factor of 1.75 is recommended.

9.5.6.3 Apparent Toughness from SENT Resistance Curves

The apparent toughness may be obtained from SENT resistance curves at the flaw growth of 0.5-1.0 mm. The appropriate level of flaw growth, at which the apparent toughness is obtained, depends on pipe wall thickness and less so on other parameters.

It is recommended that the amount of flaw growth, at which the apparent toughness is obtained, is linearly scaled between 0.5 mm for 12.7 mm (0.5 inch) wall thickness and 1.0 mm for 25.4 mm (1.0 inch).

9.5.6.4 Apparent Toughness from Shallow-Notched SENB Resistance Curves

The work by CANMET [48] has shown that the resistances of shallow-notched SENB are similar to those of SENT, of the same material. Consequently, the same procedure for the SENT specimens may be applied to shallow-notched SENB specimens.

9.5.7 Verification of Toughness Transferability

The critical issue of toughness transferability between small-scale specimens and large-scale structures at large plasticity is still an open issue. The procedures recommended for the determination of apparent toughness in the previous section contains some level of empiricism. The other challenge is that some of the available small-scale data have been generated by different test protocols which contribute to the uncertainties of the conversion factors. The recommended procedures have been confirmed valid from available data.

DNV RP-108 recognizes the uncertain nature of the resistance curve transferability. Although SENT specimens are recommended for the determination of resistance curves, the RP also recommends confirmation tests in the form of "sector" specimens, which are miniature wide plate specimens. The RP recommends revision of the SENT resistance curve if the confirmation tests indicate such revision is necessary.

Good transferability has been shown in the large-scale tests of this project between the non-pressurized pipes and CWP specimens. It is recommended that the resistance curves from the small-scale specimens be compared with limited tests of CWP specimens to confirm the transferability. Appropriate scaling or adjustment of the small-scale test results may be applied if systematical differences (beyond normal test data variations) are found.

The determination of $CTOD_A$ from resistance curves may be confirmed by applying the procedure outlined by Liu, et al [45].

10 Model Evaluation

10.1 Process of the Model Evaluation

The overall objective of this section is the evaluation of the capability and limitation of the TSC models. A number of relevant key factors were considered in the evaluation, including (1) fundamental basis of the models, (2) comparison between the experimentally measured TSC and the predicted TSC by the models, and (3) possible contributors to the agreement or the lack of agreement between the measured and predicted TSCs.

Large-scale tests covering all key input parameters and adequate ranges are important for model evaluation. However, to some extent, the scope of the experimental data available to evaluate the TSC models will always be limited. Therefore the models should be evaluated on the basis of a suite of criteria, such as their fundamental formulations, agreement with test data, and the stated limits of applicability. The pipeline industry has had a successful experience in applying weld integrity assessment procedures, developed and experimentally validated from one group of materials, to newer and modern linepipe materials and welds. For instance, the alternative girth weld flaw acceptance criteria (alternatively termed engineering critical assessment or ECA) in API 1104 Appendix A and CSA Z662 Annex K were developed from the fundamental fracture mechanics available in the 1970's and validated largely by experimental test data of late 1970's to mid 1980's. These procedures have since been applied to pipelines from grade X80 to X120. These high-strength materials did not exist when the assessment procedures were developed and adopted by the standards.

Both the experimental data and model predictions have some degree of uncertainties or variations. For instance, one example of the uncertainties of the experimental data is that the spatial variation of the material properties in a full-scale pipe may not be fully captured by the limited number of small-scale tests. An example of the uncertainties associated with the models is the representation of the stress-strain relations. In the models, these relations are idealized to have certain mathematical forms characterized by a few key parameters, such as Y/T ratio. The experimentally measured stress-strain relations conform to the idealized mathematical forms to a varying degree. The difference between the experimentally measured and idealized stress-strain relations introduces "modeling uncertainties". When a particular full-scale test is compared with the model prediction, it is often not possible to separate experimental and modeling uncertainties. Therefore, the model evaluation should focus on the overall trend. One should be extremely cautious when drawing conclusions on the basis of an individual test or comparison.

10.2 Levels of TSC Models Exercised in the Evaluation

As described in Section 9.5, the TSC models consist of four levels. In Level 4, case-specific FEA is used to generate crack driving force curves. There are many factors which can affect the driving force curves. At the present time, it is not believed that sufficient details of FEA procedures can be specified to generate the crack driving force curves consistently among end users. The Level 4 TSC models are reserved for seasoned experts with demonstrated experience in TSC calculation. While it is possible that a better conformity may be obtained by exercising the Level 4 procedures for the test data available to this project, only Levels 2 and 3 of the TSC

models were evaluated. These two levels are in the form of closed form parametric equations. The Level 1 procedures are for preliminary screening purpose. The agreement of the Level 1 procedures with the test data within this project should follow that of Level 2 when the apparent toughness is obtained from the upper shelf Charpy energy.

In the following sections, key elements relevant to the model evaluation are reviewed in Section 10.3. The determination of the toughness parameters is described in Section 10.4. The comparison of the test data and model predictions is covered extensively in Section 10.5. The overall observation of the model evaluation is given in Sections 10.6 and 10.7.

10.3 Key Elements of the Model Evaluation

10.3.1 Full-Scale Test Matrix

The 24 full-scale pipe tests shown in Section 3 and their associated small-scale material properties were used to evaluate the tensile strain design models. The test matrix and results are shown in Table 10-1. Two different pipes, namely X65 high and low Y/T pipes, were tested. The pipes were of 12.75" OD and 12.7-mm wall thickness. The high Y/T pipes had two types of girth welds which were referred to as the evenmatched and overmatched welds, respectively. The low Y/T pipes had one type of weld which overmatched the pipe strength. The tests were conducted under both pressurized and non-pressurized conditions. Each test specimen had either one or two girth welds and each girth weld had two flaws of identical size and notch location. Three flaw locations were tested, i.e., base metal, weld centerline, or HAZ.

10.3.2 Uniform Strain Zones and Reported TSCs

Most full-scale pipe test specimens had two girth welds and three uniform strain zones, as shown in Figure 10-1. There were two or four LVDTs in each uniform strain zone which measured the relative displacement between two anchor points covering the uniform strain zone. The strain values from all LVDTs in the same uniform strain zone were averaged to determine the uniform strain in that uniform strain zone. The uniform strains of all three uniform strain zones were averaged to determine the remote (uniform) strain of the entire test specimen.

In summary, the remote strain of a particular test specimen generally refers to the averaged strain of all uniform strain zones. The TSC (in Table 10-1) of a specimen is the remote strain (averaged strain of all uniform strain zones) at the critical event (i.e., the maximum load).

10.3.3 TSC Variations from Duplicate Tests

In a number of cases, duplicate tests of specimens with nominally identical conditions were performed. For instance, the two tests, 1.9 and 1.19, had nominally the same pipe material, welding procedure, flaw size, and flaw location. The nominal stress vs. remote strain relations of those two tests are shown in Figure 10-2. The TSCs of Tests 1.9 and 1.19 are 0.61% and 1.26%, respectively. The stress level at failure point of Test 1.19 is slightly higher than that of Test 1.9, by approximately 7 MPa. Similarly, as shown in Table 10-1, the two duplicate tests, 1.11 and 1.24, had 1.15% and 2.21% TSC, respectively. The stresses at failure point of Tests 1.11 and 1.24 differ by about 3 MPa. The above data demonstrate that the TSCs of duplicate tests could vary by a factor of two, while they failed at very similar stress levels.

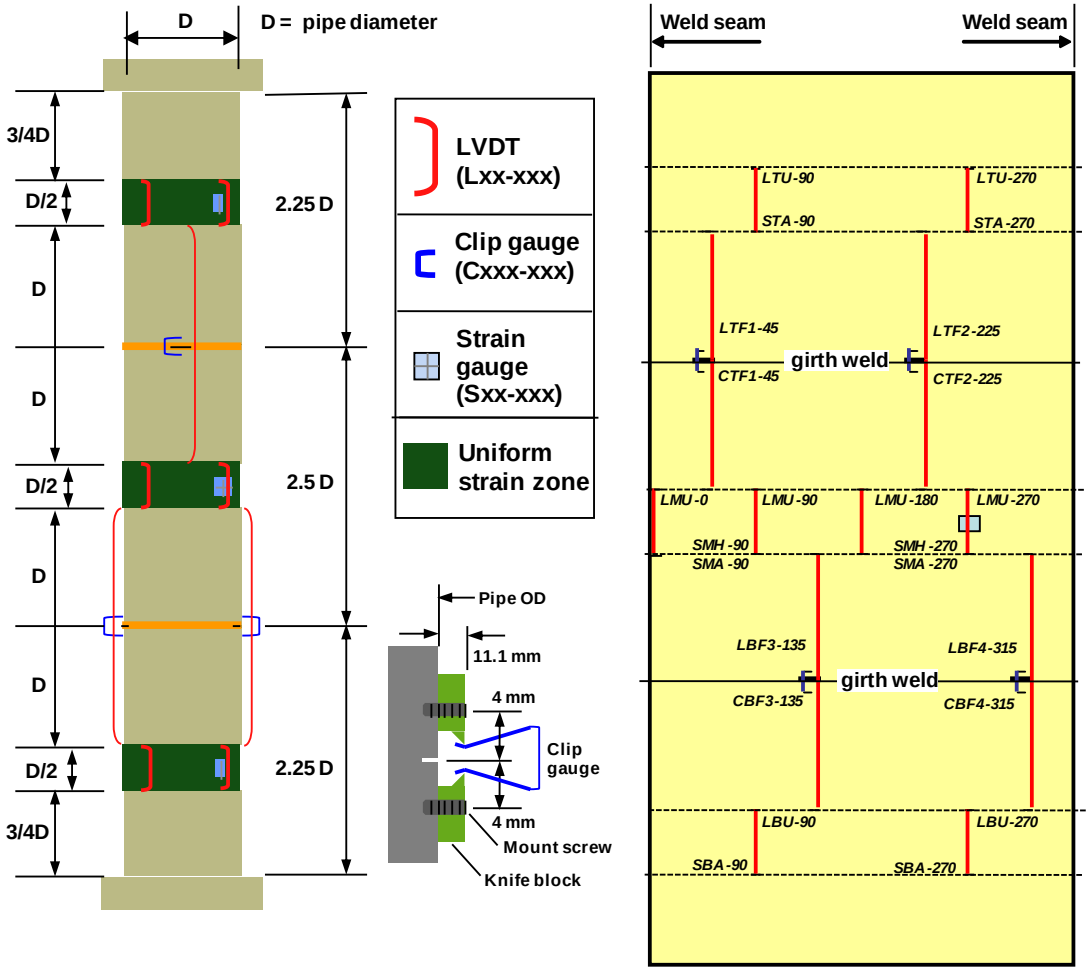

Figure 10-1 Instrumentation plan of the full-scale pipe tests

10.3.4 Variation of Tensile Properties from Small-Scale Tests

Pipe tensile properties can have variations within a certain range. As an example, the small-scale (longitudinal) stress-strain curves of the X65 high Y/T pipes are shown in Figure 10-3. It shows that the band of the stress-strain curves covers about a 4-ksi range. The tensile properties of the two pipes (X65 high Y/T and X65 low Y/T) and their welds are given in Table 10-2. The two pipes show similar strength variations, i.e., about 8 ksi for YS and 4 ksi for UTS. The Y/T ratio of the high and low Y/T pipes vary from 0.87 to 0.94 and from 0.83 to 0.93, respectively. The weld strength mismatch (measured by UTS) of the high Y/T pipe varies from -2% to 9% for the nominally evenmatched weld; and 12% to 18% for the overmatched weld. The weld strength mismatch (measured by UTS) of the low Y/T pipe varies from 14% to 25%.

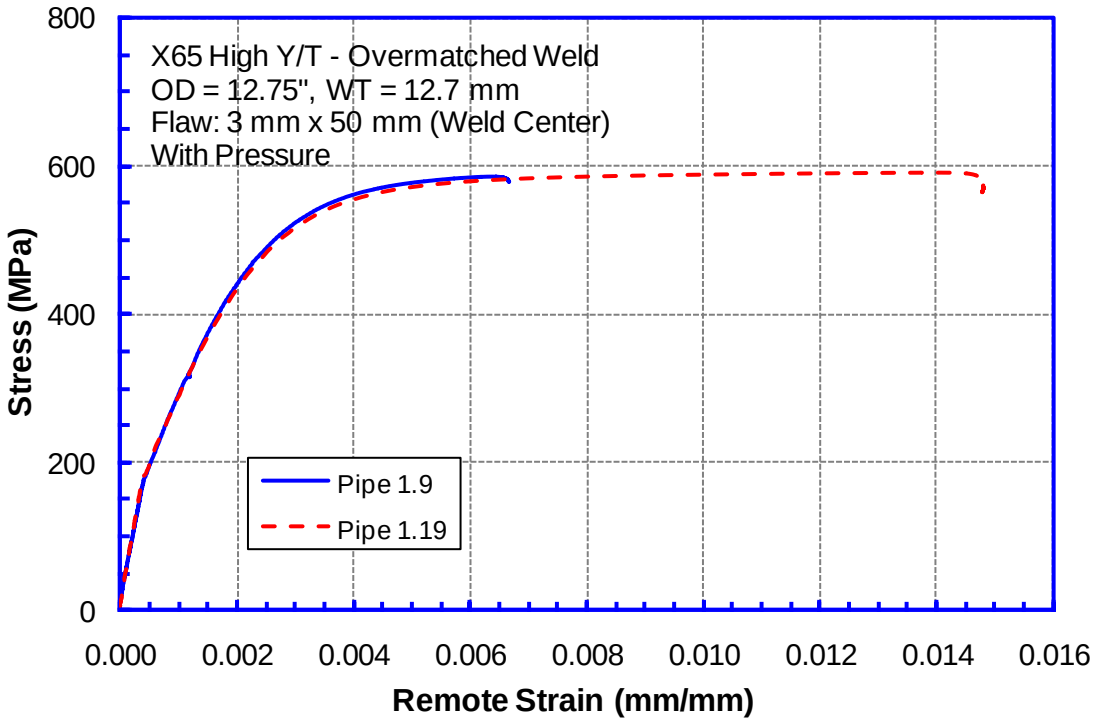

Figure 10-2 Nominal stress vs. remote strain relations of two duplicate pipe tests

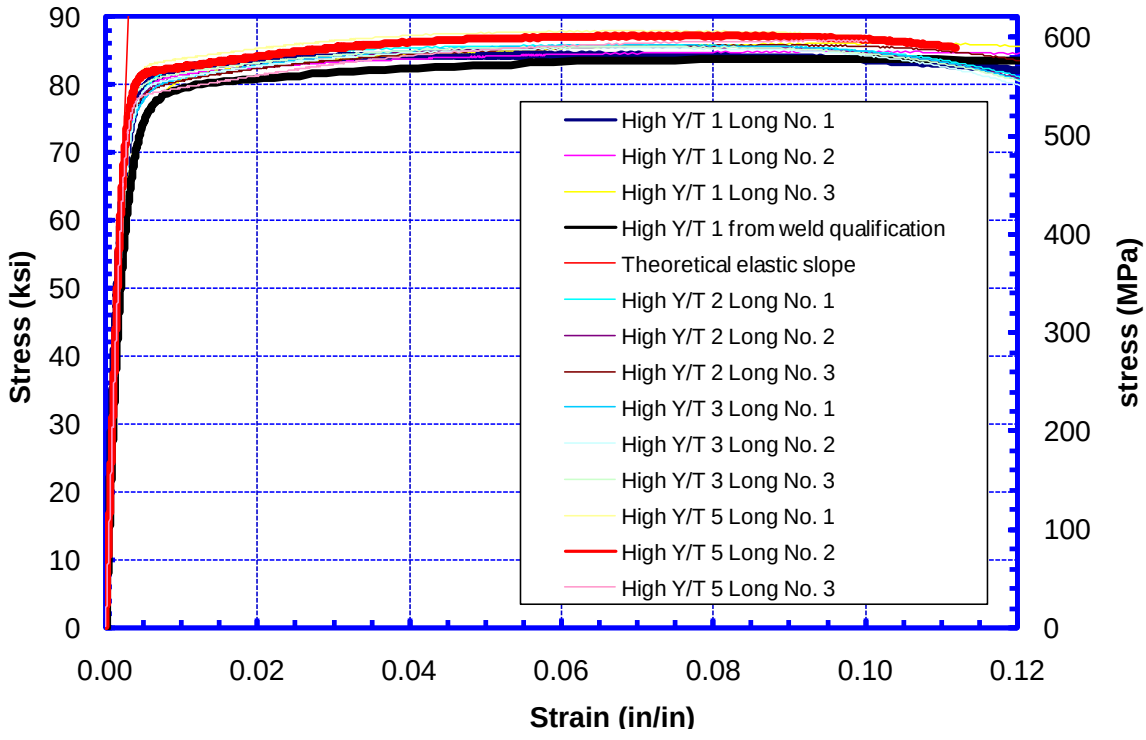

Figure 10-3 Longitudinal stress-strain curves of X65 high Y/T pipe from small-scale tests

Table 10-1 Matrix of full scale pipe tests

Test ID	Pipe Material	Temp.	Weld Mismatch	Pressure Factor	Flaw Location	a	2c	TSC at Max Load	Nominal Stress at Max Load
		(°C)				(mm)	(mm)	(%)	(Mpa)
1.1	X65 High Y/T	20	N/A	0.8	BM	3	50	0.83	590
1.2	X65 High Y/T	20	N/A	0	BM	3	50	1.88	555
1.7	X65 High Y/T	20	Even	0.8	HAZ	3	35	4.74	606
1.8	X65 High Y/T	20	Even	0	HAZ	3	35	8.07	565
1.22	X65 High Y/T	20	Even	0.8	HAZ	3	50	2.01	609
1.11	X65 High Y/T	20	Over	0.8	HAZ	3	50	1.24	599
1.24	X65 High Y/T	20	Over	0.8	HAZ	3	50	2.28	602
1.12	X65 High Y/T	20	Over	0	HAZ	3	50	2.69	568
1.13	X65 High Y/T	-20	Over	0.8	HAZ	3	50	1.59	614
1.14	X65 High Y/T	-20	Over	0	HAZ	3	50	3.12	579
1.18	X65 High Y/T	20	Over	0.8	HAZ	3	35	7.73	606
1.5	X65 High Y/T	20	Even	0.8	WM	3	35	1.58	592
1.6	X65 High Y/T	20	Even	0	WM	3	35	4.64	560
1.21	X65 High Y/T	20	Even	0.8	WM	3	50	0.72	596
1.9	X65 High Y/T	20	Over	0.8	WM	3	50	0.64	585
1.19	X65 High Y/T	20	Over	0.8	WM	3	50	1.39	592
1.10	X65 High Y/T	20	Over	0	WM	3	50	3.10	558
1.17	X65 High Y/T	20	Over	0.8	WM	3	35	2.13	605
1.23	X65 High Y/T	20	Over	0.8	WM	2	70	0.69	588
1.3	X65 Low Y/T	20	N/A	0.8	BM	3	50	1.51	487
1.4	X65 Low Y/T	20	N/A	0	BM	3	50	2.77	460
1.15	X65 Low Y/T	20	Over	0.8	HAZ	3	50	4.20	515
1.16	X65 Low Y/T	20	Over	0	HAZ	3	50	6.81	474
1.20	X65 Low Y/T	20	Over	0.8	WM	3	50	3.97	515

Table 10-2 Material property summary of X65 pipe (longitudinal) and weld (circumferential)

	X65 High Y/T Pipe					X65 Low Y/T Pipe			
	Pipe Property			Weld Mismatch at UTS		Pipe Property			Weld Mismatch at UTS
	YS (ksi)	UTS (ksi)	Y/T	Evenmatch Weld	Overmatch Weld	YS (ksi)	UTS (ksi)	Y/T	
Minimum	74.6	83.8	0.87	-2%	12%	55.9	67.6	0.83	14%
Maximum	82.2	87.9	0.94	9%	18%	64.4	71.7	0.93	25%
Median	79.0	85.9	0.93	5%	15%	61.8	69.4	0.88	16%

10.3.5 Variation of Local Flaw Response from Full-Scale Tests

Pipe and weld properties are usually not uniform along the same pipe and weld. Therefore, nominally identical flaws in the same specimen can sample different local materials and different levels of weld mismatch. The local property variation can be inferred from the CMOD curves measured from the same test specimen. For an example, the CMOD vs. remote strain relations from Tests 1.19 and 1.14 are shown in Figure 10-4 (a) and (b), respectively. Each test specimen had four nominally identical flaws and the CMOD of all flaws were recorded. It shows that the CMOD of the nominally identical flaws behaved differently. In general, one flaw eventually became dominant and led to final failure. In Test 1.19, the CMOD of one flaw became dominant at very low strain values and led to failure. On the other hand, in Test 1.14, the CMOD of all four flaws were very close until reaching the failure strain. The difference in the CMOD of the nominally identical flaws is due, in part, to the variation of the material properties in the local area near the flaw.

10.3.6 Flaw Behavior and Remote Strain Measure

To highlight the relationship between the flaws in a girth weld and the remote strain, it is useful to look at the pipe cross section that contains the flaws (termed flawed plane) and the regions where the remote strain is measured (i.e., uniform zones). As shown in Figure 10-5, the connection between the flawed plane and the uniform zones is the equivalence of longitudinal load. If the cross-sectional areas are the same at those locations, this equivalence of load leads to the equivalence of nominal stress. The action of the remote region is "transmitted" to the flawed plane through the equivalence of the nominal stress.

If the materials in the uniform zones have slightly different stress-strain behaviors, to provide the same nominal stress, the required remote strain may be different. A small difference in the stress-strain behaviors can translate to relatively large difference in strain values especially when the stress-strain curves are flat.

For example, Figure 10-6 shows three slightly different stress-strain curves. The baseline stress-strain curve was taken from the full-scale test 1.18. Two additional stress-strain curves were "created" by adding or subtracting the strength of the baseline curve by 0.5 ksi (3.5 MPa) at 0.5% strain and beyond. The range of strain values due to the slight strength difference is shown in Figure 10-7. The baseline curve establishes a one-to-one correlation. The other two curves provide the upper and lower bound strain values corresponding to the same stress produced by the baseline curve at strains greater than 1.0%. The result shows that when a flaw is subjected to the stress level corresponding to the stress at 4.0% strain of the baseline stress-strain curve, the reported strain in the uniform strain zone can vary from 2.5% to 8% (material's uniform strain) if the stress-strain curves vary by ±0.5 ksi from the baseline stress-strain curve.

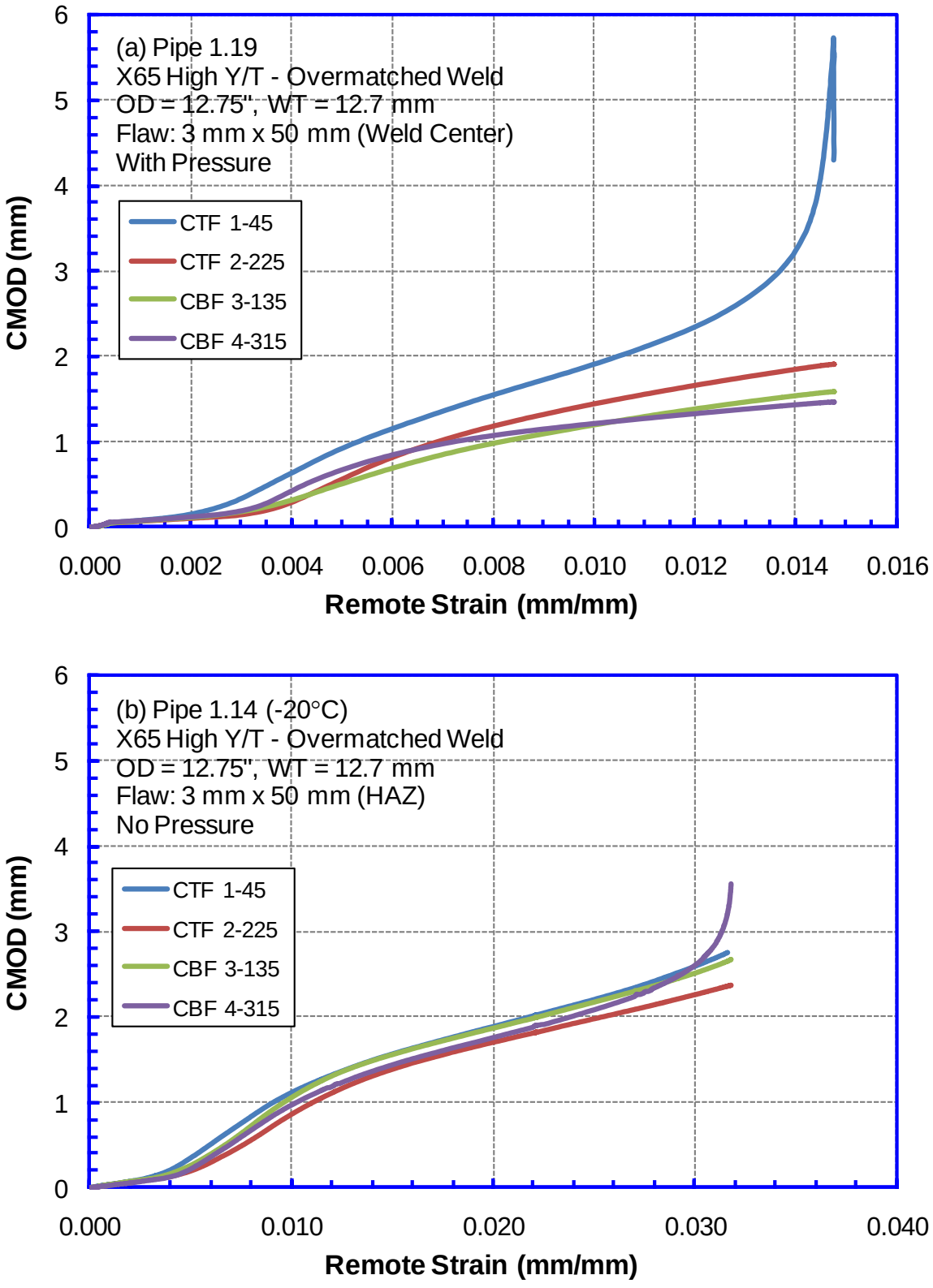

Figure 10-4 Variation of measured CMOD from identical flaws

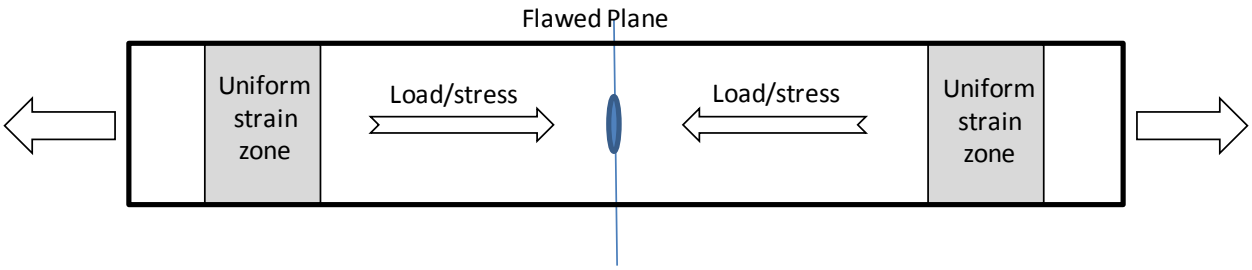

Figure 10-5 Schematic illustration of the remote regions where the strains are measured and the flawed plane where the flaw failure events are initiated

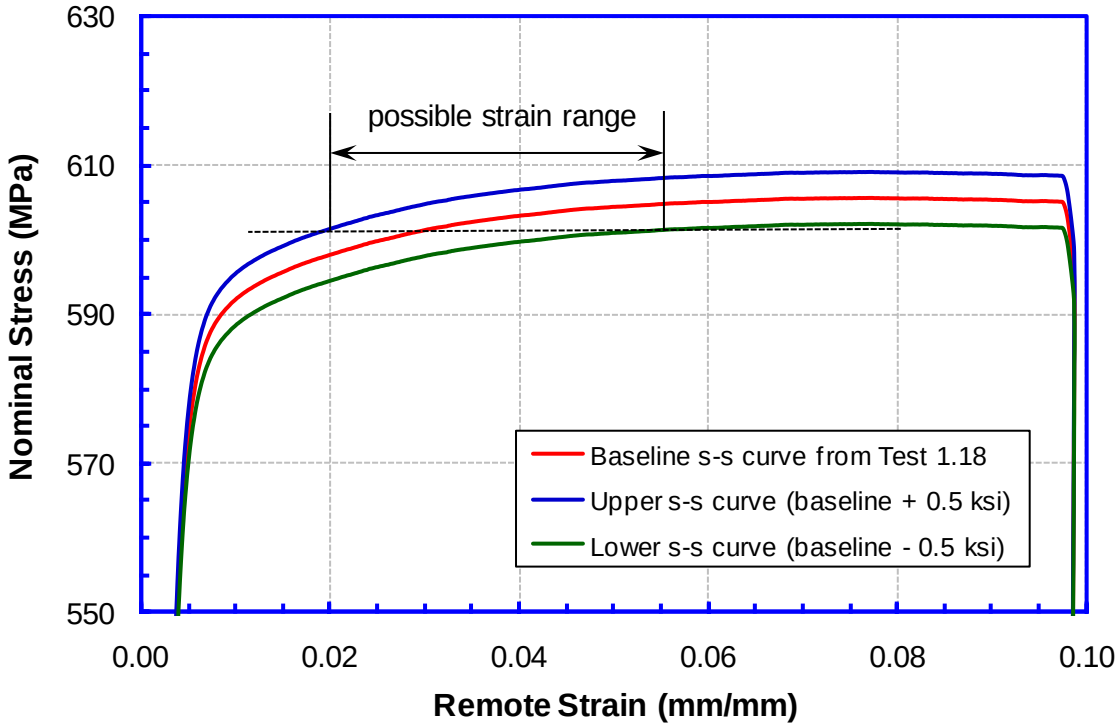

Figure 10-6 Stress-strain curves with slightly different strength levels

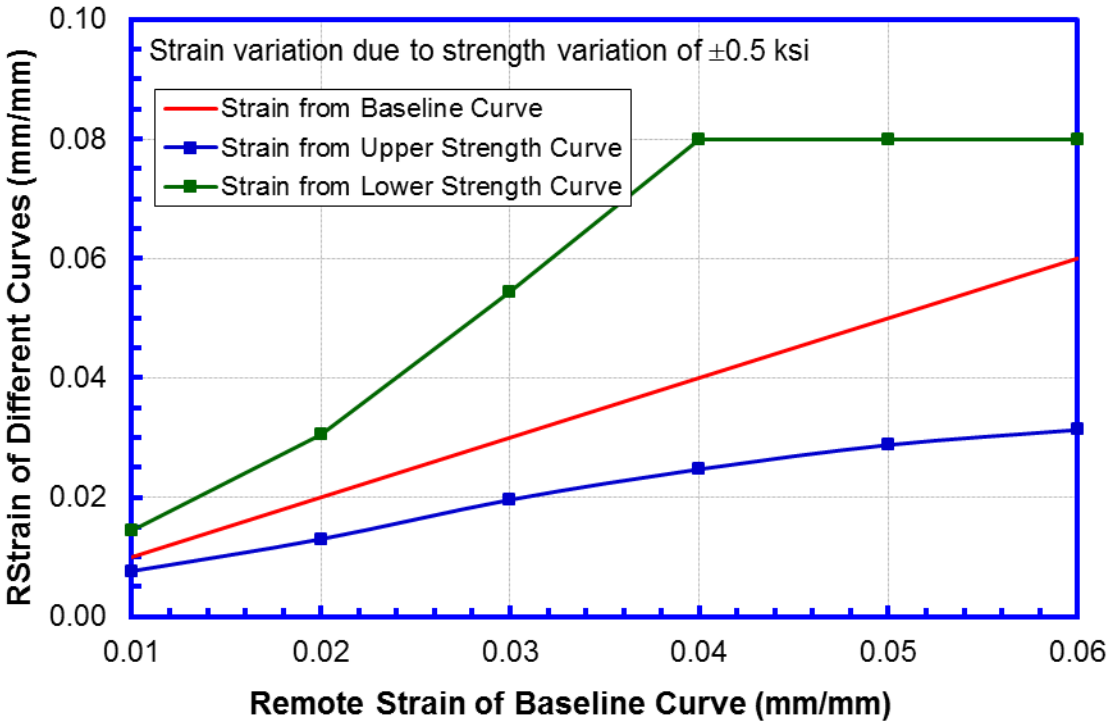

Figure 10-7 Strain values corresponding to the three stress-strain curves at the same stress level (y-axis) as a function of the strain of the baseline stress-strain curve

10.4 Determination of Fracture Toughness

10.4.1 CTOD Resistance Curves ($CTOD_R$)

The CTOD resistance curves were obtained from SENT tests. The details of the SENT tests can be found in [2]. The CTOD was calculated following the CANMET procedures [53,54]. The resistance curves of the X65 low Y/T and high Y/T pipes are shown in Figure 10-8 and Figure 10-9, respectively. The resistance curves were fitted to power functions in the form of $CTOD_R = A \times \Delta a^B$. The fitted coefficients A and B are given in Table 10-3. Multiple tests were conducted for X65 low Y/T pipe and weld materials. The test repeatability is very reliable, as shown in Figure 10-8. In general, the CTOD resistance curves of the pipe and HAZ materials are higher than those of the weld metals. The resistance curves of the pipe and HAZ materials are similar.

10.4.2 Apparent Toughness ($CTOD_A$)

The procedures in Sections 8 and 9 were used to determine the apparent toughness ($CTOD_A$). The $CTOD_A$ was calculated from Charpy energy, high constraint SENB single value CTOD, and SENT resistance curve. The $CTOD_A$ calculated from different methods are shown in Table 10-4.

The upper shelf Charpy energy and upper shelf CTOD value used for $CTOD_A$ calculations are also given for reference. The upper shelf CTOD was calculated at 99.9% of the maximum load from SENB tests. The $CTOD_A$ from the SENT resistance curves was calculated with the fitted power function by setting Δa = 0.5 mm.

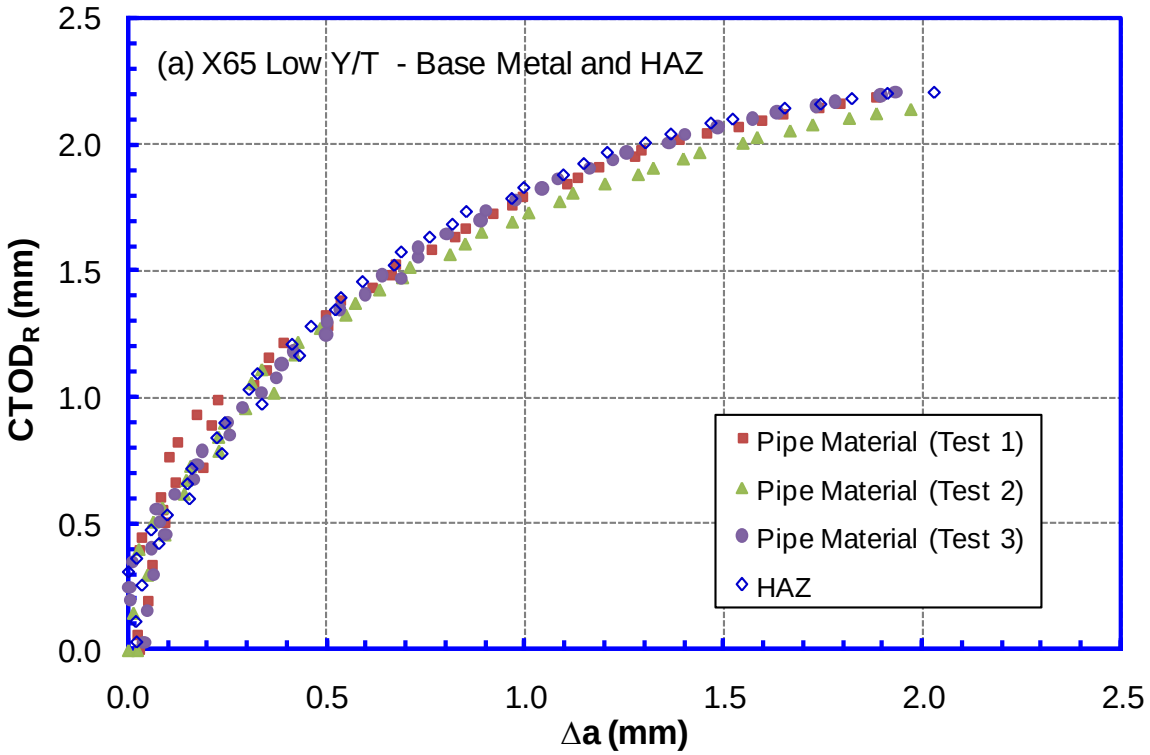

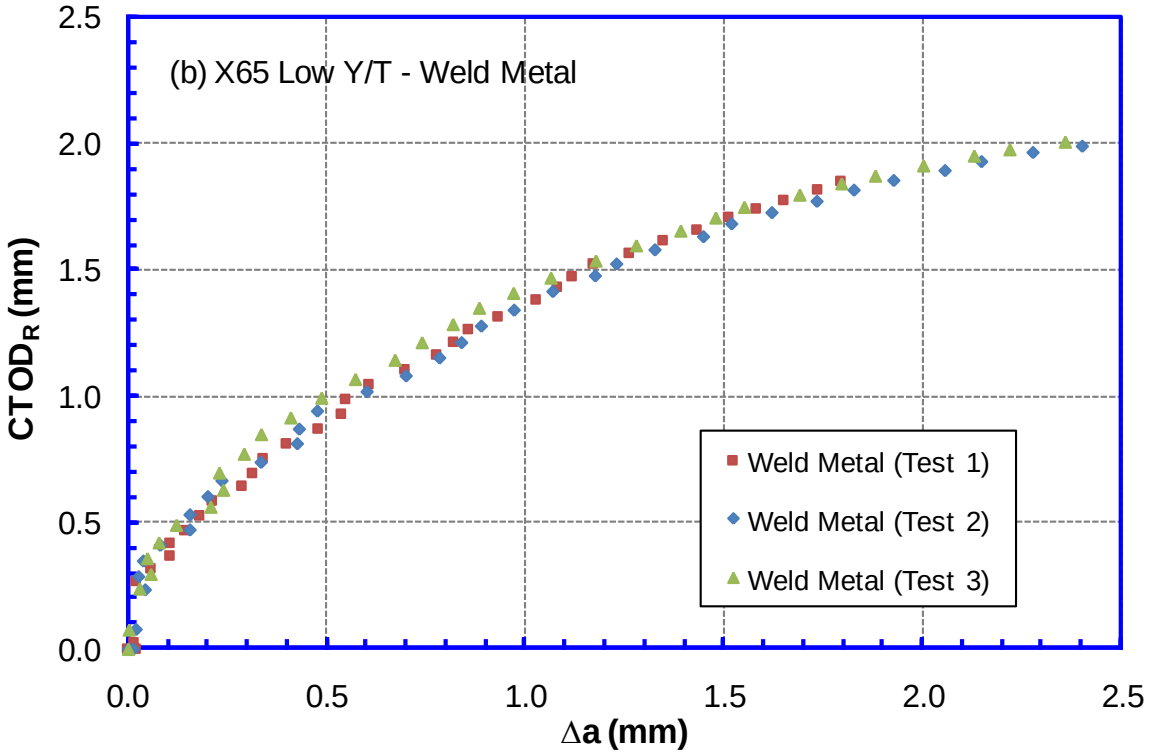

Figure 10-8 SENT resistance curves (CTOD$_R$) of X65 low Y/T pipe for (a) pipe and HAZ flaws; (b) weld metal flaws

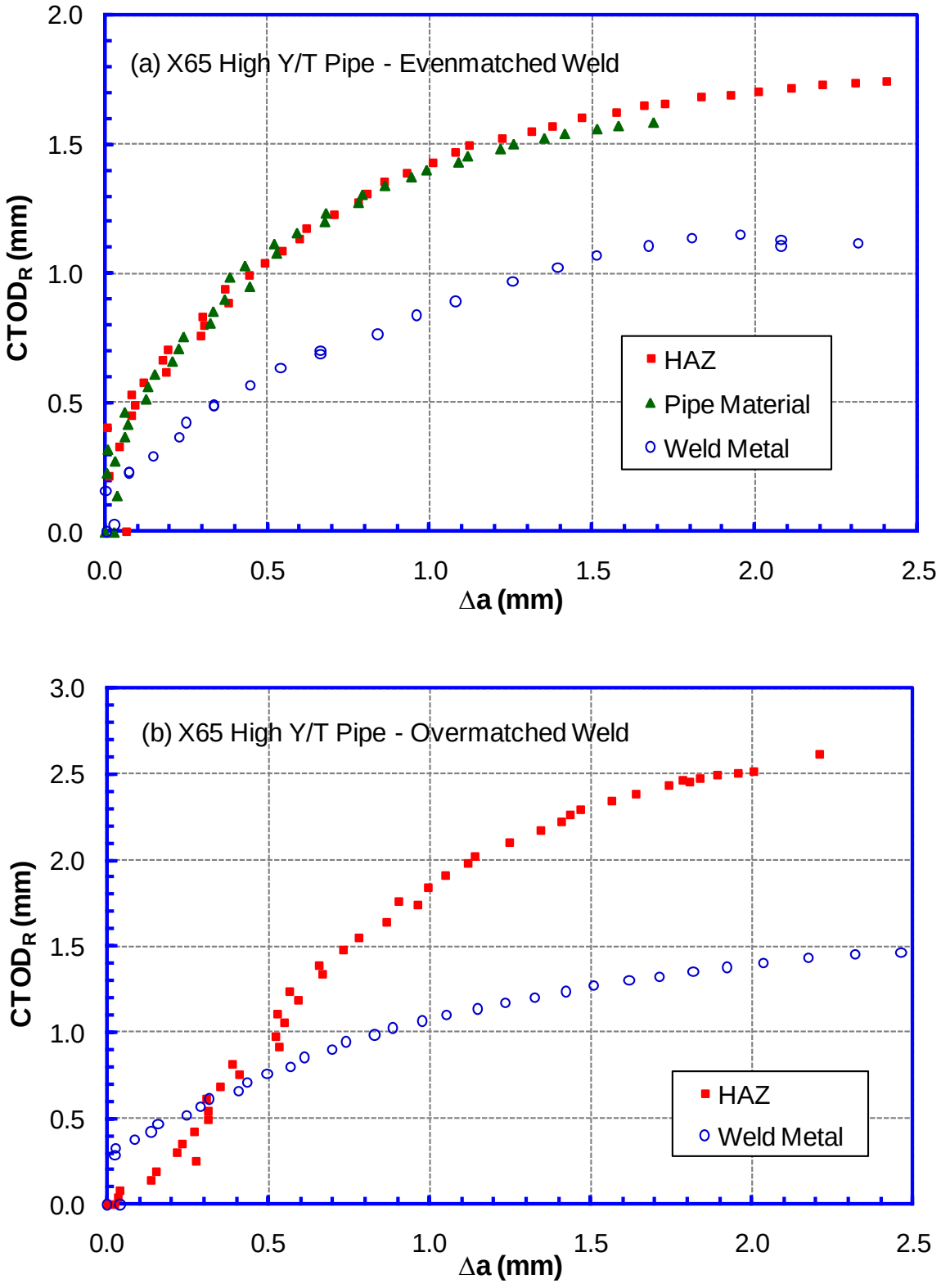

Figure 10-9 SENT resistance curves (CTOD$_R$) of X65 high Y/T pipe for (a) evenmatched weld; (b) overmatched weld

Table 10-3 Coefficients of fitted R-curves

Materials			Resistance Curve ($CTOD_R = A \times \Delta a^B$)*	
Pipe Material	Weld Attribute	Flaw Location	A	B
X65 High Y/T	None	Pipe	1.38	0.41
	Even matched	Weld	0.84	0.50
		HAZ	1.38	0.41
	Over matched	Weld	1.05	0.47
		HAZ	1.69	0.72
X65 Low Y/T	None	Pipe	1.75	0.40
	Over matched	Weld	1.34	0.52
		HAZ	1.75	0.40
*The units of $CTOD_R$ and Δa are mm.				

Table 10-4 Summary of apparent toughness ($CTOD_A$)

Material Property						Charpy and SENB		Apparent Toughness ($CTOD_A$)		
Pipe Material	Weld Attribute	Flaw Location	Yield Strength		Y/T	Upper Shelf Charpy Energy	Upper Shelf CTOD (SENB - at 99.9% Max Load)	From Charpy	From CTOD (Conversion Factor = 1.5)	From SENT R-curve (Δa = 0.5 mm)
			(ksi)	(MPa)		(J)	(mm)	(mm)	(mm)	(mm)
X65 High Y/T	None	Pipe	79.3	547.0	0.92	390.0	0.72	1.41	1.07	1.04
	Even matched	Weld	76.3	526.2	0.85	170.0	0.58	0.65	0.87	0.59
		HAZ	79.3	547.0	0.92	390.0	0.72	1.41	1.07	1.04
	Over matched	Weld	85.9	592.3	0.87	235.0	0.54	0.83	0.81	0.76
		HAZ	79.3	547.0	0.92	245.0	0.61	0.87	0.91	1.03
X65 Low Y/T	None	Pipe	61.0	420.5	0.88	300.0	0.77	1.09	1.15	1.33
	Over matched	Weld	66.2	456.4	0.80	185.0	0.44	0.66	0.65	0.93
		HAZ	61.0	420.5	0.88	300.0	0.77	1.09	1.15	1.33

10.5 Comparison of Prediction (Levels 2 and 3 Procedures) and Test Data

10.5.1 All Test Data

The tensile strain capacities were predicted using the Level 2 and Level 3 approaches for all 24 full-scale tests. For the Level 2 approach, the predictions were based on the initiation-control limit state where the $CTOD_A$ was obtained from Charpy and high-constraint CTOD toughness

tests (see Table 10-4). The Level 3 predictions were made using the toughness obtained from low-constraint SENT tests and were made using both the initiation-control and ductile-instability based limit states. The R-curves ($CTOD_R$) were obtained from SENT tests (Table 10-3) and the $CTOD_A$ was calculated from the R-curves at 0.5-mm flaw growth (Table 10-4). For both the Level 2 and Level 3 approaches, predictions were made using the median values of pipe Y/T and weld mismatch levels obtained from the small-scale tests (Table 10-2). All input parameters and predicted TSCs are provided in Table 10-5.

Table 10-5 Input parameters and predicted TSC

Test Information							Predicted TSC (Initiation Control)						Predicted TSC (Ductile Instability)		
							Toughness Charpy		Toughness SENB		Toughness SENT		Toughness SENT		
Test ID	a	2c	h	Y/T	Weld Mis-match	TSC Max Load	$CTOD_A$	TSC	$CTOD_A$	TSC	$CTOD_A$	TSC	$CTOD_R=A*\Delta a^B$		TSC
	(mm)	(mm)	(mm)			(%)	(mm)	(%)	(mm)	(%)	(mm)	(%)	A	B	(%)
1.1	3	50	0.0	0.92	1.00	0.83	1.41	1.28	1.07	0.98	1.04	0.95	1.38	0.41	0.84
1.2	3	50	0.0	0.92	1.00	1.88	1.41	1.91	1.07	1.47	1.04	1.43	1.38	0.41	1.26
1.7	3	35	0.0	0.92	1.05	4.74	1.41	2.18	1.07	1.70	1.04	1.66	1.38	0.41	1.60
1.8	3	35	0.0	0.92	1.05	8.07	1.41	3.27	1.07	2.55	1.04	2.49	1.38	0.41	2.40
1.22	3	50	0.0	0.92	1.05	2.01	1.41	1.69	1.07	1.31	1.04	1.28	1.38	0.41	1.13
1.11	3	50	0.0	0.92	1.15	1.24	0.87	1.64	0.91	1.71	1.03	1.92	1.69	0.72	2.30
1.24	3	50	0.0	0.92	1.15	2.28	0.87	1.64	0.91	1.71	1.03	1.92	1.69	0.72	2.30
1.12	3	50	0.0	0.92	1.15	2.69	0.87	2.46	0.91	2.57	1.03	2.88	1.69	0.72	3.46
1.13	3	50	0.0	0.91	1.15	1.59	0.87	1.71	0.91	1.78	1.03	1.99	1.69	0.72	2.43
1.14	3	50	0.0	0.91	1.15	3.12	0.87	2.56	0.91	2.67	1.03	2.99	1.69	0.72	3.65
1.18	3	35	0.0	0.92	1.15	7.73	0.87	2.12	0.91	2.21	1.03	2.47	1.69	0.72	3.22
1.5	3	35	0.0	0.92	1.05	1.58	0.65	1.05	0.87	1.40	0.59	0.95	0.84	0.50	1.07
1.6	3	35	0.0	0.92	1.05	4.64	0.65	1.57	0.87	2.09	0.59	1.42	0.84	0.50	1.60
1.21	3	50	0.0	0.92	1.05	0.72	0.65	0.81	0.87	1.08	0.59	0.74	0.84	0.50	0.74
1.9	3	50	0.0	0.92	1.15	0.64	0.83	1.57	0.81	1.53	0.76	1.44	1.05	0.47	1.38
1.19	3	50	0.0	0.92	1.15	1.39	0.83	1.57	0.81	1.53	0.76	1.44	1.05	0.47	1.38
1.10	3	50	0.0	0.92	1.15	3.10	0.83	2.35	0.81	2.30	0.76	2.17	1.05	0.47	2.07
1.17	3	35	0.0	0.92	1.15	2.13	0.83	2.03	0.81	1.98	0.76	1.87	1.05	0.47	1.95
1.23	2	70	0.0	0.92	1.15	0.69	0.83	2.17	0.81	2.12	0.76	2.00	1.05	0.47	1.48
1.3	3	50	0.0	0.88	1.00	1.51	1.09	1.25	1.15	1.32	1.33	1.51	1.75	0.40	1.35
1.4	3	50	0.0	0.88	1.00	2.77	1.09	1.88	1.15	1.98	1.33	2.26	1.75	0.40	2.03
1.15	3	50	0.0	0.88	1.16	4.20	1.09	2.42	1.15	2.54	1.33	2.86	1.75	0.40	2.57
1.16	3	50	0.0	0.88	1.16	6.81	1.09	3.63	1.15	3.81	1.33	4.30	1.75	0.40	3.85
1.20	3	50	0.0	0.88	1.16	3.97	0.66	1.52	0.65	1.49	0.93	2.10	1.34	0.52	2.12

The comparison of the predicted and measured TSCs of all 24 tests is shown in Figure 10-10, where the predictions were made using the initiation-control based limit state and the $CTOD_A$ obtained from SENB tests (Level 2). Figure 10-11 shows the comparison of the measured and predicted TSCs using the ductile-instability based limit state and the resistance curves measured from SENT (Level 3). A 45° line was plotted in both figures for reference. In 2 out of the 24 tests, the measured strains are less than 0.7% (enclosed in two small circles in Figure 10-10) and the measured values are much lower than the predicted ones. In 7 of the 24 tests, the measured

strains are greater than 3.5% (enclosed in a big circle in Figure 10-10) and the measured values are much higher than the predicted values. For the remaining 15 tests where the measured strains are between 0.7% and 3.5%, the measured strains match the predicted ones reasonably well.

The predictions using the initiation-control (Figure 10-10) and ductile- instability (Figure 10-11) based limit states are very similar. The correlation between the initiation-control and ductile-instability based TSC predictions are further illustrated in Figure 10-12 for all 24 tests, where the CTOD resistance curves were obtained from SENT tests and the $CTOD_A$ were determined from the resistance curves at $\Delta a = 0.5$ mm. The results demonstrate that the initiation-control and ductile-instability based models produce consistent TSC predictions.

10.5.2 Test Data with TSC between 0.7% and 3.5%

The full-scale tests with measured TSCs of 0.7-3.5% were further examined with Levels 2 and 3 procedures. The comparison of the measured and predicted TSCs from Level 2 procedures is shown in Figure 10-13. Two initiation-control based toughness options, Charpy upper shelf energy and high-constraint SENB CTOD tests, were exercised.

The comparison of the measured and predicted TSCs from Level 3 procedures is shown in Figure 10-14. The CTOD resistance curves from SENT tests were used in the ductile-instability based predictions. In the initiation-control based predictions, the $CTOD_A$ were obtained from the SENT resistance curves at 0.5-mm flaw growth. Overall, all Levels 2 and 3 toughness options provide similar predictions.

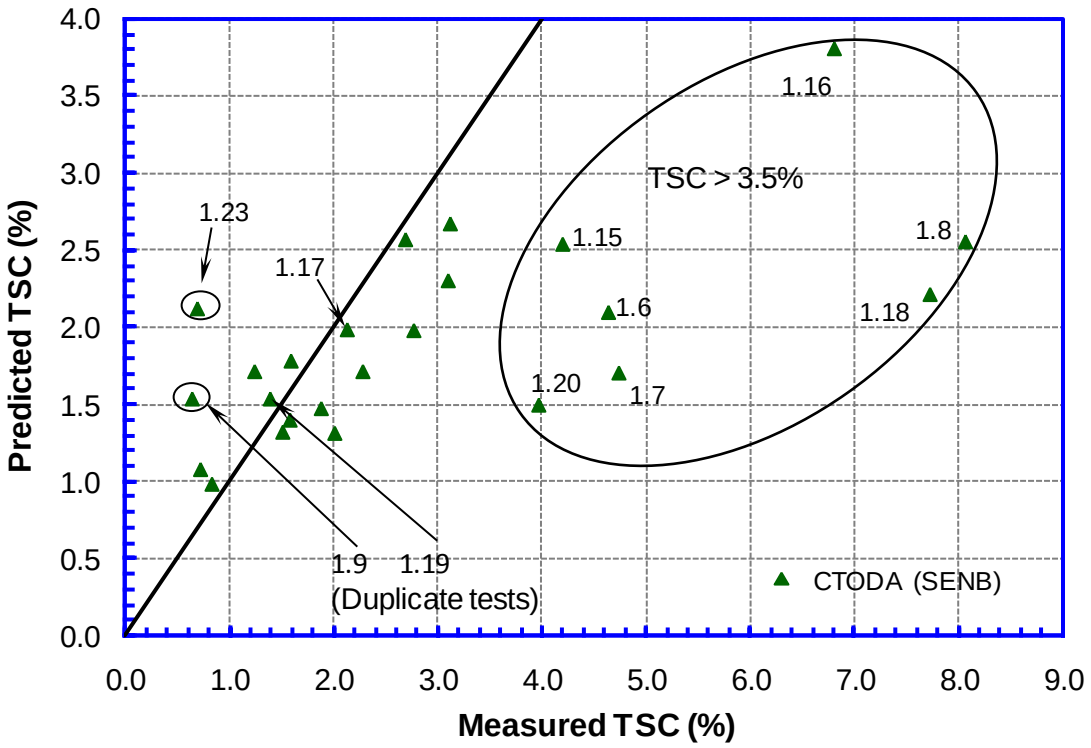

Figure 10-10 Predicted (initiation-control based) and measured TSCs of all 24 tests

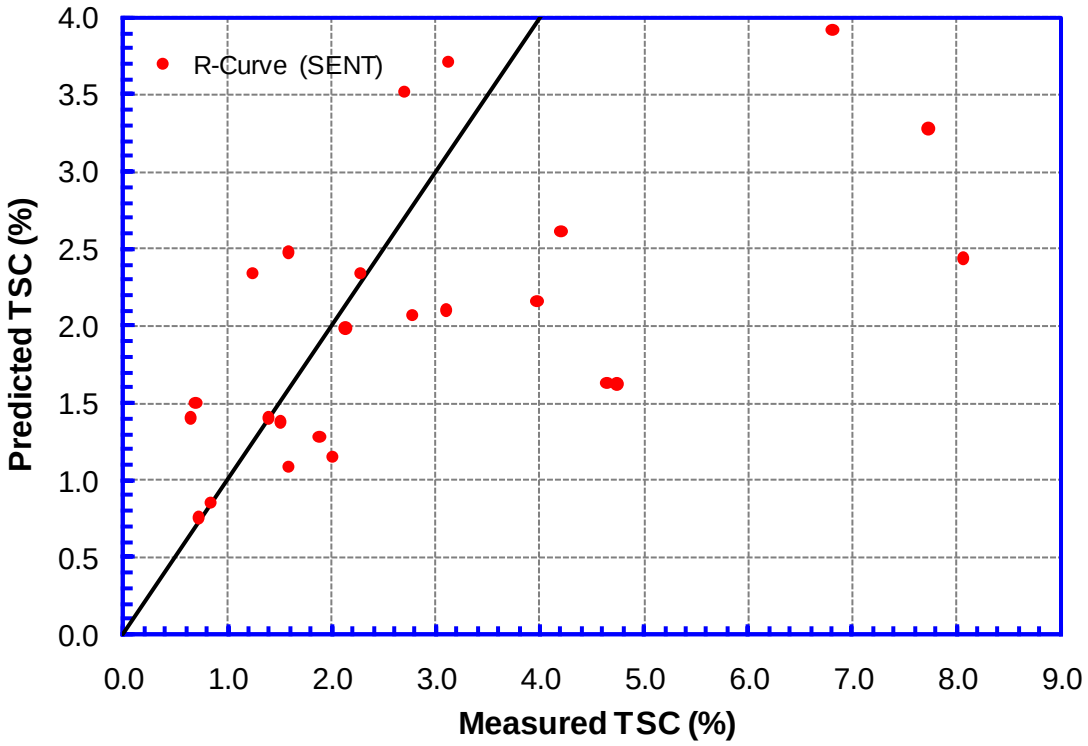

Figure 10-11 Predicted (ductile-instability based) and measured TSCs of all 24 tests

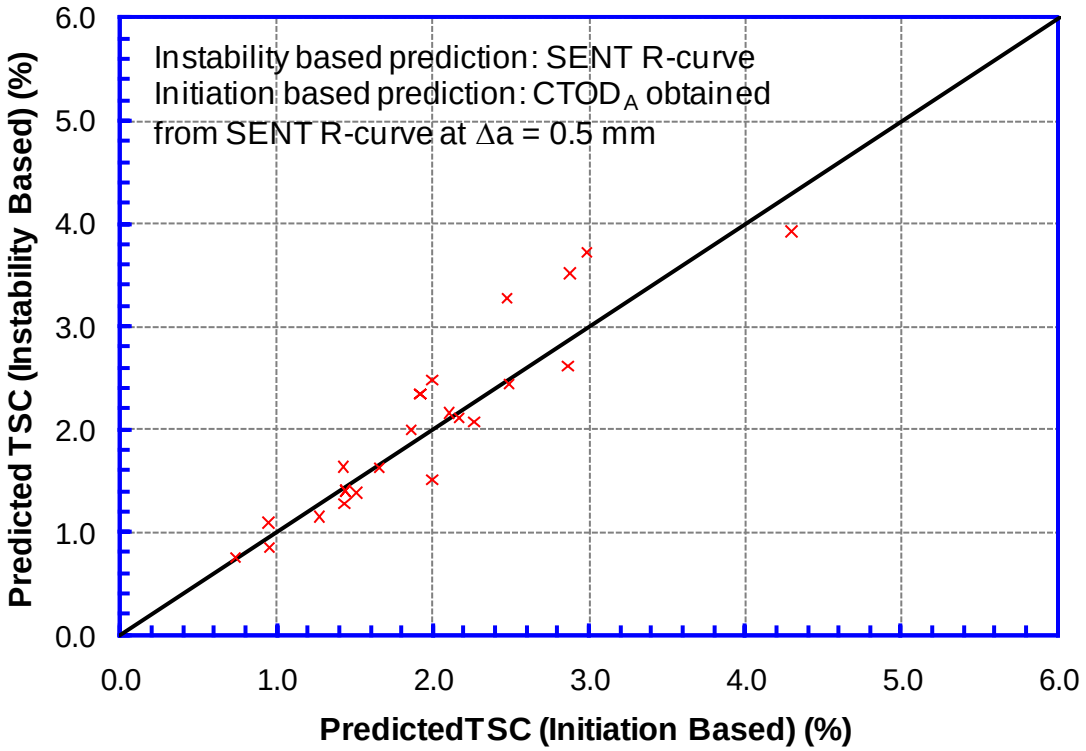

Figure 10-12 Comparison of Initiation and instability based predictions for all 24 tests

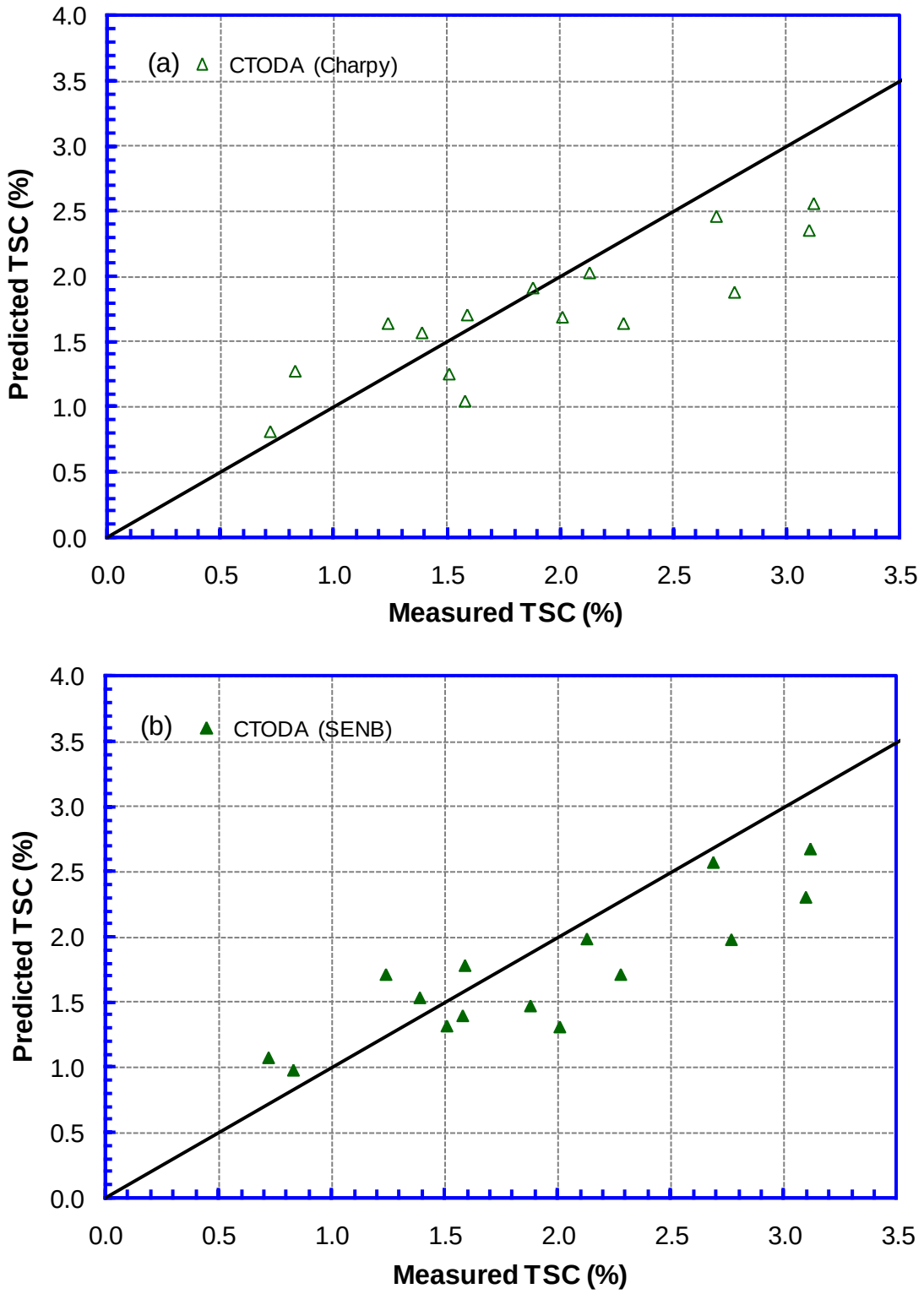

Figure 10-13 Comparison of predicted (Level 2) and measured TSC of 15 tests with strain values of 0.7-3.5% (a) $CTOD_A$ from Charpy test; (2) $CTOD_A$ from SENB test

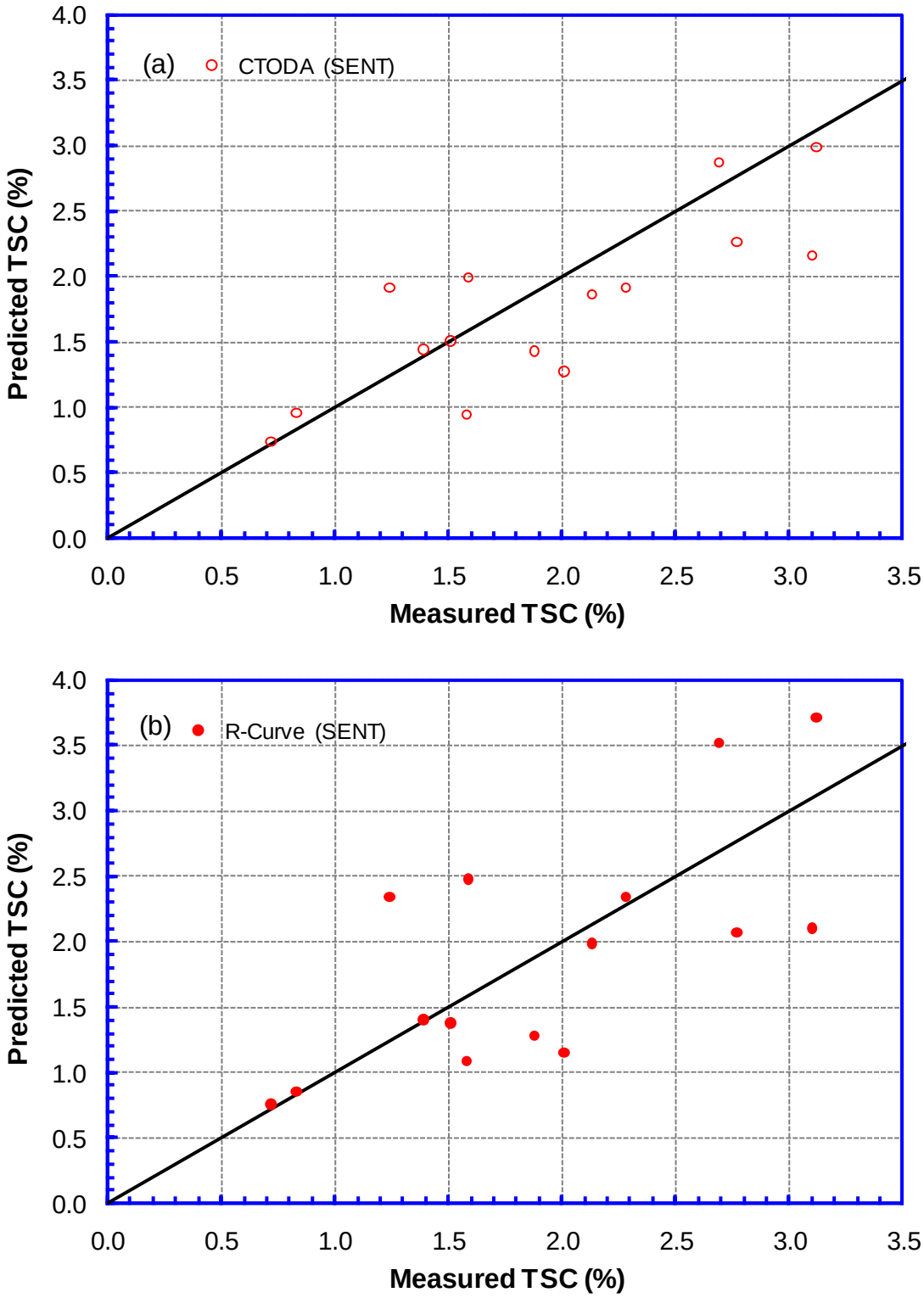

Figure 10-14 Comparison of predicted (Level 3) and measured TSC of 15 tests with strain values of 0.7-3.5% (a) $CTOD_A$ from SENT test; (b) R-curve from SENT test

10.5.3 Test Data of Low Measured TSCs

To examine the two tests with low strain values (< 0.7%), the measured nominal stress vs. remote strain relations for Tests 1.9, 1.19, and 1.23 are shown in Figure 10-15. Test 1.18 is also shown to indicate the typical stress-strain curve shape. Tests 1.9 and 1.19 were duplicate tests and the predicted TSC was about 1.6%. While this prediction matches reasonably well with the result of Test 1.19 (1.3%), it is considerably higher than the result of Test 1.9 which failed at 0.61%. Test 1.23 is useful for comparison to Test 1.9 because the specimen conditions were similar and it also produced a low strain result. Tests 1.9 and 1.23 were both overmatched with weld metal centerline notches. The measured TSCs were 0.61% and 0.66%, respectively. Test 1.23 had a 2 × 70 mm notch which was shallower than Test 1.9 (3 × 50 mm), but the flaw areas were similar. The predicted capacity of Test 1.23 was 2.2% vs. the test result of 0.66%. Tests 1.9 and 1.23 both failed relatively early in the loading cycle (just beyond yield) as shown in Figure 10-15. But, they failed by ductile fracture when the crack tore through pipe wall ending the test by leakage. As shown in Figure 10-2, the nominal failure stresses of Test 1.9 and 1.19 are very close, separated by approximately 8 MPa or 1.2 ksi.

The specimens were inspected for high-low misalignment after welding and notch geometry was checked pre and post-test. No irregularities were found. In addition, the fracture surfaces were examined and no hidden weld defects were discovered. The strength and chemical compositions of those welds were thoroughly analyzed in a post test examination. It was confirmed that the weld has proper strength as expected. However, unexpected high Oxygen contents were discovered in those welds of Tests 1.9 and 1.23 (low TSCs). The oxygen contents in the weld of Test 1.19 were within the normal range. It is suspected that the high oxygen contents may deteriorate the weld toughness. However, it should be noted that some tests failed at very high TSCs also showed high oxygen contents. The details of the strength and chemical composition analyses can be found in Appendix E.

The $CTOD_A$ measured from the residual profiles of those non-breaching-wall flaws in Tests 1.9 and 1.23 also indicated the possibility of low weld toughness. The $CTOD_A$ of some crack profiles in those two tests was about 0.5 mm which is on the lower bound of the toughness spread of the welds from the same welding procedure.

In summary, high oxygen level and low toughness may have contributed to the measured low TSCs of Tests 1.9 and 1.23. Since the nominal failure stresses of those tests are fairly close to other tests which produced high failure strains, the other contributing factor could be the flat stress-strain curve of the tested materials. Further examination of the effects of material property variation is given in Section 10.5.5.

10.5.4 Test Data of High Measured TSCs

The tests with high measured TSCs were examined by grouping them using pipe Y/T ratio and internal pressure. The measured nominal stress vs. remote strain relations for Tests 1.7, 1.17, and 1.18 (see those marked in Figure 10-10) are shown in Figure 10-16. The conditions of the three tests were similar (i.e., X65 high Y/T pipe with pressure) and the predicted TSCs of all three tests were approximately 2.1%. The measured TSC of test 1.17 was 1.9% which matches

the prediction fairly well. However, the measured TSCs of Tests 1.7 and 1.18 were 4.2% and 5.9%, respectively, which are much higher than the predicted TSCs.

The difference between the nominal stresses corresponding to the predicted and measured TSCs was also examined. Of the three tests (1.7, 1.17, and 1.18) shown in Figure 10-16, Test 1.18 showed the largest difference between the nominal stresses at the predicted and measured TSCs, which is about 5.6 MPa (as marked in Figure 10-16).

Similar results can be found in Figure 10-17 for the X65 high Y/T pipe tests without pressure (Tests 1.6 and 1.8). The largest difference between the nominal stresses at the predicted and measured TSCs of the two tests is about 8.2 MPa (from Test 1.8). The measured strains are greater than the predicted strains by a factor of more than 2.

The measured nominal stress vs. remote strain curves of the X65 low Y/T pipes tested under pressurized and non-pressurized conditions are shown in Figure 10-18 (Tests 1.3, 1.15, and 1.20) and Figure 10-19 (Tests 1.4 and 1.16), respectively. The measured and predicted TSCs of Tests 1.3 (pressurized) and 1.4 (non-pressurized) are reasonably close. However, the predicted TSCs are much lower than the measured ones in the other tests. Similar observations as those made in Figure 10-16 and Figure 10-17 can be made. Although the measured and predicted TSCs can vary by a factor of two, the maximum difference between the nominal stresses at predicted and measured TSCs is less than 14.5 MPa (in Test 1.20).

10.5.5 Impact of Small Strength Variations

The results of Figure 10-16 to Figure 10-19 clearly demonstrate that, while the measured strains at the failure events can have large differences, the differences in the corresponding stresses at the same failure events are very small. As illustrated in Figure 10-5, the flaws can only "sense" the stress transmitted from the remote regions where the strains are measured. The flaws should be expected to behave the same if the applied stress on the flawed plane is the same[3]. The remote strains that are needed to produce this same level of stress may be different, depending on the stress-strain relations.

The impact of pipe strength variation was further analyzed by the linepipe groups, i.e., by the Y/T ratio. In Figure 10-20, a representative stress-strain relation was obtained from Test 1.8 for high Y/T pipes. This stress-strain curve is also termed baseline curve. Two more curves with a strength difference ±1 ksi (6.9 MPa) were "created" by parallel-shifting the baseline curve. Using a process similar to that generated Figure 10-7, the strain range at the same stress level was estimated from the upper and lower curves.

It should be noted that the strain range is dominated by the shape of the stress-strain curve and the amount of strength variation. The absolute strength level of the baseline curve has little influence on the strain range so the single baseline curve can be used to represent the influence of strength variation with respect to the baseline curve.

[3] The context of this discussion is the stress being applied the pipe cross section where the flaw is located. The micro-scale mechanism of flaw failures is a separate subject which is not discussed here.

The experimentally measured and the predicted TSCs of the high Y/T pipes are compared in Figure 10-21 for all 19 tests. The predicted TSCs using the median values of the pipe and weld tensile properties are given as the *x* values. The corresponding measured TSCs are given as the *y* values. Three lines are also given in the plot. The middle line represents the one-to-one, i.e., perfect agreement between the measured and predicted TSCs. The upper line represents the remote strain value needed to produce the same stress level as the baseline curve when the stress-strain relation is 1 ksi (6.9 MPa) weaker than the baseline curve. By the same process, the lower line represents the remote strain when the stress-strain relation is 1 ksi (6.9 MPa) stronger than the baseline curve. The figure shows that the middle line of the prediction goes through the center of the cluster of the test data. The upper and lower bound curves due to a ±1 ksi strength variation follow the upper and lower bounds of the experimental data.

A similar process similar to the one described above was repeated for the low Y/T pipes. In Figure 10-22, a representative stress-strain relation was obtained from Test 1.16 for the low Y/T pipes. Two more curves with a strength difference ±1 ksi (6.9 MPa) were "created" by parallel-shifting the baseline curve. The experimentally measured and the predicted TSCs of the low Y/T pipes are compared in Figure 10-23 for all 5 tests. The upper and lower lines were generated in the same way as those of Figure 10-21. Most of the test data treads the upper bound curve.

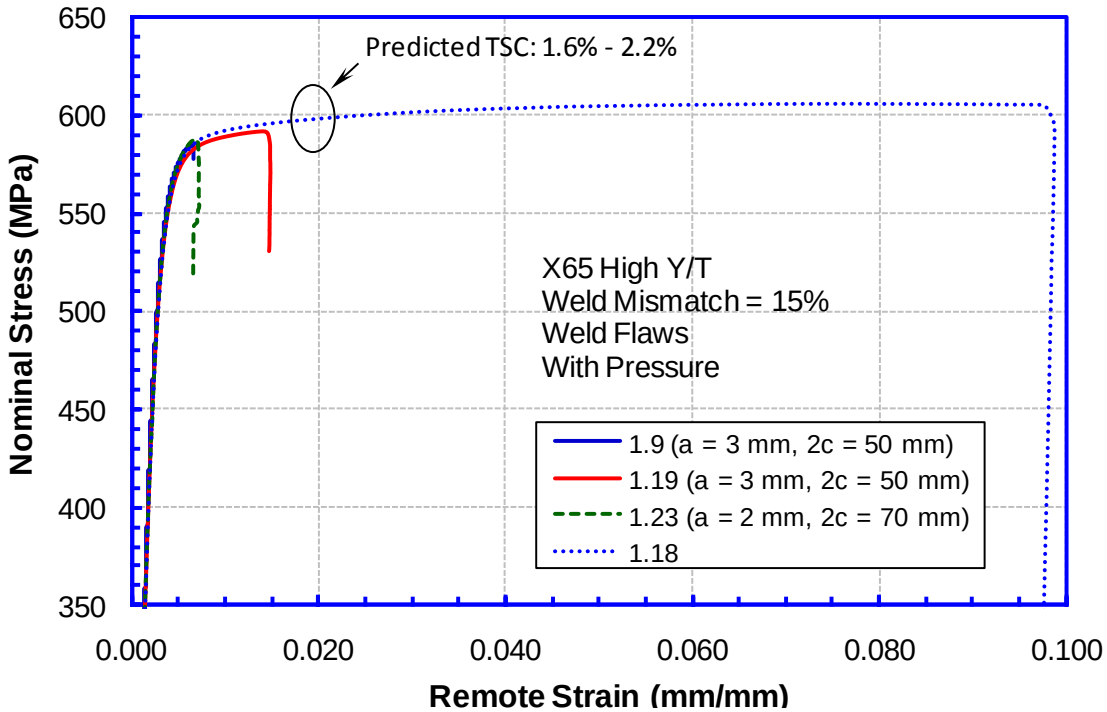

Figure 10-15 Measured nominal stress vs. remote strain relations for selected tests (1.9, 1.19, and 1.23)

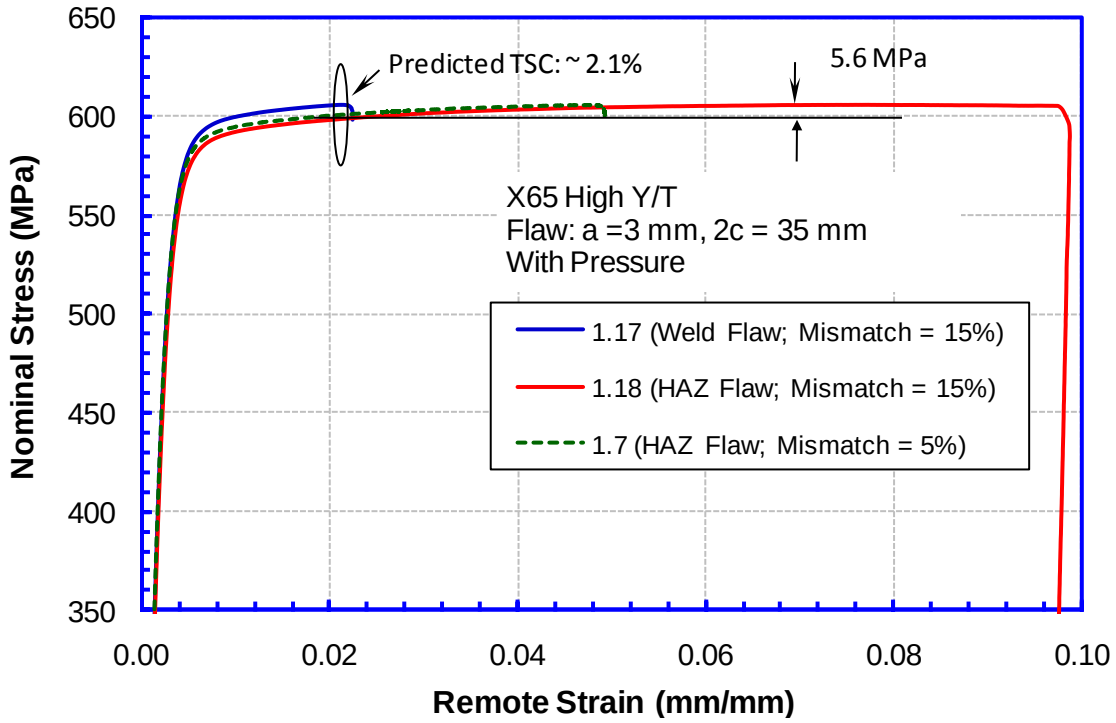

Figure 10-16 Measure nominal stress vs. remote strain relations for selected tests (X65 High Y/T pipe with pressure - 1.7, 1.17, and 1.18)

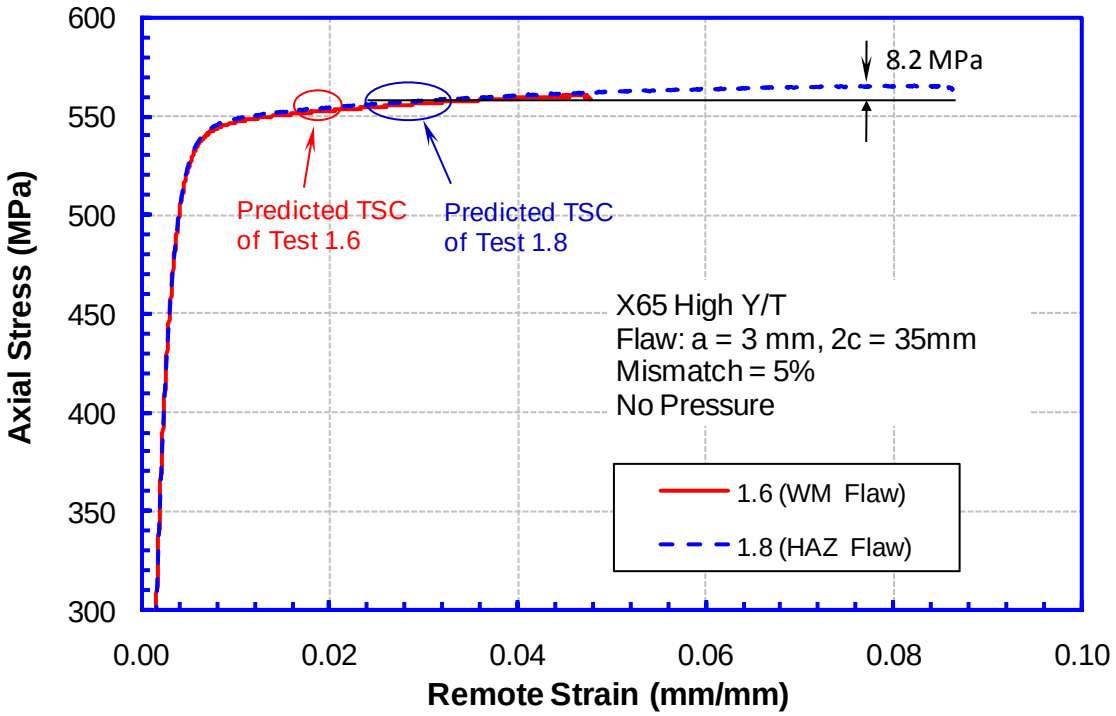

Figure 10-17 Measure nominal stress vs. remote strain relations for selected tests (X65 High Y/T pipe no pressure - 1.6 and 1.8)

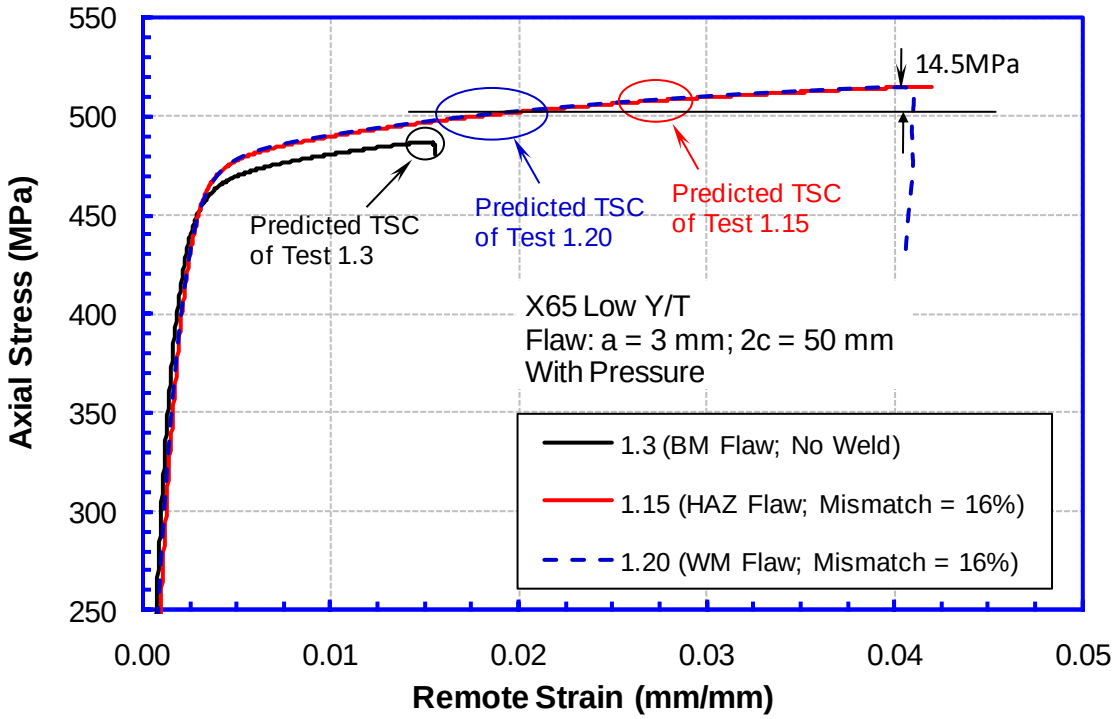

Figure 10-18 Measure nominal stress vs. remote strain relations for selected tests (X65 Low Y/T pipe with pressure – 1.3, 1.15, and 1.20)

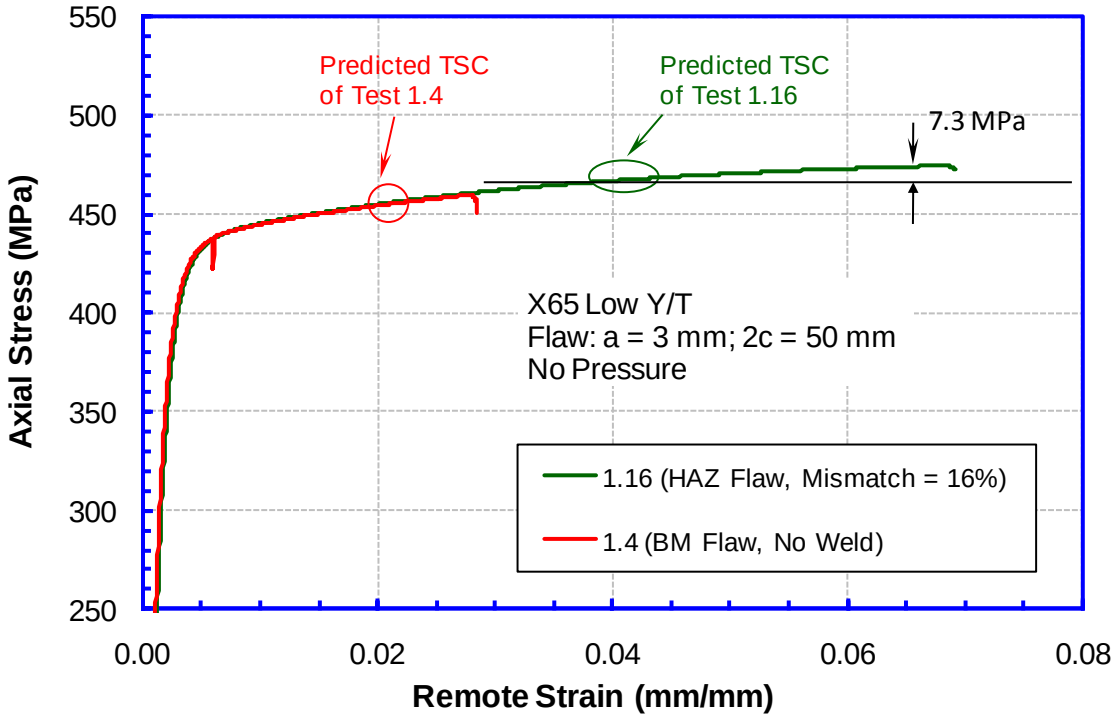

Figure 10-19 Measure nominal stress vs. remote strain relations for selected tests (X65 Low Y/T pipe no pressure - 1.4 and 1.16)

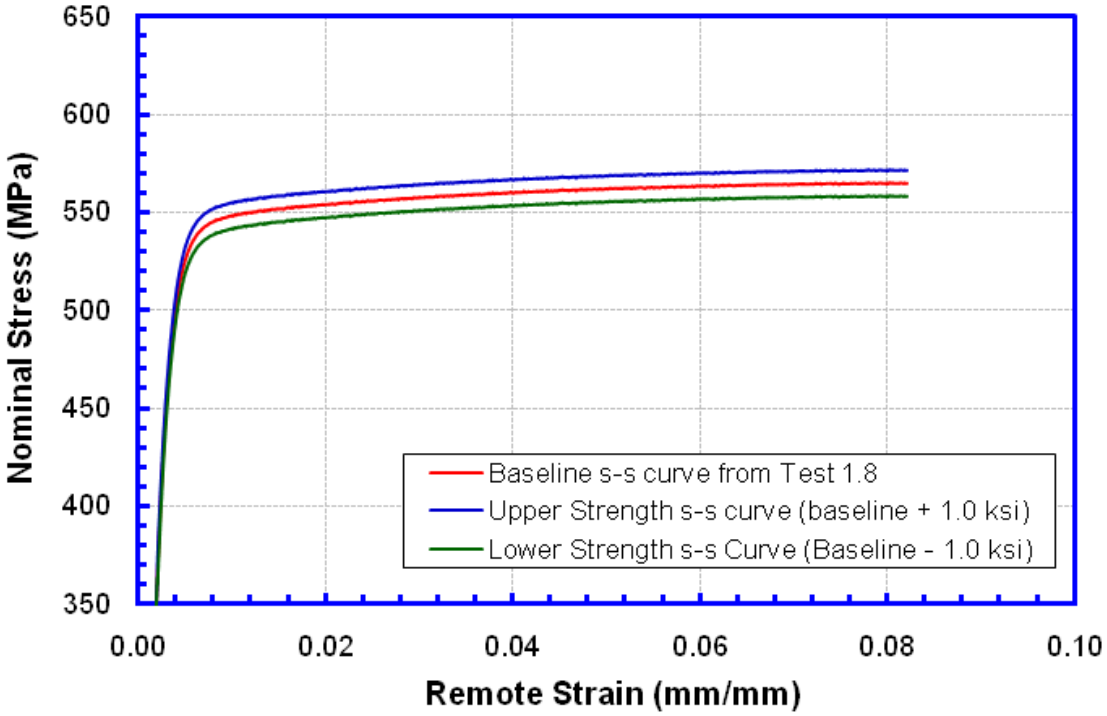

Figure 10-20 Baseline stress-strain relation of high Y/T pipe and two variations from the baseline relation

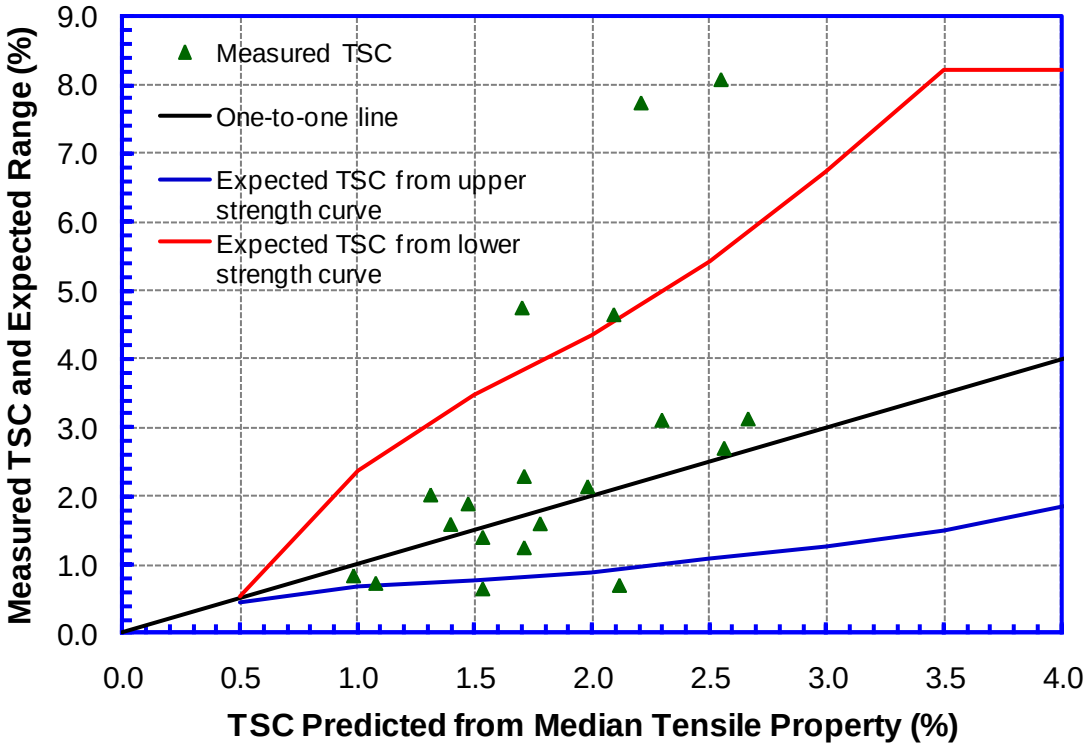

Figure 10-21 Comparison of experimentally measured and predicted TSCs of the high Y/T pipes (The TSCs are predicted using Level 2 SENB toughness option. The possible range of the TSCs from the strength variation of ±1 ksi is also shown.)

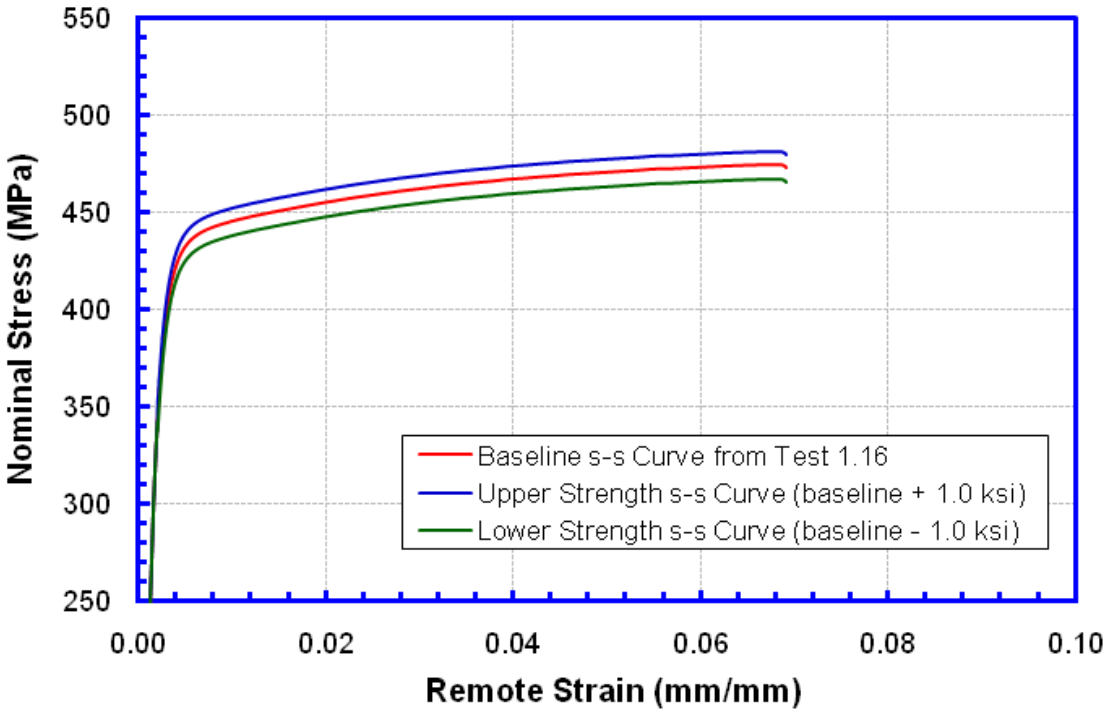

Figure 10-22 Baseline stress-strain relation of low Y/T pipe and two variations from the baseline relation

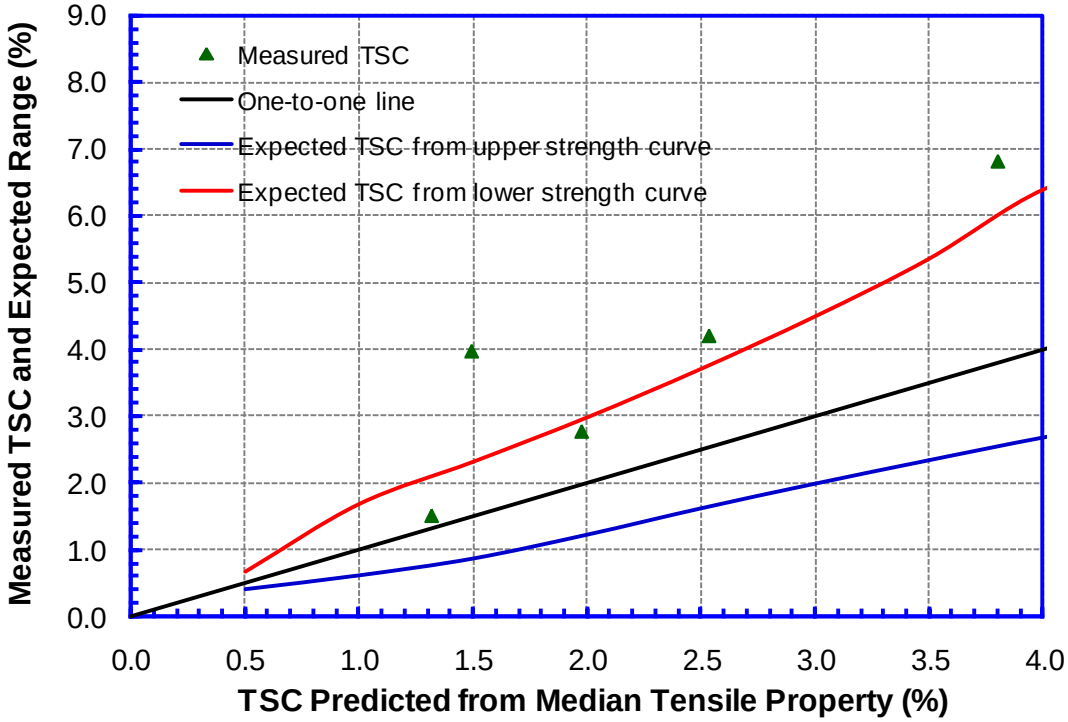

Figure 10-23 Comparison of experimentally measured and predicted TSCs of the low Y/T pipes (The TSCs are predicted using Level 2 SENB toughness option. The possible range of the TSCs from the strength variation of ±1 ksi is also shown.)

10.6 Summary of Model Evaluation

The general observations from the model evaluation are summarized as follows.

(1) TSC predictions using the ductile-instability and the initiation-control based limit state were exercised. Different toughness options were applied for the initiation-control based limit state. The consistency of the predictions from all TSC models (i.e., the initiation-control and ductile-instability based limit state) with different toughness options is similar.

(2) The predicted median TSCs trend with and go through the center of the cluster of the test data. The predicted upper and lower bound TSCs due to a ±1 ksi pipe strength variation (along the length of the pipe) follow the data scatter well.

(3) Seven of the 24 tests failed at high strain values (> 3.5%) and were under-predicted by all versions of the TSC models. One of the contributing factors is the large uncertainty associated with the measured TSCs when the strain approaches to the uniform strain where the stress-strain curve becomes very flat. The seemingly large measured TSCs are not repeatable and tend to have large variations.

(4) Two of the 24 tests failed at low strain values (< 0.7% strain) and were over-predicted by all versions of the TSC models. The possible contributors are high oxygen level of the weld metal, low toughness, and the flat stress-strain curves.

(5) The most significant contributor to the TSC variation and the difference between the measured and predicted TSCs is likely the strength variation along the length of the pipe. A small variation in the strength can lead to a large variation of the measured remote strain even when the flaw behaves consistently as expected.

For the linepipe materials tested in this project, the plastic part of the stress-strain curves is very flat. In the high strain regime, the flaw cannot "sense" the difference in the strains in remote regions as these strains produce almost identical stress. From a practical viewpoint, it is unlikely that these large strain values can be repeated consistently given the required precision and repeatability of the stress-strain curves. Therefore, there is a high possibility that large TSC variations can be expected under nominally identical conditions. The 24 full-scale tests showed a TSC range between about 0.6% and 8.1%. The two pair of duplicate tests both showed a TSC variation of a factor of two. As discussed in Section 10.1, it is often not possible to completely separate model and experimental uncertainties. However, the above observations highlighted the expected large experimental uncertainties.

Given the expected and well-documented uncertainty of the experimental data, the model should be evaluated based on the overall trend of the predictions. As shown in Figure 10-21 and Figure 10-23, the predicted median TSCs trend well with and go through the center of the cluster of test data. In addition, the predicted TSC range based on a ±1 ksi strength variation along the length of the pipe corresponds well with the scatter of the test data.

10.7 Limitations of Test Data and Model Evaluation

The model evaluation portion of this project was limited in certain respects related to the scope of the experimental work, in particular the relatively high Y/T ratio and flat stress-strain

curves of the pipe materials. The full-scale tests were conducted with two types of pipes which had a yield strength separation of approximately 10-15 ksi. The Y/T ratios of the two types of pipes were about 0.88 and 0.92, respectively. Three separate welding procedures were developed for those two types of pipes, effectively creating three weld strength levels. The characteristics of the pipe materials led to the high possibility of large TSC variations which imposed challenges and increased uncertainties to the model evaluation.

In addition, all full-scale pipes tested in this project had the same wall thickness and diameter. Additionally, girth weld high-low misalignment was accommodated in the prediction models, but no tests with misalignment were conducted. The pipe TSC is known to be weakly dependent on pipe diameter. However, pipe wall thickness and girth weld high-low misalignment are known to have significant effects on the TSCs. Therefore, while the developed tensile strain capacity prediction models covered a wide range of parameters, future full-scale testing will be necessary to validate the models in their full applicable range.

11 Discussion of Key Issues

11.1 Toughness Transferability

11.1.1 Observation of Test Data

One of the key issues in the development of tensile strain design models is the transferability of toughness measurement among specimens of different scales. As discussed in Appendix C, the relative ranking of resistance curves among SENT, CWP, and full-scale specimens is not consistent among different published data. For instance, SINTEF shows that the ranking of the resistance curves from high to low is full-scale, CWP, and SENT specimens [55]. Cheng, et al, shows that the resistance curves of full-scale and SENT specimens are the same or very close and the resistance curve CWP falls below both full-scale and SENT specimens [56].

The transferability of resistance curves between full-scale pipes and SENT was examined in great detail in this project. Section 8.3 shows the construction of (residual) resistance curves from full-scale test data using the residual flaw profiles of the flaw cross-section. The residual flaw profile reflects the flaw profile after unloading, at the termination of the test. In order to construct the flaw profile before unloading, the residual CMOD from the residual flaw profile is compared with the clip gage CMOD measured before the unloading. A nearly linear relationship is established between the residual CMOD and the measured CMOD before unloading, as shown in Figure 11-1. It is evident that the CMOD, before unloading, is approximately 10% higher than the residual CMOD.

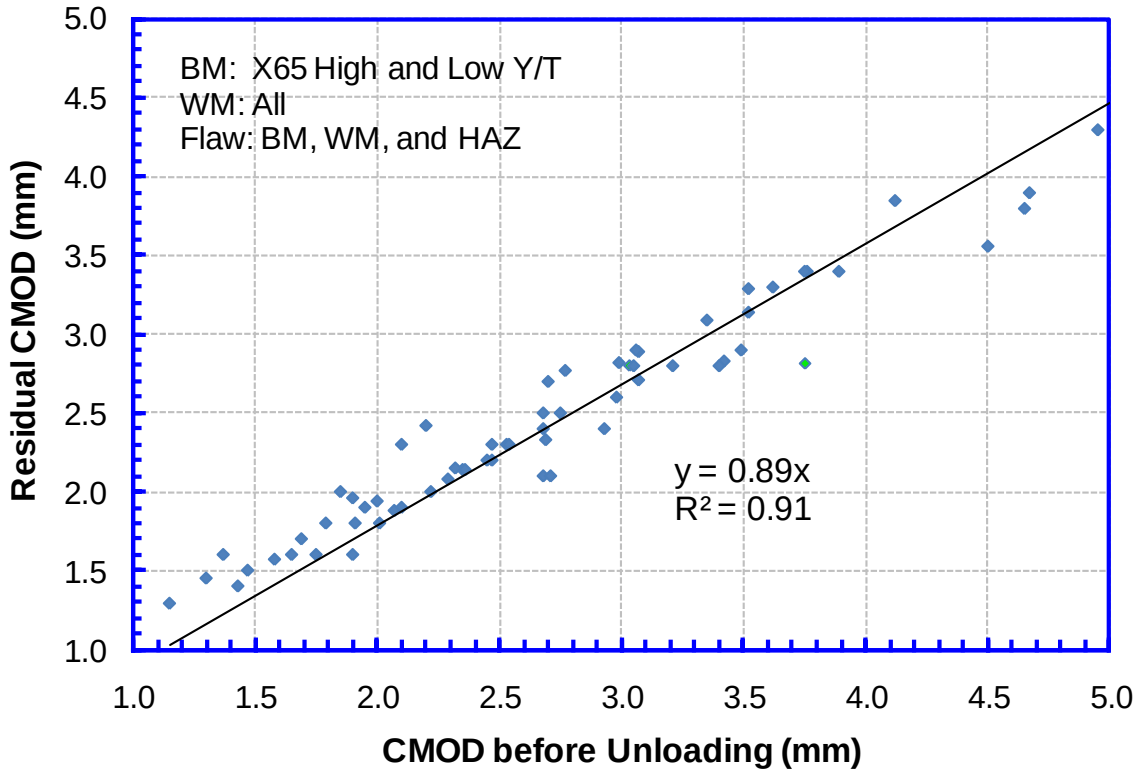

Figure 11-1 Relationship between the residual CMOD and the measured CMOD before unloading

The residual CTOD from full-scale specimens, similar to that shown in Figure 8-6, was multiplied by a factor of 1.1 to obtain the CTOD before unloading. Figure 11-2 shows the comparison of resistance curves between the full-scale pipes and the corresponding SENT for six groups of material and flaw locations. Two trends may be observed from the comparison. First, the resistance curves of the pipes are generally higher than those of SENT. Secondly, resistance curves of the full-scale pipes are slightly higher than those of SENT in some cases, but significantly higher in other cases.

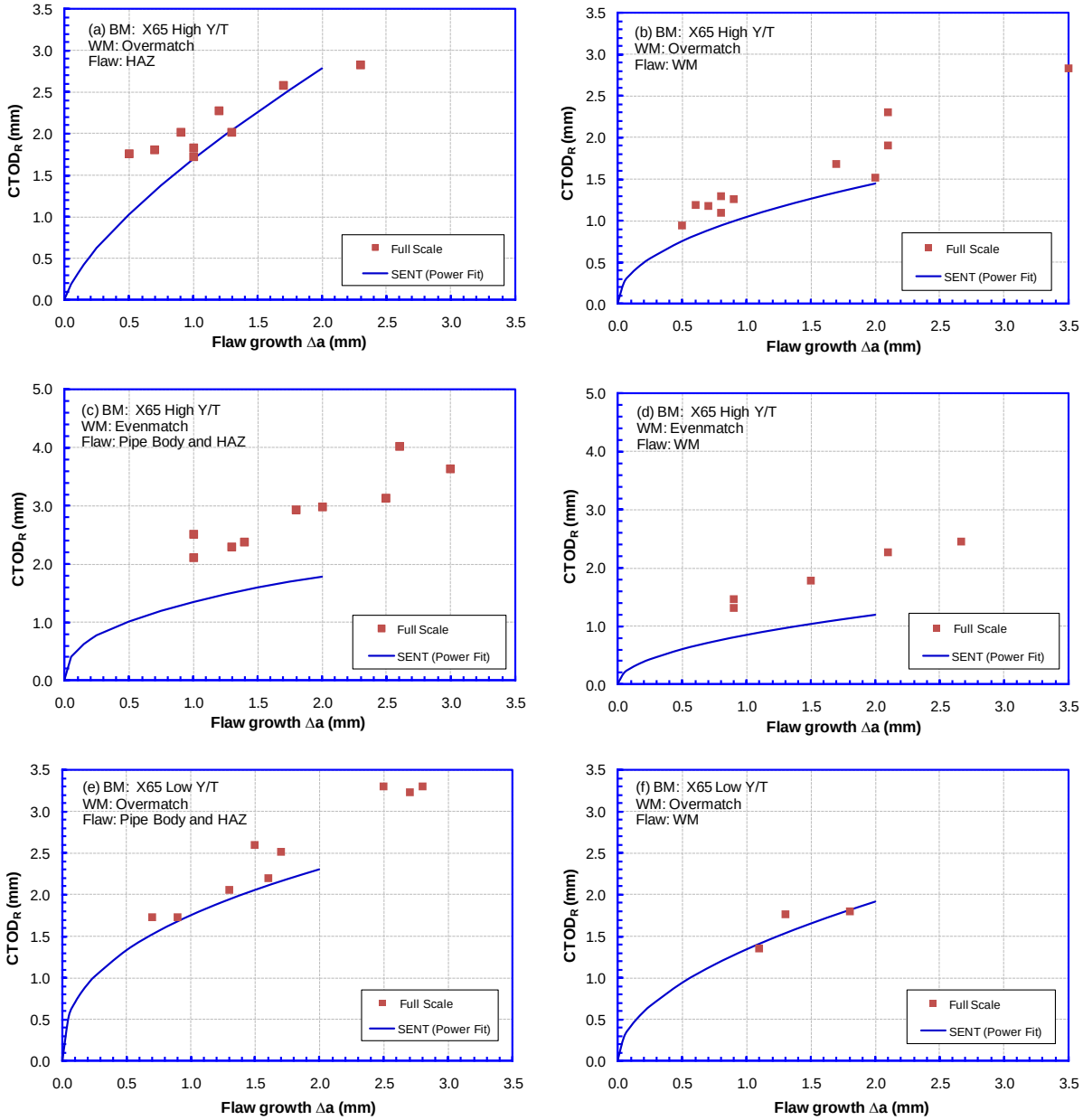

Figure 11-2 Comparison of resistance curves between full-scale pipes and SENT

11.1.2 Concluding Remarks of the Transferability of Resistance Curves

The data generated from this project demonstrate that the transferability of resistance curves between the full-scale pipes and SENT cannot be guaranteed in all cases. This observation is generally consistent with the philosophy of DNV-RP-F108 and different from the results presented by Cheng, et al [56]. The precise causes of those different observations are not known for certain. It is clear, however, that the SENT resistance curves have been generated by following different test protocols. The details of the data acquisition, and post-test data analysis of the full-scale tests, can also affect the presented resistance curves. However these details are not sufficiently provided in some publications, and will not allow significant verification.

There is a strong library of evidence to suggest that the transferability of resistance curves, between full-scale pipes and SENT specimen, should not be automatically assumed in all cases. More in-depth analysis of past and future data is necessary to establish the transferability. Such analysis can only be done if the details of the instrumentation plan, data acquisition method, and post-test data processing procedure are provided for review and verification.

11.2 Strength Variation along Pipe Length and Strain Based Design

As discussed in Sections 10.3.6 and 10.5.5, a relatively small variation of the pipe strength in the uniform strain zone can lead to a large variation of measured TSCs. The effect of pipe strength and TSC variation to strain based design is discussed in this section. For example, in a full-scale pipe test (as shown in Figure 11-3 (a)), the material properties near the flaw are assumed to be known and the flaw fails at a nominal stress of 556 MPa. If the pipe strength is 1 ksi stronger in one uniform zone and 1 ksi weaker in the other than the baseline property, the measured TSCs in the two uniform zones are 1.1% and 5.6%, respectively as shown in Figure 11-4. The large difference in the measured TSCs seems to create great uncertainty in strain-based design.

However, as shown in Figure 11-3 (b), if the same pipe were installed in the field and subjected to longitudinal tension from ground movement hazards. If the pipe were to fail at the predicted nominal stress level as in the tensile strain model, the strain demands of the two pipes would be 1.1% and 5.6%, respectively. The pipe with the lower strength has the higher capacity, and at the same time, has the higher strain demand. The strain demand and strain capacity match each other. Therefore, the large strain capacity variation due to pipe strength variation is balanced out the same variation of the strain demand. This analysis confirms that strain-based design is feasible even there is a large variation of strains due to the pipe strength variation. It highlights the need to examine the strain demand and strain capacity in the same framework. This same analysis also indicates that the possible large strain variation needs to be considered when test data are compared with deterministic tensile strain capacity prediction models.

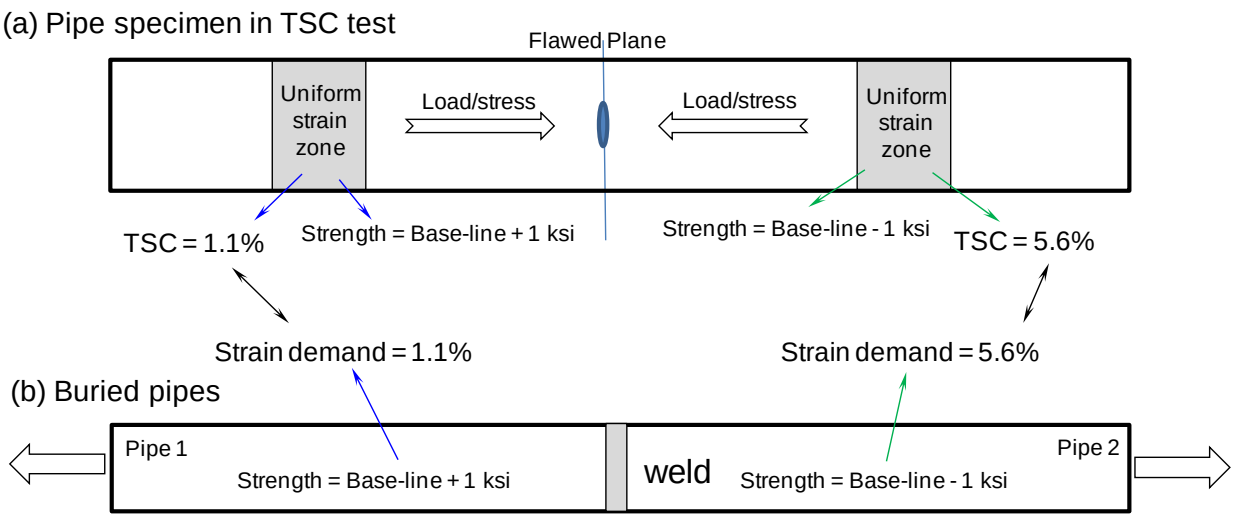

Figure 11-3 Strain capacity vs. strain demand

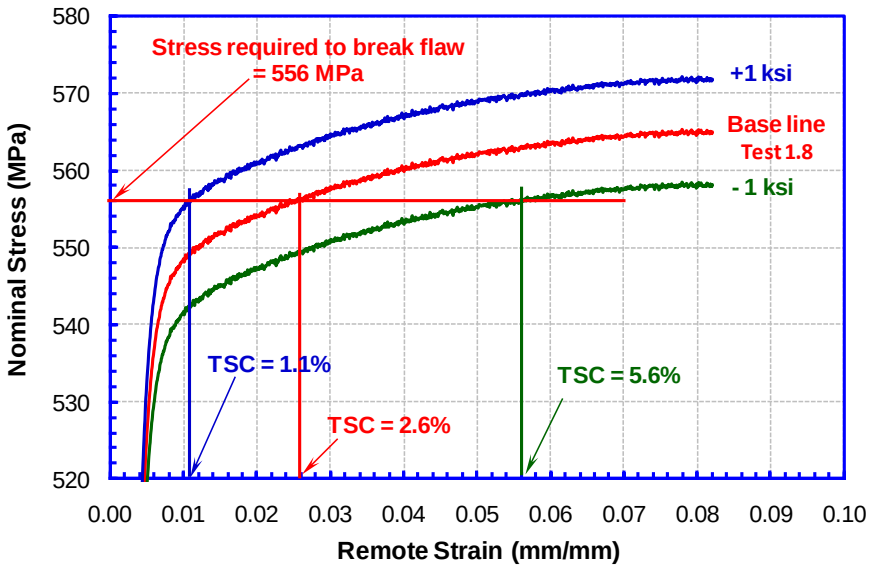

Figure 11-4 TSC variation vs. strength variation

12 Concluding Remarks

A major research program has been undertaken to develop tensile strain design models with the support of a multitude of test specimens. The central output of this second project of the consolidated program is the tensile strain design procedures. The procedures involve three essential elements: (1) linepipe specification, (2) welding procedure qualification, and (3) tensile strain design models. The main focus of this project is the third element, i.e., tensile strain design models. The tensile strain design procedures consist of recommendations in the three essential elements. In most cases, background information and rationale are provided along with the recommendations. The recommendations are not meant to be all-inclusive. Appropriate national and international standards should be followed in conjunction with the recommendations presented here. All phases of a pipeline life, including installation, commissioning, and operation should be considered to ensure safe operation over its entire life.

The tensile strain design models are structured with the following overarching principles. First, a flexible framework is established for the adoption of the current technology and the incorporation of future development. Secondly, the most appropriate approach for the tensile strain design of a particular project depends on the scale of the project and many design and maintenance considerations. No single approach may be appropriate for all projects. Thirdly, a framework of a multi-level approach is proposed which allows for the use of a wide variety of material toughness test options.

A four-level approach is proposed for the tensile strain design models. The Level 1 procedure provides estimated tensile strain capacity (TSC) in a tabular format for quick initial assessment. The apparent toughness is estimated from upper shelf Charpy impact energy. The Level 2 procedure contains a set of parametric equations. The tensile strain capacity can be computed from these equations with the input of pipe's dimensional parameters and material property parameters, including apparent toughness. The apparent toughness is estimated from either upper shelf Charpy energy or upper shelf toughness of standard CTOD test specimens. The Level 3 procedure uses the same set of equations as in Level 2. The toughness options are expanded to the toughness obtained from newer lower-constraint tests. In this level, two limit states, based on either initiation control or ductile instability, can be analyzed. The Level 4 procedure allows the use of direct FEA calculation to develop crack driving force relations. The same limit states as those in Level 3 may be analyzed. The Level 4 procedures should only be used by seasoned experts in special circumstances where lower level procedures are judged inappropriate.

The tensile strain design models may be used for the following purposes.

(1) The determination of tensile strain capacity for given material properties and flaw size.

(2) The determination of acceptable flaw sizes for given material properties and target tensile strain capacity.

(3) The selection of material properties to achieve a target strain capacity for a given flaw size.

(4) The optimization of the tensile strain capacity by balancing the requirements of material parameters, such as weld strength (thus weld strength mismatch level) versus toughness.

The essential features of the tensile strain design models are as follows:

(1) Two limits states are recognized: (1) initiation control and (2) ductile instability.

(2) Two weld bevel geometries are recognized: (1) narrow-groove, typical of mechanized GMAW welds and (2) standard groove, typical of FCAW and SMAW welds.

(3) There are no inherent limits on pipe grade. The linepipe tensile properties are represented by its longitudinal *Y*/*T* ratio, which serves as a representation of linepipes strain hardening capacity.

(4) linepipeThe weld should not have gross strength undermatching.

(5) The target optimum strain range of the models is from 1.0% to one half of the pipe's uniform elongation.

(6) The models are applicable to one single flaw in a girth weld. If multiple flaws were to exist in a single girth weld, the flaws need to be sufficiently far apart, so that the existence of other flaws does not affect the behavior of the flaw being evaluated.

(7) No flaw interaction rules are established and applied in the models.

(8) No embedded safety factor is applied or implied.

(9) The models should not be used for flaw acceptance after repair welding without further evaluation.

(10) The potential impact of material anisotropy on the tensile strain capacity is not considered in the models.

The fundamental basis of the tensile strain models does not assume or rely on material property data of any particular grade. The parametric representation of the tensile property of the linepipes and welds was developed using a material database which covered grades from X65 to X100. The tensile strain design models are, in principle, applicable to all GMAW and FCAW/SMAW processes, provided that appropriate mechanical property data are within the applicable range of the models. However, the validation of the models is limited to mechanized GMAW processes at this time.

One of the major focuses of the test program is the effects of internal pressure on tensile strain capacity. A large number of paired tests, full-scale pipes with and without pressure, were conducted to investigate the effects of internal pressure. The experimental test results conclusively demonstrated that the internal pressures equivalent to Classes 1 and 2 designs could reduce the strain capacity of pipelines with circumferential planar flaws, by as much as 50% or more. The magnitude of the pressure effects is confirmed by the numerical analysis. The effects of the internal pressure have been incorporated into the tensile strain design models.

There are a couple of critical issues facing the tensile strain design.

(1) The treatment of pop-in events in the toughness testing has to be addressed. The assurance of upper shelf ductile behavior, is necessary to achieve adequate tensile strain capacity.

(2) The transferability of resistance curves between small-scale test specimens and large-scale structure remains an open issue. It is almost certain, from both available test data and theoretical analysis, that the transferability cannot be universally assured for all conditions.

(3) The variation of pipe tensile properties needs to be better understood and quantified. This process will involve more rigorous inspection of testing procedures and dedicated and consistent post-test data processing procedures.

(4) Unified and workable linepipe specifications sufficient for the tensile strain capacity, compressive strain capacity, and strain demand are needed.

(5) Flaws tend to interact at much greater distances under strain-based design conditions than under stress-based design conditions. The present flaw interaction rules are not applicable to strain-based design. New flaw interaction rules should be established for strain-based design.

(6) The tolerance of buried flaws under strain-based design conditions has, for a large part, not been investigated. It is expected that the buried flaws of the same size as surface-breaking flaws, are less detrimental to girth weld integrity. The investigation of the buried flaws should yield benefits to the industry.

The tensile strain design is a complex subject. Significant progress has been made through the joint effort of this project team. At the same, more issues have been discovered through this investigation process. More work, particularly of different wall thicknesses and a broader range of material properties, will help the confirmation of the current work and resolve some of the remaining issues.

Parallel to the development of tensile strain design models around the world, there has been the development and application of non-standardized material test methods. A few notable examples of those test methods are: all weld metal tensile test, single-edge-notched tension (SENT) test, curved wide plate (CWP) test, and full-scale pressurized pipe (FSPP) tests. Although SENT, CWP and FSPP tests have been around for a while, the type and precision of the test data required for tensile strain designs are different from those required for the traditional stress-based design. The tests conducted from this program show that the reported value from a test, such as the tensile strain capacity or toughness resistance curve, depends on (1) the setup of data acquisition and (2) post-test data processing for raw test data, to customarily used final data. For instance, the tensile strain capacity reported in the literature is variably from (1) averaged strain over the entire specimen length, (2) a section of specimen straddling the girth weld with flaws, or (3) a zone away from girth weld flaws and specimen ends. Assuming the material behaves the same, the raw data from those measurements would be different. Certain measurements, such as flaw growth from unloading compliance, are more sensitive in one specimen form than the other. Consequently, it is critical that the details of the test protocol and post-test data processing procedures are reported along with test data summary for those non-standardized tests. Any validation of tensile design models should be conducted with the full knowledge of test protocol and post-test data processing procedures.

13 References

1 "Guidelines for Constructing Natural Gas and Liquid Hydrocarbon Pipelines Through Areas Prone to Landslide and Subsidence Hazards," prepared by C-CORE, D. G. Honegger Consulting, and SSD, Inc., PRCI Catalog No. L52292, January 2009.

2 Wang, Y.-Y., Liu, M., Long, X., Stephens, M., Petersen, R., and Gordon, R., "Validation & Documentation of Tensile Strain Limit Design Models for Pipelines," PRCI Project ABD-1, DOT Agreement DTPH56-06-T000014, Final report, August 2, 2011.

3 Hukle, M. W., Horn, A. M., Hoyt, D. S., and LeBleu, Jr., J. B., "Girth Weld Qualification for High Strain Pipeline Applications," *Proceeding of the 24th International Conference on Offshore Mechanics and Arctic Engineering (OMAE2005)*, June 12-17, Kalkidiki, Greece, 2005.

4 Denys, R., Lefevre, A., and Baets, P. D., "A Rational Approach to Weld and Pipe Material Requirements for a Strain Based Pipeline Design," *Proceedings of Applications & Evaluation of High-Grade Linepipes in Hostile Environments*, Pacifico Yokohama, Japan, November 7-8, 2002, pp. 121-157.

5 Wang, Y.-Y., Liu, M., Chen, Y., and Horsley, D., "Effects of Geometry, Temperature, and Test Procedure on Reported Failure Strains from Simulated Wide Plate Tests," *Proceedings of 6th International Pipeline Conference*, Paper No. IPC2006-10497, September 25-29, 2006, Calgary, Alberta, Canada.

6 Denys, R.M. and Lefevre A.A., "Ugent guidelines for curved wide plate testing", *Pipeline Technology Conference*, Paper number Ostend2009-110, Ostend, Belgium, October 12-14, 2009.

7 "Update of Weld Design, Testing, and Assessment Procedures for High Strength Pipeline," project funded by the U.S. Department of Transportation Pipeline and Hazardous Materials Safety Administration, Contract No. DTPH56-07-T-000005.

8 DNV OS-F101, "Submarine Pipeline System," 2000.

9 DNV-RP-F108, "Fracture control for pipeline installation methods introducing cyclic plastic strain", 2006.

10 Wang, Y.-Y., Rudland, D., Denys, R., and Horsley, D. J., "A Preliminary Strain-Based Design Criterion for Pipeline Girth Welds," *Proceedings of the International Pipeline Conference 2002*, Calgary, Alberta, Canada, September 29-October 3, 2002.

11 Wang, Y.-Y., Cheng, W., McLamb, M., Horsley, D., Zhou, J., and Glover, A., "Tensile Strain Limits of Girth Welds with Surface-Breaking Defects Part I an Analytical Framework," in *Pipeline Technology, Proceedings of the 4th International Conference on Pipeline Technology*, Edited by Rudi Denys, Ostend, Belgium, May 9-13, 2004.

12 Wang, Y.-Y., Horsley, D., Cheng, W., Glover, A., McLamb, M., and Zhou, J., "Tensile Strain Limits of Girth Welds with Surface-Breaking Defects Part II Experimental Correlation and Validation," in *Pipeline Technology, Proceedings of the 4th International*

Conference on Pipeline Technology, Edited by Rudi Denys, Ostend, Belgium, May 9-13, 2004.

13 Horsley, D. and Wang, Y.-Y., "Weld Mismatch Effects on the Strain Limits of X100 Girth Welds," in *Pipeline Technology, Proceedings of the 4th International Conference on Pipeline Technology,* Edited by Rudi Denys, Oostende, Belgium, May 9-12, 2004.

14 Wang, Y.-Y., Cheng, W., and Horsley, D., "Tensile Strain Limits of Buried Defects in Pipeline Girth Welds," *Proceedings of the International Pipeline Conference 2004*, Calgary, Alberta, Canada, October 4-8, 2004.

15 CSA Z662, "Oil and Gas Pipeline Systems," Canadian Standards Association, 2007.

16 Østby, E, "New strain-based fracture mechanics equations including the effects of biaxial loading, mismatch and misalignment", *Proceeding of the 24th International Conference on Offshore Mechanics and Arctic Engineering*, Paper No. OMAE2005-67518, June 12-17, 2005, Halkidiki, Greece.

17 Sandivk, A., Østby, E, Naess A., Sigurdsson G., and Thaulow, C., "Fracture control – offshore pipelines: probabilistic fracture assessment of surface cracked ductile pipelines using analytical equations", *Proceeding of the 24th International Conference on Offshore Mechanics and Arctic Engineering*, Paper No. OMAE2005-67517, June 12-17, 2005, Halkidiki, Greece.

18 Nyhus, B., Østby, E, Knagenhjelm, H.O., Black, S., and RØstadsand, P.A., "Fracture control – offshore pipelines: experimental studies on the effect of crack depth and asymmetric geometries on the ductile tearing resistance", *Proceeding of the 24th International Conference on Offshore Mechanics and Arctic Engineering*, Paper No. OMAE2005-67532, June 12-17, 2005, Halkidiki, Greece.

19 Minnaar, K. Gioielli, P.C., Macia, M.L., Bardi, F., Biery, N.E., and Kan, W.C., "Predictive FEA modeling of pressurized full-scale tests", *Proceedings of the 17th International Offshore and Polar Engineering Conference*, July, 1-6, 2007, Lisbon, Portugal, P3114.

20 Fairchild, D.P., Cheng, W., Ford, S.J., Minnaar, K., Biery, N.E., Kumar, A., and Nissley, N.E., "Recent advances in curved wide plate testing and implications for strain-based design", *Proceedings of the 17th International Offshore and Polar Engineering Conference*, July, 1-6, 2007, Lisbon, Portugal, P3013.

21 Kibey, S.A., Minnaar, K., Cheng, W., and Wang, X., "Development of a physics-based approach for the predictions of strain capacity of welded pipelines", *Proceedings of the 19th International Offshore and Polar Engineering Conference*, June, 21-26, 2009, Osaka, Japan, P132.

22 Kibey, S., Issa, J.A., Wang, X., and Minnaar, K., "A simplified, parametric equation for prediction of tensile strain capacity of welded pipelines", *Pipeline Technology Conference*, October 12-14, 2009, Paper No. Ostend2009-039, Ostend, Belgium.

23 Otsuka, A., et al., "Effect of Stress Triaxiality on Ductile Fracture Initiation of Low Strength Steel," *J. of the Society of Material Science*, Japan, Vol. 29, No. 322, pp. 717-723, 1980.

24 Toyoda, M., et al., "Criterion for Ductile Cracking for the Evaluation of Steel Structure under Large Scale Cyclic Loading," *Proc. Of 20th International Conference on Offshore Mechanics and Arctic Engineering*, OMAE 2001-MAT-3103, 2001.

25 Igi, S. and Suzuki, N., "Tensile Strain Limits of X80 High-Strain Pipelines," *Proceedings of the 17th International Offshore and Polar Engineering Conference*, Lisbon, Portugal, July 1-6, 2007.

26 Mohr. W. C., "Strain-Based Design of Pipelines," final report to MMS, October 2003.

27 Mohr, W., "Weld Area Mismatch and Pressure Effects in Strain-Based Design," *Proceedings of the 4th International Conference on Pipeline Technology*, Edited by Rudi Denys, Ostend, Belgium, May 9-13, 2004, pp. 279-290.

28 Liu, M., Wang, Y.-Y., and Horsley, D., "Significance of HAZ Softening on Strain Concentration and Crack Driving Force in Pipeline Girth Welds," *Proceeding of the 24th International Conference on Offshore Mechanics and Arctic Engineering* , OMAE 2005, June 13-17, Kalkidiki, Greece.

29 Wang, Y.-Y., Liu, M., Horsley, D., and Zhou, J., "A Quantitative Approach to Tensile Strain Capacity of Pipelines," 6th International Pipeline Conference, Paper No. IPC2006-10474, September 25-29, 2006, Calgary, Alberta, Canada.

30 Ostby, E., and Hellesvik, A., "Fracture Control of Offshore Pipeline JIP: Results from Large Scale Testing of the Effects of Biaxial Loading on the Strain Capacity of Pipes with Defects,'" *Proceedings of the 17th International Offshore and Polar Engineering Conference* (ISOPE 2007), Lisbon, Portugal, July 1-6, 2007.

31 Gioielli, P.C., Minnaar, K., Macia, M.L., and Kan, W.C, "Large-scale testing methodology to measure the influence of pressure on tensile strain capacity of a pipeline", *Proceedings of the 17th International Offshore and Polar Engineering Conference* (ISOPE 2007), Lisbon, Portugal, July 1-6, 2007.

32 Igi, S., Sakimoto, T., Suzuki, N., Muraoka, R., and Arakawa, T., "Tensile strain capacity of X80 pipeline under tensile loading with internal pressure", *Proceedings of the 8th International Pipeline Conference (IPC2010)*, Calgary, Alberta, Canada, Sept. 27-Oct. 1, 2010.

33 Wang, Y.-Y. and Liu, M., "The Role of Anisotropy, Toughness Transferability, and Weld Misalignment in the Strain Based Design of Pipelines," Proceedings of the 17th International Offshore and Polar Engineering Conference (ISOPE 2007), Lisbon, Portugal, July 1-6, 2007.

34 Wang, Y.-Y. and Liu, M., "Weld Integrity from the Perspective of Strain-Based Design of Large Diameter and High Strength Pipelines," Special Issue of the Proceedings of

"Pipeline Technology Now and Then" at the 8th International Welding Symposium, 8WS, November 16-18, 2008, Kyoto, Japan.

35 Kibey, S. A., Minnaar, K., Issa, J. A., and Gioielli, P. C., "Effect of Misalignment on the Tensile Strain Capacity of Welded Pipelines," *Proceedings of the 18th International Offshore and Polar Engineering Conference (ISOPE 2008)*, Vancouver, Canada, July 6-11, 2008.

36 Wang, Y.-Y., Liu, M., Stephens, M., Petersen, R., and Horsley, D., "Recent Development in Strain-Based Design in North America," *Proceedings of the 19th International Offshore and Polar Engineering Conference (ISOPE 2009)*, Osaka, Japan, July 21-26, 2009.

37 Igi, S., Sakimoto, T., Suzuki, N., Muraoka, R., and Arakawa, T., "Tensile Strain Capacity of X80 Pipeline under Tensile Loading with Internal Pressure," *Proceedings of the 8th International Pipeline Conference*, Paper No. IPC2010-31281, September 27 – October 1, 2010, Calgary, Alberta, Canada

38 Liu, M. and Wang, Y.-Y., "Significance of Biaxial Stress on the Strain Concentration and Crack Driving Force in Pipeline Girth Welds with Softened HAZ," *Proceedings of the 26th International Conference on Offshore Mechanics and Arctic Engineering (OMAS 2007)*, San Diego, California, USA, June 10-15, 2007.

39 McMeeking, R. M. and Parks, D. M., "On Criteria for *J*-Dominance of Crack Tip Fields in Large-Scale Yielding," *Elastic-Plastic Fracture*, ASTM STP 668, ASTM, pp. 175-194, 1979.

40 Begley, J. A. and Landes, J. D., "The *J*-Integral as a Fracture Criterion," *Fracture Toughness, Part II*, ASTM STP 514, ASTM, pp.1-20, 1972.

41 Shih, C. F. and German, M. D., "Requirements for a One Parameter Characterization of Crack Tip Fields by the HRR Singularity," *International Journal of Fracture*, Vol. 17, No. 1, pp.27-42, 1981.

42 Shih, C. F., "Relationships between the J-Integral and the Crack Opening Displacement for Stationary and Extending Cracks," *Journal of the Mechanics and Physics of Solids*, Vol. 29, pp. 305-326, 1981.

43 Wallin, K., "The Effects of T-Stress on the Master Curve Transition Temperature To," ECF 13, San Sebastian, Spain, 2000.

44 Wang, Y.Y., Liu, M., and Horsley, D., "Apparent toughness from constraint considerations and direct testing", *Proceedings of the 17th International Offshore and Polar Engineering Conference* (ISOPE 2007), Lisbon, Portugal, July 1-6, 2007.

45 Liu, M., Wang, Y.Y., and Long, X., "Enhanced apparent toughness approach to tensile strain design", *Proceedings of the 8th International Pipeline Conference (IPC2010)*, Calgary, Alberta, Canada, Sept. 27-Oct. 1, 2010.

46 Wang, Y.-Y., Kirk, M. T., and Reemsnyder, H., "Inference Equations for Fracture Toughness Testing: Numerical Analysis and Experimental Verification," *28th National*

Symposium on Fatigue and Fracture Mechanics, ASTM STP 1321, J. Underwood, etc., Eds., Saratoga Springs, NY, June 25-27, 1996.

47 Gianetto, J., Tyson, B., Wang, Y.-Y., Bowker, J., Park, D., and Shen, G., "Properties and Microstructure of Weld Metal and HAZ Regions in X100 Single and Dual Torch Girth Welds," *Proceedings of the 8th International Pipeline Conference,* Paper No. IPC2010-31411, September 27 – October 1, 2010, Calgary, Alberta, Canada.

48 Park, D.Y., Tyson, W.R., Gianetto, J.A., Shen, G, and Eagleson, R.S., "Evaluation of fracture toughness of X100 pipe steel using SE(B) and clamped SE(T) single specimens," *Proceedings of the 8th International Pipeline Conference (IPC2010),* September 27 – October 1, Calgary, Alberta, Canada, 2010.

49 Liu, M., Wang, Y.-Y., and Horsley, D., "Significance of HAZ softening on strain concentration and crack driving force in pipeline girth weld", *Proceeding of the 24th International Conference on Offshore Mechanics and Arctic Engineering (OMAE2005),* June 12-17, Kalkidiki, Greece, 2005.

50 Quintana, M. A., "Background of All-Weld Metal Tensile test Protocol," in Weld Design, Testing, and Assessment Procedures for High Strength Pipelines," Topical Report 277-T-02, May 2011.

51 Wang, Y.-Y., Zhou, H., Liu, M., Tyson, W., Gianetto, J., Weeks, T., McColskey, J. D., Quintana, M. A., and Rajan, V. B., "Weld Design, Testing, and Assessment Procedures for High Strength Pipelines," Summary Report 277, May 2011.

52 Bannister, A. C., "Determination of fracture toughness from Charpy impact energy: procedure and validation" SINTAP Sub-Task 3.3 Report, 1998.

53 Shen, G. and Tyson, W.R., Evaluation of CTOD from J-integral for SE(T) specimens, *Pipeline Technology 2009.*

54 Shen, G., Gianetto, J.A. and Tyson, W.R, Measurement of J-R curves using single-specimen technique on clamped SE(T) specimens, *Proceedings of the Nineteenth International Offshore and Polar Engineering Conference,* June 21-26, 2009.

55 DNV/SINTEF/TWI, "Fracture Control for Installation Methods Introducing Cyclic Plastic Strains, Development of Guidelines for Reeling of Pipelines," a JIP performed jointed by DNV, SINTEF, and TWI.

56 Cheng, W., Tang, H., Gioielli, P., Minnaar, K., Macia, M., "Test Methods for Characterization of Strain Capacity: Comparison of R-Curves from SENT/CWP/FS Tests," Pipeline Technology Conference, 12-14 October 2009, Ostend, Belgium.

Appendix A TSC Look-Up Tables for Level 1 Models

Table- A-1 TSC look-up table - GMAW (Y/T = 0.81)

Y/T	Mismatch Level	Misalignment (mm)	Flaw Depth, a (mm)	Flaw Length, 2c (mm)	Tensile Strain Capacity (%)																	
					Wall Thickness = 12.7 mm						Wall Thickness = 19.1 mm						Wall Thickness = 25.4 mm					
					$CTOD_A$ (mm)						$CTOD_A$ (mm)						$CTOD_A$ (mm)					
					0.6	0.8	1.0	1.2	1.4	1.6	0.6	0.8	1.0	1.2	1.4	1.6	0.6	0.8	1.0	1.2	1.4	1.6
0.81	1.00	1.6	2.0	25.0	1.2%	1.6%	1.9%	2.2%	2.5%	2.7%	2.3%	2.8%	3.2%	3.5%	3.7%	3.8%	3.3%	3.7%	3.9%	4.1%	4.2%	4.3%
			2.0	50.0	0.8%	1.1%	1.4%	1.6%	1.8%	2.0%	1.5%	2.0%	2.3%	2.6%	2.8%	3.0%	2.3%	2.8%	3.0%	3.2%	3.4%	3.5%
			4.0	25.0	0.8%	1.0%	1.2%	1.4%	1.6%	1.8%	1.3%	1.7%	2.0%	2.3%	2.5%	2.7%	2.0%	2.4%	2.8%	3.0%	3.2%	3.4%
			4.0	50.0		0.6%	0.7%	0.9%	1.0%	1.1%	0.7%	0.9%	1.2%	1.4%	1.6%	1.7%	1.0%	1.3%	1.6%	1.8%	2.0%	2.2%
			6.0	25.0	0.7%	0.8%	1.0%	1.2%	1.3%	1.5%	1.0%	1.3%	1.6%	1.9%	2.1%	2.3%	1.5%	1.9%	2.3%	2.5%	2.7%	2.9%
			6.0	50.0				0.6%	0.7%	0.7%		0.7%	0.8%	1.0%	1.1%	1.3%	0.7%	0.9%	1.1%	1.3%	1.5%	1.7%
		2.4	2.0	25.0	0.7%	0.9%	1.1%	1.3%	1.4%	1.6%	1.6%	2.0%	2.3%	2.5%	2.7%	2.8%	2.6%	3.0%	3.2%	3.3%	3.4%	3.5%
			2.0	50.0		0.7%	0.9%	1.0%	1.1%	1.3%	1.1%	1.4%	1.7%	1.9%	2.1%	2.2%	1.8%	2.2%	2.5%	2.6%	2.7%	2.8%
			4.0	25.0	0.6%	0.7%	0.9%	1.0%	1.1%	1.2%	1.0%	1.3%	1.5%	1.7%	1.9%	2.1%	1.6%	2.0%	2.2%	2.5%	2.6%	2.8%
			4.0	50.0			0.6%	0.6%	0.7%	0.8%	0.6%	0.7%	0.9%	1.1%	1.2%	1.3%	0.8%	1.1%	1.3%	1.5%	1.7%	1.8%
			6.0	25.0		0.6%	0.8%	0.9%	1.0%	1.1%	0.8%	1.1%	1.3%	1.5%	1.6%	1.8%	1.3%	1.6%	1.9%	2.1%	2.3%	2.4%
			6.0	50.0					0.6%	0.6%		0.6%	0.7%	0.8%	0.9%	1.0%	0.6%	0.8%	1.0%	1.1%	1.3%	1.4%
		3.2	2.0	25.0							1.1%	1.4%	1.5%	1.7%	1.8%	1.9%	2.0%	2.3%	2.5%	2.6%	2.7%	2.7%
			2.0	50.0							0.7%	1.0%	1.2%	1.3%	1.4%	1.5%	1.4%	1.7%	1.9%	2.0%	2.1%	2.2%
			4.0	25.0							0.7%	0.9%	1.1%	1.2%	1.4%	1.5%	1.3%	1.6%	1.8%	1.9%	2.1%	2.2%
			4.0	50.0									0.7%	0.8%	0.9%	1.0%	0.6%	0.8%	1.0%	1.2%	1.3%	1.4%
			6.0	25.0							0.6%	0.8%	1.0%	1.1%	1.2%	1.3%	1.0%	1.3%	1.5%	1.7%	1.8%	1.9%
			6.0	50.0										0.6%	0.7%	0.8%		0.6%	0.8%	0.9%	1.0%	1.1%
	1.15	1.6	2.0	25.0	2.2%	2.8%	3.3%	3.8%	4.1%	4.5%	3.8%	4.6%	5.1%	5.4%	5.7%	5.8%	5.1%	5.6%	5.9%	6.0%	6.1%	6.2%
			2.0	50.0	1.5%	2.0%	2.4%	2.8%	3.1%	3.4%	2.7%	3.3%	3.9%	4.2%	4.5%	4.7%	3.8%	4.4%	4.7%	4.9%	5.0%	5.1%
			4.0	25.0	1.4%	1.8%	2.2%	2.5%	2.9%	3.1%	2.3%	2.9%	3.4%	3.8%	4.1%	4.4%	3.3%	3.9%	4.4%	4.7%	5.0%	5.1%
			4.0	50.0	0.8%	1.1%	1.3%	1.5%	1.8%	2.0%	1.3%	1.7%	2.0%	2.4%	2.6%	2.9%	1.7%	2.3%	2.7%	3.0%	3.3%	3.6%
			6.0	25.0	1.2%	1.5%	1.8%	2.1%	2.3%	2.6%	1.8%	2.3%	2.8%	3.1%	3.4%	3.7%	2.6%	3.2%	3.7%	4.0%	4.3%	4.5%
			6.0	50.0	0.6%	0.8%	0.9%	1.1%	1.2%	1.4%	0.9%	1.2%	1.5%	1.7%	2.0%	2.2%	1.2%	1.6%	2.0%	2.3%	2.5%	2.8%
		2.4	2.0	25.0	1.3%	1.7%	2.0%	2.3%	2.5%	2.7%	2.8%	3.4%	3.8%	4.1%	4.3%	4.4%	4.2%	4.6%	4.8%	5.0%	5.1%	5.1%
			2.0	50.0	1.0%	1.3%	1.6%	1.8%	2.0%	2.2%	2.0%	2.5%	2.9%	3.2%	3.4%	3.6%	3.1%	3.6%	3.8%	4.0%	4.2%	4.3%
			4.0	25.0	1.0%	1.3%	1.5%	1.8%	2.0%	2.2%	1.8%	2.2%	2.6%	2.9%	3.2%	3.4%	2.7%	3.3%	3.6%	3.9%	4.1%	4.3%
			4.0	50.0	0.7%	0.9%	1.0%	1.2%	1.4%	1.5%	1.0%	1.3%	1.6%	1.8%	2.1%	2.3%	1.4%	1.9%	2.2%	2.5%	2.7%	2.9%
			6.0	25.0	0.9%	1.2%	1.4%	1.6%	1.8%	1.9%	1.5%	1.9%	2.2%	2.5%	2.7%	2.9%	2.2%	2.7%	3.1%	3.4%	3.6%	3.8%
			6.0	50.0	0.6%	0.7%	0.8%	0.9%	1.0%	1.2%	0.8%	1.0%	1.2%	1.4%	1.6%	1.8%	1.0%	1.4%	1.7%	1.9%	2.1%	2.3%
		3.2	2.0	25.0							1.9%	2.3%	2.6%	2.8%	2.9%	3.1%	3.3%	3.6%	3.8%	3.9%	4.0%	4.1%
			2.0	50.0							1.4%	1.7%	2.0%	2.2%	2.4%	2.5%	2.4%	2.8%	3.0%	3.2%	3.3%	3.4%
			4.0	25.0							1.3%	1.6%	1.9%	2.1%	2.3%	2.5%	2.2%	2.6%	2.9%	3.1%	3.3%	3.4%
			4.0	50.0							0.8%	1.0%	1.2%	1.4%	1.6%	1.7%	1.2%	1.5%	1.8%	2.0%	2.2%	2.4%
			6.0	25.0							1.1%	1.4%	1.7%	1.9%	2.1%	2.2%	1.8%	2.2%	2.5%	2.7%	2.9%	3.1%
			6.0	50.0							0.6%	0.8%	1.0%	1.1%	1.3%	1.4%	0.9%	1.1%	1.4%	1.6%	1.8%	1.9%
	1.30	1.6	2.0	25.0	2.9%	3.7%	4.4%	5.0%	5.5%	5.8%	5.0%	6.0%	6.6%	7.0%	7.3%	7.5%	6.6%	7.2%	7.5%	7.7%	7.8%	7.9%
			2.0	50.0	2.0%	2.6%	3.2%	3.7%	4.1%	4.5%	3.5%	4.4%	5.0%	5.5%	5.8%	6.1%	5.0%	5.6%	6.0%	6.3%	6.4%	6.5%
			4.0	25.0	1.8%	2.4%	2.9%	3.4%	3.8%	4.1%	3.0%	3.8%	4.5%	5.0%	5.4%	5.7%	4.3%	5.1%	5.7%	6.1%	6.4%	6.6%
			4.0	50.0	1.1%	1.4%	1.7%	2.1%	2.3%	2.6%	1.6%	2.2%	2.7%	3.1%	3.5%	3.8%	2.3%	3.0%	3.5%	4.0%	4.3%	4.6%
			6.0	25.0	1.5%	1.9%	2.4%	2.7%	3.1%	3.4%	2.4%	3.1%	3.6%	4.1%	4.5%	4.8%	3.4%	4.2%	4.8%	5.2%	5.5%	5.8%
			6.0	50.0	0.8%	1.0%	1.2%	1.4%	1.6%	1.8%	1.2%	1.6%	1.9%	2.3%	2.6%	2.9%	1.6%	2.1%	2.6%	3.0%	3.3%	3.6%
		2.4	2.0	25.0	1.8%	2.3%	2.7%	3.0%	3.3%	3.6%	3.8%	4.5%	4.9%	5.3%	5.5%	5.7%	5.4%	5.9%	6.2%	6.4%	6.5%	6.6%
			2.0	50.0	1.3%	1.7%	2.1%	2.4%	2.7%	3.0%	2.6%	3.3%	3.8%	4.2%	4.5%	4.7%	4.0%	4.6%	5.0%	5.2%	5.4%	5.5%
			4.0	25.0	1.3%	1.7%	2.1%	2.4%	2.6%	2.9%	2.3%	3.0%	3.5%	3.9%	4.2%	4.4%	3.6%	4.3%	4.7%	5.1%	5.3%	5.5%
			4.0	50.0	0.9%	1.2%	1.4%	1.6%	1.8%	2.0%	1.3%	1.7%	2.1%	2.5%	2.7%	3.0%	1.9%	2.5%	2.9%	3.3%	3.6%	3.8%
			6.0	25.0	1.2%	1.5%	1.8%	2.1%	2.4%	2.6%	1.9%	2.5%	2.9%	3.3%	3.6%	3.9%	2.9%	3.6%	4.0%	4.4%	4.7%	4.9%
			6.0	50.0	0.8%	0.9%	1.1%	1.3%	1.4%	1.6%	1.0%	1.3%	1.6%	1.9%	2.1%	2.4%	1.4%	1.8%	2.2%	2.5%	2.8%	3.1%
		3.2	2.0	25.0							2.6%	3.1%	3.4%	3.7%	3.9%	4.0%	4.3%	4.7%	4.9%	5.1%	5.2%	5.3%
			2.0	50.0							1.8%	2.3%	2.7%	3.0%	3.2%	3.3%	3.2%	3.7%	4.0%	4.2%	4.3%	4.4%
			4.0	25.0							1.7%	2.2%	2.5%	2.8%	3.1%	3.2%	2.9%	3.4%	3.8%	4.1%	4.3%	4.4%
			4.0	50.0							1.0%	1.3%	1.6%	1.9%	2.1%	2.3%	1.5%	2.0%	2.4%	2.7%	2.9%	3.1%
			6.0	25.0							1.5%	1.9%	2.2%	2.5%	2.7%	2.9%	2.4%	2.9%	3.3%	3.6%	3.8%	4.0%
			6.0	50.0							0.8%	1.1%	1.3%	1.5%	1.7%	1.9%	1.2%	1.5%	1.8%	2.1%	2.3%	2.5%

Table- A-2 TSC look-up table - GMAW (Y/T = 0.87)

Y/T	Mismatch Level	Misalignment (mm)	Flaw Depth, a (mm)	Flaw Length, 2c (mm)	Tensile Strain Capacity (%)																	
					Wall Thickness = 12.7 mm						Wall Thickness = 19.1 mm						Wall Thickness = 25.4 mm					
					$CTOD_A$ (mm)						$CTOD_A$ (mm)						$CTOD_A$ (mm)					
					0.6	0.8	1.0	1.2	1.4	1.6	0.6	0.8	1.0	1.2	1.4	1.6	0.6	0.8	1.0	1.2	1.4	1.6
0.87	1.00	1.6	2.0	25.0	0.7%	1.0%	1.2%	1.4%	1.6%	1.8%	1.5%	1.9%	2.2%	2.5%	2.6%	2.8%	2.4%	2.7%	2.9%	3.1%	3.2%	3.2%
			2.0	50.0		0.7%	0.9%	1.0%	1.2%	1.3%	1.0%	1.3%	1.6%	1.8%	2.0%	2.2%	1.7%	2.0%	2.2%	2.4%	2.5%	2.6%
			4.0	25.0		0.6%	0.8%	0.9%	1.0%	1.2%	0.9%	1.1%	1.4%	1.6%	1.8%	1.9%	1.4%	1.7%	2.0%	2.2%	2.4%	2.5%
			4.0	50.0					0.6%	0.7%		0.6%	0.8%	0.9%	1.1%	1.2%	0.7%	0.9%	1.1%	1.3%	1.5%	1.6%
			6.0	25.0			0.6%	0.7%	0.8%	0.9%	0.7%	0.9%	1.1%	1.3%	1.4%	1.6%	1.1%	1.4%	1.6%	1.8%	2.0%	2.1%
			6.0	50.0									0.6%	0.7%	0.8%	0.9%		0.6%	0.8%	0.9%	1.1%	1.2%
		2.4	2.0	25.0			0.6%	0.7%	0.8%	0.9%	1.0%	1.3%	1.5%	1.7%	1.8%	1.9%	1.8%	2.1%	2.3%	2.4%	2.5%	2.5%
			2.0	50.0				0.6%	0.6%	0.7%	0.7%	0.9%	1.1%	1.2%	1.4%	1.5%	1.2%	1.5%	1.7%	1.9%	2.0%	2.0%
			4.0	25.0					0.6%	0.7%	0.6%	0.8%	1.0%	1.1%	1.3%	1.4%	1.1%	1.3%	1.6%	1.7%	1.9%	2.0%
			4.0	50.0									0.6%	0.7%	0.8%	0.8%		0.7%	0.9%	1.0%	1.1%	1.2%
			6.0	25.0								0.7%	0.8%	0.9%	1.1%	1.2%	0.9%	1.1%	1.3%	1.4%	1.6%	1.7%
			6.0	50.0											0.6%	0.6%			0.6%	0.7%	0.8%	0.9%
		3.2	2.0	25.0							0.6%	0.8%	0.9%	1.0%	1.1%	1.2%	1.3%	1.5%	1.7%	1.8%	1.8%	1.9%
			2.0	50.0								0.6%	0.7%	0.8%	0.9%	0.9%	0.9%	1.1%	1.3%	1.4%	1.5%	1.5%
			4.0	25.0									0.6%	0.7%	0.8%	0.9%	0.8%	1.0%	1.2%	1.3%	1.4%	1.5%
			4.0	50.0												0.6%	0.4%	0.5%	0.7%	0.8%	0.9%	0.9%
			6.0	25.0									0.6%	0.6%	0.7%	0.8%	0.7%	0.8%	1.0%	1.1%	1.2%	1.3%
			6.0	50.0																0.6%	0.7%	0.7%
	1.15	1.6	2.0	25.0	1.6%	2.0%	2.5%	2.8%	3.1%	3.4%	2.9%	3.6%	4.0%	4.3%	4.5%	4.7%	4.1%	4.6%	4.8%	5.0%	5.1%	5.2%
			2.0	50.0	1.1%	1.4%	1.8%	2.1%	2.3%	2.5%	2.0%	2.6%	3.0%	3.3%	3.6%	3.8%	3.0%	3.5%	3.8%	4.0%	4.1%	4.2%
			4.0	25.0	1.0%	1.3%	1.6%	1.9%	2.1%	2.3%	1.7%	2.2%	2.6%	2.9%	3.2%	3.5%	2.6%	3.1%	3.5%	3.8%	4.0%	4.2%
			4.0	50.0	0.6%	0.8%	1.0%	1.1%	1.3%	1.4%	0.9%	1.2%	1.5%	1.8%	2.0%	2.2%	1.3%	1.7%	2.1%	2.4%	2.6%	2.8%
			6.0	25.0	0.8%	1.1%	1.3%	1.5%	1.7%	1.9%	1.4%	1.8%	2.1%	2.4%	2.7%	2.9%	2.0%	2.5%	2.9%	3.2%	3.4%	3.6%
			6.0	50.0		0.6%	0.7%	0.8%	0.9%	1.0%	0.7%	0.9%	1.1%	1.3%	1.5%	1.7%	0.9%	1.2%	1.5%	1.8%	2.0%	2.2%
		2.4	2.0	25.0	0.9%	1.2%	1.4%	1.6%	1.7%	1.9%	2.1%	2.5%	2.9%	3.1%	3.3%	3.4%	3.3%	3.6%	3.9%	4.0%	4.1%	4.2%
			2.0	50.0	0.7%	0.9%	1.1%	1.3%	1.4%	1.5%	1.4%	1.8%	2.1%	2.4%	2.6%	2.7%	2.4%	2.8%	3.0%	3.2%	3.3%	3.4%
			4.0	25.0	0.7%	0.9%	1.1%	1.2%	1.4%	1.5%	1.3%	1.6%	1.9%	2.2%	2.4%	2.6%	2.1%	2.5%	2.8%	3.1%	3.2%	3.4%
			4.0	50.0		0.6%	0.7%	0.8%	0.9%	1.0%	0.7%	1.0%	1.2%	1.4%	1.5%	1.7%	1.1%	1.4%	1.7%	1.9%	2.1%	2.3%
			6.0	25.0	0.6%	0.8%	1.0%	1.1%	1.2%	1.3%	1.1%	1.4%	1.6%	1.9%	2.0%	2.2%	1.7%	2.1%	2.4%	2.6%	2.8%	3.0%
			6.0	50.0			0.6%	0.6%	0.7%	0.8%	0.6%	0.7%	0.9%	1.0%	1.2%	1.3%	0.8%	1.0%	1.3%	1.5%	1.6%	1.8%
		3.2	2.0	25.0							1.4%	1.7%	1.9%	2.0%	2.2%	2.3%	2.5%	2.8%	3.0%	3.1%	3.2%	3.2%
			2.0	50.0							1.0%	1.2%	1.4%	1.6%	1.7%	1.9%	1.8%	2.1%	2.3%	2.5%	2.6%	2.7%
			4.0	25.0							0.9%	1.2%	1.4%	1.5%	1.7%	1.8%	1.6%	1.9%	2.2%	2.4%	2.5%	2.6%
			4.0	50.0								0.7%	0.8%	1.0%	1.1%	1.2%	0.8%	1.1%	1.3%	1.5%	1.7%	1.8%
			6.0	25.0							0.8%	1.0%	1.2%	1.3%	1.5%	1.6%	1.3%	1.6%	1.9%	2.1%	2.2%	2.4%
			6.0	50.0								0.6%	0.7%	0.8%	0.9%	1.0%	0.6%	0.8%	1.0%	1.2%	1.3%	1.4%
	1.30	1.6	2.0	25.0	2.2%	2.9%	3.4%	3.9%	4.3%	4.6%	4.0%	4.8%	5.4%	5.8%	6.0%	6.3%	5.5%	6.0%	6.4%	6.6%	6.7%	6.8%
			2.0	50.0	1.5%	2.0%	2.5%	2.9%	3.2%	3.5%	2.8%	3.5%	4.0%	4.5%	4.8%	5.0%	4.0%	4.7%	5.0%	5.3%	5.5%	5.6%
			4.0	25.0	1.4%	1.9%	2.3%	2.6%	2.9%	3.2%	2.4%	3.0%	3.6%	4.0%	4.4%	4.6%	3.5%	4.2%	4.7%	5.1%	5.3%	5.5%
			4.0	50.0	0.9%	1.1%	1.4%	1.6%	1.8%	2.0%	1.3%	1.7%	2.1%	2.5%	2.8%	3.0%	1.8%	2.4%	2.8%	3.2%	3.5%	3.8%
			6.0	25.0	1.2%	1.5%	1.8%	2.1%	2.4%	2.6%	1.9%	2.4%	2.9%	3.3%	3.6%	3.9%	2.8%	3.4%	3.9%	4.3%	4.6%	4.8%
			6.0	50.0	0.6%	0.8%	1.0%	1.1%	1.3%	1.4%	0.9%	1.3%	1.5%	1.8%	2.0%	2.3%	1.3%	1.7%	2.1%	2.4%	2.7%	2.9%
		2.4	2.0	25.0	1.3%	1.7%	2.0%	2.3%	2.5%	2.7%	2.9%	3.5%	3.9%	4.2%	4.5%	4.6%	4.4%	4.9%	5.2%	5.3%	5.5%	5.5%
			2.0	50.0	1.0%	1.3%	1.6%	1.8%	2.0%	2.2%	2.0%	2.6%	3.0%	3.3%	3.5%	3.8%	3.2%	3.7%	4.1%	4.3%	4.5%	4.6%
			4.0	25.0	1.0%	1.3%	1.5%	1.8%	2.0%	2.2%	1.8%	2.3%	2.7%	3.0%	3.3%	3.5%	2.8%	3.4%	3.8%	4.1%	4.4%	4.5%
			4.0	50.0	0.7%	0.9%	1.0%	1.2%	1.4%	1.5%	1.0%	1.3%	1.6%	1.9%	2.1%	2.3%	1.5%	1.9%	2.3%	2.6%	2.9%	3.1%
			6.0	25.0	0.9%	1.2%	1.4%	1.6%	1.8%	1.9%	1.5%	1.9%	2.3%	2.6%	2.8%	3.0%	2.3%	2.8%	3.2%	3.6%	3.8%	4.0%
			6.0	50.0	0.6%	0.7%	0.8%	0.9%	1.1%	1.2%	0.8%	1.0%	1.3%	1.5%	1.7%	1.8%	1.1%	1.4%	1.7%	2.0%	2.2%	2.4%
		3.2	2.0	25.0							2.0%	2.4%	2.7%	2.9%	3.0%	3.2%	3.4%	3.8%	4.0%	4.2%	4.3%	4.4%
			2.0	50.0							1.4%	1.7%	2.0%	2.3%	2.5%	2.6%	2.5%	2.9%	3.2%	3.4%	3.5%	3.6%
			4.0	25.0							1.3%	1.6%	1.9%	2.2%	2.3%	2.5%	2.2%	2.7%	3.0%	3.3%	3.5%	3.6%
			4.0	50.0							0.8%	1.0%	1.2%	1.4%	1.6%	1.7%	1.2%	1.5%	1.8%	2.1%	2.3%	2.5%
			6.0	25.0							1.1%	1.4%	1.7%	1.9%	2.1%	2.3%	1.9%	2.3%	2.6%	2.9%	3.1%	3.2%
			6.0	50.0							0.6%	0.8%	1.0%	1.2%	1.3%	1.4%	0.9%	1.2%	1.4%	1.6%	1.8%	2.0%

Table- A-3 TSC look-up table - GMAW (Y/T = 0.92)

Y/T	Mismatch Level	Misalignment (mm)	Flaw Depth, a (mm)	Flaw Length, 2c (mm)	Tensile Strain Capacity (%)																	
					Wall Thickness = 12.7 mm						Wall Thickness = 19.1 mm						Wall Thickness = 25.4 mm					
					$CTOD_A$ (mm)						$CTOD_A$ (mm)						$CTOD_A$ (mm)					
					0.6	0.8	1.0	1.2	1.4	1.6	0.6	0.8	1.0	1.2	1.4	1.6	0.6	0.8	1.0	1.2	1.4	1.6
0.92	1.00	1.6	2.0	25.0		0.6%	0.7%	0.8%	0.9%	1.0%	1.0%	1.3%	1.5%	1.7%	1.8%	1.9%	1.7%	2.0%	2.1%	2.3%	2.3%	2.4%
			2.0	50.0				0.6%	0.7%	0.7%	0.7%	0.9%	1.1%	1.2%	1.4%	1.5%	1.1%	1.4%	1.6%	1.7%	1.8%	1.9%
			4.0	25.0					0.6%	0.7%	0.6%	0.7%	0.9%	1.1%	1.2%	1.3%	0.9%	1.2%	1.4%	1.6%	1.7%	1.8%
			4.0	50.0										0.6%	0.7%	0.8%		0.6%	0.8%	0.9%	1.0%	1.1%
			6.0	25.0								0.6%	0.7%	0.8%	1.0%	1.1%	0.7%	0.9%	1.1%	1.3%	1.4%	1.5%
			6.0	50.0												0.6%				0.6%	0.7%	0.8%
		2.4	2.0	25.0							0.6%	0.8%	0.9%	1.0%	1.1%	1.1%	1.2%	1.4%	1.5%	1.6%	1.7%	1.7%
			2.0	50.0									0.6%	0.7%	0.8%	0.9%	0.8%	1.0%	1.1%	1.2%	1.3%	1.4%
			4.0	25.0									0.6%	0.7%	0.7%	0.8%	0.7%	0.9%	1.0%	1.1%	1.2%	1.3%
			4.0	50.0																0.6%	0.7%	0.8%
			6.0	25.0											0.6%	0.7%		0.7%	0.8%	0.9%	1.0%	1.1%
			6.0	50.0																		0.6%
		3.2	2.0	25.0												0.6%	0.8%	0.9%	1.0%	1.1%	1.1%	1.2%
			2.0	50.0														0.7%	0.8%	0.8%	0.9%	0.9%
			4.0	25.0														0.6%	0.7%	0.8%	0.8%	0.9%
			4.0	50.0																		
			6.0	25.0															0.6%	0.6%	0.7%	0.8%
			6.0	50.0																		
	1.15	1.6	2.0	25.0	1.1%	1.5%	1.8%	2.0%	2.3%	2.5%	2.3%	2.8%	3.1%	3.4%	3.6%	3.8%	3.3%	3.7%	4.0%	4.1%	4.2%	4.3%
			2.0	50.0	0.8%	1.0%	1.3%	1.5%	1.7%	1.9%	1.5%	2.0%	2.3%	2.6%	2.8%	3.0%	2.4%	2.8%	3.1%	3.3%	3.4%	3.5%
			4.0	25.0	0.7%	1.0%	1.2%	1.4%	1.5%	1.7%	1.3%	1.7%	2.0%	2.3%	2.5%	2.7%	2.0%	2.5%	2.8%	3.1%	3.3%	3.4%
			4.0	50.0		0.6%	0.7%	0.8%	0.9%	1.0%	0.7%	1.0%	1.2%	1.4%	1.6%	1.7%	1.0%	1.4%	1.6%	1.9%	2.1%	2.3%
			6.0	25.0	0.6%	0.8%	0.9%	1.1%	1.2%	1.4%	1.0%	1.3%	1.6%	1.9%	2.1%	2.2%	1.6%	2.0%	2.3%	2.6%	2.8%	2.9%
			6.0	50.0				0.6%	0.6%	0.7%		0.7%	0.8%	1.0%	1.1%	1.3%	0.7%	1.0%	1.2%	1.4%	1.6%	1.7%
		2.4	2.0	25.0	0.6%	0.8%	0.9%	1.0%	1.1%	1.2%	1.5%	1.9%	2.1%	2.3%	2.5%	2.6%	2.5%	2.9%	3.1%	3.2%	3.3%	3.3%
			2.0	50.0		0.6%	0.7%	0.8%	0.9%	1.0%	1.0%	1.3%	1.6%	1.8%	1.9%	2.0%	1.8%	2.1%	2.4%	2.5%	2.6%	2.7%
			4.0	25.0		0.6%	0.7%	0.8%	0.9%	1.0%	0.9%	1.2%	1.4%	1.6%	1.8%	1.9%	1.6%	1.9%	2.2%	2.4%	2.5%	2.7%
			4.0	50.0					0.6%	0.7%		0.7%	0.8%	1.0%	1.1%	1.2%	0.8%	1.1%	1.3%	1.5%	1.6%	1.8%
			6.0	25.0			0.6%	0.7%	0.8%	0.9%	0.8%	1.0%	1.2%	1.4%	1.5%	1.6%	1.3%	1.6%	1.8%	2.0%	2.2%	2.3%
			6.0	50.0									0.6%	0.8%	0.9%	1.0%	0.6%	0.8%	0.9%	1.1%	1.2%	1.4%
		3.2	2.0	25.0							0.9%	1.1%	1.3%	1.4%	1.5%	1.6%	1.9%	2.1%	2.3%	2.4%	2.4%	2.5%
			2.0	50.0							0.6%	0.8%	1.0%	1.1%	1.2%	1.3%	1.3%	1.6%	1.7%	1.9%	2.0%	2.0%
			4.0	25.0							0.6%	0.8%	0.9%	1.0%	1.1%	1.2%	1.2%	1.4%	1.6%	1.8%	1.9%	2.0%
			4.0	50.0									0.6%	0.7%	0.8%	0.8%	0.6%	0.8%	1.0%	1.1%	1.2%	1.3%
			6.0	25.0								0.7%	0.8%	0.9%	1.0%	1.1%	1.0%	1.2%	1.4%	1.5%	1.7%	1.8%
			6.0	50.0											0.6%	0.7%		0.6%	0.7%	0.8%	1.0%	1.1%
	1.30	1.6	2.0	25.0	1.7%	2.2%	2.7%	3.0%	3.4%	3.6%	3.2%	3.9%	4.4%	4.8%	5.0%	5.2%	4.6%	5.1%	5.4%	5.6%	5.8%	5.9%
			2.0	50.0	1.2%	1.6%	1.9%	2.2%	2.5%	2.8%	2.2%	2.8%	3.3%	3.7%	3.9%	4.2%	3.3%	3.9%	4.3%	4.5%	4.7%	4.8%
			4.0	25.0	1.1%	1.5%	1.8%	2.0%	2.3%	2.5%	1.9%	2.4%	2.9%	3.2%	3.6%	3.8%	2.8%	3.5%	3.9%	4.2%	4.5%	4.7%
			4.0	50.0	0.7%	0.9%	1.1%	1.2%	1.4%	1.6%	1.1%	1.4%	1.7%	2.0%	2.2%	2.5%	1.5%	1.9%	2.3%	2.6%	2.9%	3.1%
			6.0	25.0	0.9%	1.2%	1.4%	1.7%	1.9%	2.1%	1.5%	2.0%	2.3%	2.7%	2.9%	3.2%	2.3%	2.8%	3.2%	3.6%	3.8%	4.1%
			6.0	50.0		0.6%	0.7%	0.9%	1.0%	1.1%	0.8%	1.0%	1.2%	1.5%	1.6%	1.8%	1.1%	1.4%	1.7%	2.0%	2.2%	2.4%
		2.4	2.0	25.0	1.0%	1.2%	1.5%	1.7%	1.8%	2.0%	2.3%	2.8%	3.1%	3.4%	3.6%	3.7%	3.6%	4.1%	4.3%	4.5%	4.6%	4.7%
			2.0	50.0	0.7%	1.0%	1.2%	1.3%	1.5%	1.6%	1.6%	2.0%	2.3%	2.6%	2.8%	3.0%	2.6%	3.1%	3.4%	3.6%	3.7%	3.8%
			4.0	25.0	0.7%	1.0%	1.1%	1.3%	1.5%	1.6%	1.4%	1.8%	2.1%	2.4%	2.6%	2.8%	2.3%	2.8%	3.1%	3.4%	3.6%	3.8%
			4.0	50.0		0.6%	0.8%	0.9%	1.0%	1.1%	0.8%	1.0%	1.3%	1.5%	1.7%	1.8%	1.2%	1.5%	1.8%	2.1%	2.3%	2.5%
			6.0	25.0	0.7%	0.9%	1.0%	1.2%	1.3%	1.4%	1.2%	1.5%	1.8%	2.0%	2.2%	2.4%	1.8%	2.3%	2.6%	2.9%	3.1%	3.3%
			6.0	50.0			0.6%	0.7%	0.8%	0.9%	0.6%	0.8%	1.0%	1.1%	1.3%	1.4%	0.9%	1.1%	1.4%	1.6%	1.8%	2.0%
		3.2	2.0	25.0							1.5%	1.8%	2.0%	2.2%	2.3%	2.4%	2.7%	3.1%	3.3%	3.4%	3.5%	3.6%
			2.0	50.0							1.0%	1.3%	1.5%	1.7%	1.9%	2.0%	1.9%	2.3%	2.5%	2.7%	2.8%	2.9%
			4.0	25.0							1.0%	1.2%	1.4%	1.6%	1.8%	1.9%	1.7%	2.1%	2.4%	2.6%	2.8%	2.9%
			4.0	50.0							0.6%	0.8%	0.9%	1.1%	1.2%	1.3%	0.9%	1.2%	1.4%	1.6%	1.8%	1.9%
			6.0	25.0							0.9%	1.1%	1.3%	1.4%	1.6%	1.7%	1.4%	1.8%	2.1%	2.3%	2.4%	2.6%
			6.0	50.0								0.6%	0.7%	0.9%	1.0%	1.1%	0.7%	0.9%	1.1%	1.3%	1.4%	1.6%

Table- A-4 TSC look-up table – FCAW/SMAW (Y/T = 0.81)

Y/T	Mismatch Level	Misalignment (mm)	Flaw Depth, a (mm)	Flaw Length, 2c (mm)	Tensile Strain Capacity (%)																	
					Wall Thickness = 12.7 mm						Wall Thickness = 19.1 mm						Wall Thickness = 25.4 mm					
					$CTOD_A$ (mm)						$CTOD_A$ (mm)						$CTOD_A$ (mm)					
					0.6	0.8	1.0	1.2	1.4	1.6	0.6	0.8	1.0	1.2	1.4	1.6	0.6	0.8	1.0	1.2	1.4	1.6
0.81	1.00	1.6	2.0	25.0	1.3%	1.8%	2.2%	2.6%	2.9%	3.1%	2.1%	2.5%	2.8%	3.1%	3.3%	3.4%	2.5%	2.8%	3.0%	3.1%	3.3%	3.3%
			2.0	50.0	1.0%	1.3%	1.6%	1.9%	2.2%	2.4%	1.5%	1.9%	2.2%	2.4%	2.7%	2.8%	1.8%	2.2%	2.4%	2.6%	2.7%	2.8%
			4.0	25.0	0.9%	1.2%	1.6%	1.9%	2.2%	2.4%	1.4%	1.9%	2.2%	2.5%	2.8%	3.0%	2.0%	2.4%	2.7%	2.9%	3.0%	3.1%
			4.0	50.0	0.6%	0.7%	0.9%	1.1%	1.2%	1.4%	0.8%	1.0%	1.3%	1.6%	1.8%	2.0%	1.0%	1.3%	1.6%	1.9%	2.1%	2.2%
			6.0	25.0	0.8%	1.1%	1.3%	1.6%	1.9%	2.1%	1.2%	1.6%	2.0%	2.3%	2.5%	2.7%	1.7%	2.1%	2.4%	2.7%	2.8%	3.0%
			6.0	50.0			0.6%	0.7%	0.9%	1.0%	0.6%	0.8%	1.0%	1.2%	1.4%	1.6%	0.7%	1.0%	1.3%	1.5%	1.7%	1.9%
		2.4	2.0	25.0	1.0%	1.3%	1.6%	1.9%	2.1%	2.3%	1.7%	2.0%	2.3%	2.5%	2.7%	2.8%	2.1%	2.4%	2.6%	2.7%	2.8%	2.9%
			2.0	50.0	0.7%	1.0%	1.2%	1.4%	1.7%	1.9%	1.2%	1.5%	1.8%	2.0%	2.2%	2.3%	1.6%	1.8%	2.1%	2.2%	2.4%	2.5%
			4.0	25.0	0.7%	1.0%	1.2%	1.5%	1.7%	2.0%	1.1%	1.5%	1.8%	2.1%	2.3%	2.5%	1.7%	2.0%	2.3%	2.5%	2.6%	2.7%
			4.0	50.0		0.6%	0.7%	0.9%	1.0%	1.2%	0.6%	0.9%	1.1%	1.3%	1.5%	1.7%	0.9%	1.1%	1.4%	1.6%	1.8%	1.9%
			6.0	25.0	0.7%	0.9%	1.1%	1.3%	1.6%	1.8%	1.0%	1.3%	1.6%	1.9%	2.1%	2.3%	1.5%	1.8%	2.1%	2.3%	2.5%	2.6%
			6.0	50.0			0.6%	0.7%	0.8%	0.9%		0.7%	0.8%	1.0%	1.2%	1.4%	0.6%	0.9%	1.1%	1.3%	1.5%	1.7%
		3.2	2.0	25.0							1.3%	1.6%	1.8%	2.0%	2.2%	2.3%	1.8%	2.0%	2.2%	2.3%	2.4%	2.5%
			2.0	50.0							0.9%	1.2%	1.4%	1.6%	1.8%	1.9%	1.3%	1.6%	1.8%	1.9%	2.0%	2.1%
			4.0	25.0							0.9%	1.2%	1.5%	1.7%	1.9%	2.1%	1.4%	1.7%	2.0%	2.1%	2.3%	2.4%
			4.0	50.0								0.7%	0.9%	1.1%	1.2%	1.4%	0.7%	1.0%	1.2%	1.4%	1.5%	1.7%
			6.0	25.0							0.8%	1.1%	1.4%	1.6%	1.8%	2.0%	1.2%	1.6%	1.8%	2.0%	2.2%	2.3%
			6.0	50.0								0.6%	0.7%	0.9%	1.0%	1.2%	0.6%	0.8%	1.0%	1.1%	1.3%	1.4%
	1.15	1.6	2.0	25.0	2.3%	3.0%	3.6%	4.0%	4.5%	4.8%	3.3%	3.9%	4.4%	4.7%	5.0%	5.2%	3.8%	4.2%	4.5%	4.7%	4.9%	5.0%
			2.0	50.0	1.7%	2.2%	2.7%	3.1%	3.5%	3.8%	2.4%	3.0%	3.4%	3.8%	4.1%	4.3%	2.9%	3.3%	3.7%	3.9%	4.1%	4.3%
			4.0	25.0	1.6%	2.1%	2.6%	3.1%	3.5%	3.9%	2.3%	3.0%	3.5%	3.9%	4.3%	4.5%	3.1%	3.6%	4.0%	4.3%	4.6%	4.7%
			4.0	50.0	0.9%	1.2%	1.5%	1.8%	2.1%	2.4%	1.3%	1.8%	2.2%	2.5%	2.8%	3.1%	1.7%	2.2%	2.6%	2.9%	3.2%	3.4%
			6.0	25.0	1.3%	1.8%	2.2%	2.6%	3.0%	3.3%	2.0%	2.6%	3.1%	3.5%	3.9%	4.1%	2.7%	3.3%	3.7%	4.1%	4.3%	4.5%
			6.0	50.0	0.7%	0.9%	1.1%	1.3%	1.5%	1.7%	1.0%	1.3%	1.7%	2.0%	2.3%	2.5%	1.3%	1.7%	2.1%	2.4%	2.7%	2.9%
		2.4	2.0	25.0	1.7%	2.2%	2.6%	3.0%	3.4%	3.7%	2.6%	3.2%	3.6%	3.9%	4.1%	4.3%	3.2%	3.6%	3.9%	4.1%	4.2%	4.3%
			2.0	50.0	1.3%	1.7%	2.0%	2.4%	2.7%	3.0%	2.0%	2.4%	2.8%	3.1%	3.4%	3.6%	2.4%	2.8%	3.1%	3.4%	3.6%	3.7%
			4.0	25.0	1.2%	1.7%	2.1%	2.5%	2.8%	3.1%	1.9%	2.5%	2.9%	3.3%	3.6%	3.8%	2.6%	3.1%	3.5%	3.8%	4.0%	4.1%
			4.0	50.0	0.8%	1.1%	1.3%	1.6%	1.8%	2.0%	1.1%	1.5%	1.8%	2.1%	2.4%	2.6%	1.4%	1.9%	2.2%	2.5%	2.8%	3.0%
			6.0	25.0	1.2%	1.5%	1.9%	2.2%	2.6%	2.9%	1.7%	2.2%	2.6%	3.0%	3.3%	3.6%	2.3%	2.9%	3.3%	3.5%	3.8%	3.9%
			6.0	50.0	0.7%	0.8%	1.0%	1.2%	1.4%	1.6%	0.9%	1.2%	1.4%	1.7%	2.0%	2.2%	1.1%	1.5%	1.8%	2.1%	2.4%	2.6%
		3.2	2.0	25.0							2.1%	2.5%	2.9%	3.1%	3.3%	3.5%	2.7%	3.1%	3.3%	3.5%	3.6%	3.7%
			2.0	50.0							1.6%	1.9%	2.3%	2.5%	2.7%	2.9%	2.1%	2.4%	2.7%	2.9%	3.1%	3.2%
			4.0	25.0							1.5%	2.0%	2.4%	2.7%	2.9%	3.2%	2.2%	2.7%	3.0%	3.2%	3.4%	3.6%
			4.0	50.0							0.9%	1.2%	1.5%	1.8%	2.0%	2.2%	1.2%	1.6%	1.9%	2.2%	2.4%	2.6%
			6.0	25.0							1.4%	1.8%	2.2%	2.5%	2.8%	3.0%	2.0%	2.5%	2.8%	3.1%	3.3%	3.4%
			6.0	50.0							0.7%	1.0%	1.2%	1.5%	1.7%	1.9%	1.0%	1.3%	1.6%	1.8%	2.1%	2.3%
	1.30	1.6	2.0	25.0	2.8%	3.6%	4.3%	4.9%	5.4%	5.8%	4.0%	4.7%	5.3%	5.7%	6.1%	6.3%	4.7%	5.2%	5.6%	5.8%	6.0%	6.2%
			2.0	50.0	2.1%	2.7%	3.3%	3.8%	4.2%	4.6%	3.0%	3.6%	4.2%	4.6%	4.9%	5.2%	3.5%	4.1%	4.5%	4.8%	5.0%	5.2%
			4.0	25.0	1.9%	2.6%	3.2%	3.7%	4.2%	4.6%	2.8%	3.6%	4.2%	4.7%	5.2%	5.5%	3.7%	4.4%	4.9%	5.3%	5.6%	5.8%
			4.0	50.0	1.2%	1.5%	1.9%	2.3%	2.6%	2.9%	1.6%	2.2%	2.6%	3.1%	3.4%	3.8%	2.1%	2.7%	3.1%	3.5%	3.9%	4.1%
			6.0	25.0	1.6%	2.2%	2.7%	3.2%	3.6%	4.0%	2.4%	3.1%	3.7%	4.2%	4.7%	5.0%	3.3%	4.0%	4.5%	4.9%	5.2%	5.5%
			6.0	50.0	0.9%	1.1%	1.4%	1.6%	1.9%	2.1%	1.2%	1.6%	2.0%	2.4%	2.7%	3.0%	1.6%	2.1%	2.5%	2.9%	3.2%	3.5%
		2.4	2.0	25.0	2.1%	2.7%	3.2%	3.7%	4.1%	4.4%	3.2%	3.9%	4.3%	4.7%	5.0%	5.3%	4.0%	4.4%	4.8%	5.0%	5.2%	5.4%
			2.0	50.0	1.6%	2.1%	2.5%	2.9%	3.3%	3.6%	2.4%	3.0%	3.4%	3.8%	4.1%	4.4%	3.0%	3.5%	3.8%	4.1%	4.4%	4.5%
			4.0	25.0	1.6%	2.1%	2.5%	3.0%	3.4%	3.7%	2.3%	3.0%	3.5%	4.0%	4.3%	4.6%	3.2%	3.8%	4.2%	4.6%	4.9%	5.1%
			4.0	50.0	1.0%	1.3%	1.6%	1.9%	2.2%	2.5%	1.4%	1.8%	2.2%	2.6%	2.9%	3.2%	1.8%	2.3%	2.7%	3.0%	3.3%	3.6%
			6.0	25.0	1.4%	1.9%	2.3%	2.7%	3.1%	3.4%	2.0%	2.6%	3.2%	3.6%	4.0%	4.3%	2.8%	3.5%	3.9%	4.3%	4.6%	4.8%
			6.0	50.0	0.8%	1.0%	1.3%	1.5%	1.7%	1.9%	1.1%	1.4%	1.8%	2.1%	2.4%	2.6%	1.4%	1.8%	2.2%	2.5%	2.8%	3.1%
		3.2	2.0	25.0							2.5%	3.1%	3.5%	3.8%	4.1%	4.3%	3.4%	3.8%	4.1%	4.3%	4.5%	4.6%
			2.0	50.0							1.9%	2.4%	2.8%	3.1%	3.3%	3.6%	2.5%	3.0%	3.3%	3.5%	3.7%	3.9%
			4.0	25.0							1.9%	2.4%	2.9%	3.2%	3.6%	3.8%	2.7%	3.2%	3.6%	3.9%	4.2%	4.4%
			4.0	50.0							1.1%	1.5%	1.8%	2.1%	2.4%	2.7%	1.5%	1.9%	2.3%	2.6%	2.9%	3.1%
			6.0	25.0							1.7%	2.2%	2.7%	3.0%	3.4%	3.6%	2.4%	3.0%	3.4%	3.7%	4.0%	4.2%
			6.0	50.0							0.9%	1.2%	1.5%	1.8%	2.1%	2.3%	1.2%	1.6%	1.9%	2.2%	2.5%	2.7%

Table- A-5 TSC look-up table – FCAW/SMAW (Y/T = 0.87)

Y/T	Mismatch Level	Misalignment (mm)	Flaw Depth, a (mm)	Flaw Length, 2c (mm)	Tensile Strain Capacity (%)																	
					Wall Thickness = 12.7 mm						Wall Thickness = 19.1 mm						Wall Thickness = 25.4 mm					
					$CTOD_A$ (mm)						$CTOD_A$ (mm)						$CTOD_A$ (mm)					
					0.6	0.8	1.0	1.2	1.4	1.6	0.6	0.8	1.0	1.2	1.4	1.6	0.6	0.8	1.0	1.2	1.4	1.6
0.87	1.00	1.6	2.0	25.0	0.9%	1.2%	1.5%	1.7%	2.0%	2.2%	1.4%	1.7%	2.0%	2.2%	2.3%	2.5%	1.8%	2.0%	2.2%	2.3%	2.4%	2.4%
			2.0	50.0	0.6%	0.8%	1.1%	1.3%	1.5%	1.6%	1.0%	1.3%	1.5%	1.7%	1.9%	2.0%	1.3%	1.5%	1.7%	1.8%	2.0%	2.0%
			4.0	25.0	0.6%	0.8%	1.0%	1.2%	1.4%	1.6%	0.9%	1.2%	1.5%	1.7%	1.9%	2.1%	1.3%	1.6%	1.9%	2.0%	2.2%	2.3%
			4.0	50.0			0.6%	0.7%	0.8%	0.9%		0.7%	0.8%	1.0%	1.2%	1.3%	0.7%	0.9%	1.1%	1.3%	1.4%	1.6%
			6.0	25.0		0.7%	0.8%	1.0%	1.2%	1.4%	0.8%	1.0%	1.3%	1.5%	1.7%	1.9%	1.1%	1.5%	1.7%	1.9%	2.0%	2.1%
			6.0	50.0						0.6%			0.6%	0.8%	0.9%	1.0%		0.7%	0.8%	1.0%	1.2%	1.3%
		2.4	2.0	25.0	0.6%	0.8%	1.1%	1.3%	1.4%	1.6%	1.1%	1.4%	1.6%	1.8%	1.9%	2.0%	1.5%	1.7%	1.9%	2.0%	2.0%	2.1%
			2.0	50.0		0.6%	0.8%	1.0%	1.1%	1.2%	0.8%	1.0%	1.2%	1.4%	1.5%	1.6%	1.1%	1.3%	1.4%	1.6%	1.7%	1.8%
			4.0	25.0		0.6%	0.8%	1.0%	1.1%	1.3%	0.7%	1.0%	1.2%	1.4%	1.6%	1.8%	1.1%	1.4%	1.6%	1.8%	1.9%	2.0%
			4.0	50.0				0.6%	0.7%	0.8%		0.6%	0.7%	0.8%	1.0%	1.1%	0.6%	0.7%	0.9%	1.1%	1.2%	1.3%
			6.0	25.0		0.6%	0.7%	0.9%	1.0%	1.2%	0.6%	0.9%	1.1%	1.3%	1.5%	1.6%	1.0%	1.3%	1.5%	1.6%	1.8%	1.9%
			6.0	50.0										0.7%	0.8%	0.9%		0.6%	0.7%	0.9%	1.0%	1.1%
		3.2	2.0	25.0							0.9%	1.1%	1.3%	1.4%	1.5%	1.6%	1.3%	1.4%	1.6%	1.7%	1.8%	1.8%
			2.0	50.0							0.6%	0.8%	1.0%	1.1%	1.2%	1.3%	0.9%	1.1%	1.2%	1.3%	1.4%	1.5%
			4.0	25.0							0.6%	0.8%	1.0%	1.2%	1.3%	1.4%	0.9%	1.2%	1.4%	1.5%	1.6%	1.7%
			4.0	50.0									0.6%	0.7%	0.8%	0.9%		0.6%	0.8%	0.9%	1.0%	1.2%
			6.0	25.0								0.7%	0.9%	1.1%	1.2%	1.4%	0.8%	1.1%	1.3%	1.4%	1.5%	1.6%
			6.0	50.0										0.6%	0.7%	0.8%			0.6%	0.7%	0.9%	1.0%
	1.15	1.6	2.0	25.0	1.7%	2.2%	2.7%	3.1%	3.4%	3.7%	2.5%	3.0%	3.4%	3.7%	4.0%	4.2%	3.0%	3.4%	3.6%	3.8%	4.0%	4.1%
			2.0	50.0	1.2%	1.6%	2.0%	2.3%	2.6%	2.9%	1.8%	2.3%	2.6%	2.9%	3.2%	3.4%	2.2%	2.6%	2.9%	3.1%	3.3%	3.4%
			4.0	25.0	1.1%	1.5%	1.9%	2.3%	2.6%	2.9%	1.7%	2.2%	2.7%	3.0%	3.3%	3.6%	2.4%	2.8%	3.2%	3.5%	3.7%	3.8%
			4.0	50.0	0.7%	0.9%	1.1%	1.3%	1.6%	1.8%	1.0%	1.3%	1.6%	1.9%	2.1%	2.4%	1.2%	1.6%	2.0%	2.2%	2.5%	2.7%
			6.0	25.0	1.0%	1.3%	1.6%	1.9%	2.2%	2.5%	1.4%	1.9%	2.3%	2.7%	3.0%	3.3%	2.0%	2.6%	2.9%	3.2%	3.4%	3.6%
			6.0	50.0		0.7%	0.8%	0.9%	1.1%	1.3%	0.7%	1.0%	1.2%	1.5%	1.7%	1.9%	0.9%	1.3%	1.6%	1.8%	2.1%	2.3%
		2.4	2.0	25.0	1.2%	1.6%	2.0%	2.3%	2.6%	2.8%	2.0%	2.5%	2.8%	3.1%	3.3%	3.4%	2.6%	2.9%	3.1%	3.3%	3.4%	3.5%
			2.0	50.0	0.9%	1.2%	1.5%	1.8%	2.0%	2.3%	1.5%	1.8%	2.2%	2.4%	2.6%	2.8%	1.9%	2.2%	2.5%	2.7%	2.9%	3.0%
			4.0	25.0	0.9%	1.2%	1.5%	1.8%	2.1%	2.3%	1.4%	1.8%	2.2%	2.5%	2.8%	3.0%	2.0%	2.4%	2.8%	3.0%	3.2%	3.3%
			4.0	50.0	0.6%	0.8%	0.9%	1.1%	1.3%	1.5%	0.8%	1.1%	1.3%	1.6%	1.8%	2.0%	1.1%	1.4%	1.7%	1.9%	2.1%	2.3%
			6.0	25.0	0.9%	1.1%	1.4%	1.6%	1.9%	2.1%	1.2%	1.6%	2.0%	2.3%	2.6%	2.8%	1.8%	2.2%	2.5%	2.8%	3.0%	3.2%
			6.0	50.0		0.6%	0.7%	0.9%	1.0%	1.1%	0.6%	0.8%	1.0%	1.3%	1.5%	1.6%	0.8%	1.1%	1.3%	1.6%	1.8%	2.0%
		3.2	2.0	25.0							1.6%	1.9%	2.2%	2.5%	2.6%	2.8%	2.2%	2.5%	2.7%	2.8%	3.0%	3.1%
			2.0	50.0							1.2%	1.5%	1.7%	2.0%	2.1%	2.3%	1.6%	1.9%	2.1%	2.3%	2.4%	2.6%
			4.0	25.0							1.1%	1.5%	1.8%	2.1%	2.3%	2.5%	1.7%	2.1%	2.4%	2.6%	2.7%	2.9%
			4.0	50.0							0.7%	0.9%	1.1%	1.3%	1.5%	1.7%	0.9%	1.2%	1.4%	1.6%	1.8%	2.0%
			6.0	25.0							1.0%	1.4%	1.7%	1.9%	2.1%	2.3%	1.5%	1.9%	2.2%	2.4%	2.6%	2.8%
			6.0	50.0								0.7%	0.9%	1.1%	1.2%	1.4%	0.7%	0.9%	1.2%	1.4%	1.6%	1.7%
	1.30	1.6	2.0	25.0	2.1%	2.8%	3.3%	3.8%	4.3%	4.6%	3.2%	3.8%	4.3%	4.7%	5.0%	5.3%	3.8%	4.3%	4.6%	4.9%	5.1%	5.3%
			2.0	50.0	1.6%	2.1%	2.5%	2.9%	3.3%	3.6%	2.3%	2.8%	3.3%	3.7%	4.0%	4.3%	2.8%	3.3%	3.7%	3.9%	4.2%	4.4%
			4.0	25.0	1.4%	1.9%	2.4%	2.8%	3.2%	3.6%	2.1%	2.8%	3.3%	3.8%	4.1%	4.5%	2.9%	3.5%	4.0%	4.3%	4.6%	4.8%
			4.0	50.0	0.9%	1.2%	1.4%	1.7%	2.0%	2.2%	1.2%	1.6%	2.0%	2.3%	2.7%	2.9%	1.6%	2.0%	2.4%	2.8%	3.1%	3.3%
			6.0	25.0	1.2%	1.6%	2.0%	2.4%	2.7%	3.1%	1.8%	2.4%	2.9%	3.3%	3.7%	4.0%	2.5%	3.1%	3.6%	4.0%	4.3%	4.5%
			6.0	50.0	0.7%	0.8%	1.0%	1.2%	1.4%	1.6%	0.9%	1.2%	1.5%	1.8%	2.1%	2.3%	1.2%	1.6%	1.9%	2.2%	2.5%	2.8%
		2.4	2.0	25.0	1.6%	2.0%	2.5%	2.9%	3.2%	3.5%	2.5%	3.1%	3.5%	3.8%	4.1%	4.3%	3.2%	3.7%	4.0%	4.2%	4.4%	4.5%
			2.0	50.0	1.2%	1.6%	1.9%	2.3%	2.5%	2.8%	1.9%	2.3%	2.7%	3.0%	3.3%	3.5%	2.4%	2.8%	3.1%	3.4%	3.6%	3.8%
			4.0	25.0	1.2%	1.5%	1.9%	2.3%	2.6%	2.9%	1.8%	2.3%	2.7%	3.1%	3.4%	3.7%	2.5%	3.0%	3.4%	3.8%	4.0%	4.2%
			4.0	50.0	0.8%	1.0%	1.2%	1.4%	1.7%	1.9%	1.0%	1.4%	1.7%	2.0%	2.2%	2.5%	1.3%	1.7%	2.1%	2.4%	2.7%	2.9%
			6.0	25.0	1.1%	1.4%	1.7%	2.1%	2.3%	2.6%	1.5%	2.0%	2.4%	2.8%	3.1%	3.4%	2.2%	2.7%	3.1%	3.5%	3.8%	4.0%
			6.0	50.0	0.6%	0.8%	0.9%	1.1%	1.3%	1.4%	0.8%	1.1%	1.3%	1.6%	1.8%	2.0%	1.0%	1.4%	1.7%	2.0%	2.2%	2.4%
		3.2	2.0	25.0							2.0%	2.4%	2.8%	3.1%	3.3%	3.5%	2.7%	3.1%	3.4%	3.6%	3.8%	3.9%
			2.0	50.0							1.5%	1.9%	2.2%	2.4%	2.7%	2.9%	2.0%	2.4%	2.7%	2.9%	3.1%	3.2%
			4.0	25.0							1.4%	1.8%	2.2%	2.5%	2.8%	3.1%	2.1%	2.6%	2.9%	3.2%	3.4%	3.6%
			4.0	50.0							0.8%	1.1%	1.4%	1.6%	1.9%	2.1%	1.1%	1.5%	1.8%	2.0%	2.3%	2.5%
			6.0	25.0							1.3%	1.7%	2.0%	2.4%	2.6%	2.9%	1.9%	2.3%	2.7%	3.0%	3.3%	3.5%
			6.0	50.0							0.7%	0.9%	1.1%	1.4%	1.6%	1.7%	0.9%	1.2%	1.4%	1.7%	1.9%	2.1%

Table- A-6 TSC look-up table – FCAW/SMAW (Y/T = 0.92)

Y/T	Mismatch Level	Misalignment (mm)	Flaw Depth, a (mm)	Flaw Length, 2c (mm)	Tensile Strain Capacity (%)																	
					Wall Thickness = 12.7 mm						Wall Thickness = 19.1 mm						Wall Thickness = 25.4 mm					
					$CTOD_A$ (mm)						$CTOD_A$ (mm)						$CTOD_A$ (mm)					
					0.6	0.8	1.0	1.2	1.4	1.6	0.6	0.8	1.0	1.2	1.4	1.6	0.6	0.8	1.0	1.2	1.4	1.6
0.92	1.00	1.6	2.0	25.0	0.6%	0.8%	1.0%	1.2%	1.3%	1.5%	0.9%	1.2%	1.4%	1.5%	1.6%	1.7%	1.2%	1.4%	1.5%	1.6%	1.7%	1.7%
			2.0	50.0		0.6%	0.7%	0.8%	1.0%	1.1%	0.7%	0.8%	1.0%	1.2%	1.3%	1.4%	0.9%	1.0%	1.2%	1.3%	1.4%	1.4%
			4.0	25.0			0.7%	0.8%	0.9%	1.1%	0.6%	0.8%	1.0%	1.2%	1.3%	1.5%	0.9%	1.1%	1.3%	1.4%	1.5%	1.6%
			4.0	50.0						0.6%			0.6%	0.7%	0.8%	0.9%		0.6%	0.7%	0.9%	1.0%	1.1%
			6.0	25.0				0.7%	0.8%	0.9%		0.7%	0.9%	1.0%	1.2%	1.3%	0.8%	1.0%	1.2%	1.3%	1.4%	1.5%
			6.0	50.0											0.6%	0.7%				0.7%	0.8%	0.9%
		2.4	2.0	25.0		0.6%	0.7%	0.8%	1.0%	1.1%	0.7%	0.9%	1.1%	1.2%	1.3%	1.4%	1.0%	1.2%	1.3%	1.4%	1.5%	1.5%
			2.0	50.0				0.6%	0.7%	0.8%		0.7%	0.8%	0.9%	1.0%	1.1%	0.7%	0.9%	1.0%	1.1%	1.2%	1.2%
			4.0	25.0				0.6%	0.7%	0.9%		0.7%	0.8%	1.0%	1.1%	1.2%	0.7%	1.0%	1.1%	1.2%	1.3%	1.4%
			4.0	50.0										0.6%	0.6%	0.7%			0.6%	0.7%	0.8%	0.9%
			6.0	25.0				0.6%	0.7%	0.8%		0.6%	0.7%	0.9%	1.0%	1.1%	0.6%	0.8%	1.0%	1.1%	1.2%	1.3%
			6.0	50.0												0.6%				0.6%	0.7%	0.8%
		3.2	2.0	25.0							0.6%	0.7%	0.9%	1.0%	1.1%	1.2%	0.9%	1.0%	1.1%	1.2%	1.3%	1.3%
			2.0	50.0									0.6%	0.8%	0.8%	0.9%	0.6%	0.7%	0.9%	0.9%	1.0%	1.1%
			4.0	25.0									0.7%	0.8%	0.9%	1.0%	0.6%	0.8%	0.9%	1.1%	1.1%	1.2%
			4.0	50.0												0.6%				0.6%	0.7%	0.8%
			6.0	25.0									0.6%	0.7%	0.8%	0.9%		0.7%	0.9%	1.0%	1.1%	1.1%
			6.0	50.0																	0.6%	0.7%
	1.15	1.6	2.0	25.0	1.3%	1.7%	2.1%	2.4%	2.7%	3.0%	2.0%	2.4%	2.8%	3.0%	3.2%	3.4%	2.4%	2.8%	3.0%	3.2%	3.3%	3.4%
			2.0	50.0	0.9%	1.2%	1.5%	1.8%	2.0%	2.3%	1.4%	1.8%	2.1%	2.3%	2.6%	2.7%	1.8%	2.1%	2.3%	2.5%	2.7%	2.8%
			4.0	25.0	0.9%	1.2%	1.5%	1.7%	2.0%	2.3%	1.3%	1.7%	2.1%	2.4%	2.7%	2.9%	1.8%	2.3%	2.6%	2.8%	3.0%	3.1%
			4.0	50.0		0.7%	0.8%	1.0%	1.2%	1.3%	0.7%	1.0%	1.2%	1.4%	1.7%	1.9%	1.0%	1.3%	1.5%	1.8%	2.0%	2.1%
			6.0	25.0	0.7%	1.0%	1.2%	1.5%	1.7%	1.9%	1.1%	1.5%	1.8%	2.1%	2.4%	2.6%	1.6%	2.0%	2.3%	2.6%	2.8%	2.9%
			6.0	50.0			0.6%	0.7%	0.8%	0.9%		0.7%	0.9%	1.1%	1.3%	1.5%	0.7%	1.0%	1.2%	1.4%	1.6%	1.8%
		2.4	2.0	25.0	0.9%	1.2%	1.5%	1.8%	2.0%	2.2%	1.6%	1.9%	2.2%	2.5%	2.6%	2.8%	2.1%	2.4%	2.6%	2.7%	2.8%	2.9%
			2.0	50.0	0.7%	0.9%	1.2%	1.4%	1.6%	1.8%	1.1%	1.4%	1.7%	1.9%	2.1%	2.3%	1.5%	1.8%	2.0%	2.2%	2.3%	2.4%
			4.0	25.0	0.7%	0.9%	1.2%	1.4%	1.6%	1.8%	1.1%	1.4%	1.7%	2.0%	2.2%	2.4%	1.6%	1.9%	2.2%	2.4%	2.6%	2.7%
			4.0	50.0		0.6%	0.7%	0.8%	1.0%	1.1%	0.6%	0.8%	1.0%	1.2%	1.4%	1.6%	0.8%	1.1%	1.3%	1.5%	1.7%	1.8%
			6.0	25.0	0.7%	0.8%	1.0%	1.2%	1.4%	1.6%	0.9%	1.2%	1.5%	1.8%	2.0%	2.2%	1.4%	1.7%	2.0%	2.2%	2.4%	2.6%
			6.0	50.0				0.6%	0.7%	0.8%		0.6%	0.8%	0.9%	1.1%	1.3%	0.6%	0.8%	1.0%	1.2%	1.4%	1.6%
		3.2	2.0	25.0							1.2%	1.5%	1.8%	2.0%	2.1%	2.3%	1.7%	2.0%	2.2%	2.3%	2.4%	2.5%
			2.0	50.0							0.9%	1.1%	1.4%	1.5%	1.7%	1.8%	1.3%	1.5%	1.7%	1.9%	2.0%	2.1%
			4.0	25.0							0.9%	1.1%	1.4%	1.6%	1.8%	2.0%	1.3%	1.6%	1.9%	2.1%	2.2%	2.4%
			4.0	50.0								0.7%	0.8%	1.0%	1.2%	1.3%	0.7%	0.9%	1.1%	1.3%	1.4%	1.6%
			6.0	25.0							0.8%	1.0%	1.3%	1.5%	1.7%	1.9%	1.2%	1.5%	1.7%	1.9%	2.1%	2.2%
			6.0	50.0									0.7%	0.8%	0.9%	1.1%		0.7%	0.9%	1.1%	1.2%	1.3%
	1.30	1.6	2.0	25.0	1.7%	2.2%	2.7%	3.1%	3.5%	3.8%	2.5%	3.1%	3.5%	3.9%	4.2%	4.4%	3.2%	3.6%	3.9%	4.2%	4.4%	4.5%
			2.0	50.0	1.2%	1.6%	2.0%	2.3%	2.6%	2.9%	1.8%	2.3%	2.7%	3.0%	3.3%	3.5%	2.3%	2.7%	3.1%	3.3%	3.5%	3.7%
			4.0	25.0	1.1%	1.5%	1.9%	2.2%	2.5%	2.9%	1.7%	2.2%	2.6%	3.0%	3.4%	3.7%	2.3%	2.9%	3.3%	3.6%	3.9%	4.1%
			4.0	50.0	0.7%	0.9%	1.1%	1.3%	1.5%	1.7%	0.9%	1.3%	1.6%	1.8%	2.1%	2.4%	1.2%	1.6%	1.9%	2.2%	2.5%	2.7%
			6.0	25.0	1.0%	1.3%	1.6%	1.9%	2.1%	2.4%	1.4%	1.9%	2.3%	2.7%	3.0%	3.3%	2.0%	2.5%	3.0%	3.3%	3.6%	3.8%
			6.0	50.0		0.7%	0.8%	0.9%	1.1%	1.2%	0.7%	0.9%	1.2%	1.4%	1.6%	1.8%	0.9%	1.2%	1.5%	1.8%	2.0%	2.2%
		2.4	2.0	25.0	1.2%	1.6%	2.0%	2.3%	2.6%	2.8%	2.0%	2.5%	2.9%	3.2%	3.4%	3.6%	2.7%	3.1%	3.4%	3.6%	3.8%	3.9%
			2.0	50.0	1.0%	1.3%	1.5%	1.8%	2.0%	2.3%	1.5%	1.9%	2.2%	2.5%	2.7%	2.9%	2.0%	2.3%	2.6%	2.8%	3.0%	3.2%
			4.0	25.0	0.9%	1.2%	1.5%	1.8%	2.0%	2.3%	1.4%	1.8%	2.2%	2.5%	2.8%	3.1%	2.0%	2.5%	2.8%	3.1%	3.4%	3.6%
			4.0	50.0	0.6%	0.8%	0.9%	1.1%	1.3%	1.5%	0.8%	1.1%	1.3%	1.5%	1.8%	2.0%	1.1%	1.4%	1.7%	1.9%	2.2%	2.4%
			6.0	25.0	0.8%	1.1%	1.3%	1.6%	1.8%	2.1%	1.2%	1.6%	1.9%	2.2%	2.5%	2.8%	1.7%	2.2%	2.6%	2.9%	3.1%	3.3%
			6.0	50.0		0.6%	0.7%	0.8%	1.0%	1.1%	0.6%	0.8%	1.0%	1.2%	1.4%	1.6%	0.8%	1.1%	1.3%	1.5%	1.8%	2.0%
		3.2	2.0	25.0							1.6%	2.0%	2.3%	2.5%	2.8%	2.9%	2.3%	2.6%	2.9%	3.1%	3.2%	3.3%
			2.0	50.0							1.2%	1.5%	1.8%	2.0%	2.2%	2.4%	1.7%	2.0%	2.2%	2.4%	2.6%	2.7%
			4.0	25.0							1.1%	1.5%	1.8%	2.0%	2.3%	2.5%	1.7%	2.1%	2.4%	2.7%	2.9%	3.1%
			4.0	50.0							0.7%	0.9%	1.1%	1.3%	1.5%	1.6%	0.9%	1.2%	1.4%	1.6%	1.8%	2.0%
			6.0	25.0							1.0%	1.3%	1.6%	1.9%	2.1%	2.3%	1.5%	1.9%	2.2%	2.5%	2.7%	2.9%
			6.0	50.0								0.7%	0.9%	1.1%	1.2%	1.4%	0.7%	0.9%	1.1%	1.3%	1.5%	1.7%

Appendix B Linepipe Specifications for SBD

B.1 Scope of the Section

This appendix examines the specifications of linepipe and girth weld tensile properties necessary for strain-based design with particular focus on the tensile strain capacity. Test data are drawn from multiple public sources. Details of the test data can be found in the cited references.

The appendix is intended to be self-contained. Some of the materials presented here may have been cited in the main body of the report.

B.2 Current Linepipe Specifications

B.2.1 Specifications in Codes and Standards

Traditional pipeline design is primarily based on the need for pressure containment. Tests for linepipe tensile properties are straightforward. For large diameter submerged-arc or combined submerged-arc and gas-metal-arc welded pipes, the required tests related to tensile properties are tensile tests in the hoop direction and cross-weld tensile tests [1,2]. For PSL 1 pipes the specified properties are minimum yield strength, minimum ultimate tensile strength (UTS) and minimum elongation for pipe body tests. For cross-weld tensile tests, only minimum UTS is specified. For PSL 2 pipes, additional requirements include maximum yield strength, maximum UTS, and maximum Y/T ratio for pipe body tests.

The form of test specimen can be either flattened rectangular strap or round bars from non-flattened pieces. The gauge diameter of test specimens is given as a function of pipe diameter and wall thickness in API 5L and ISO 3183 [1,2].

B.2.2 Specifications for Strain-Based Design

TransCanada PipeLines Ltd. installed one kilometer of a trial section of X100 pipeline in the fall of 2002 [3] and then two kilometers of X100 pipeline in the winter season of 2003-2004 [4]. A 5.5 kilometer section of X100 pipeline was installed in 2006 with fully strain-based design requirements [5]. Additional requirements on the linepipe were implemented to supplement those in CSA Z245.1-02 [6]. Some of these supplemental requirements are (1) round bar tensile tests for hoop properties, (2) tensile tests in the form of strip specimens for longitudinal properties, (3) different minimum and maximum yield strengths for the hoop and longitudinal directions, (4) different maximum Y/T ratios for hoop and longitudinal directions, and (5) minimum uniform elongation in the longitudinal direction. Multiple stress ratios at predefined strain intervals were also required for the longitudinal tensile properties to ensure that “round–house” stress-strain relations were achieved [7].

B.3 Key Issues Affecting Strain-Based Design

B.3.1 Definition of Yield Strength

One of the most fundamental material properties in pipeline design and service, is the pipe yield strength. The yield strength is typically reported as the strength at 0.5% total strain or the strength at the 0.2% offset strain [1,2]. In response to the requirements for strain-based design, a number of pipe manufacturers have developed manufacturing processes aimed at improving the stress strain response of the linepipes, including having round-house stress-strain curves (without obvious yield point and Luder's extension), high strain hardening, and resistance to strain aging during pipe coating [8,9,10]. One of the interesting features of the round-house stress-strain curves is the nonlinear stress-strain response prior to yielding, as shown in Figure- B-1 [8]. As the yield strength is measured at either 0.5% total strain or 0.2% offset strain, the reported yield strength, as given in Figure- B-1 and Table- B-1, could be much lower than the "physical" yield strength, which may be understood as the "knee" of the stress-strain curve. The low yield strength directly leads to the reported low *Y*/*T* ratio.

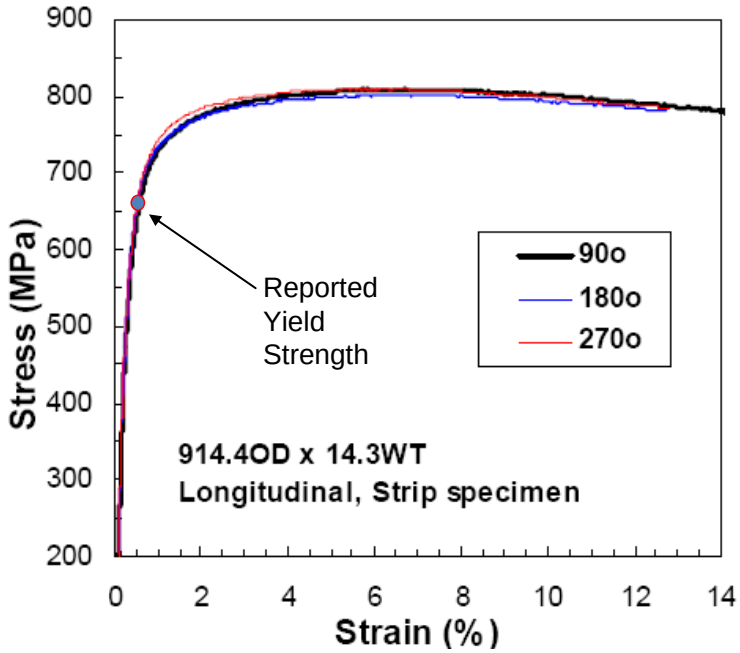

Figure- B-1 Stress-strain curves of a high-strain pipe and the associated yield strength by current codes [8]

B.3.2 Variation of Tensile Properties

The need for weld strength overmatch for strain-based design will require tight control of the spread (standard deviation) of pipe tensile properties. At the same time, any specifications aimed at achieving such tight control need to incorporate the natural variation of pipe tensile properties in the normal production environment. A ~2005-vintage 36-inch OD and ¾-inch wall thickness X100 pipe was tested at CANMET. The room-temperature stress-strain curves from round and strap specimens, cut from different clock positions, are shown in Figure- B-2 and Figure- B-3, respectively. The variation in yield strength within the given section of pipe is in the range of 80-90 MPa. This variation is higher than the estimated yield strength variation of 50-60 MPa (at

0.5% total strain) from published data by Tsuru, et al. [11]. Data published by Ishikawa, et al., seem to suggest a much smaller variation [12].

Table- B-1 Reported Strength Values by current codes [8]

Pipe No.	Direction	Base metal tensile properties *1					Trans weld
		YS (MPa)	TS (MPa)	Y/T (%)	uEl (%)	σ_r *2 $\sigma_{1.5}/\sigma_{0.5}$	TS (MPa)
A	Trans.	713	824	87	-	-	819
	Longi.	668	835	80	7.3	1.17	-
B	Trans.	713	836	85	-	-	825
	Longi.	659	811	81	6.9	1.18	-

*1 Trans: round bar specimen, Longi.: Rectangular strip specimen

*2 Stress ratio, defined by the ratio of stress at ε=1.5% to that at ε=0.5% (σ1.5/σ0.5)

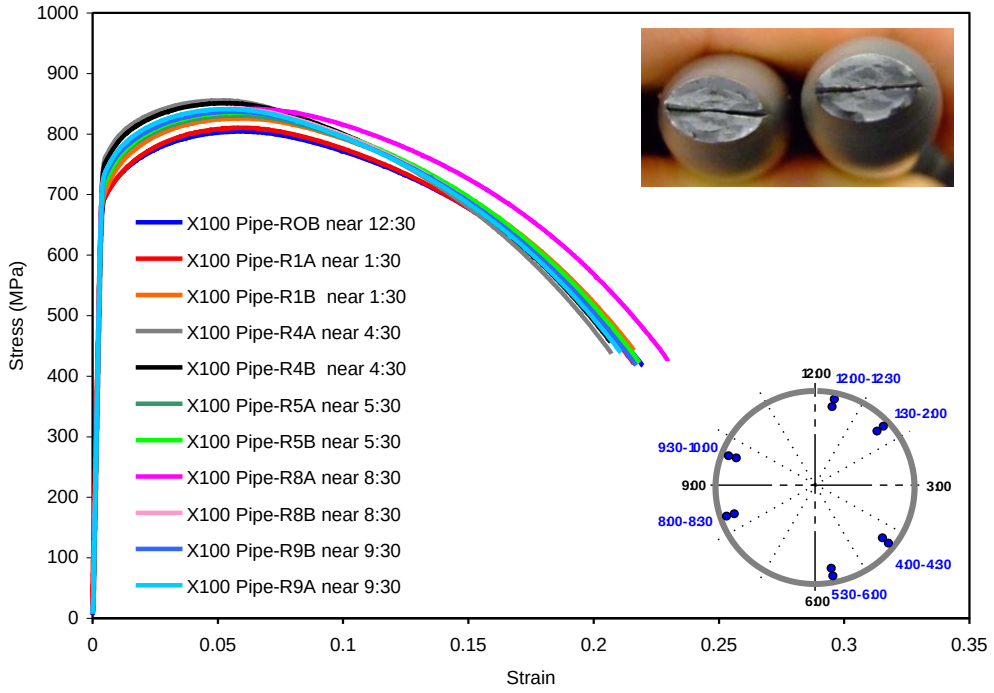

Figure- B-2 Stress-strain curves for tests using large diameter round specimens cut longitudinal to the pipe axis (LPA) at the different clock positions. Insert: image of fracture surfaces

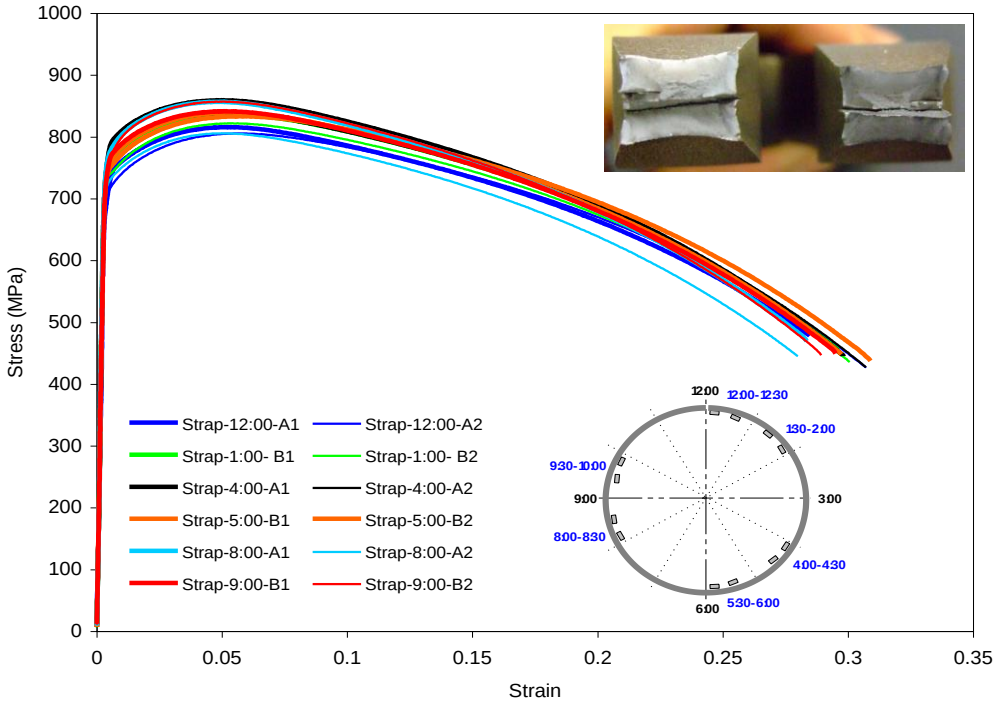

Figure- B-3 Stress-strain curves for tests using square strap tensile specimens cut longitudinal to the pipe axis (LPA) at different clock positions. Insert: image of fracture surfaces

B.3.3 Dependence on Specimen Type

The stress-strain curves from the round bar and square cross-section strap in Figure- B-2 and Figure- B-3 are compared in Figure- B-4 using the highest and lowest curve from each specimen type. There are some differences between the curves of the different specimen types, however, there is a general agreement up to UTS. The total elongation from the strap specimens is much greater than that from the round bar specimens. The difference is attributable to the different specimen cross-section (round versus square) and the ratio of gage width (diameter) to gage length. Both types of specimen had the same gage length of 2 inches while the cross-sectional areas were different. These results show that the specification for the total elongation has to be defined in the context of a consistent specimen type with consistent dimensions.

Pipe tensile properties are, in most cases, obtained from room temperature tests. Past tests done on modern X70 and X100 pipe steels indicated that the increase in ultimate tensile strength (UTS) at low test temperatures is greater than the increase of the yield strength, resulting in enhanced strain hardening behavior at low temperatures. The change in the tensile behavior, particularly the strain hardening capacity, is important in understanding the tensile strain capacity. Hoop tensile properties of an X70 pipe are compared in Figure- B-5 [13]. There is a marked increase in both strength and strain hardening capacity at -20ºC, consistent with prior observations. A similar trend is observed in the X56 pipes, as shown in Figure- B-6.

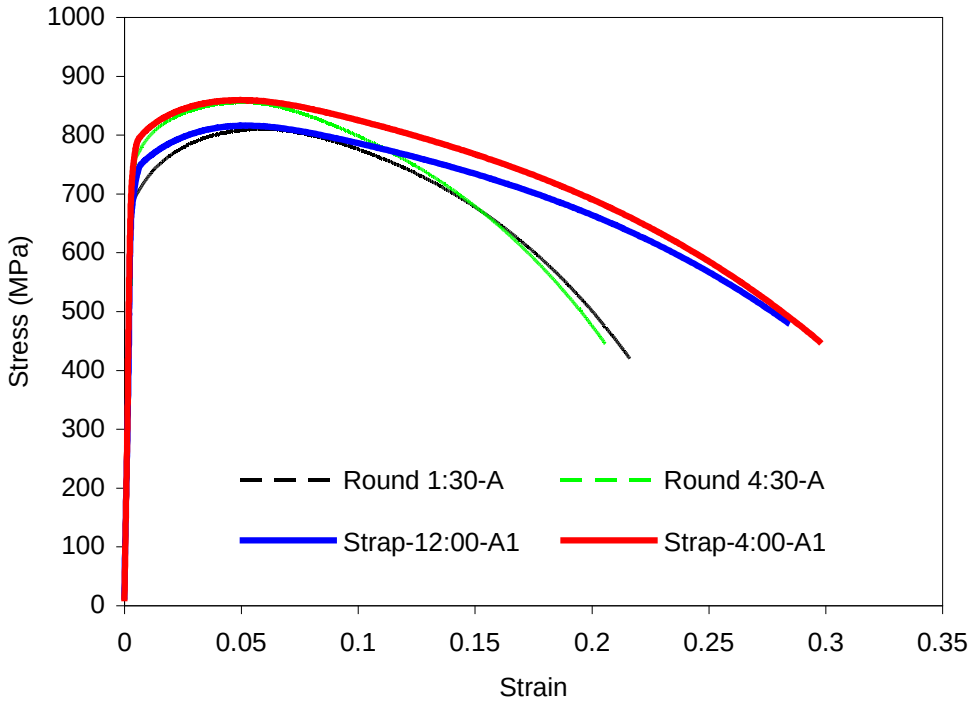

Figure- B-4 Comparison of stress-strain curves between the round bar and square cross-section strap

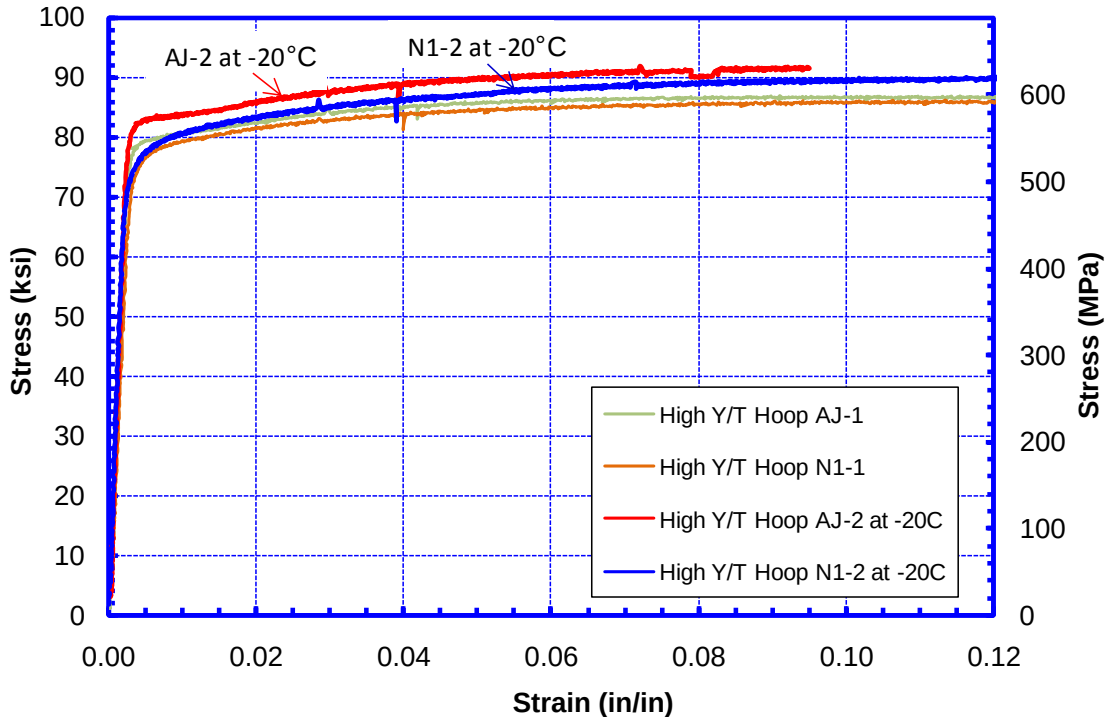

Figure- B-5 Hoop tensile property of an X70 pipe at room temperature and -20ºC [13]

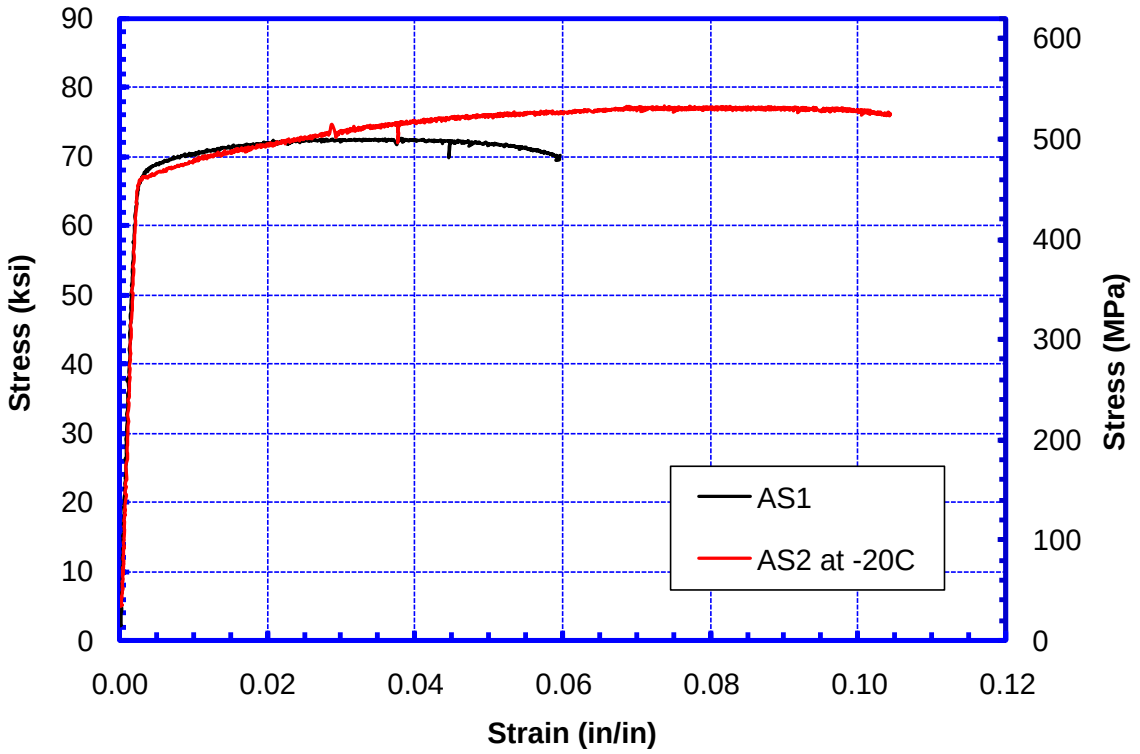

Figure- B-6 Hoop tensile stress-strain curves of an X56 pipe at room temperature and -20ºC [13]

B.4 Features of Tensile Properties of Girth Welds

B.4.1 Dependence on Test Type

There are no consensus standards for all-weld-metal (AWM) tensile testing. Significant work has been carried out in recent years by CANMET to determine the variability of weld metal tensile properties [14,15]. One such example, from a 36-inch (914-mm) diameter and 0.75-inch (19-mm) wall thickness X100 single-torch girth weld, is shown in Figure- B-7 [14]. The specimens from the ID show a much higher yield strength (910-920 MPa) than those from the OD (750-780 MPa). The ultimate tensile strengths of the ID and OD specimens are very close at approximately 940 MPa.

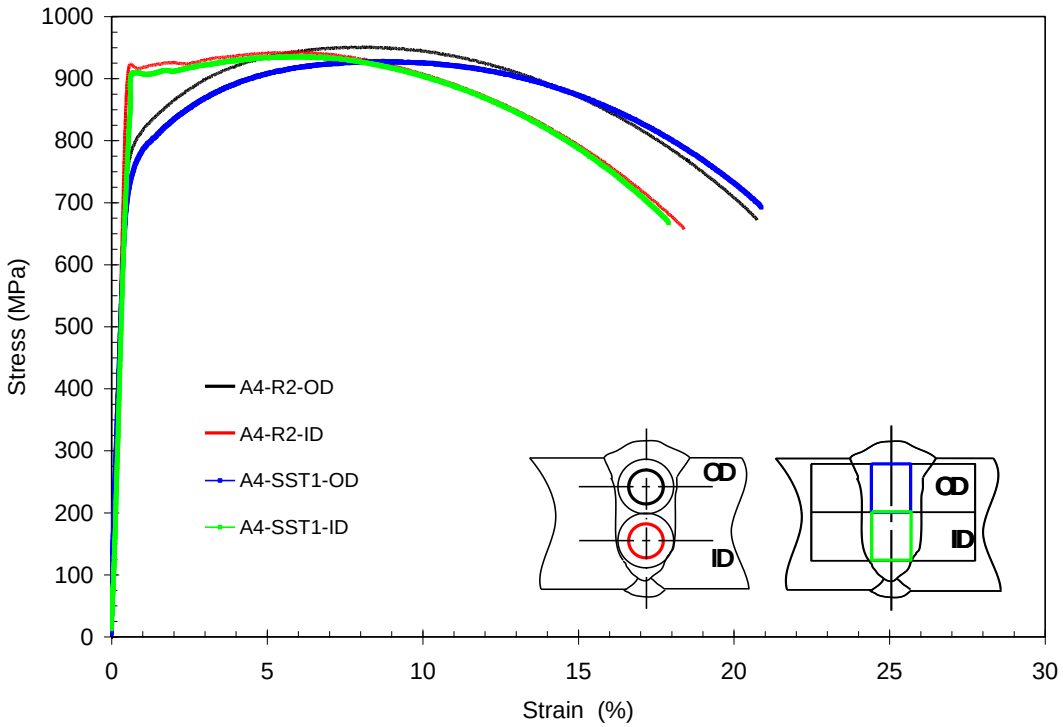

Figure- B-7 All-weld-metal tensile properties from round bar (R1) and split strip (SS) specimens [14]

Stress-strain curves of the two round bars, and one rectangular strip from a single-torch weld, are compared in Figure- B-8. The three curves exhibit the highest degree of difference at the region around the yield points. The ID-biased round bar specimen gives the highest yield strength, whereas the OD-biased round bar gives the lowest yield strength. The strength of rectangular strip specimens generally falls between those of ID and OD round bar specimens. These results follow the same trend observed previously for similar X100 pipeline welds [15].

B.4.2 Variation of Properties

Rectangular all-weld strip specimens were extracted from six rolled girth welds made from pipes of the same heat. The stress-strain curves are shown in Figure- B-9. There is generally a very good consistency among the welds.

B.4.3 Dependence on Test Temperature

Examples of the effect of temperature on the AWM tensile stress-strain curve are shown in Figure- B-10[13]. For reference, the stress-strain curve of the pipe, in longitudinal direction, is also provided. The AWM stress-strain curves of an X100 weld are given in Figure- B-11. Trends similar to those observed for the tensile properties of the base pipe, are evident for the weld metals. In both cases, there is a marked increase in both the tensile strength and strain hardening capacity of the weld metal, except in the case of the ID biased round tensile specimen of the X100 weld, where there is only an increase in the uniform strain (engineering strain at the point of UTS). Further low temperature (-20°C) AWM tensile testing is underway at CANMET

to establish the differences in tensile properties, using both round and strip tensile specimens for two series of single and dual torch welds.

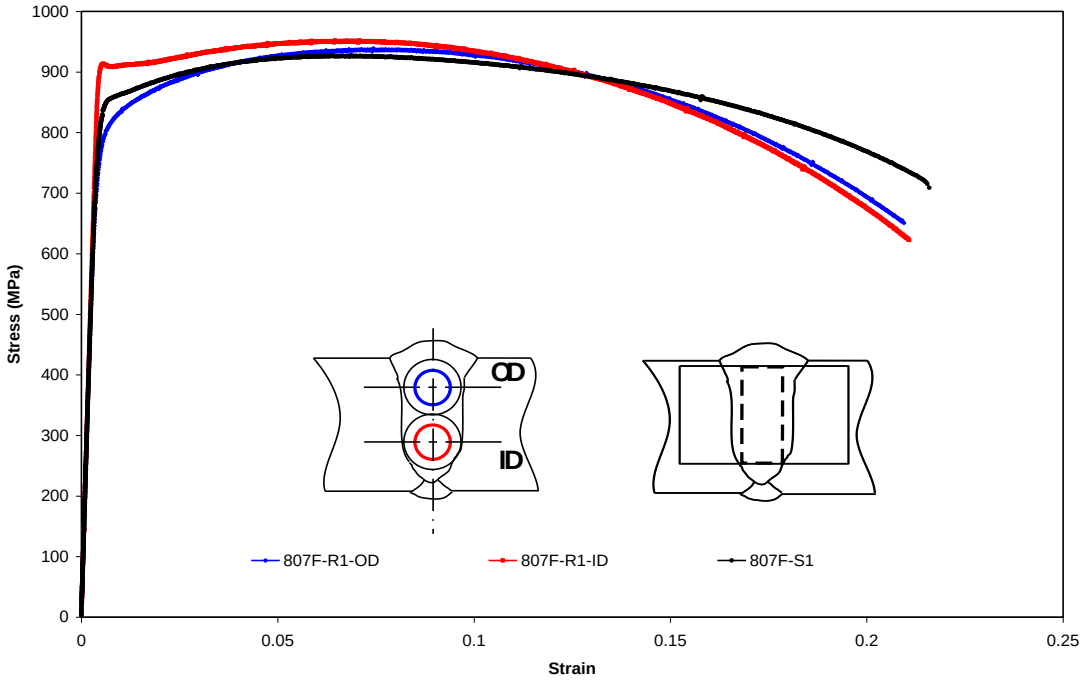

Figure- B-8 Stress-strain curves of weld metal from three specimens of different location and type

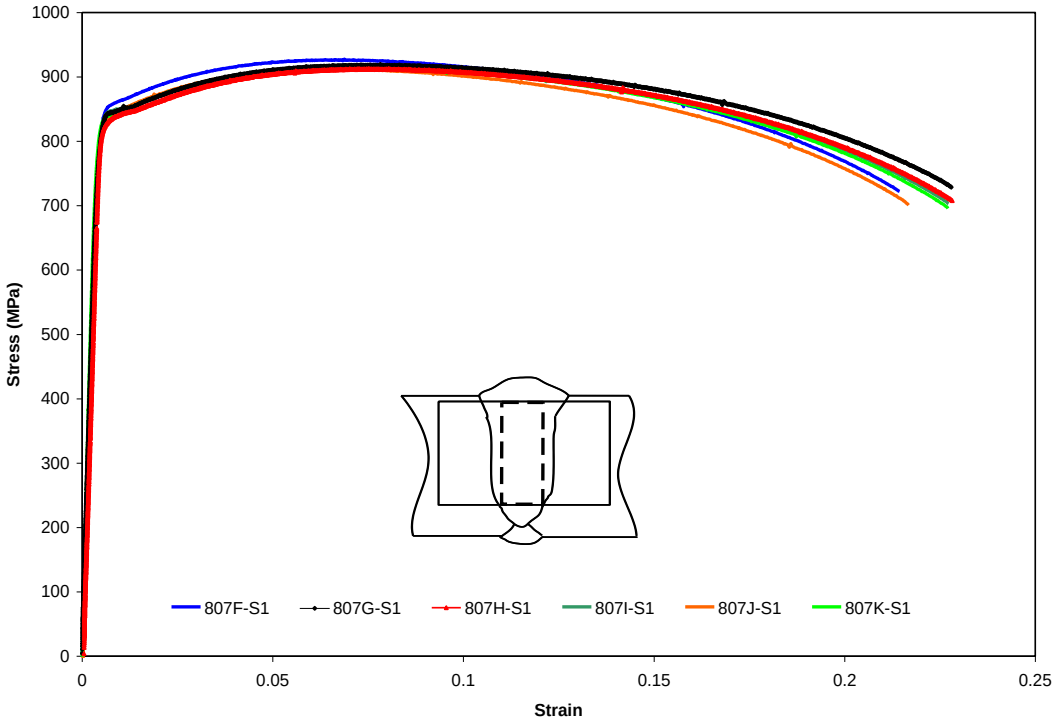

Figure- B-9 Stress-strain curves of the weld metal using strip specimens from six rolled welds

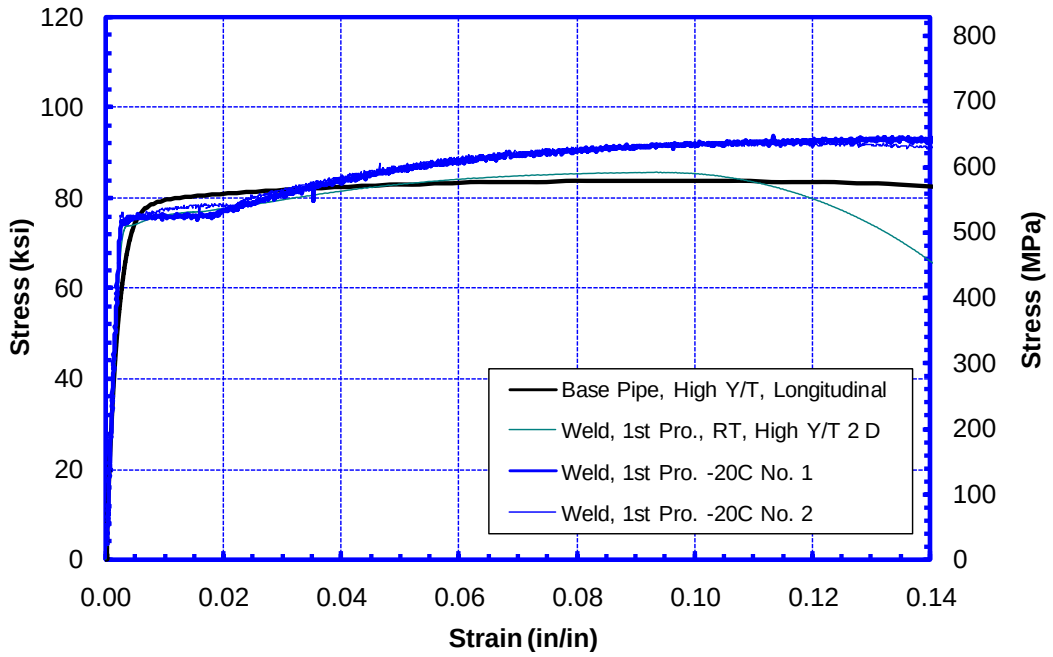

Figure- B-10 Stress-strain curves of an X70 pipe at room temperature and weld metal at room temperature and -20ºC [13]

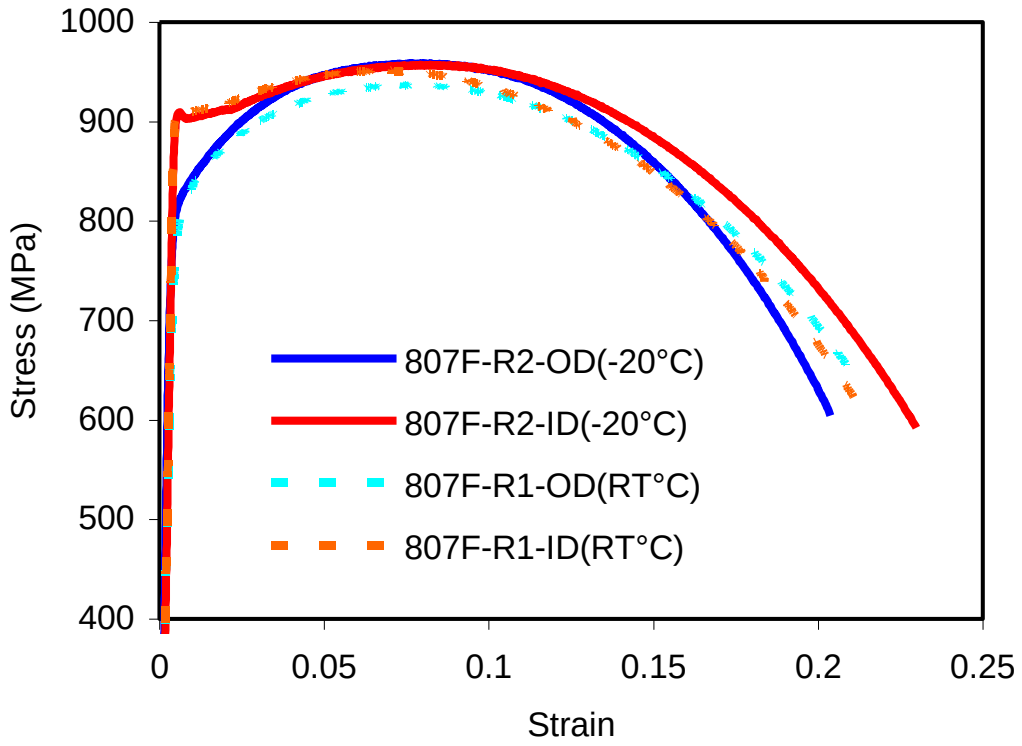

Figure- B-11 All-weld-metal tensile properties of an X100 single torch weld at room temperature and -20ºC

B.5 Effects of Strain Aging

B.5.1 Effects of Strain Aging on Linepipe Properties

Numerous studies have been conducted on the effects of strain aging on the tensile properties of high strength pipe. The results of these studies are briefly summarized here:

Strain aging can increase the yield strength by 60 MPa or more [16].

The change in UTS by strain aging is generally much smaller than that by yield strength [16].

(a) Strain aging can change the stress-strain curve from round-house shape to discontinuous yielding [16].
(b) There is a strong correlation between the change in stress-strain curves and the (1) amount of pre-straining, (2) strain aging temperature, and (3) duration of the temperature hold [17].
(c) The tensile property change may vary at different pipe wall thickness locations since those locations experience different amount of pre-strain [10].
(d) Most reported linepipe steels don't experience significant strain aging effects at temperatures below 200°C at the typical duration of anti-corrosion coating, (e.g. FBE coating, of approximately 5 minutes).

B.5.2 Effects of Strain Aging on Weld Properties

Narayanan et al. studied the strain aging effects of ferritic weld metal deposited with gas shielded flux cored arc welding (FCAW-G) process [18]. A multi-pass procedure was used to deposit weld metal in a 19-mm thick joint. All-weld-metal tensile samples were subjected to varying levels of strain, aged at 170ºC for 20 minutes and reloaded to failure. The tensile tests showed increased yield strength and UTS in comparison to the as-deposited values, confirming the effects of strain aging. There was also a change in the strain hardening behavior and decrease in the uniform elongation with the strain aging.

B.6 Representation of Weld Strength Mismatch

It is generally agreed that weld strength overmatching is highly desirable for strain-based design as the overmatching weld metal prevents strain localization and shields the weld from overall deformation in the presence of hoop stress (from internal pressure). The most prevalent way of defining overmatching uses the yield strengths of base metal (pipe material) and weld metal. Implementing overmatching requirements is not as easy as it seems. The ranges of stress-strain curves revealed in the CANMET work exemplify this challenge as shown in Figure- B-12 [19]. Depending on the "pairing" of the stress-strain curves, the yield strength of the weld metal can be as much as 150 MPa higher than that of the base pipe (880 MPa vs. 730 MPa) or as low as slightly below that of the base pipe. The mismatch level could therefore range from 0% to 20% overmatching. The range shown in Figure- B-12, from the same pipe and girth weld, is entirely due to the natural variation of the pipe properties and differences in the type of all-weld-metal tensile specimens. Other possible contributing factors to strength variations, but not included in Figure- B-12, are (1) strain aging effects, (2) variability from the non-linear stress-strain response prior to yielding (e.g. Figure- B-2), (3) joint-to-joint variation and (4) heat-to-heat variations.

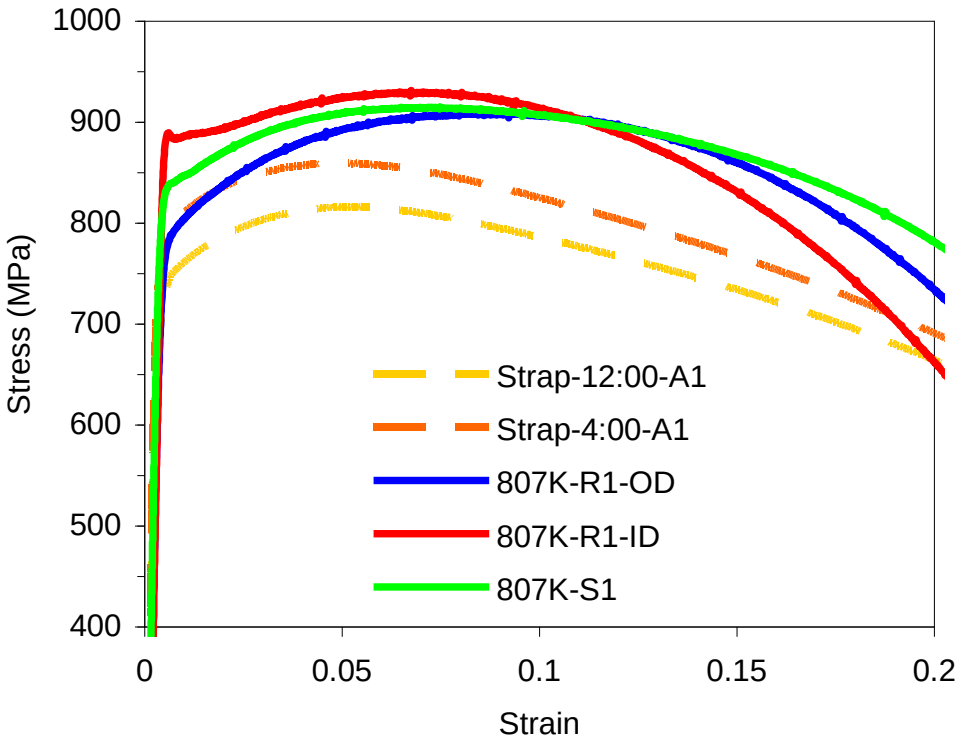

Figure- B-12 Comparison of AWM stress-strain curves (round bar biased to OD and ID and strip specimens) with longitudinal stress-strain curves of the X100 pipe (strap tensile specimens in dashed curves) [19]

B.7 Definition of "Round-House"

Some of the recent efforts to produce pipes with superior strain capacity have focused on having "round-house" stress strain curves. The presence of yield point elongation, or Luder's extension, tends to initiate buckling, and therefore reduces the compressive strain capacity of the pipe. Therefore, having round-house stress strain curves is critical to achieving high compressive strain capacity.

Conceptually, the round house stress strain curve is such that the yielding is continuous. i.e., the stress increases smoothly and gradually with the increase of strain. Experience has shown that such stress-strain curves are achievable before the pipes are subjected to anti-corrosion coating. However, a yield plateau can appear after anti-corrosion coating. Sometimes a slight drop in load can occur around the yield point. It is not known how small the yield plateau or load drop can be before a stress-strain curve would be disqualified as not having round-house behavior. The application of multiple stress ratios by TransCanada [5] is meant to give rise to the round-house stress-strain response. However, such definition may not exclude small Luder's extension or a small drop in stress values.

A more robust definition of round-house behavior is needed. The definition should focus on two factors: (1) the magnitude of the stress drop and (2) the strain interval over which the drop occurs. It may be argued that an isolated small drop or plateau in stress over a very small strain

range, would not adversely affect tensile strain capacity, particularly if the overall strain hardening trend was continuous.

B.8 Summary and Recommendations

The sensitivity of strain based design to linepipe and weld tensile properties is well established. There are significant technical and practical challenges in acquiring adequate properties. The current specifications in codes and standards are not sufficient to guarantee tensile properties adequate for strain-based design. The following considerations are recommended:

1. At a minimum, full stress-strain curves will be required for pipe and weld tensile properties. While most test labs do not presently produce full stress-strain curves, some are capable of generating these curves, when required.
2. The quality of the full stress-strain curves may vary and should be checked and confirmed. One particularly obvious "marker" is the reported elastic slope of the stress strain curves. While small deviation from the theoretical value is understandable and tolerable, in some egregious cases the reported slope has been much lower than the theoretical value or even, in some cases, much greater than the theoretical value. While the elastic slope is generally not viewed as a material parameter in strain-based design, the elastic slope directly affects the reported yield strength. This influence is particularly acute for stress-strain curves of high-strength steel, exhibiting non-linear behavior prior to the yield point, (see Figure- B-1). An incorrect elastic slope can directly lead to incorrect yield strength, hence incorrect Y/T ratio and an incorrect conclusion on the pass/fail of the strength requirement. It also affects the qualification of the weld strength mismatch, if the mismatch is defined at the yield strength. It is recommended that consistent test data-screening and evaluation procedures be implemented in project applications.
3. The effect of test temperature on the strain hardening behavior is a relatively new issue. It is not known whether the increased strain hardening rate and uniform strain shown in this paper are limited to certain linepipes and welds. Clearly, more investigation is needed, given the importance of strain hardening capacity on tensile strain limit. With respect to the overall approach to strain-based design, consistency in test temperature should be considered. Although the pipeline industry has been conducting toughness tests (e.g., Charpy and CTOD) at the minimum design temperature or lower, tensile tests are mostly done at room temperature. Yet tests specific for strain-based design, such as curved-wide-plate tests, may be done at yet another temperature. Clearly, there is a need to (1) understand the temperature effects on tensile properties, (2) move towards a uniform test temperature so the test results can be better correlated. Interestingly, many labs are not equipped to do low temperature tensile tests, certainly not at the production rates needed for large-scale projects.
4. The yield strength according to current definitions, either at 0.5% total strain or at 0.2% offset strain, can exhibit large specimen-to-specimen variations. This is particularly true for longitudinal property measurement in some of the high strength pipes. It is recommended that the strain at which the yield strength is measured be graduated (increased) with pipe strength level. This recommendation is consistent with that of Klein et al. [16].

5. The shape of stress-strain curves can vary from changes in the material properties (aged vs. non-aged) and from changes in test specimen geometry and specimen position relative to the pipe and weld. It is insufficient to define weld strength mismatch on the basis of either yield strength or UTS. Given the relatively large spread in the yield strengths of both pipe and weld metals, defining strength mismatch on the basis of yield strength can be problematic in understanding and controlling the weld properties. The UTS of both pipes and welds tends to show less variation than the yield strength for the same welds. The strength mismatch on the basis of UTS is preferred to that based on yield strength. If a single value indicator is desired, mismatch based on UTS may be used as a first order tool.
6. Strain hardening capacity is a critical parameter for strain-based design. The customary representation of strain hardening by *Y*/*T* ratio is not adequate if the reported yield strength does not represent the material's physical yield point.
7. For large-scale application of strain-based design, consistent tensile test protocols, including both linepipe and girth welds, are needed.
8. In the absence of a universally accepted definition of round-house behavior, the following definition is proposed: "a stress-strain curve is deemed to have round-house shape, if the stress value does not drop by more than 0.5% of UTS over any continuous strain range of 0.2% when the strain is less than 50% of uniform elongation." Such a definition would allow for a plateau or even drop in stress value, provided that this occurs within a small strain increment of 0.2%. The implementation of such a definition is possible with digital records of stress-strain curves and some stress-strain curve screening software.

B.9 References

1 "Specification for Linepipe," API Specification 5L, 44th Edition, October 1, 2007.

2 "Petroleum and Natural Gas Industries – Steel Pipe for Pipeline Transportation System," ISO 3183, 2007.

3 Glover, A., Zhou, J., Horsley, D., Suzuki, N., Endo, S. and Takehara, J., "Design Application and Installation of an X100 Pipeline," Proceedings of 22nd International Conference on Offshore Mechanics and Arctic Engineering, Paper No. OMAE2003-37429, Cancun, Mexico, 2003.

4 Glover, A., Horsley, D., Dorling, D. and Takehara, J., "Construction and Installation of X100 Pipelines," Proceedings of the 5th International Pipeline Conference, Paper No. IPC04-0328, Calgary, Canada, 2004.

5 Ishikawa, N., Okatsu, M., Endo, S., Kondo, J., Zhou, J. and Taylor, D. "Mass Production and Installation of X100 Pipeline for Strain-Based Design Application," Proceedings of 7th International Pipeline Conference (IPC2008), September 29-October 3, 2008, Calgary, Alberta, Canada.

6 "Steel Pipe," CSA Z245.1-02, Canadian Standards Association, Mississauga, ON, Canada, 2002.

7 Zhou, J., Taylor, D., and Hodgkinson, D., "Further Large-Scale Implementation of Advanced Pipeline Technologies," Proceedings of 7th International Pipeline Conference (IPC2008), September 29-October 3, 2008, Calgary, Alberta, Canada.

8 Ishikawa, N., Okatsu, M., Shimamura, J., Endo, S., Shikanai, N., Muraoka, R., Kondo, J., and Suzuki, N. "Material Development and Strain Capacity of Grade X100 High Strain Linepipe

Produced by Heat Treatment Online Process," Proceedings of 7th International Pipeline Conference, September 29-October 3, 2008, Calgary, Alberta, Canada.

9 Hara, T., Terada, Y., Shinohara, Y., Hitoshi, A. and Doi, N., "Metallurgical Design and Development of High Deformable X100 Linepipe Steels Suitable for Strain Based Design," Proceedings of 7th International Pipeline Conference, September 29-October 3, 2008, Calgary, Alberta, Canada.

10 Seo, D., Yoo, J., Song, W. and Kang, K., "Development of X100 Linepipe Steel with High Deformation Capacity," Proceedings of 7th International Pipeline Conference, September 29-October 3, 2008, Calgary, Alberta, Canada.

11 Tsuru, E., Shinohara, Y., and Asahi, H., "Evaluation of Precept of Strain Capacity of High Strength UOE Linepipes Used in Strain-Based Design Applications," Proceedings of the 17th International Offshore and Polar Engineering Conference (ISOPE 2007), Lisbon, Portugal, July 1-6, 2007.

12 Ishikawa, N., Okatsu, M., Shimamura, J., Endo, S., Shikanai, N., Muraoka, R., Kondo, J., and Suzuki, N. "Material Development and Strain Capacity of Grade X100 High Strain Linepipe Produced by Heat Treatment Online Process," Proceedings of 7th International Pipeline Conference, September 29-October 3, 2008, Calgary, Alberta, Canada.

13 Wang, Y.-Y., Liu, M., Stephens, M., Petersen, R., and Horsley, D., "Recent Development in Strain-Based Design in North America," Proceedings of the 19th International Offshore and Polar Engineering Conference (ISOPE 2009), Osaka, Japan, July 21-26, 2009.

14 Gianetto, J.A., Bowker, J.T., Bouchard, R., Dorling, D.V. and Horsley, "Tensile and Toughness Properties of Pipeline Girth Welds," *Welding in the World*, Vol. 51, No. 5/6, 2007.

15 Gianetto, J.A., Bowker, J.T., Dorling, D.V., Taylor, D., Horsley, D. and Fiore, S.R., "Overview of Tensile and Toughness Testing Protocols for Assessment of X100 Pipeline Girth Welds," Proceedings of 7th International Pipeline Conference (IPC2008), IPC2008-64668, Calgary, Alberta, Canada, October 2008.

16 Klein, R., Collins, L., Hamad, F., Chen, X. and Bai, D., "Determination of mechanical properties of high strength linepipe," Proceedings of 7th International Pipeline Conference (IPC2008), September 29-October 3, 2008, Calgary, Alberta, Canada.

17 Duan, D., Zhou, J., Rothwell, B., Horsley, D. and Pussegoda, N., "Strain aging effects in high strength linepipe materials," Proceedings of 7th International Pipeline Conference (IPC2008), September 29-October 3, 2008, Calgary, Alberta, Canada.

18 Narayanan, B., Brady, N., Wang, Y.-Y. and Ogborn, J., "Effect of Strain Ageing on Yield Strength and Post Yield Behavior of FCAW-G Ferritic Weld Metal," Proceedings of the 8th International Pipeline Conference, Paper No. IPC2010-31371, September 27 – October 1, 2010, Calgary, Alberta, Canada.

19 Gianetto, J., Tyson, W., Wang, Y-Y., Park, D-Y, Bowker, J. and Shen, G., "Mechanical Properties and Microstructure of Weld Metal and HAZ Regions in X100 Single and Dual Torch Girth Welds," Proceedings of 8th International Pipeline Conference (IPC2010), IPC2010-31411, Calgary, Alberta, Canada, October 2010.

Appendix C Toughness Considerations for SBD

C.1 Scope of This Section

Girth weld toughness is one of the key inputs in strain-based design. A few key issues are examined here. The resolution of these issues is critical to the strain-based design.

C.2 Key Toughness Considerations for Strain-Based Design

C.2.1 Dependence of Resistance Curves on Specimen Type

Tensile strain capacity models, on the basis of instability analysis, rely on the toughness of resistance curves to determine the instability point. Therefore it is useful to examine the similitude of resistance curves among specimens of different types. It is particularly important to establish the similitude between the laboratory small-scale specimens and the actual large structure, as the small-scale test results are used to predict the large-scale behavior.

Curved wide plate (CWP) specimens have been used as a quasi-structural specimen to evaluate the tensile strain capacity of pipeline girth welds [1,2]. For small-scale specimens, the standard three-point bend CTOD specimen has been widely used to quantify girth weld toughness. In recent years the low-constraint SENT specimen is increasingly being used because it is viewed as a more appropriate measure of girth weld toughness than the SENB specimen [3,4].

The resistance curves from different specimen types are compared here. In the early tests by SINTEF, the resistance curve of the "Sector" specimen was shown to be the highest, followed by SENT, and then SENB, as shown in Figure- C-1 [5]. Tests conducted at CANMET showed that the resistance curves from SENT were generally higher than those from SENB, as shown in Figure- C-2 [6]. Recently published results by Cheng, et al. showed that the resistance curves of SENT specimens were markedly higher than that of SENB specimens, as shown in Figure- C-3 [4]. Cheng, et al., also showed that there is a good similitude of resistance curves between the full-scale and SENT specimens, as shown in Figure- C-4 [4]. The resistance curves of the CWP specimens are somewhat lower than both the SENT and full-scale specimens.

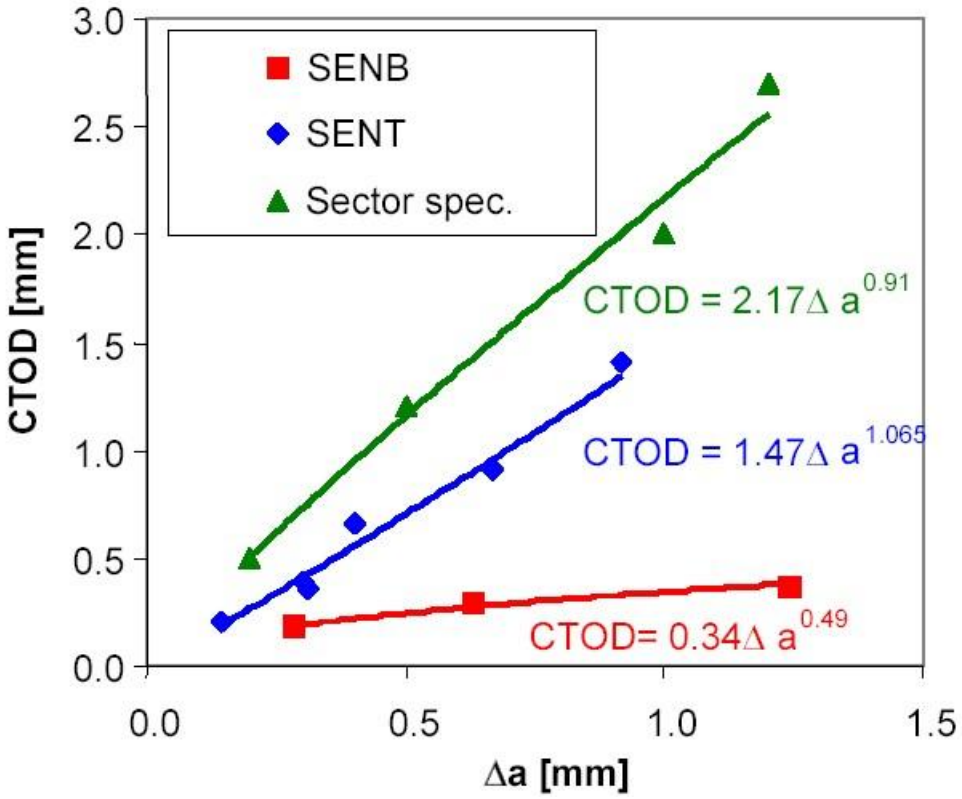

Figure- C-1 CTOD resistance curves of three types of specimens

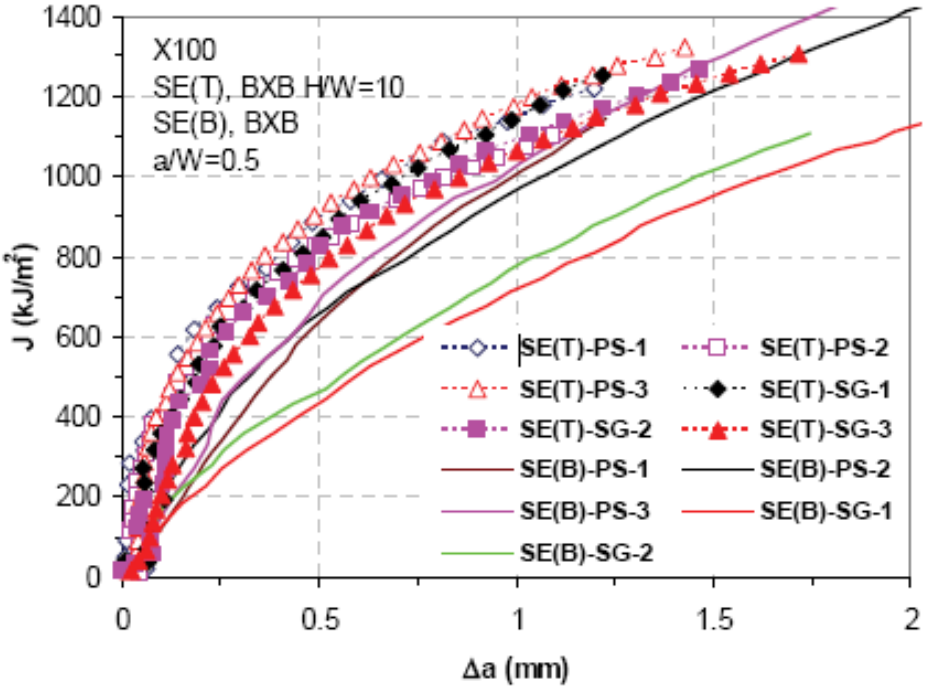

Figure- C-2 Dependence of *J* resistance curves on specimen type and side groove of X100 base pipe [6]. PS: plane-sided (non-side-grooved). SG: side-grooved.

.

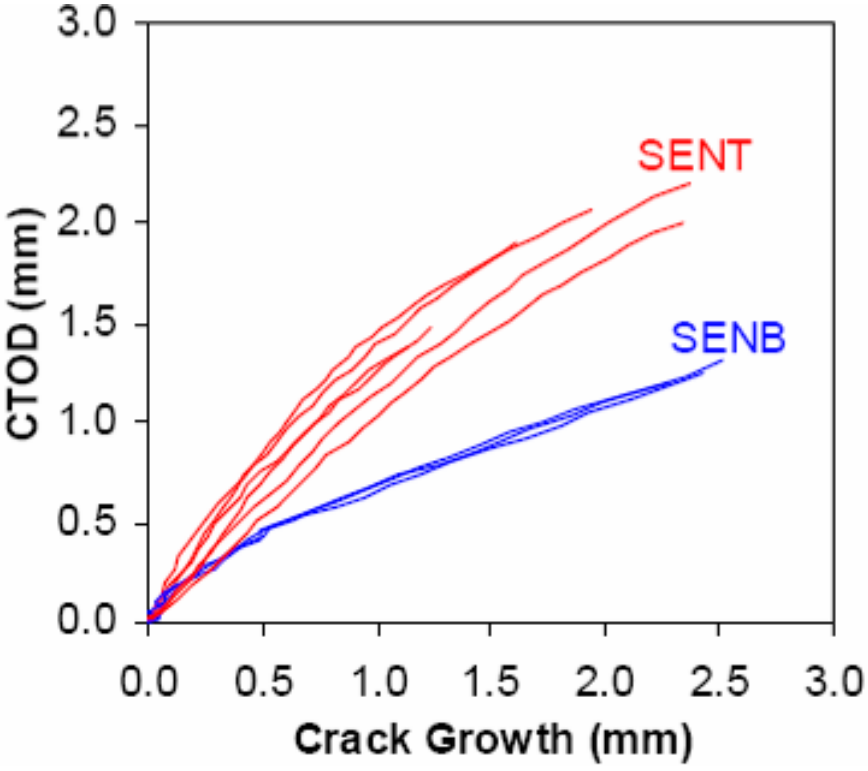

Figure- C-3 Measured CTOD R-curves of X65 welds [4]

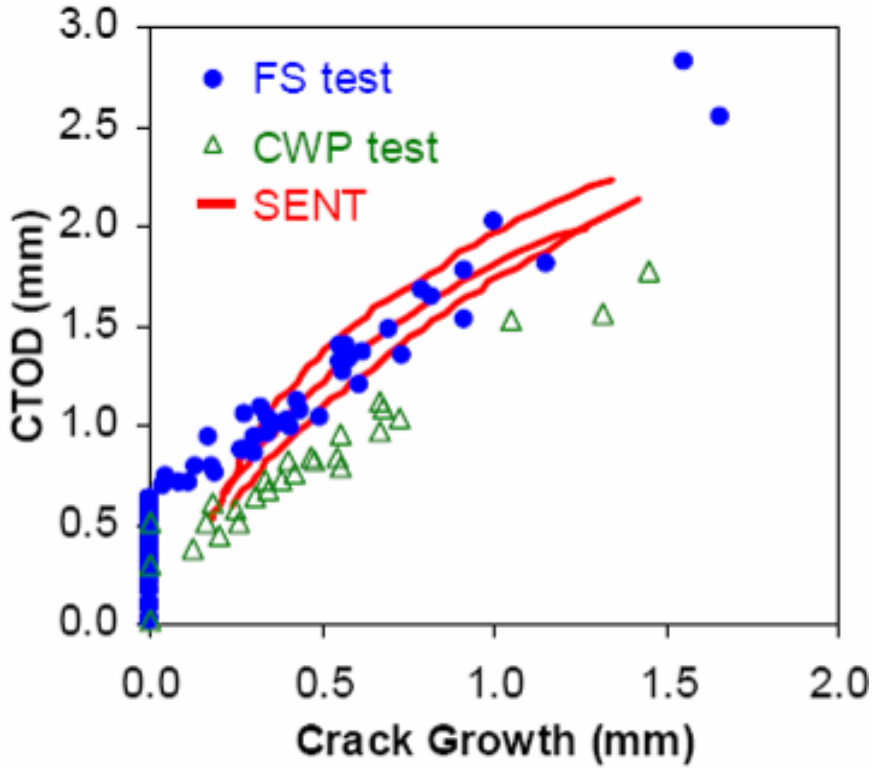

Figure- C-4 Measured CTOD R-curves of X70 base pipe from full-scale (FS), CWP, and SENT specimens [4]

C.2.2 Pop-in and Occasional Low Values of HAZ Toughness

The extensive small-scale toughness data of the X65 and X80 welds in previous sections showed that the weld metal toughness tend to have smaller scatter than the HAZ toughness. Furthermore, the HAZ generally had higher upper shelf toughness and lower transition temperature. These observations are generally consistent with the CTOD toughness data generated on X100 welds by Gianetto, et al., as shown in Figure- C-5 [7].

It is the most interesting to compare the HAZ toughness, shown in Figure- C-5, between the single-torch and dual-torch welds. There are three test results from each weld. On the basis of averaged toughness, the single-torch weld has lower toughness than dual-torch welds. This is contrary to prior observations [8]. More in-depth examination shows that two of the specimens in each weld type have the same toughness (0.27 vs. 0.27 mm and 0.14 vs. 0.14 mm). The difference is the third pair, in which the single-torch weld had 0.04 mm while the dual-torch had 0.28 mm. The question is whether one could draw conclusion on the relative toughness between the two types of the weld based on this single pair of toughness data.

An occasional low HAZ toughness is often attributable to a local brittle zone (LBZ). The structural significance of the LBZ has been the subject of considerable debate. Some argue that LBZ exists in virtually all welds. Finding the low toughness from the LBZ, from the toughness testing viewpoint, is only a matter of statistics in notch location with respect to LBZ. The CTOD toughness data presented in this paper shows that there can be considerable scatter in HAZ toughness when the test temperature is lower than approximately -20ºC. If the low toughness test results are a matter of statistics, one would not be able to conclude that the single-torch weld is worse than the dual-torch weld on the basis of a single pair of test data.

The low CTOD toughness found in modern pipeline girth welds is often associated with pop-in events at test temperature common for welding procedure qualifications, generally from 0ºC to -20ºC. The pop-in events are usually associated with some degree of load drop, but in most cases, specimens do not fracture. The toughness transition curves are helpful in determining whether the bulk material is brittle. In most cases, the bulk material is ductile. Therefore, one may conclude that the low toughness is associated with local brittle microstructure.

The more important question is, "what would be the appropriate toughness for the prediction of large-scale structural behavior?" Using the absolute lowest value of CTOD toughness can lead to unnecessary conservatism and weld repair. A more appropriate approach is taking into account the local nature of the microstructure that leads to the pop-in related low toughness. One might assume the low toughness exists over a small, but finite width of a weld path, say one weld pass height. The structural significance of a weld flaw may be assessed by assuming a flaw larger than the initial size, say initial height plus one weld bead height, and by using the bulk toughness as opposed to the low pop-in value. The essential argument here is that the flaws may pop through the LBZ but become stable after the pop-through event, provided that the pop-in is small enough and that the dynamic toughness of the surrounding material is high enough. If the low toughness zone is local and the structural stability is maintained with the larger-size flaw, this approach is appropriate and would not lead to an overly conservative assessment. In field girth welding of pipelines, an overly conservative assessment can lead to unnecessary repairs.

Since repair welds tend to have an inferior quality when compared to mechanized welds, unnecessary repairs lead to an overall lower quality of the completed welds.

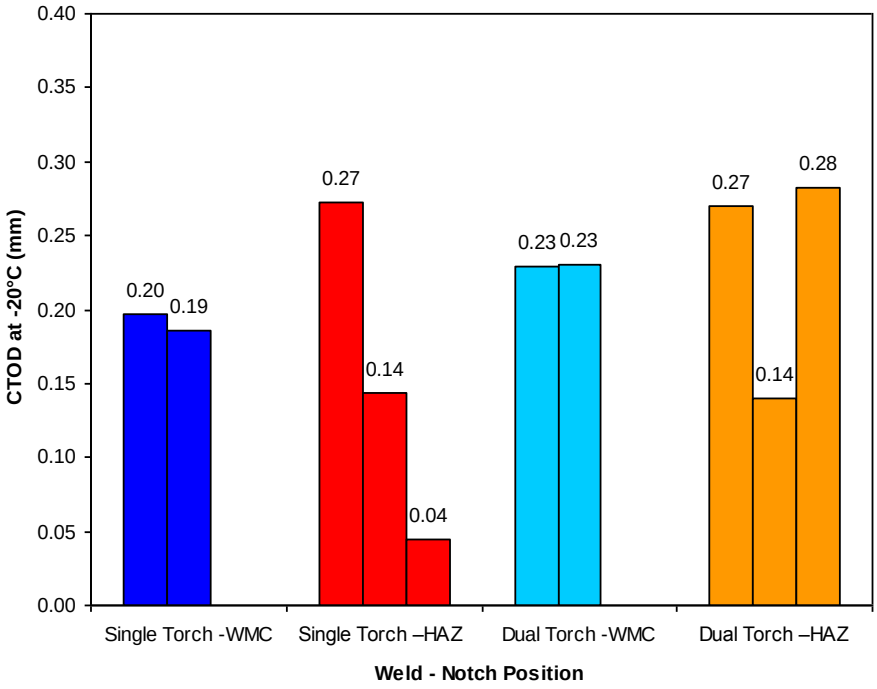

Figure- C-5 CTOD toughness of the X100 weld at -20ºC [7]

C.2.3 Effects of Weld Strength Mismatch on Toughness

Having weld strength overmatching is beneficial in achieving high tensile strain capacities. Given the variation of tensile properties of the linepipes and girth welds, there is a range of weld strength mismatch level for a given pipeline project [9]. To guarantee a minimum level of weld strength mismatch, the mean and upper level of strength mismatch would have to be higher than the specified minimum level. Some published work has showed that overly high overmatching may reduce the measured toughness, as shown in Figure- C-6 [10]. Kocak, et al., observed that a softer environment should relax the conditions for brittle fracture for HAZ flaws [11]. They also stated [12] that "for highly overmatched welds, the loss of crack tip constraint on shallow cracked overmatched SENB specimens was almost fully compensated by the mismatch (overmatch) induced constraint, and hence low toughness values, similar to the deep notched specimens, were obtained." To achieve the overall high tensile strain capacity, the benefits of weld strength overmatch should be considered in conjunction with toughness considerations.

In addition to the material's response to weld strength mismatch, it is worth noting that the current CTOD toughness test standards were developed assuming homogeneous material properties. Within a certain strength mismatch range, the inference equations used to convert the measured parameters, such as load and CMOD (crack mouth opening displacement) to the CTOD value, are valid [13]. Beyond those established ranges, the application of those inference equations should be examined.

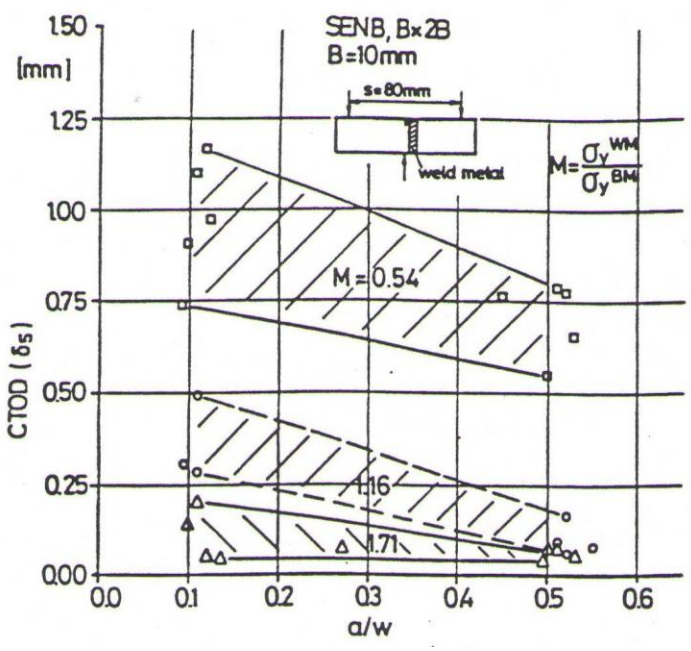

Figure- C-6 CTOD toughness as a function of weld strength mismatch and relative flaw depth (constraint) [10]

C.2.4 Effects of Side Groove in Toughness Test Specimens

Work at CANMET and others have shown that the resistance curves of SENT and SENB specimens with side grooves are lower than those from plane-sided (without side groove) specimens. An example of such results is shown in Figure- C-7 for SENT specimens [14].

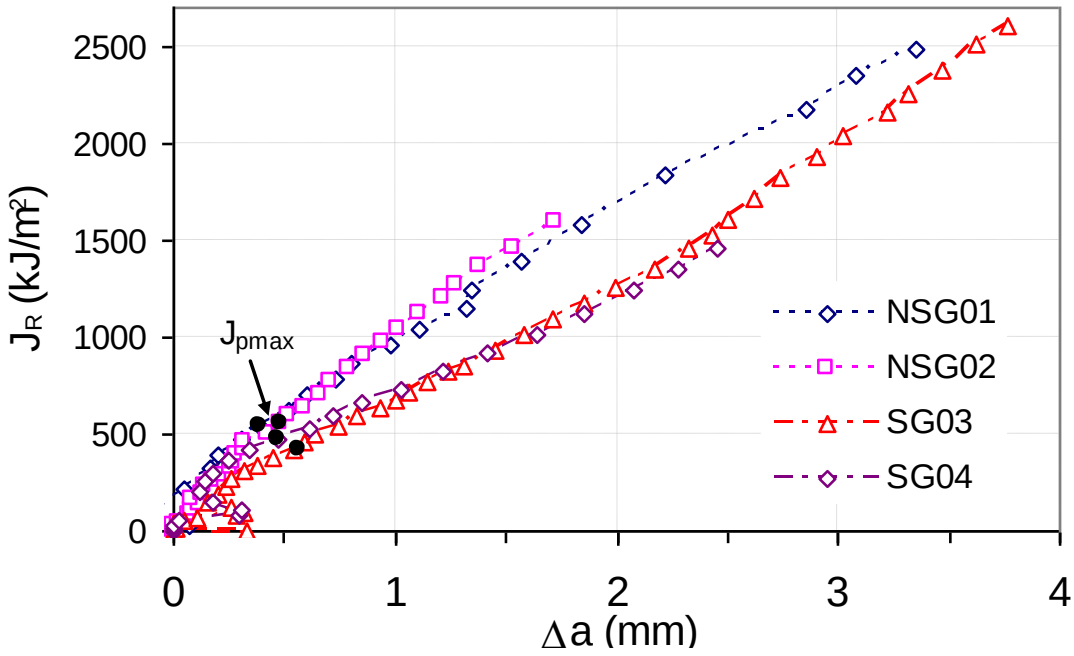

Figure- C-7 Effects of side groove on the J-resistance curves from SENT specimens [14]. NSG: Non-side-grooved. SG: side grooved

C.2.5 Effects of Flaw Depth

The work at CANMET has also shown that the resistance curves of SENT specimens are dependent on the initial flaw depth, as shown in Figure- C-8 [6]. It is therefore important to consider the influence of the initial flaw depth when selecting the appropriate small-scale test specimens for the prediction of large-scale behavior.

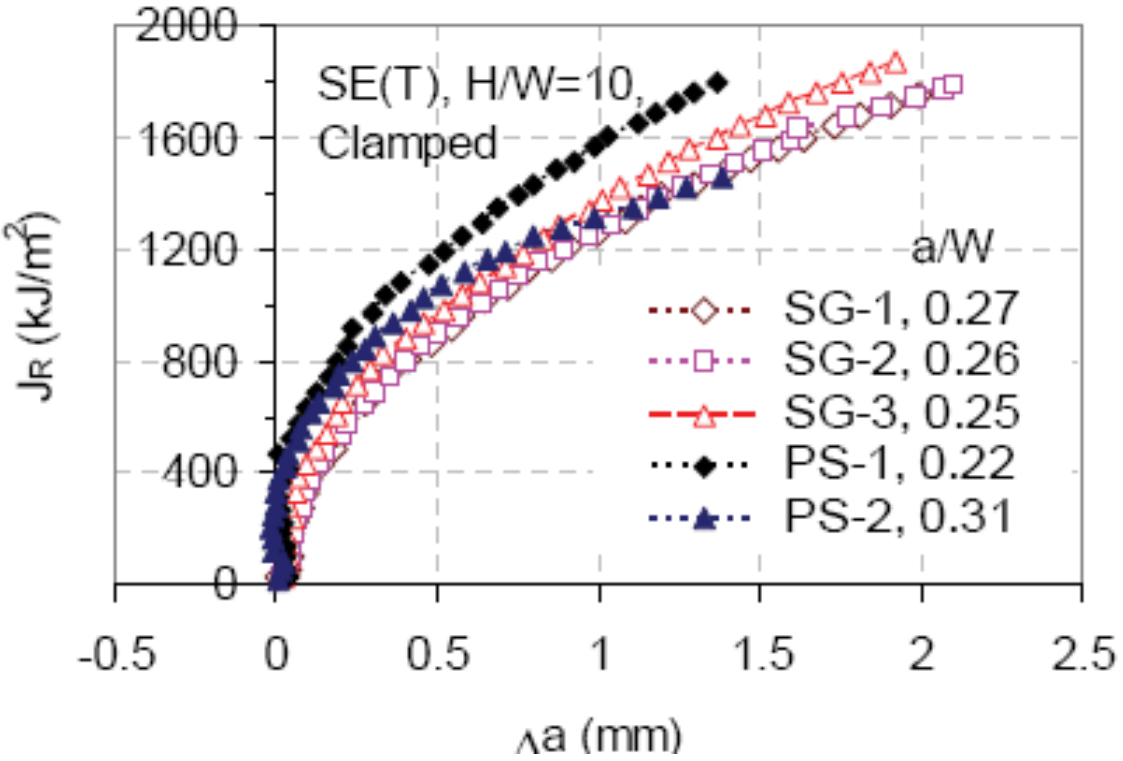

Figure- C-8 Effects of side groove and initial flaw depth on the J-resistance curves of SENT specimens [6]

C.3 Observations on Toughness

1. The similitude of resistance curves among specimens of different forms is not consistent in currently published data. Further investigation is needed to fully establish the similitude.
2. The resistance curves of low-constraint specimens are dependent on a number of test parameters, such as side groove and flaw depth.
3. Due to the dependence of resistance curves on test specimen parameters, appropriate windows of applicability need to be defined when applying the small-scale test results for the prediction of large-scale behavior.
4. Occasional low CTOD toughness, particularly those from pop-in events, likely exists in many girth welds. It is suggested that the occasional low values should be analyzed on a case-by-case basis. Requirements of weld integrity on the basis of the occasional low toughness could be counter-productive for overall pipeline safety.

5. To understand the overall material behavior and the significance of occasional low CTOD toughness, more emphasis should be placed on the generation and use of toughness transition curves.
6. Typical triplicate CTOD tests for HAZ toughness may not be sufficient for strain-based design, due to the possible large variations of toughness values, particularly for flaws located in HAZ. The CTOD tests should be supplemented by Charpy transition curves, which can be generated quickly and inexpensively. The transition curves provide a clearer picture of overall material behavior, i.e., upper shelf vs. lower shelf behavior, than toughness values at a single temperature, when these toughness values have large variations.
7. Strain-based design, on the basis of overall upper shelf toughness, is more representative of the expected large-scale behavior than the lowest value at a given temperature when the scatter of the toughness value is considered. A low risk of brittle (cleavage) fracture requires adequate demonstration through toughness testing. If high-constraint tests do not present evidence of cleavage, the risk of brittle fracture is low. However, if such specimens fail in a brittle manner then enough low-constraint tests must be done to ensure that the risk of brittle fracture is acceptably low.
8. To achieve the overall high tensile strain capacity, the benefits of weld strength overmatch should be considered in conjunction with toughness considerations.
9. In addition to the constraint effects, the volume of materials being sampled along the highly-stressed crack front should be considered in predicting large-scale behavior.

The HAZ toughness may pose one of the greatest challenges in understanding the weld properties. It has been demonstrated that HAZ tends to have lower transition temperature and higher upper shelf toughness than the weld metal. At the same time, very low toughness values are possible, mostly through pop-in events. For some of the welds tested, the SENT specimens gave much lower transition temperature than those from Charpy and SENB specimens. The relevant transition temperature for large-scale specimens is not known. There is very little information on the transition temperature of large-scale structures, since the testing of such structures in meaningful quantities can be prohibitively expensive. More research on the transition behavior of large structures, from both a theoretical basis and a practical application, is needed.

C.4 References

1 Denys, R., Lefevre, A., and Baets, P. D., "A Rational Approach to Weld and Pipe Material Requirements for a Strain Based Pipeline Design," Proceedings of Applications & Evaluation of High-Grade Linepipes in Hostile Environments, Pacifico Yokohama, Japan, pp. 121-157, November 7-8, 2002.

2 Wang, Y.-Y., Liu, M., Chen, Y., and Horsley, D., "Effects of Geometry, Temperature, and Test Procedure on Reported Failure Strains from Simulated Wide Plate Tests," 6th International Pipeline Conference, Paper No. IPC2006-10497, September 25-29, 2006, Calgary, Alberta, Canada.

3 Ostby, E., "Fracture Control-Offshore Pipelines - New Strain-Based Fracture Mechanics Equations Including the Effect of Biaxial Laoding, Mismatch, and Misalignment," Proceedings of 24th

International Conference on Offshore Mechanics and Arctic Engineering, Kalkidiki, Greece June 12-17, 2005.

4 Cheng, W., Tang, H., Gioielli, P., Minnaar, K., Macia, M., "Test Methods for Characterization of Strain Capacity: Comparison of R-Curves from SENT/CWP/FS Tests," Pipeline Technology Conference, 12-14 October 2009, Ostend, Belgium.

5 DNV/SINTEF/TWI, "Fracture Control for Installation Methods Introducing Cyclic Plastic Strains, Development of Guidelines for Reeling of Pipelines," a JIP performed jointed by DNV, SINTEF, and TWI.

6 Shen, G., Gianetto, J. A., Tyson, W. R., 2009, ―Measurement of J-R Curves Using Single-Specimen Technique on Clamped SE(T) Specimens,‖ Proc. 19th Intl. Offshore and Polar Eng. Conf., ISOPE, pp. 92–99.

7 Gianetto, J., Tyson, B., Wang, Y.-Y., Bowker, J., Park, D., and Shen, G., "Properties and Microstructure of Weld Metal and HAZ Regions in X100 Single and Dual Torch Girth Welds," *Proceedings of the 8th International Pipeline Conference*, Paper No. IPC2010-31411, September 27 – October 1, 2010, Calgary, Alberta, Canada.

8 Hamad, F., Collins, L. and Volkers, R., 2008 "Effects of GMAW Procedure on the Heat-Affected Zone (HAZ) Toughness of X80 (Grade 550) Linepipe," 7th Int. Pipeline Conf., ASME, IPC2008-64097, pp. 1-17.

9 Wang, Y.-Y., Liu, M., Gianetto, J., and Tyson, B., "Considerations of Linepipe and Girth Weld Tensile Properties for Strain-Based Design of Pipelines," *Proceedings of the 8th International Pipeline Conference*, Paper No. IPC2010-31376, September 27 – October 1, 2010, Calgary, Alberta, Canada.

10 Kocak, M. and Schwalbe, K.-H., "Fracture of Welded Joints: Strength Mismatch Effect," IIW Doc. X-F-003-94, April 1994.

11 Kocak, M., Es-Souni, M., Chen, L., and Schwalbe, K.-H., "Microstructure and weld metal matching effects on heat affected zone toughness," Proceedings of the 8th International Conference OMAE-ASME, The Hague, the Netherlands, March 19-23, 1989, pp. 623-633.

12 Kocak, M. and Denys, R., "CTOD and Wide Plate Testing of Welds with Particular Emphasis on Mis-Matched Welded Joints," Keynote Lecture, 10th European Conference on Fracture, 20-23 September 1994, Berlin, F.R.G.

13 Pisarski, H. G., Wang, Y.-Y., Kirk, M. T., and Gordon, J. R., "The Effect of Yield Strength Mismatch on CTOD and *J* Estimation Procedure for Weld Metal Fracture Toughness Determination," Proceedings of the 14th International Conference on Offshore Mechanics and Arctic Engineering, Copenhagen, Denmark, Volume III, 1995, pp. 427-434.

14 Shen, G., et al., "Fracture Toughness Evaluation of High Strength Steel Pipe," 2008 ASME Pressure Vessel and Piping Division Conference, July 27-31, 2008, Chicago, Illinois, USA.

Appendix D Examination of Toughness Transferability

D.1 Introduction

The fracture toughness is usually obtained from small-scale laboratory tests such as the single-edge-notched-bend (SENB) specimen. It is well known that the traditional SENB specimen is a high-constraint fracture test specimen. It tends to underestimate the material's toughness for flaws in pipes due to its high constraint level. The constraint level of the SENB specimen usually increases as the a/W ratio increases (a – flaw depth, W – specimen width). The a/W ratio of the traditional SENB specimen is about 0.5.

Compared with the traditional SENB specimen, the single-edge-notched-tension (SENT) specimen can generate a lower constraint level at the flaw. Therefore, it has been proposed to be a low constraint test for measuring the material's toughness for flaws in pipes.

The curved wide plate (CWP) specimen is believed to provide a better representation of the constraint level in a pipe than the SENB and SENT specimens. However, the CWP tests are not considered as a small scale specimen.

The similitude of the tension loaded specimens is examined in this appendix. In addition to the above specimens, full-scale pipes are added to the analysis.

D.2 FE Model and Matrix

The transferability of the fracture toughness from different specimens is studied using the GTN model. The GTN model was initially developed by Gurson [1] and later improved by Tvergaard [2,3] and Koplik and Needleman [4]. The model simulates the mechanism of void nucleation, growth, and coalescence in porous metals exposed to severe triaxial stress state, as that near a crack tip.

Three test specimen forms, including SENT, CWP, and full scale pipe (FSP), were selected for analyses. The SENT specimen has a B×B configuration (i.e., square cross section). The width (W) and wall thickness (B) of the specimen are 11.57 mm. The specimen was clamp loaded and the "day-light" length of the specimen is 10 times of the specimen width (10W). Similar to the SENT specimen, the wall thickness of the CWP and FSP specimens was kept at 11.57 mm. The outside diameter (OD) of the CWP and FSP specimens was 312 mm (nominally 12-inch OD). The length of the model is greater than five times that of the OD (> 5OD) to avoid any boundary effect. The widths of the weld and heat affected zone (HAZ) are 6.96 mm and 2.00 mm, respectively.

The FE models of the three test specimens are presented in Figure- D-1. The flaws were located in the center of the weld metal (WM). For SENT specimens, the flaw was modeled as a through wall crack. For the CWP and FSP specimens, the flaw was a surface breaking semi-elliptic crack of 50-mm long, located on ID surface. Due to the symmetry of geometry and loading conditions, only a quarter of the specimen was modeled for each case. The material parameters of a high strength linepipe steel in [5] were used in the analysis. The stress-strain curves of the pipe and weld materials are shown in Figure- D-2.

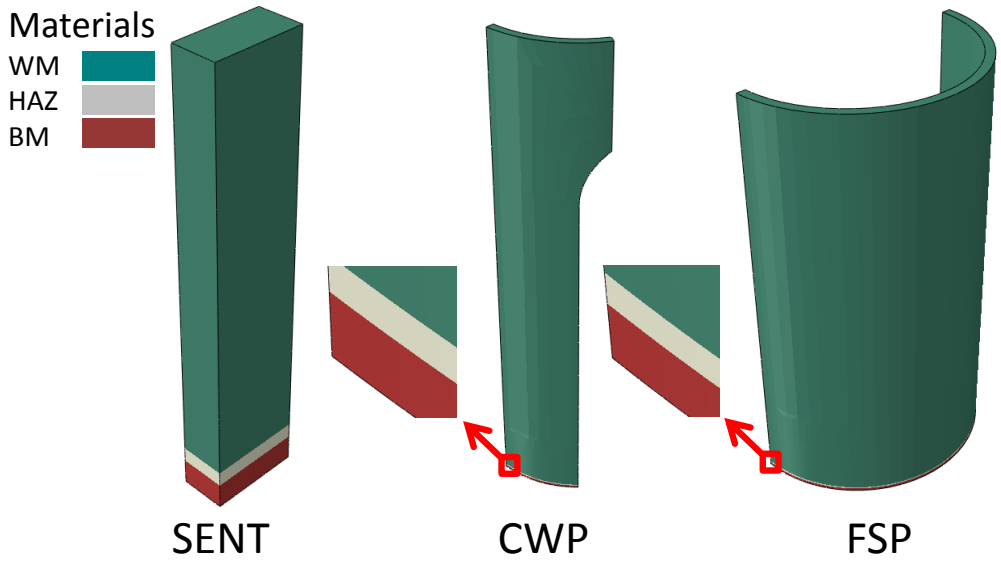

Figure- D-1 FEA models

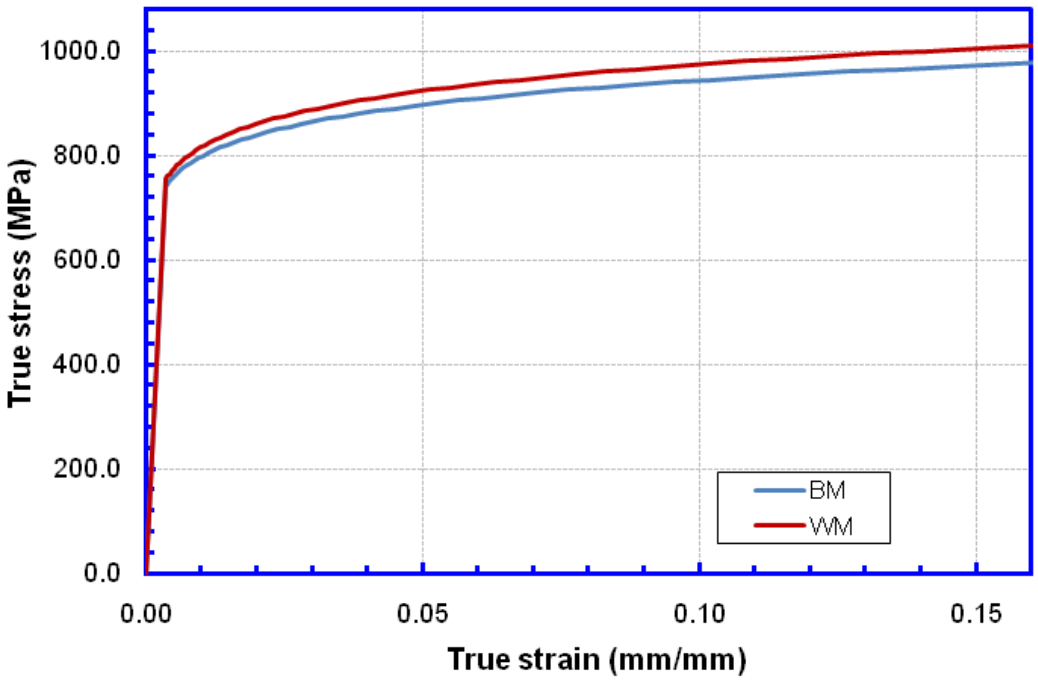

Figure- D-2 Stress-strain curves of X100 pipe and weld

The effect of specimen type on fracture toughness was studied for the SENT, CWP, and FSP specimens. The flaw depths of all the specimens were fixed at 3 mm.

ABAQUS/Explicit was used in the simulation and three-dimensional (3-D) eight-node brick (linear) elements were used. The elements were removed when the build-in failure criteria of the GTN model were reached to simulate the flaw growth.

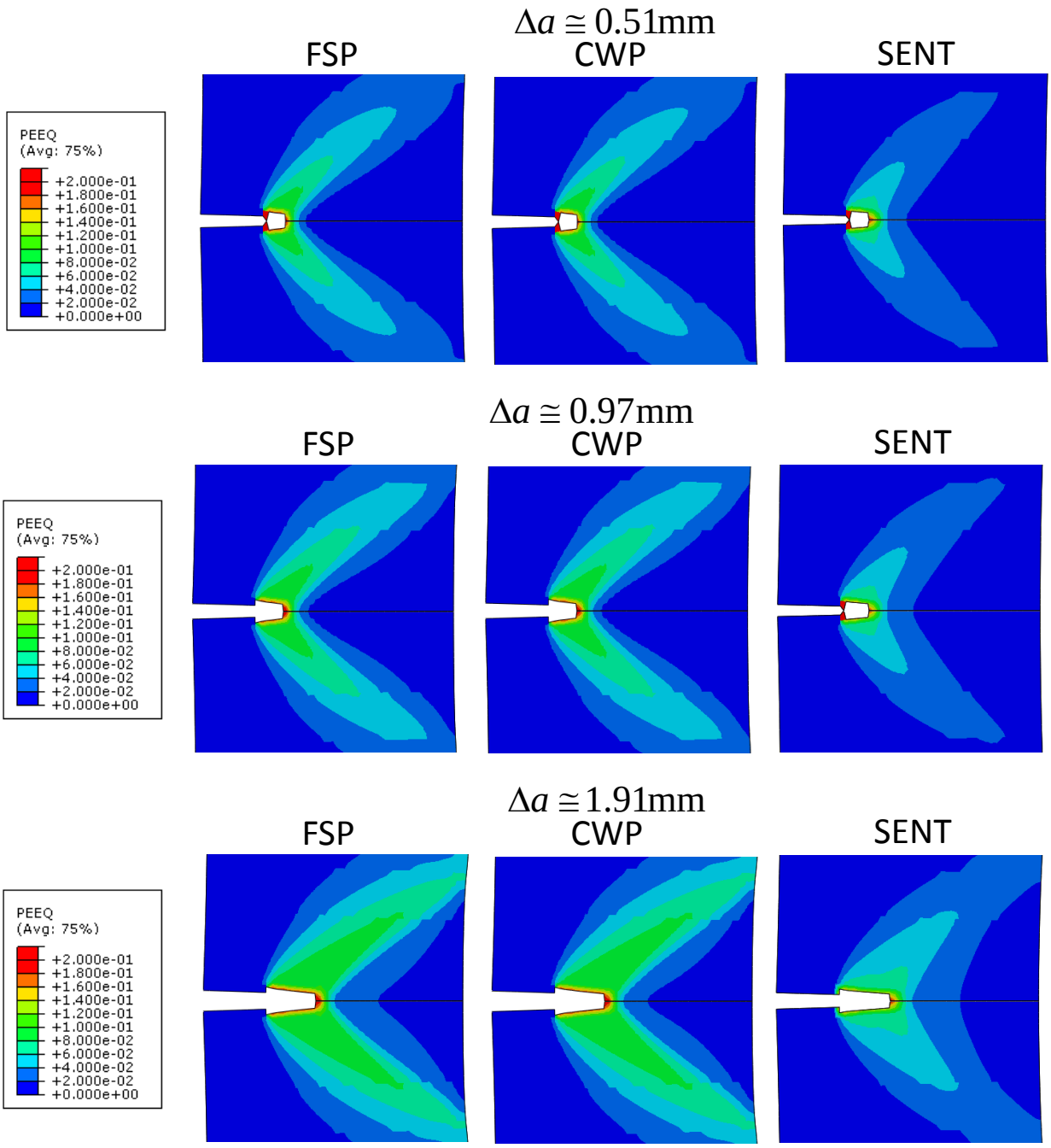

Figure- D-3 Equivalent plastic strain (PEEQ) contour near the crack tip with initial flaw depth a_0 = 3 mm

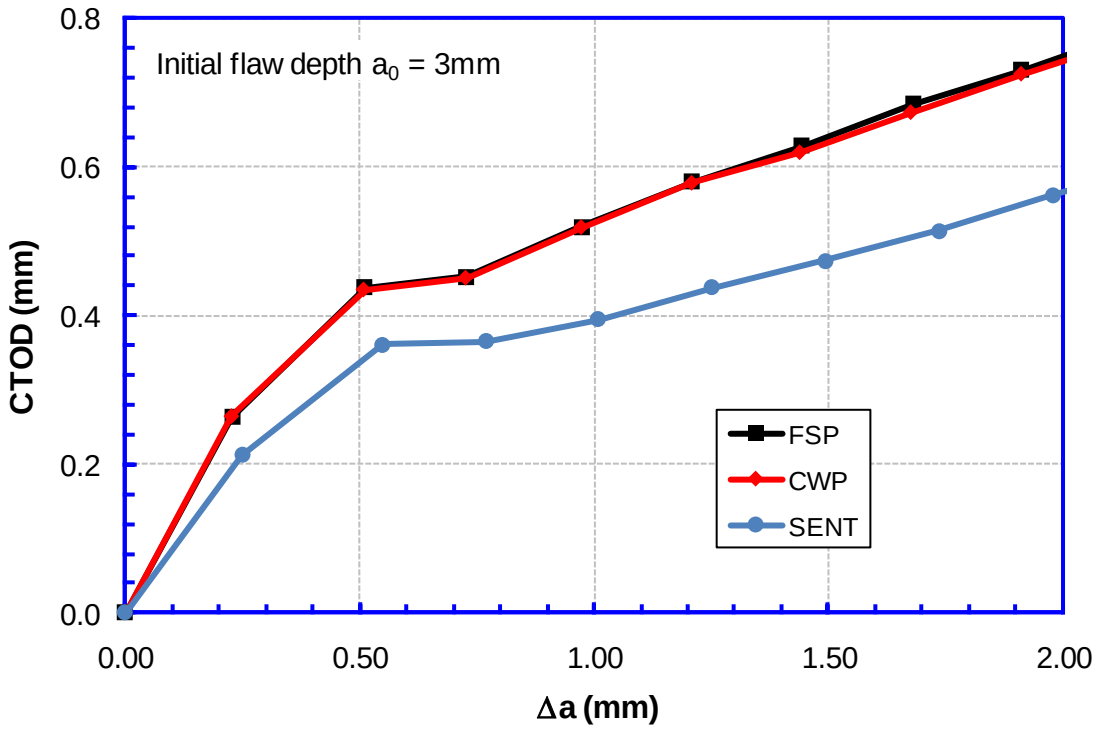

Figure- D-4 Simulated CTOD resistance curve

D.3 Preliminary Analysis Results

The equivalent plastic strain fields near the crack tip are shown in Figure- D-3 at the same amount of flaw growth among different specimens. The initial flaw depth is 3 mm (i.e., a_0/W = 0.26) for all specimens. The FSP and CWP generate almost the same deformation fields near the crack tip, which supports the similarity of the damage process in the two specimen/structure types. SENT generates a similar deformation pattern near the crack tip, compared to FSP and CWP, but the magnitude of the deformation is lower. There is a good similitude between the CWP and the FSP. The SENT specimen generates lower plastic strain for the given amount of flaw growth from the same initial a_0/W, which indicates that the corresponding crack opening of SENT would be lower than those of CWP and FSP.

The CTOD resistance curves from the same models are shown in Figure- D-4. The CTOD was calculated as the separation of the crack surface 0.25-mm behind the original flaw tip (i.e., 2.75 mm from the crack mouth). The removal of elements in the GTN simulation prevents the direct computation of CTOD at the original flaw depth (3 mm). It clearly showed that the resistance curves obtained from CWP and FSP are identical. The resistance curve from the SENT specimen is about 20% lower than those of the CWP and FSP. The results are consistent with the plastic strain contour shown in Figure- D-3.

The overall results show that there is a good similitude between CWP and FSP. The crack-tip state of SENT is different from those of CWP and FSP. The difference in the crack-tip state leads to the lower resistance curve of SENT specimens.

D.4 References

1 Gurson, A.L., Continuum theory of ductile rupture by void nucleation and growth: Part I – Yield criteria and flow rules for porous ductile media. Journal of Engineering Materials and Technology 99, 2-15: 1977.

2 Tvergaard, V. Influence of voids on shear band instabilities under plane strain conditions. Interational Journal of Fracture 17, 389-407: 1981.

3 Tvergaard, V. Ductile fracture by cavity nucleation between larger voids. Journal of the Mechanics and Physics of Solids 30, 265-286: 1982.

4 Koplik J and Needleman, A. Void growth and coalescence in porous plastic solids. International Journal of Solids and Structures 24, 835-853: 1988.

5 Liu, M. and Wang, Y-Y., Applying Gurson type of damage models to low constraint tests of high strength steels and weld. 6th International Pipeline Conference 2006, Calgary, Canada.

Appendix E Supplementary Tests on ABD-1 Girth Welds

E.1 Introduction

Several full scale tests in this project failed at much smaller strain levels than nominally identical duplicate tests, raising concerns about the consistency of the girth welds tested in the program. To help provide further insight into the girth weld properties and evaluate the consistency of the girth welds, a series of supplementary tests were performed on girth weld samples.

The variation in failure strains was most evident in the following full scale tests:

Table- E-1 Failure Strains in Full Scale Pipe Tests

Test	Weld Procedure	Flaw Size	Flaw Location	Strain at Max Load
1.9	15% Overmatch	3 x 50 mm	Weld	0.64%
1.19	15% Overmatch	3 x 50 mm	Weld	1.39%
1.23	15% Overmatch	2 x 70 mm	Weld	0.69%
1.21	Even Matched	3 x 50 mm	Weld	0.72%

Samples 1.9, 1.19 and 1.23 were all fabricated from the high Y/T Grade X65 pipe with a PGMAW weld procedure that produced a nominal weld metal overmatch of 15%. Sample 1.21 was fabricated from the same high Y/T pipe but using a PGMAW weld procedure that produced an approximately even matched weld. The main concern is that specimens 1.9 and 1.23 behaved like even matched girth welds as opposed to 15% overmatched welds.

E.2 Details of Girth Weld Samples

Although the flaw regions from the full scale tests were all stamped with weld identification number and preserved, the off cuts form the full scale tests were not all stamped (since no further testing of these sections was envisaged). As a result, it was not possible to identify the girth weld sections away from the failed notch location in all the specimens of interest. Nevertheless, the following girth weld samples, provided by CRES and C-Fer, were used for supplementary tests:

CRES

- 1.19: Girth weld with original flaw regions cut out.
- 1.23: Girth weld sections between original flaw regions.

C-Fer

- 1.9 : Failed region at original flaw
- 1.19: Failed region at original flaw
- 1.21: Failed region at original flaw (Note, 1.21 was an even matched weld)
- 1.23: Failed region at original flaw
- 776-CL: Original 15% Overmatch Girth Weld that was not tested
- 776-CN: Original 15% Overmatch Girth Weld that was not tested

In addition to the samples listed above, C-Fer also supplied the failed regions of all the full scale test welds with the exception of 1.11 and 1.18.

E.3 Supplementary Tests

The following tests were performed in this study:

- All Weld Metal Tensile Tests : 1.19, 1.23, 776-CL and 776-CN
- Weld metal Chemistries : 1.9, 1.19. 1.21, 1.23, 776-CL and 776-CN
- Hardness Surveys : 1.9, 1.19. 1.21, 1.23, 776-CL and 776-CN

E.4 Results

E.4.1 All weld Metal Tensile Results

The all weld metal tensile results from the supplementary tests are summarized below and presented as stress strain curves in Figure- E-1 together with a summary of the original properties determined in previous small-scale tests.

Table- E-2 Results of All Weld Metal Tensile Tests

Specimen	YS (ksi)	TS (ksi)	YS (MPa)	TS (MPa)	Source	Status
1.19-1	78.9	103.2	544	712	CRES	Previously Tested
1.19-2	81.7	102.5	563	707	CRES	Previously Tested
1.23-1	85.8	97.5	592	672	CRES	Previously Tested
1.23-2	89.0	98.3	614	678	CRES	Previously Tested
776-CL	86.6	101.5	597	700	C-Fer	Not Tested
776-CN	89.3	101.7	616	701	C-Fer	Not Tested

It can be seen from Figure- E-1 that the all weld metal stress strain curves for the samples that were previously tested (Specimens 1.19 and 1.23) exhibited continuous yielding as opposed to Specimens 776-CL and 776-CN which were not previously tested. This is considered to be a result of the previous loading the welds encountered during the full scale test. Furthermore since the girth welds that have previously been tested will have seen some level of straining during the full scale tests, strain aging may affect the measured yield strength in the subsequent tensile tests. Although strain aging may affect the measured yield strength in the small scale tensile tests, it usually has very small effect on the material tensile strength. Given the above, it is considered more appropriate to compare the tensile strength values in Table- E-2 to determine the degree of weld metal overmatch.

The original small scale tests on the second production girth welds exhibited the following average all weld metal tensile properties:

- Yield Strength: 85.9 ksi (592 MPa)
- Tensile Strength: 98.5 ksi (679 MPa)

The measured tensile strength values in the supplementary all weld metal tensile tests (Specimens 1.19, 1.23 and the untested 776-CL & CN) all agree with the original average strength, confirming that welds 1.19 and 1.23 provide approx 15% overmatch.

The uniform strains to maximum load in the all weld metal tensile tests were also compared. The results, which are summarized in Table- E-3, highlight that welds 1.19 and 776-CL & CN all exhibited uniform strains to maximum load of over 10% but weld 1.23 exhibited approx 4% strain to maximum load. Although welds 1.19 and 1.23 were previously tested in full scale tests, the difference in the measured strains to maximum load is unusual. This highlights that although welds 1.19 and 1.23 have similar strength, weld 1.23 has a much lower ductility than weld 1.19.

Table- E-3 Uniform Strains to Maximum Load in All Weld Metal Tensile Tests

Specimen	YS (ksi)	TS (ksi)	Source	Max Load Strain in Full Scale Test	Uniform Strain in All weld Metal Test	Status
1.19-1	78.9	103.2	CRES	1.39%	> 10%	Previously Tested
1.19-2	81.7	102.5	CRES		> 10%	Previously Tested
1.23-1	85.8	97.5	CRES	0.69%	3.5%	Previously Tested
1.23-2	89.0	98.3	CRES		4.0%	Previously Tested
776-CL	86.6	101.5	C-Fer	N.A.	> 10%	Not Tested
776-CN	89.3	101.7	C-Fer		> 10%	Not Tested

E.4.2 Hardness Results

The results of the Hardness tests, which were performed on the weld centerline with 1-mm spacing, are summarized in Table- E-4.

Table- E-4 Summary of Hardness Test Results

Source	CRES		C-Fer					
Specimen	1.19	1.23	1.23	1.19	1.9	776-CL	776-CN	1.21
Average	233	223	262	251	259	228	221	277
Min	215	208	239	229	253	193	211	271
Max	249	233	275	273	262	244	234	286

It can be seen from Table- E-4 that the hardness results of the untested welds (776-CL & CM) agree well with the 1.19 and 1.23 results from the samples removed outside of the flaw regions and as a result experienced relatively low local strains. The C-Fer results (all from the immediate flaw regions were high local strains and necking were present) exhibit much higher hardness values.

E.4.3 Weld Metal Chemistries

Weld metal chemistry analyses were performed on selected samples. The weld metal chemistries were measured on the weld center line at the mid thickness location. Although the weld metal chemistries were consistent, the measured oxygen and nitrogen (O_2 and N_2) contents showed a large variation. The measured O_2 and N_2 contents are presented in Table- E-5.

All the welds listed in Table- E-5were welded with K Nova Ni and pulsed GMAW with 85/15% Ar/CO_2 shielding gas with the exception of weld 1.21 which was welded with Lincoln L56 and short arc GMAW with 50/50% Ar/CO_2.

Table- E-5 Results of Weld Metal Chemistry Analysis

Specimen	Source	Status	Oxygen	Nitrogen
1.9	C-Fer	Previously Tested	0.046	
1.9	C-Fer	Previously Tested	0.038	0.009
1.19-1	CRES	Previously Tested	0.028	
1.19-2	CRES	Previously Tested	0.029	0.005
1.19-3	C-Fer	Previously Tested	0.022	
1.19-4	C-Fer	Previously Tested	0.028	0.007
1.21-1	C-Fer	Previously Tested	0.050	0.007
1.23-1	CRES	Previously Tested	0.049	
1.23-3	CRES	Previously Tested	0.048	0.008
1.23-4	C-Fer	Previously Tested	0.047	
1.23-5	C-Fer	Previously Tested	0.037	0.006
776-CL	C-Fer	Not Tested	0.025	
776-CL	C-Fer	Not Tested	0.030	0.005
776-CN	C-Fer	Not Tested	0.028	
776-CN	C-Fer	Not Tested	0.029	0.005

The weld metal oxygen and nitrogen contents for the untested welds (776-CL & CN) and weld 1.19 are consistent with the normal expectation for PGMAW girth welds, i.e., Oxygen ~ 0.025% and Nitrogen ~ 0.005%. In comparison, the oxygen and nitrogen contents in welds 1.9 and 1.23 are much higher than expected. High oxygen levels in weld metal (i.e., Oxygen > 0.040% or 400 ppm) can result in an increased number of inclusions which in turn can lead to reduced tensile ductility and a reduction in ductile fracture toughness. The high oxygen contents in welds 1.9 and 1.23 (low strain welds) are an indication that the toughness in these welds may be lower than welds 1.19 and 776-CN & CL. This is also consistent with the reduced uniform strain values measured in weld 1.23.

E.4.4 Additional Weld Metal Chemistry Analysis

To provide additional information on the variability of weld metal chemistry (in particular oxygen and nitrogen), all the samples provided by C-Fer were analyzed for oxygen and nitrogen. In addition, oxygen and nitrogen measurements were made on several trial welds made by CRC using the following weld process / shielding gas combinations.

- Short Arc with 100% CO_2
- Short Arc with 50% CO_2
- PGMAW with 85/15% Ar/ CO_2
- PGMAW with 75/25% Ar/ CO_2
- PGMAW with 50/50% Ar/ CO_2

The measured oxygen contents in the CRC trial welds are summarized in Table- E-6. The measured oxygen and nitrogen contents in full scale pipe tests are summarized in Table- E-7.

Table- E-6 Weld Metal Oxygen Levels in CRC Trial Welds

Weld Process	Shielding Gas	Oxygen (%)
Short Arc GMAW	100% CO_2	0.045
	50/50% Ar/CO_2	0.036
PGMAW	85/15% Ar/CO_2	0.028
	75/25% Ar/CO_2	0.031
	50/50% Ar/CO_2	0.037

Table- E-7 Weld Metal Chemistry Analysis for Full Scale Pipe Tests

C-Fer Spec Number	Pipe	Weld Process	Weld Metal Matching	Flaw Size (mm)	Flaw Location	Internal Pressure	Strain at Max Load (%)	Oxygen (%)	Nitrogen (%)
1.5	High Y/T	PGMAW	Even	3 x 35	WCL	High	1.58	0.049	0.006
1.6						Low	4.64	0.048	0.007
1.7					HAZ	High	4.74	0.048	0.006
1.8						Low	8.07	0.049	0.006
1.9	High Y/T	PGMAW	Over	3 x 50	WCL	High	0.64	0.042	0.009
1.10						Low	3.10	0.028	0.006
1.11					HAZ	High	1.24	-	-
1.12						Low	2.69	0.026	0.006
1.13						High	1.59	0.025	0.006
1.14						Low	3.12	0.030	0.007
1.15	Low Y/T	Short Arc	Over	3 x 50	HAZ	High	4.20	0.065	0.005
1.16						Low	6.81	0.061	0.005
1.17	High Y/T	PGMAW	Over	3 x 35	WCL	High	2.13	0.049	0.005
1.18					HAZ		7.73	-	-
1.19				3 x 50	WCL		1.39	0.029	0.007
1.20	Low Y/T	Short Arc	Over	3 x 50	WCL	High	3.97	0.055	0.005
1.21	High Y/T	PGMAW	Even	3 x 50	WCL	High	0.72	0.050	0.007
1.22					HAZ		2.01	0.044	0.005
1.23	High Y/T	PGMAW	Over	2 x 70	WCL	High	0.69	0.042	0.007
1.24				3 x 50	HAZ		2.28	0.030	0.005
-				NA	NA	NA	NA	0.030	0.005
-				NA	NA	NA	NA	0.029	0.005

It can be seen from Table- E-6 that the trial CRC PGMAW welds produced oxygen contents that varied from 0.028% to 0.037% depending on the shielding gas. PGMAW is normally used with either 85/15% Ar/CO_2 or 75/25% Ar/CO_2 shielding gas. Although PGMAW is not normally used with 50/50% Ar/CO_2 gas, due to issues with porosity and spatter, this weld process / shielding gas combination was evaluated to determine how the increase in CO_2 in the shielding gas influenced the measured oxygen content in the weld metal. The results from the CRC trial welds are consistent with the measured oxygen levels one would expect with the different shielding gas combinations, i.e., 0.025 – 0.030% Oxygen for 85/15% Ar/CO_2.

The measured oxygen and nitrogen contents form the girth welds in the full scale pipe samples that were tested at C-Fer show a wide range of oxygen content (0.025% to 0.050%).

Indeed some of the full scale girth welds, which were all fabricated with 85/15% Ar/CO_2 shielding gas, produced oxygen levels that were larger than the CRC PGMAW trial weld fabricated using a 50/50% Ar/CO_2 shielding gas.

The reason for both the broad spread and the unusually high oxygen contents in the girth welds from the full scale pipe tests is not obvious. Possible factors include:

- Contaminated shielding gas,
- Improperly labeled shielding gas,
- Use of incorrect shielding gas,
- Ineffective shielding due to shielding gas flow rates that were either too high (causing turbulence) or too low,
- Temporary lack of Shielding due to a draft from a window or door,
- Excess lubricant on welding wire.

Regardless of the cause for the spread in measured oxygen level, it could be concluded from a quick review of Table- E-7 that not all the PGMAW girth welds with high oxygen levels exhibited low strains to failure indicating the weld metal oxygen content may not have influenced the full scale test results. Nevertheless, it must be noted that the full scale test program considered a large number of test variables making a direct evaluation of the effect of high weld metal oxygen content difficult. The tests where PGMAW weld metal oxygen content is most important are the samples notched at the weld centerline, i.e., Tests 1.5, 1.6, 1.9, 1.10, 1.17, 1.19, 1.21, and 1.23. If this set of data is further reduced to the tests where the girth welds had similar sized flaws (i.e., 3 x 50 mm or 2 x 70 mm) and internal pressure (Tests 1.9, 1.19, 1.21, and 1.23), the following conclusions can be drawn from the full scale test data:

- The girth welds with oxygen contents greater than 0.040% (400 ppm) had failure strains of 0.64%, 0.69% and 0.72% as compared to the failure strain of 1.39% for Test 1.19 which had an oxygen content of 0.029%.

This conclusion would indicate that full scale tests with girth welds that a) had a high oxygen content and b) were notched at the weld centerline are likely to exhibit uncharacteristically low strains to failure. In comparison, HAZ notched samples with high oxygen content might not be affected by the oxygen level since the available test data confirms that the high oxygen weld metal still provides the target strength overmatch. Moreover, since the HAZ notched samples failed either along the HAZ or through the HAZ into the parent pipe, the toughness and ductility of the weld metal is not critical provided the weld metal provides the target level of overmatch.

It is noted that there are several full scale tests on WCL notched pressurized pipe with PGMAW weld metal oxygen contents > 400 ppm that failed at moderate strains (e.g., Test 1.5 : Failure Strain = 1.58% and Test 1.17 : Failure Strain = 2.13%). In these cases, the flaw size was 3 x 35 mm which would have resulted in a reduced crack driving force. Nevertheless, it is recognized that all PGMAW WCL notched samples with oxygen content > 400 ppm may have failed at lower strains than would have been the case had the oxygen content been closer to 250 ppm normally expected for PGMAW welds.

E.5 Summary

Although it was not possible to perform more extensive testing on the full scale test welds that failed at low strains due to difficulties with material traceability, the following conclusions can be drawn from the tests performed on the available material:

- All weld metal tensile tests showed no evidence of under or even matching in the second generation production welds. The all weld metal tensile strengths are consistent with the previous small scale tests as part of the project.
- The all weld metal tensile tests did exhibit a wide range of uniform strains to maximum load (less than 4% to more than 10%) with the lowest values recorded for weld 1.23 which failed at 0.69% strain in a full scale test. The low uniform strain to maximum load in weld 1.23 indicates that although this weld did overmatch the base pipe by 15 – 20%, it exhibited much lower ductility than other nominally identical test welds.
- Weld metal chemistries confirmed higher oxygen (0.050%) in some of the test welds fabricated with pulsed GMAW and 85/15% Ar/CO_2 shielding gas. The oxygen levels are much higher than the typical oxygen levels (0.025%) expected in pulsed GMAW welds. Higher oxygen content will result in an increased number of inclusions and a reduction in toughness and ductility. All three of the full scale test welds (1.9, 1.21 and 1.23) that failed at low strains had elevated oxygen levels.
- Given the consistency of the weld metal chemistry results within a test weld, the high oxygen and nitrogen levels are unlikely to be a result of temporary lack of shielding due to a draft. The most likely cause of the high oxygen and nitrogen levels is contaminated shielding gas, an incorrectly identified gas cylinder or use of an incorrect shielding gas.

In summary, the supplementary tests on the test welds did not highlight any evidence of under strength girth welds but did confirm some of the girth welds, including all three of the full scale test welds that failed at low strains, had high weld metal oxygen levels which is likely to promote a reduction in toughness and ductility which in turn could reduce the strain to failure. This may have contributed to the low failure strains in Tests 1.9, 1.21, and 1.23 which had girth welds with high oxygen content in combination with large flaw sizes (3 x 50 mm or 2 x 70 mm) and internal pressure, which would have increased the crack tip driving force[4].

- Test 1.9 Failure Strain = 0.64% Oxygen Content = 0.042%
- Test 1.21 Failure Strain = 0.72% Oxygen Content = 0.050%
- Test 1.23 Failure Strain = 0.69% Oxygen Content = 0.042%

[4] There were welds that had high oxygen level but failed at relatively high strains. Those welds either had smaller flaws or were tested without internal pressure. Both of those conditions promoted low crack driving forces.

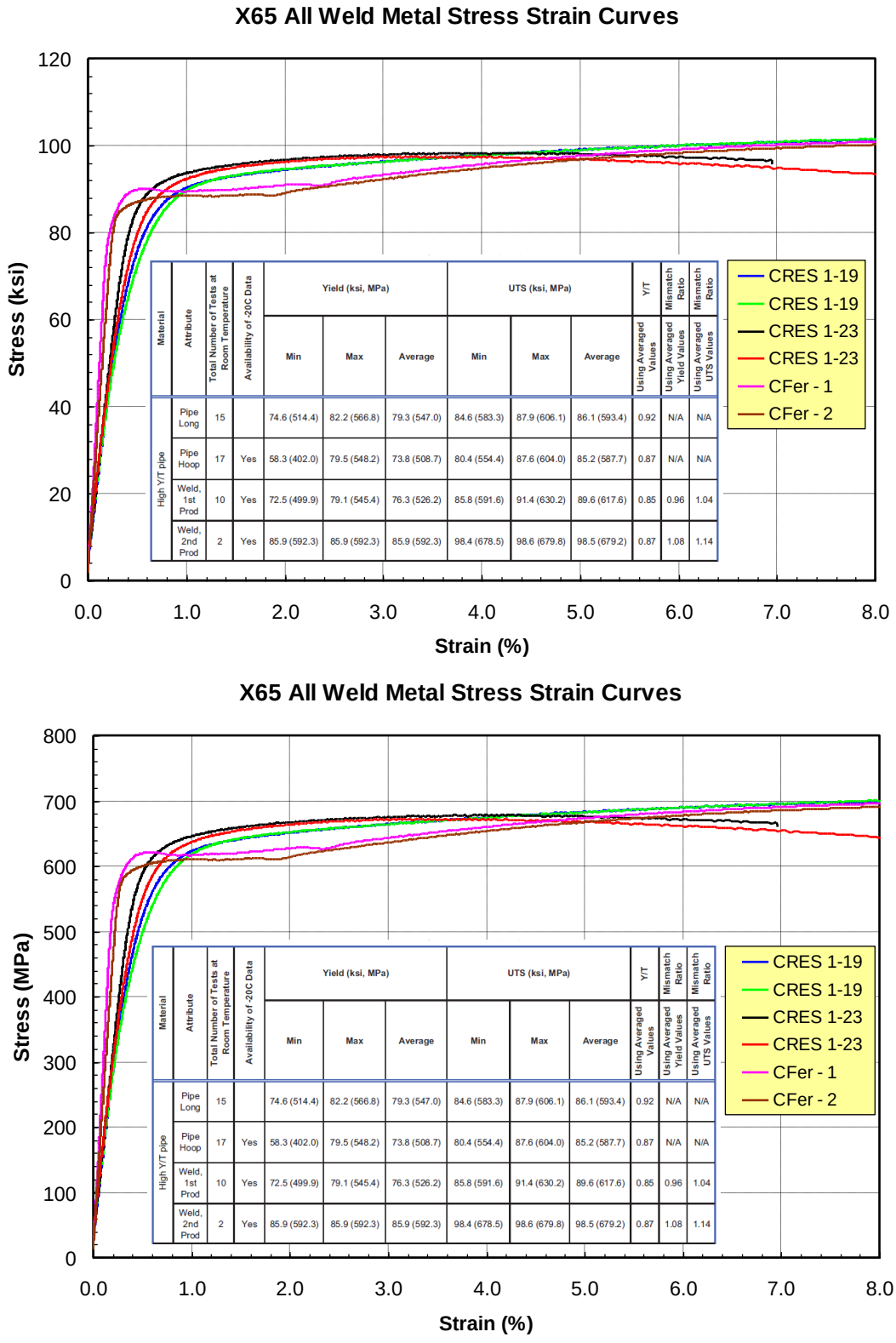

Material	Attribute	Total Number of Tests at Room Temperature	Availability of -20C Data	Yield (ksi, MPa)			UTS (ksi, MPa)			Y/T	Mismatch Ratio	Mismatch Ratio
				Min	Max	Average	Min	Max	Average	Using Averaged Values	Using Averaged Yield Values	Using Averaged UTS Values
High Y/T pipe	Pipe Long	15		74.6 (514.4)	82.2 (566.8)	79.3 (547.0)	84.6 (583.3)	87.9 (606.1)	86.1 (593.4)	0.92	N/A	N/A
	Pipe Hoop	17	Yes	58.3 (402.0)	79.5 (548.2)	73.8 (508.7)	80.4 (554.4)	87.6 (604.0)	85.2 (587.7)	0.87	N/A	N/A
	Weld, 1st Prod	10	Yes	72.5 (499.9)	79.1 (545.4)	76.3 (526.2)	85.8 (591.6)	91.4 (630.2)	89.6 (617.6)	0.85	0.96	1.04
	Weld, 2nd Prod	2	Yes	85.9 (592.3)	85.9 (592.3)	85.9 (592.3)	98.4 (678.5)	98.6 (679.8)	98.5 (679.2)	0.87	1.08	1.14

Figure- E-1 All Weld Metal Stress Strain Curves (Top Plot - ksi : Bottom Plot – MPa)